Damage Repair of Bridge Superstructures using Bonded Composite Patching

By

Jacob Noel McNutt

Thesis

Submitted to the Faculty of the

Graduate School of Vanderbilt University

in partial fulfillment of the requirements

for the degree of

MASTER OF SCIENCE

in

Civil Engineering

August, 2011

Nashville, Tennessee

Approved:

Professor P.K. Basu

Professor Curtis Byers

To my wife, Anita, my very own miracle

and

To my parents, Eddie and Melissa, ever encouraging

ACKNOWLEDGEMENTS

This work would not be possible without the financial support of the Tennessee Department of Transportation. Material and service support also provided by Sika Corporation, Newport Composites and Adhesives, Concrete Products Inc., Gerdau Ameristeel, Lafarge Materials, East Kentucky Power Cooperative, and Vanderbilt Physics machine shop.

I am grateful to my wise and knowledgeable advisor, Dr. P. K. Basu. He is wise and a wellspring of knowledge. I am also grateful to Dr. Curtis Byers for taking the time and energy to help me throughout the research. I am thankful to all those who helped me in various ways to complete this research project; Niko Nordendal, Ozgur Yapar, Adrian Bennett, Lisa Brown, Ghina Nakad, and Catie Gay. I would also like to thank Dr. David Delapp, who was more than knowledge in the lab. Gratitude is also due to John Fellenstein and Bob Patchin in the physics machine shop who were critical in creating several lab devices.

Lastly, I would like to thank my family and friends for their support. I would like to thank my wife for her support and love. She is always positive and helped me in any way I asked and then some. I would like to thank my parents for their wisdom, love, and support and I want to thank my siblings, Maggie and Ben, for inspiring me to be more than I am.

TABLE OF CONTENTS

LIST OF TABLES

Page

Chapter I

Chapter II

Chapter III

Chapter V

Chapter VI

APPENDIX B

LIST OF FIGURES

Page

Chapter I

Chapter II

Chapter III

Chapter IV

Chapter V

Chapter VI

APPENDIX B

LIST OF NOMENCLATURE

Nomenclature Specific to Chapter I; Review of Research Literature

A_c = area of the FRP composite

A_{con} = area of concrete section

A_f = are of fiber composite

A_s = area of the substrate

A_{s1} = area of primary tensile reinforcing steel

A_{s2} = area of top reinforcing steel

b_c = concrete beam width; (mm)

b_{FRP} = composite width; (mm)

b_p = width of the FRP composite

CFRP = Carbon Fiber Reinforced Polymer

E_f = modulus of fiber composite

E_{FRP} = modulus of composite; (MPa)

E_{con} = modulus of concrete

E_s = substrate tensile modulus

E_{s1} = tensile modulus of primary tension reinforcing steel

E_{s2} = modulus of top reinforcing steel

FRP = Fiber Reinforced Polymer

f'_c = concrete compressive strength; (MPa)

f_t = concrete tensile strength; (MPa)

G_a = shear modulus of the adhesive

G_f = interfacial fracture energy; (MPa-mm)

I_s = moment of inertia of steel substrate section

l = length of beam

L = bond length; (mm)

L_b = bond length

L_d = distance from the loaded section to the end of the FRP laminate

$M_{bd,end}$ = composite plate end moment when debonding occurs

$M_{db,f}$ = flexural debonding moment when no shear stresses are present

P = applied load

q = applied uniform load

s = slip

s_f = slip at zero bond strength; (mm)

s_m = slip corresponding to bond strength

s_o = local slip at maximum bond strength; (mm)

t_a = adhesive thickness

u_c = displacement of concrete section of beam

u_f = displacement of fiber composite

u_{s1} = displacement of primary tension reinforcing steel

u_{s2} = displacement of top reinforcing steel

$V_{db.end}$ = composite plate end shear force

$V_{db,s}$ = shear debonding force when the beam section is not subjected to any bending moment

W_s = the substrate section modulus

x = distance along beam

Y = deflection of composite beam

α = shape parameter

α' = shape parameter

τ_m = bond strength

σ_P = the bond stress; (MPa)

Nomenclature Specific to Chapter I; Review of Current Practice and Design Guidelines

A_s = area of nonprestressed tension reinforcement; $(in)^2$

A'_s = area of compression reinforcement; $(in)^2$

ASTM = American Society of Testing and Materials

b_{FRP} = width of the FRP reinforcement

c = depth of the concrete compression zone; (in)

C_E = environment reduction factor

CPS = Concrete Surface Profile

d_f = effective depth of the FRP composite

d_{FRP} = effective depth of the FRP reinforcement

d_s = distance from the extreme compression fiber to the centroid of A_s; (in)

d'_s = distance from the extreme compression fiber to the centroid of A'_s; (in)

$E_a = 2G_a (1+v_a)$ Young's Modulus of adhesive; (ksi)

E_f = design tensile modulus of elasticity; (psi)

f'_c = compressive strength of concrete

$f_{c,s}$ = compressive stress of the concrete under service loading

f_{fe} = FRP composite strength

$f_{ps,s}$ = stress experienced by the steel strands

f_s = stress of the steel tensile reinforcement; (ksi)

f'_s = stress of the compression reinforcement; (ksi)

f_{fu} = design ultimate tensile strength; (psi)

f_{fu}^* = manufacturer specified ultimate tensile strength; (psi)

$f_{s,s}$ = stress of the reinforcing steel under service loads

G_a = shear modulus from ASTM D5656; (ksi)

h = height of the section; (in)

ICRI = International Concrete Repair Institute

I_T = moment inertia of the transformed FRP section; (in^4)

kd = depth of the neutral axis under service loads

k_1, k_2 = modification factors

k_2 = multiplier for locating the resultant of the compression force

L_d = development length of composite patch

L_e = active bond length

M_u = factored moment at the reinforcement end; (kips)

n = number of FRP plies

N_b = FRP reinforcement strength per unit width

R_n is the nominal strength of the structural member

S_{DL} is the dead load effects

S_{LL} is the live load effect

s_v is the spacing of the FRP reinforcement

t_a = thickness of the adhesive layer; (in)

t_f = thickness of the FRP composite

t_{FRP} = thickness of the FRP composite; (in)

T_{FRP} = tension force in the FRP reinforcement; (kips)

V_a = 0.35 Poisson's ratio

V_c = nominal shear strength provided by the concrete

V_{FRP} = nominal shear strength provided by the FRP reinforcement

V_n = nominal shear capacity of a concrete member

V_p = component of the effective prestressing force in the shear direction

V_s = nominal shear strength provided by transverse reinforcing steel

V_u = factored shear force at the reinforcement end; (kips)

w_{FRP} = width of the FRP reinforcement

α = angle between FRP principal direction and the longitudinal member axis

α_1 = ACI parameter defining concrete compressive stress block

β_1 = ACI parameter defining concrete compressive stress block

ε^u_{FRP} is the tensile failure strain according to ASTM D3039

ε_{fd} = rupture strain of the FRP composite systems

ε_{fu} = design ultimate strain

ε_{fu}^* = manufacturer specified design ultimate strain

ε_{pe} = effective strain of the prestressing strands after losses

ε_{pnet} = net tensile strain in the strands beyond decompression

ε_{sy} = strain at which steel yields.

κ_v = bond-reduction factors

τ_a = limiting shear stress from ASTM D5656

ϕ_{FRP} = resistance factor determined from reliability analysis

ψ_f = strength reduction factor for FRP composite materials

Nomenclature for Chapter II through Chapter VI

a = distance from edge of beam to location of point load

a_i = constant

A_{beam} = total area of steel beam

A_v = area of steel shear reinforcement

A_s = area of the mild, or primary, tensile reinforcing steel

A'_s = area of compression, or tope, reinforcing steel

A_{ps} = area of prestressing steel strands

b_{fl} = width of steel flange

b_p = width of composite patch

$(b_p)_{max}$ = maximum width of composite patch

$(b_p)_{min}$ = minimum width of composite patch

b_w = beam width

c_b = distance from the bottom extreme fiber of steel beam to the neutral axis

c_t = distance from the top extreme fiber of steel beam to the neutral axis

d = distance from top of beam to depth of primary tensile reinforcing steel

d = total height of steel beam

$\bar{d}$ = average depth of tensile steel for prestressed concrete beam

d' = depth of compression, or top, reinforcing steel

d_{ps} = depth of the prestressed steel strands

d_{rup} = depth from top of beam to tensile strain of rupture for concrete

d_s = depth of tensile mild reinforcing steel

e = eccentricity of point loads from center line of beam

E = modulus of elasticity of beam

E_c = modulus of elasticity of concrete

E_s = modulus of elasticity of steel

f'_c = compressive strength of concrete

f_p = stress of composite patch

f_{pu} = ultimate stress capacity of composite patch

f_s = stress of mild, or primary, reinforcing steel

f'_s = stress of compression, or top, reinforcing steel

f_y = yield stress of reinforcing steel

$F_{adhesive}$ = force of the adhesive

F_c = compressive force of the concrete section

F_p = force of the composite patch

F_{patch} = force of the composite patch

$(F_p)_{tot}$ = force experienced by composite patch for shear reinforcing

FRP = fiber reinforced polymer

F_s = force of the primary reinforcing steel

F_t = force created from the tensile strength of concrete

H = height of concrete beams

h_{cr} = height of crack in concrete

I = moment of inertia of beam

ICRI = International Concrete Repair Institute

L = length of beam

L_p = length of composite patch

L_{pd} = development length of composite patch

M_{app} = applied moment

M_n = moment capacity

$(M_n)_{existing}$ = moment capacity of beam before repair

$(M_n)_{new}$ = moment capacity of the beam after repair

P = point load

P_{xp2} = point load applied to composite repaired beam

P_{xp3} = point load applied to composite repaired beam

P_u = ultimate load applied to beam

q = self-weight of beam

s = spacing of the steel shear reinforcing stirrups

s_p = spacing of the composite patch shear reinforcing

t_a = thickness of the adhesive

t_{fl} = thickness of steel beam flange

t_p = thickness of the composite patch

t_w = thickness of the steel beam web

u = displacement horizontal springs system symbolizing composite adhesive undergo

u_b = horizontal displacement of beam

u_p = horizontal displacement of composite patch

U_{beam} = total potential energy of a composite patched beam

$U_{H.S}$ = strain energy of the horizontal springs of mechanistic model

$U_{V.S}$ = strain energy of the vertical springs of mechanistic model

v = displacement vertical spring system symbolizing composite adhesive undergo

v_b = vertical displacement of beam

v_p = vertical displacement of composite patch

V = sum of non-conservative forces applied to the composite patched beams

V_{app} = applied shear

V_n = shear capacity of beam

$(V_n)_{existing}$ = shear capacity of beam before repair

$(V_n)_{new}$ = shear capacity of beam after repair

w_p = width of composite patch

x = length along span of beam

$x_{fd\text{-}f}$ = location to which composite patch must remain fully developed

$x_{fd\text{-}o}$ = location at which composite patch must be fully developed

x_{p2} = location of point load application of composite repaired beam

x_{p3} = location of point load application of composite repaired beam

y_b = distance from the bottom of the beam to its neutral axis

y_c = distance from the centroid of the concrete to a datum location

y_c = the distance from the most extreme tensile fiber of the steel beam to the centroid of the area acting in compression.

$\overline{y_c}$ = distance from the neutral axis to the centroid of the compression section

y_s = distance from the centroid of the primary reinforcing steel to a datum location

y_t = distance from the most extreme tensile fiber of the steel beam to the centroid of the area acting in tension

α_s = angle measured from the longitudinal direction of the beam up to the direction of the steel shear reinforcement

α_p = angle measured from the longitudinal direction of the beam up to the direction of the steel shear reinforcement

ε_c = strain of the concrete

ε_s = strain of the primary reinforcing steel

γ = ratio of prestressing steel strand yield stress to mild steel yield stress

λ = ACI variable for type of concrete

Π_{beam} = total energy of a composite patched beam

Chapter I

INTRODUCTION

Motivation

Bridges are critical links in America's transportation infrastructure. Nearly one third of the 599,766 bridges of the National Bridge Inventory (NBI) are either structurally deficient, functionally obsolete, or both. *Structurally deficient* bridges are defined by restrictions of vehicle weight, closed entirely, or a necessity of structural rehabilitation. Structurally deficient bridges have elements which need to be monitored or repaired. Such bridges are not in danger of imminent collapse or is unsafe; only that the bridges must be closely monitored, inspected, or repaired. A *functionally obsolete* bridge was designed according to design codes which are no longer accepted by modern standards. Such insufficiencies could include inadequate lane or shoulder widths, vertical clearances, prone to flooding, and or other environmental concerns.

Most of the bridges currently in use were constructed in the 20th century. These structures were designed and built to last 50 years minimum; most are already 45 years old and are deteriorating. Such deterioration is the results of excessive use and exposure to harsh environmental elements. Steel bridges are corroding and cracking from fatigue while concrete structures crack, spall, scour, and delaminate from a host of attacks. Bridges often age at an accelerated rate because they are subject to heavier, larger, and faster traffic loads than the predicted design values. Additional damage is caused by

vehicle collision into piers and beams. The onslaught of corrosion varies according to traffic patterns of use, geographic location, and the degree of exposure to the elements.

Steel bridge deterioration is primarily attributed to the factors listed below; figures 1 through 3 show examples of steel bridge with such wear.

- Inadequate fatigue life; which leads to fracture points at large stress concentrations such as bolt opening, weld roots, or locations of radical change in geometry.
- Loss of material; occurs commonly due to atmospheric corrosion including salt induced corrosion and rust
- Stress corrosion cracking; causes sudden failure of ductile steel members under tension loads
- According to recent estimates of FHWA, the current annual cost of bridge corrosion is $13.3 billion.
- Error and mistakes in design, fabrication and erection

Deterioration of concrete bridges is caused by a wide variety factors, listed below. Several figures of different damages to concrete beams are shown in figures 4 to 8.

- Chloride-ion penetration; leads to corrosion of the reinforcing steel followed by delamination and spalling of concrete
- Carbonation; breaks down the matrix structure of cement, reducing the pH of the concrete making it more brittle and cause reinforcing steel to corrode

Figure 1. Corroded girder of Chesterfield Bridge in Virginia

Figure 2. Corrosion of diagonal steel brace in additional to impact damage

Figure 3. Collapse of Silver Bridge in 1967, caused by fatigue failure of eye bar pin

- Leaching, scaling, and efflorescence; leads to degradation of concrete by surface erosion, creation of internal voids and loss of strength of concrete
- Map cracks; caused by alkali-silicate reaction produces a gel which expands in volume with absorption of water leading to eventual rupture of concrete
- Sulfate and acids attack; cause cured cement to expand inducing internal stresses making the concrete prone to cracking and disintegration
- Freeze-thaw and thermal cycles; cause cracking of concrete
- Accidents; such as fire damage and collision impact

- Overstress condition; causes undesirable cracking and concrete distress caused by exposure to heavier than design loads or unaccounted differential foundation settlement
- Substandard construction materials
- Poor workmanship; such as improper placement, inadequate or incorrect compaction and curing
- Errors and mistakes in design

Figure 4. Reinforced concrete beam with vertical crack

Figure 6. Diagonal shear cracks near support

Figure 5. Severe spalling and delamination, exposing corroded reinforcing steel

Figure 6. Overhead vehicle impact damage to bottom of prestressed girder

Figure 7. Deterioration of prestressed girder end, exposing anchorage

Figure 8. Diagonal crack in prestressed girder

FRP Composite Repair

With the ever growing materials science field, many new materials are becoming available for retrofitting applications. Beginning in the 1980's, fiber reinforced polymers, or FRPs, began its distinct presence in the civil engineering community as a viable option for structural repair and post strengthening. Such materials are typically comprised of resin matrix embedded with carbon, glass, and, less commonly, aramid fibers. FRP laminates are lightweight and incredibly strong compared with the classic patch materials, namely steel, grout, cement, and concrete; making it ideal for placement.

However, the higher cost of the FRP patch material coupled with its unfamiliarity in the engineering community, may also have limited its use. Since the economic turmoil of the Great Recession, the sharp rise in the price of building materials, such as steel, makes FRP retrofitting solutions increasingly attractive for bridge repair (Kelly and Grecia, 2010). In this post-recession era, with politicians crying for budget cuts on all

fronts, it is no doubt a daunting task for bridge managements to find an answer to the estimated price tag of about $140 billion for replacing all the deficient and/or obsolete bridges within a few years (Schust, 2008).

For some time, the aerospace industry has been using patch repair techniques for the body of aircrafts, first, using metal patches, and later with bonded laminated composite patches (Ahn, Basu, et al., 2010; Ahn & Basu, 2011). The use of laminated fiber reinforced polymers for repairing localized damages of types described above is characterized by the following attributes.

- Easy and quick installation
- Savings in labor and shut-down costs
- Durable, lightweight, and high strength to weight ratios
- Customizable with respect to shape, size, and strength

Currently, a new variety of repair strategies are being investigated for adoption into practice. Of these, laminated fiber-reinforced materials attract the most attention because they are typically very light-weight, have incredibly high strength, and are easily installed in the field. This evolution of new materials for retrofitting damaged bridge structures from technical, economic and operational points of view is movement in the right direction for effective management of the national bridge inventory.

However, there is a need to thoroughly evaluate the practicality of such repair solutions for acceptance in practice. This requires a joint effort by researchers and professionals; calling for short- and long-term experimental and mathematical studies. As part of this effort, viable repair materials and schemes need to be evaluated in the

laboratory, under a variety of simulated conditions of deterioration and environmental attacks. Repair solutions which satisfy the expectations of civil engineering professionals and researchers with laboratory performance, should then be implemented on a carefully selected prototype bridge. The choice of such a bridge and the repair solution is guided by issues of the degree and cause of damage or deterioration, objectives of repair, and the cost of implementation and bridge instrumentation.

In order to increase FRP composites use, significant investigations into the nature and behavior of the FRP materials are being undertaken through research efforts at several universities. Such efforts are primarily funded by governmental agencies. Early researches have primarily focused on strengthening existing structures to accommodate heavier traffic loads and increasing earthquake resistance of bridge piers by retrofitting.

Review of Research Literature

The European civil engineering community first considered FRP composite systems as a viable repair solution nearly five decades ago (Meier, 1995). Research into the practical use of FRP systems was spearheaded in the 1960's by the Swiss Federal Laboratories for Materials Testing and Research, or EMPA for short. Interest in FRP composite systems rose from the many drawbacks of post-strengthening structures with steel; and continues to be the motivation for investigating FRP composites in the USA today. The early work completed by the researchers involved selecting fiber and adhesive types and finding feasible, safe employment of fibers systems. Researchers initially debated the benefits and drawbacks of various fiber material and mechanical

properties, including fiber ratios and prestressing, in addition to finding cost/saving ratios for civil engineering projects.

These efforts concluded that carbon fiber reinforced polymers (CFRP) were the optimum fiber type and was a practical repair system for repairing beams, girders, towers, and columns. These early research efforts found utilizing CFRP composite systems could strengthen all these structural members with a number of reinforcing schemes. The reinforcing schemes pertinent to beams and girders will be discussed in greater detail in what follows. The practical issues of FRP composite field application was initially explored by these early researchers (Meier, 1995). Given the burgeoning state of the technology, the importance of proper installation for satisfactory performance of composite systems was not clearly understood. The first observed FRP composite failures included (Meier, 1995):

- Sudden failure of FRP with little warning
- Compressive failure of concrete of the structural members
- FRP peeling from uneven concrete surfaces
- FRP peeling of thin composites under loading
- Concrete shearing in tensile regions
- Delamination of composite plies

Methods to avoid some of these failure states have been developed over time, such as composite delamination, while others have not (Meier, 1995; Teng and Cheng, 2009).

Another important first step made early in the research of composite application to civil engineering structures was to study the effects of weathering. The composite materials available to the Swiss researchers were run through hundreds of freeze-thaw cycles to find if the fibrous materials suffered from repeated temperature changes and water expansion. The materials were additionally heated to extreme temperatures in an oven to find the effects of heat on the adhesives and fibers (Meier, 1995).

These first efforts exploring FRP composite as a viable post-strengthening or repair solution made progress into narrowing the ever widening composite field to feasible materials, projects, and reinforcing schemes. However, such early research made little effort to develop FRP composite reinforcement design and standardization. The reinforcing schemes were varied widely, making it difficult to identify the effectiveness of the composite materials or their application. Many areas were left to be explored including composite material testing; quantification of the physical properties of the composite components, mechanical behavior, and proper steps at standardized testing. Questions about the effects of chemical degradation and environmental exposure were also left for future examiners to answer. Though several case studies were performed, the long term performance of the FRP composite systems was not explored. Neither were the effects of fatigue failure from cyclic loading despite such loading being common in many civil engineering structures.

Previous research on FRP applications in engineering has enabled increased understanding of the material for engineering applications. Retrofitting deficient structures with FRP laminates was initiated in Switzerland in the 1960's (Meier, 1995). Since then, several attempts have been made to advance the concept for wider

applications in the remediation, strengthening and life-extension of civil engineering structures.

Current research has sought many of the answers to the questions left by initial researchers. The research efforts have become specialized and focus on each element of a typical FRP composite system specifically: substrate materials, surface preparations, adhesives, FRP fibrous materials, and protective coatings. Studies have been conducted into the specific use of FRP composite system to repair structural members deficient in shear, flexural, torsional, and axial capacity. Some researchers endeavor to find optimum reinforcing schemes, others to create accurate stress distribution models, and still others to characterize the long term performance of FRP composites.

Given the ever expanding FRP composite industry, new composite products have become available for use and research. CFRP grids have been researched as a reinforcing system of walls (Joshi, 2004). FRP rods have been studied as reinforcing of concrete slabs instead of conventional steel bars (Nanni, 2004). Investigations have also been undertaken into the use of FRP rods as post-strengthening placed in epoxy filled holes of in-place walls and beams (Joshi, 2004). Flexible FRP fabrics have been employed in practice and the laboratory setting to strengthen beams and columns (Jumaat et al., 2006). The nature, however, of this research effort focuses on the application of FRP composite systems to repair, or post-strengthen, beams and girders; specifically those of bridge super-structures. As such, the state-of-the-art research work pertinent to such applications follows.

There are several distinct FRP composite systems capable of effectively retrofitting bridge and building beams. Most of these systems are designed to reinforce

concrete beams, though most are appropriate for steel beams. These systems are externally bonded to the structural members via epoxy or resins and can employ FRP composite bars, strips, and fiber fabrics. The FRP systems are available in many forms; manufacturers can supply the fibers cured in resin, impregnated in resin, or simply as dry fibers. There are two primary reinforcing schemes for post-strengthening of beams to increase the moment capacity and a variety of reinforcing patterns for enhancing the shear capacity of beams.

One retrofitting technique for increasing moment capacity is called *near-surface fiber reinforced polymer* (NS-FRP) and it is applicable to concrete beams. This system requires grooves to be saw-cut into the tensile face of the beam. These grooves are filled with resin or epoxy, in which FRP strips or rods are carefully placed. Figure 9 shows the employment of a typical NS-FRP system.

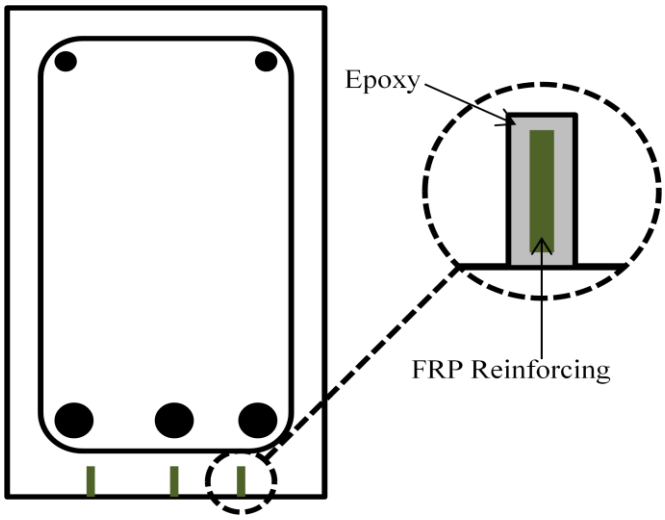

Figure 9. Typical NS-FRP reinforcing system utilizing composite strips

Both analytical and experimental research has been conducted to increase understanding of this FRP composite reinforcing system. Most investigations explore the bond behavior

and capacity because it is typically the adhesive of the FRP composite system which fails first (Sena-Cruz, 2004). Elaborate experimental tests have delved into the importance of bond length, the bond-slip behavior of the adhesive, as well as adhesive capacity and other mechanical properties. The conclusions of a series of test are summarized below (Sena-Cruz, 2004).

- Nonlinear branch before the peak pullout force increased with bond length, L_b;
- Peak pullout force increased with L_b;
- Bond strength ranged from 10MPa to 14MPa, with a tendency to decrease with an increase of L_b;
- Ratio between the maximum tensile stress in the CFRP laminate and its tensile strength increased with L_b;
- Loaded end slip at peak pullout force showed a tendency of a nonlinear increase with L_b;
- Envelop of the pullout force-slip relationship of the cyclic tests was similar to the curve obtained in the corresponding monotonic test;
- Continuous decrease of the peak pullout force was observed in the unloading/reloading cycles carried before the test peak pullout force. The test peak pullout force, however was not affected by this effect;
- Unloading branches of the loading cycles performed in the post-peak regime, no slip at the free end was recovered;
- Stiffness (i.e. average cyclic inclination) up to the peak pullout force was decreased with the cyclic loading. At the initiation of the softening phase, the stiffness increased slightly, followed by a smooth decrease.

As mentioned above, the adhesive bond is critical to accurately predict the failure and life-span of the FRP application. One model mathematically derived to characterize the bond stress is given by equation 1 (Sena-Cruz, 2004). The stress is described in terms of bond strength, slip, and displacement with two shape parameters. This expression can correctly predict the behavior of experimental data.

$$\tau(s) = \begin{cases} \tau_m \left(\frac{s}{s_m}\right)^{\alpha}, \text{if } s \leq s_m \\ \tau_m \left(\frac{s}{s_m}\right)^{-\alpha'}, \text{if } s \geq s_m \end{cases} \quad (1)$$

NS-FRP composite systems have several drawbacks. The system poses several risks to the field technicians and the bridge superstructure. The system requires technicians to saw grooves into the bottom of the beams, creating several safety issues. There are significant risks to the bridge super structure if the grooves intersect with in-place reinforcing steel; technicians could make the grooves too deep or simply in the wrong place due to the difficulty of overhead sawing. Penetrating the reinforcing steel only promotes corrosion and/or additional repair work.

Externally bonding plates or fiber fabrics to beams and girders are non-invasive and eliminates the need to further damage the beams or girders in an attempt to repair them. Since less beam preparation is necessary, composite systems of plates and fabrics require less labor which is an additional cost savings. There has been a steady increase of interest in research into the effect of applying of externally bonded plates and fiber fabrics.

There are several successful externally bonded plate and fiber fabric reinforcing schemes (Teng and Cheng, 2009). Figure 10 shows a typical diagram of applying FRP composites to augment the moment, or flexural, capacity of inadequate beams.

Figure 10. Common flexural reinforcing scheme

To provide shear strength to a concrete member, the designer can choose from several reinforcing schemes, summarized in figure 11.

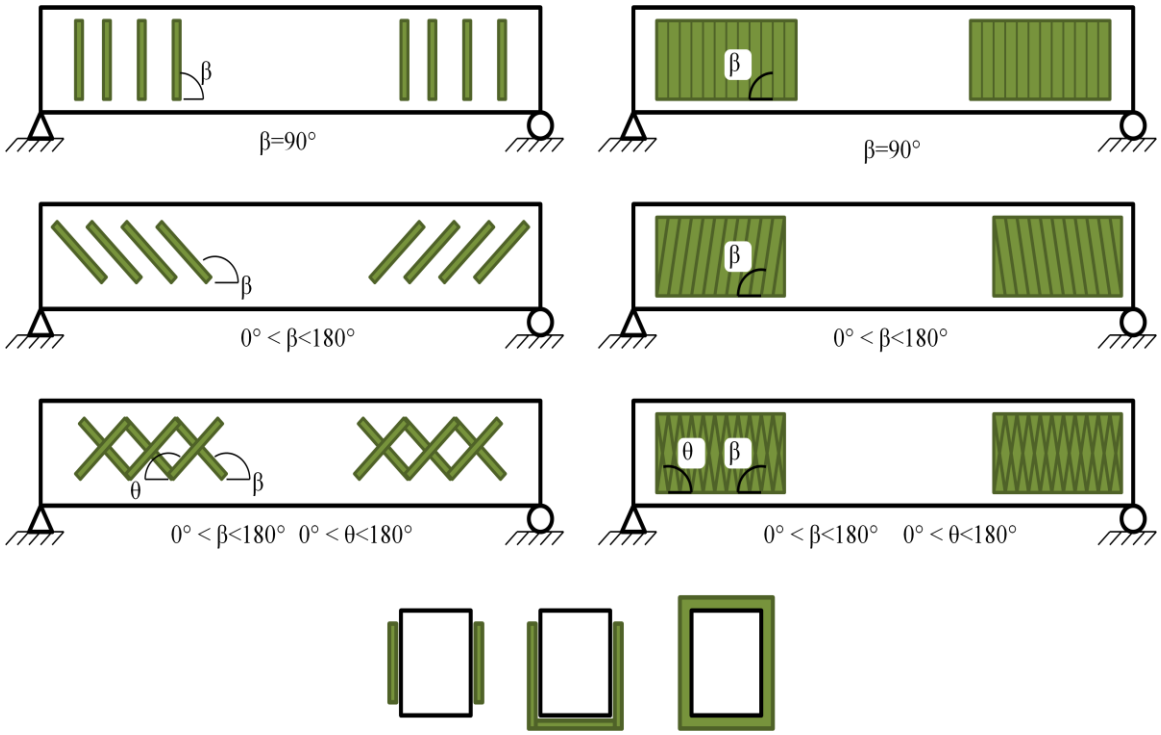

Figure 11. Common shear strengthening schemes

Observe that the FRP composite materials can be placed solely on the sides of the beam, called *side plates*, along the sides and bottom, called *U-jackets*, or can encompass the entire beam, called *complete wrapping*. Fiber direction can be oriented at the discretion of the design engineer.

Several failure modes have been indentified (Teng and Cheng, 2009). A majority of the failures of FRP composite patching schemes used to increase moment capacity of beams are attributed to debonding of either the FRP composite or separation of the concrete cover. The failures modes are illustrated in figure 12.

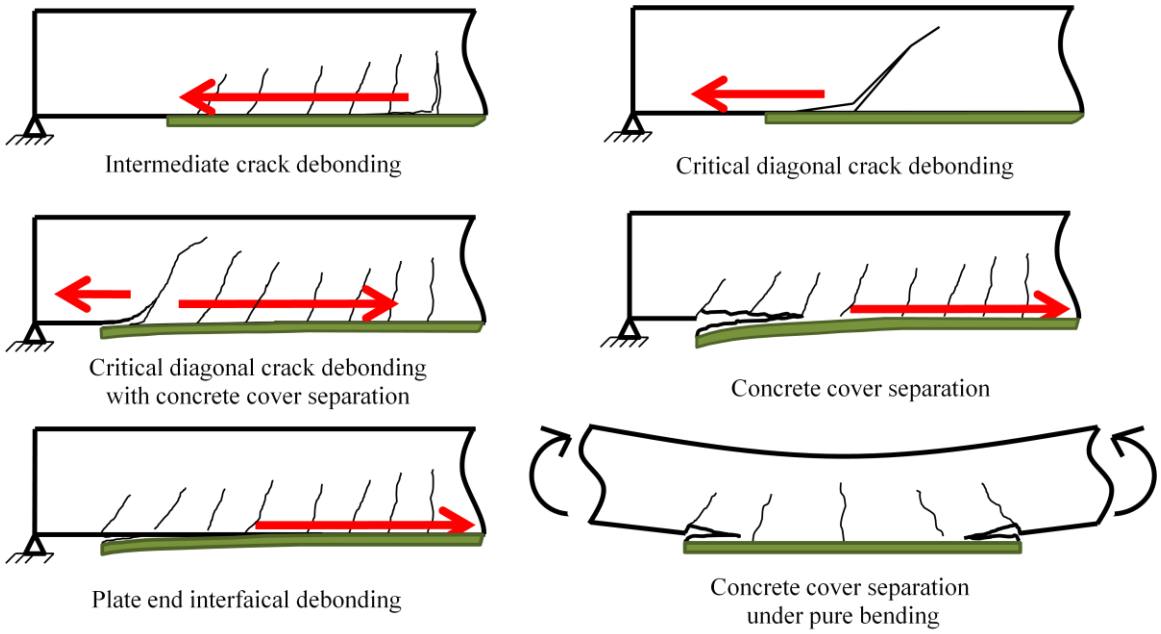

Figure 12. Debonding failure modes

Intermediate crack debonding is caused by flexural cracking. The crack creates local debonding at its origin. As loading increases, debonding travels toward the end of the patch; effectively separating the composite from the substrate. Intermediate crack debonding is a common failure of shallow beams with externally bonded composites. Concrete cover separation is caused by crack propagation along the length of the primary tensile reinforcement. The failure begins at a crack near the end of the plate and travels along the length of the reinforcing steel. Another failure type is end of plate interfacial debonding. This failure is caused by high shear and normal stresses in the adhesive near

the end of the composite patch. These stresses exceed the adhesive capacity, which is typically the weakest component and cause the FRP composite to debond from the substrate. The debonding tends to travel inward to the center of the beam. This type of failure typically occurs when the FRP composite is significantly narrower than the beam to which it is adhered. If the patch is wide enough, the failure mode is likely to be concrete cover separation. The final type of flexural failure mode is critical diagonal crack debonding. This failure occurs in regions of the beam with high shear stress, low shear reinforcement, and low moment. Shear cracks developing near the end of the composite plate, causing local debonding that propagates toward the end of the composite. If enough reinforcing steel is present in the beam, this failure mode is unlikely to occur. Instead concrete cover separation is probable. Additional failure states include composite fiber rupture and concrete crushing, both are illustrated in figure 13.

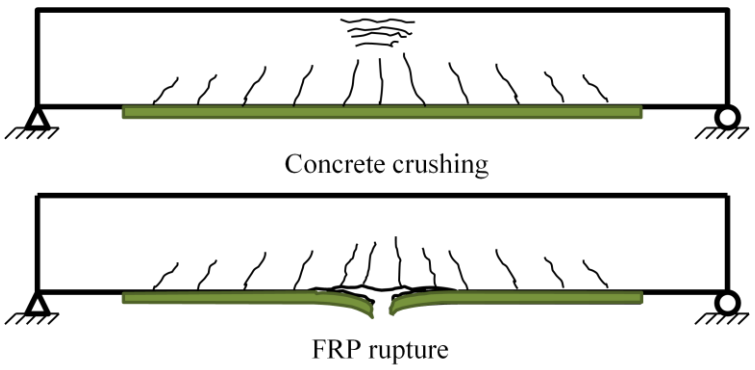

Figure 13. Common flexural failures of beam-FRP composite systems

The most commonly observed failure of composite patch repair systems for increasing the shear capacity of beams are composite fiber rupture and debonding (Teng and Cheng, 2009). FRP rupture typically occurs when the beam specimen is completely

wrapped with composite strips. U-jackets and side plates generally debond from the substrate due to induced shear stresses exceeding the adhesive capacity.

Great effort has been put forth to understand debonding failures, approaching the subject experimentally, mechanistically, and numerically. Given the wealth of tools available to study the mechanical and physical properties, stress and strain behavior, and failure phenomenon of composite adhesives, numerous equations and mathematical models have been developed. One researcher in particular, Teng, has focused attention on deriving empirical formulas to describe bond behavior and stress distributions, reproduced below in its entirety (Teng and Cheng, 2009).

$$\sigma_p = \alpha\beta_W\beta_L\sqrt{\frac{E_{FRP}\sqrt{f_c'}}{t_{FRP}}} \tag{2}$$

$$\beta_W = \sqrt{\frac{2-\frac{b_{FRP}}{b_c}}{1+\frac{b_{FRP}}{b_c}}} \tag{3}$$

$$\beta_L = \begin{cases} 1 \text{ if } L \geq L_e \\ \sin\left(\frac{\pi L}{2L_e}\right) \text{ if } L > L_e \end{cases} \tag{4}$$

$$L_e = \sqrt{\frac{E_{FRP}t_{FRP}}{\sqrt{f_c'}}} \tag{5}$$

The bond-slip relationship was also derived, as shown below.

$$\tau = \tau_{max}\frac{s}{s_o} \text{ if } s \leq s_o \tag{6}$$

$$\tau = \tau_{max}\frac{s_f - s}{s_f - s_o} \text{ if } s_o < s \leq s_f \quad (7)$$

$$\tau = 0 \text{ if } s > s_f \quad (8)$$

where; $s_f = \frac{2G_f}{\tau_{max}}$

$s_o = 0.0195\beta_W f_t$

$\tau_{max} = 1.5\beta_W f_t$

$G_f = 0.308\beta_W^2\sqrt{f_t}$

Another model which describes the stress distribution of composite patching is derived from a strength approach (Colombi et al., 2006; Taljsten, 1997). The model is base on the application of linear, elastic mechanics to the interface of the composite patch and the substrate. The model requires several assumptions, including:

- Each component exhibits elastic stress-strain relationships
- A perfect bond exists between the substrate and composite section
- The adhesive layer is considered thin, so that stress does not vary across the thickness
- The bending stiffness of the beam is much greater than that of the FRP patch

The bending resistance of the composite patch and normal interfacial stresses in the bonding zone are ignored. The bond-slip relationship between the substrate and composite patch is modeled with equation 9 and the tensile stress distribution of the composite is given by equation 10.

$$\tau(x) = \frac{G_a P}{2 t_a E_s W_s}\left(\frac{a\lambda e^{-\lambda x} + 1}{\lambda^2}\right) \quad (9)$$

$$\sigma_c(x) = \frac{b_p G_a P}{2 t_a A_c E_s W_s}\frac{x + a\left(1 - e^{-\lambda x}\right)}{\lambda^2} \quad (10)$$

$$\text{where, } \lambda^2 = \frac{G_a b_p}{s}\left(\frac{1}{E_c A_c} + \frac{1}{E_s A_s} + \frac{h}{2 E_s A_s}\right)$$

Another viable model for the stress distribution of the composite patch is based on the transformed section (Colombi et al., 2006; Moy et al. 2002). This model is suitable for steel beams and is defined in equation 11. The required assumptions of the model include:

- Each component exhibits elastic stress-strain relationships
- A perfect bond exists between the substrate and composite section
- Plane sections remain plane during bending

$$\sigma_c(x) = m\frac{P(x + a)}{2I}y \quad (11)$$

$$\text{where, } y = \frac{.5 A_s h}{A_s + \left(\frac{E_c}{E_s}\right)}$$

$$I = I_s + A_s(.5h - y)^2 + \left(\frac{E_c}{E_s}\right) A_c y^2$$

The last two models were verified using experimental data from steel beams with composite patches (Colombi et al., 2006).

The development of powerful numerical tools, notably commercial finite element software, has allowed the researchers to perform realistic parametric studies of various substrates post-strengthened with FRP composite patches. Some studies simply provide confirmation of other analytical models. Such investigations have corroborated the models proposed above by equations 9, 10, and 11 (Colombi et al., 2006). These confirmations serve to build confidence in models, thereby increasing the popularity of the models among researchers and engineers.

Other finite element analysis studies explore unknown details of various substrates repaired with FRP composites. One study seeks to find the effects of composite patching of steel members with fatigue cracking (Colombi, 2003). The researchers utilized experiments performed on steel plates with notched holes which are retrofitted with composite strips, as shown in figure 14. The motivation of the study was to perform a parametric study including the effects of patch stiffness, adhesive thickness, composite prestressing, and area of debonding on the stress intensity factor were analyzed. Plane stress condition is assumed for the region located near the crack tip.

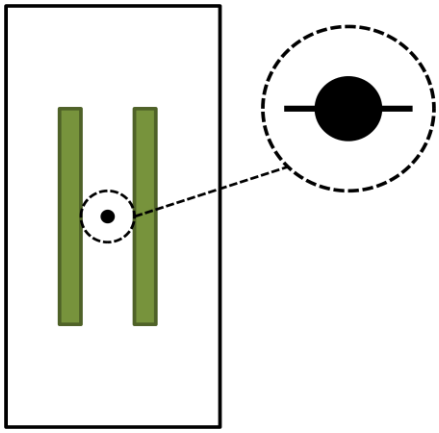

Figure 14. Notched hole steel plate specimen reinforced with FRP laminates

The results of the finite element modeling are intuitive. Composite reinforcing reduces the stress intensity factors regardless of crack size. As the modulus of elasticity of the laminate increases, the stress intensity factor is found to decrease. FRP strips without prestressed fibers were more effective at strengthening plates with long cracks as opposed to shorter cracks. For short cracks, the reduction of stress field intensity is insignificant. Since the relative stiffness of the steel plate is higher than the composite material, the stress range does not alter in the presence of composite patches. The most effective use of composite patching occurs when the fatigue crack reaches the outer edge of the laminated FRP patch. This is expected if the patch covers a large portion of the crack and plastic zone.

Prestressing the fibers causes no reduction in stress intensity factors, but does promote crack closure. An increase in composite thickness will reduce crack stress intensity values. Increasing the thickness of the adhesive will also decrease stress intensity values. An increase in adhesive thickness allows for more shear deformation in that region. Finally, increasing the debonded area resulted in a decrease of stress intensity values. The largest debonded area is defined as a ratio of one to two; meaning that the length of the major axis is twice as long as the length of the minor axis. This largest value still results in a stress intensity value that is less than those of the steel plate alone (Colombi, 2003).

Current research explores correct modeling of debonding failure. Teng and Chen have developed a model which incorporates any combination of moments and shear forces with an interaction curve between plate end moments and shear force (Teng and Cheng, 2009). This curve is given by equation 12.

$$\left(\frac{V_{db,end}}{V_{db,s}}\right)^2 + \left(\frac{M_{db,end}}{M_{db,f}}\right)^2 = 1 \qquad (12)$$

These relationships are expounded by equations 13 and 14.

$$M_{db,end} = \frac{0.488\, M_{u,0}}{(\alpha_{flex}\alpha_{axial}\alpha_W)^{\frac{1}{9}}} \leq M_{u,0} \qquad (13)$$

$$\text{where, } \alpha_{flex} = \frac{\left[(EI)_{c,FRP} - (EI)_{c,0}\right]}{\left[(EI)_{c,0}\right]}$$

$$\alpha_{axial} = \frac{E_{FRP}t_{FRP}}{(E_c d)}$$

$$\alpha_W = \frac{b_c}{b_{FRP}} \leq 3$$

$$V_{db,s} = V_c + \varepsilon_{v,e}\overline{V}_s \qquad (14)$$

$$\text{where, } \overline{V}_s = A_{sv}E_{sv}\frac{d_e}{s_v}$$

$$\varepsilon_{v,e} = \frac{10}{\sqrt{\alpha_{flex}\alpha_E\alpha_t\alpha_W}}$$

$$\alpha_E = \frac{E_{FRP}}{E_c}$$

$$\alpha_t = \left(\frac{t_{FRP}}{d}\right)^{1.3}$$

Intermediate debonding stress is modeled by equation 15. The equation was developed by extensive finite element modeling (Lu et al., 2007).

$$\tau_{dbic} = 0.114(4.41 - \alpha)\tau_{max}\sqrt{\frac{E_{FRP}}{t_{FRP}}} \quad (15)$$

where, $\tau_{max} = 1.5\beta_w f_t$

$$\alpha = 3.41\frac{L_{ee}}{L_d}$$

$$L_{ee} = 0.228\sqrt{E_{FRP}f_{FRP}}$$

For shear FRP applications, the debonding stress distribution is non-uniform (Teng and Cheng, 2009). This is because the FRP composite has varying bond lengths in relationship to the size and orientation of shear cracks. A representation of the effective stress distribution, $f_{FRP,e}$, is given by equation 16.

$$f_{FRP,e} = D_{FRP}\sigma_{FRP,max} \quad (16)$$

where, $\sigma_{FRP,max} = \min\left\{\begin{matrix} f_{FRP} \\ \alpha\beta_w\beta_L\sqrt{\frac{E_{FRP}}{t_{FRP}}\sqrt{f'_c}} \end{matrix}\right\}$

$$D_{FRP} = \begin{cases} \frac{2}{\pi\lambda}\frac{1-\cos\left(\frac{\pi\lambda}{2}\right)}{\sin\left(\frac{\pi\lambda}{2}\right)} & \text{if } \lambda \le 1 \\ 1 - \frac{\pi - 2}{\pi\lambda} & \text{if } \lambda > 1 \end{cases}$$

$$\alpha = 0.427$$

$$\beta_w = \begin{cases} 1 & \text{if } \lambda \le 1 \\ \sin\left(\frac{\pi\lambda}{2}\right) & \text{if } \lambda > 1 \end{cases}$$

$$\beta_L = \sqrt{\frac{2 - \left(\frac{w_{FRP}}{s_{FRP}\sin(\beta)}\right)}{1 + \left(\frac{w_{FRP}}{s_{FRP}\sin(\beta)}\right)}} \ge \frac{\sqrt{2}}{2}$$

$$\lambda = \frac{L_{max}}{L_e}$$

$$L_{max} = \left\{ \begin{matrix} \frac{f_{FRP,e}}{\sin(\beta)} \text{ for U} - \text{jackets} \\ \frac{h_{FRP,e}}{2\sin(\beta)} \text{ for side plates} \end{matrix} \right\}$$

Some research has been performed to estimate the deflections of FRP composite repaired beams. This research is helpful to predict serviceability requirements of the code and also in the prediction of composite patched beams before failure. One pertinent research effort utilized the energy variation method to calculate the deflection of reinforced concrete beams retrofitted with FRP composite material (Gorji, 2009).

Utilizing the principle of conservation of energy, equation 17 was derived. The basic assumption is that the beam material properties do not vary along the length of the beam and that the composite patch runs the full span of the beam. Assuming a parabolic variation, equation 17 yields equation 18; this is the displacement expression for the beam.

$$Q = \frac{1}{2}\int_0^l E_c A_c (u_c')^2 dx + \frac{1}{2}\int_0^l E_{s1} A_{s2} (u_{s1}')^2 dx + \frac{1}{2}\int_0^l E_{s2} A_{s2} (u_{s2}')^2 dx + \frac{1}{2}\int_0^l E_f A_f (u_f')^2 dx - \int_0^l q(x) Y(x) dx \qquad (17)$$

$$Y = \frac{q[l^2 x(l-x) + x^2(l-x)^2]}{24 d_1^2 (E_c A_c z_1^2 + E_{s1} A_{s1} + E_{s2} A_{s2} z_2^2 + E_f A_f z_3^2)} \qquad (18)$$

Current research has left much to be desired by engineers. Despite significant gains in knowledge, FRP reinforcing systems for civil engineering application are

commonly designed and implemented by the companies which manufacture them. The cause for this lies in the unique nature of FRP laminates and respective adhesives. There is an urgent need to standardize FRP composite materials, including adhesive, in a way which promotes practicing civil engineers to confidently design FRP composite repairs of bridge superstructures or building frames.

Such efforts are underway and are necessary to break the ties that allow manufacturers to monopolize the design and application of composite systems. One distinct effort in this direction is to standardize FRP composite materials testing. Some researchers have made headway towards having a recognized ASTM standard for characterizing FRP materials specifically for civil engineering applications (Bank, 2003). Currently, the practice is to use existing general ASTM standards to test the composite materials. Such tests do not directly reflect the nature of civil engineering uses of FRP composites; including long term material and mechanical properties or the composite response to environmental or corrosive attacks.

Another area in need of urgent attention is the long-term behavior of the FRP composite systems. Work conducted by Diab and Wu investigated the effects of aging on FRP systems, the results of which point to a need for additional and intense research (2008). The research conducted included both experimental and numerical explorations. A finite element model, with a precisely programmed aging parameter, closely related the results of experimental studies of long term behavior of FRP composites. The researchers found that the length necessary to properly develop the required strength significantly increases over time, almost 45% over 1500 days. Given this drastic

weakening of the adhesive, the researchers simply concluded further tests and analysis are necessary (Diab and Wu, 2008).

Another area of interest that needs to be further explored is the application of more than one ply of FRP composite reinforcing. Adding plies of composite fibers create a host of stress concentrations which have yet to be accurately mapped reliably (Hart-Smith, 1995). Researchers and industry scientists in the aerospace industry lead the effort of properly examining multi-ply composite systems and the use of tapering the ends of added plies (Soutis and Hu, 1997). Efforts to incorporate multi-ply and tapered composite systems into composite repair schemes of civil engineering structures have begun (Gao et al, 2006). Such efforts have only concluded that using more than one ply increases the capacity of beams and that an ideal taper length and placement can be identified.

Though not necessary to design composite repairs of beams, it would also be beneficial for engineers if the composite manufactures would dissect the relationship between fibrous material and adhesives. Engineers can only choose adhesives deemed consistent with an individual FRP material. Instead, engineers should have the freedom to decide which composite fiber materials and adhesives are best suited for a particular civil engineering application.

Ideally, civil engineers should be capable of designing FRP reinforcing systems without relying on the expertise of the composite manufacturer. In order for this goal to be realized, engineers must have standardized material information, verified and safe design equations, and information about the long term behavior of structures repaired with FRP composites.

Review of Current Practice and Design Guidelines

It is not uncommon to find a significant time delay between academic research and field practice. There are established engineering code provisions for repairing steel and concrete bridge superstructures. Only provisional guidelines for repair using FRP composite systems have been written by respected civil engineering associations, namely the National Cooperative Highway Research Program (NCHRP) and the American Concrete Institute (ACI).

AASHTO Guidelines

The American Association of State Highway and Transportation Officials (AASHTO) produced a guide of bridge superstructure repair techniques (Benedetta, 2007). This report encompasses repair of reinforced concrete, steel, prestressed concrete beams, and truss members and joints. Developed methods are intended to restore members suffering from excessive corrosion, impact damaged, overloading, or excessive fatigue loading. Details are presented below.

AASHTO provides several methods to repair reinforced concrete beams with insufficient flexure and/or shear capacity. Several steps are necessary to prepare the substrate and surface. The first step typically is jacking the superstructure to relieve dead-load stresses. Relieving these stresses is always recommended. Jacking is especially helpful for repairs requiring form work. The next step is to clean the defective

area. Blast cleaning the area is an appropriate and common practice. A qualified structural engineer must determine the state of repair. Common solutions include coating exposed rebar with a protective layer of epoxy, applying shotcrete, or constructing formwork repairs. Formed repairs rebuild members with fresh concrete. These repairs are the most common because they are considered to create more permanent repairs.

Shear repairs are typically simpler. Reinforcing steel is added to the structural member. An experienced engineer examines the steel reinforcing details to identify appropriate sites to insert additional shear reinforcing. At suitable sites, holes are drilled at 45 degree angles perpendicular the shear cracks. These holes are filled with epoxy and reinforcing steel rebar is carefully placed in the epoxy.

Prestressed concrete beams pose more complex repair problems. Prestressed beams generally have less concrete covering the steel reinforcement. Repair solutions typically require mechanical devices and novel approaches. Successful repair systems have been implemented by the Departments of Transportation (DOT) in Florida and Pennsylvania. In Florida, DOT engineers used cable splices to reconnect and tension the prestressing steel cables. The splices are secured to the ends of the beam and tightened using threaded couplers. Pennsylvania DOT utilized post tensioning to repair prestressed beams. The post tensioning strands are strewn along the length of the beam and fastened to steel plates attached to either end of the damaged beams. After tightening the new steel cables, forms are assembled along the beams around the steel cables. Concrete is then placed over the cables to secure and protect them.

AASHTO provides multiple solutions for repairing deficient steel members, depending on the extent of damage. Solutions typically involve replacing corroded

sections with sound steel sections. Such sections are removed by sawing or torching, and a new section is welded in place; the replacement steel can be either rolled or fabricated. The new section is typically primed and painted to protect the steel from corrosion.

Impact damaged steel superstructures can be repaired with heat treatments. The deformed section is heated with torches to increase the member flexibility. Once sufficiently heated, the section can be manipulated into its original shape. AASHTO provides several heating patterns which will avoid creating residual stresses and overheating.

The allowable bridge repair techniques detailed by AASHTO have several limitations, including high costs and is labor intensive. However, the civil engineering community is making significant steps to incorporate FRP composite repairs. Following are two series of documents describing recommended FRP composite design and application practices. The first series was developed by NCHRP and the second by ACI.

NCHRP Guidelines

The National Cooperative Highway Research Program has prepared a report with the purpose to exhaustively gather previously conducted research on FRP systems, from which a technically sound design guide is created (Zureick et al., 2010). The report adopts the load and resistance factored design, LFRD, design philosophy. The guide provides the civil engineering community with a design strategy for flexural, shear, torsional, and axial loading.

In the report preamble, a compendium of analytical, experimental, and technical research and reports were collected from domestic and international sources are presented in an attempt to provide the most recent and pertinent information. Despite the large amount of experimental work, additional experiments were conducted and the resulting data was considered. *AASHTO LFRD Bridge Design Specifications* load combinations are used not only to expedite the field application of the design criteria developed but to also build confidence in the design procedure.

LFRD designs are based on statistical considerations. These methods are used to describe variability in loads and material properties. The methods also provide useful failure criteria. An excellent example of the importance of statistical methods is defining the mechanical properties of some materials; the more variable the strength of the material, the higher the acceptable nominal strength must be. The report describes all the statistical variables representing loading combinations and material strengths. The physical and mechanical properties of the FRP systems manufactured in a factory setting will differ greatly from those created in the field. Factory cured FRP systems typically have greater strength than those installed on the job site. Additionally, controlled environment cured FRP composites have significantly less variability. This difference is critical in civil engineering application, where most FRP systems will be assembled in the field. The tensile strength of the FRP materials was characterized with a two-parameter Weibull distribution.

Pre-manufactured systems are typically shells, plates, and strips and other precured FRP laminates. Field assembled FRP systems typically require fibers to be impregnated with resin; either by hand or with transportable impregnators. Because of

the unique nature of FRP systems, machine impregnators are specific to the fibers and resin type. Field assembled composite systems have greater variability than those manufactured in a controlled setting. Consequently the nominal strengths of each system are significantly different. One advantage of field assembled systems is that they are generally better suited for complex structures that include multiple types of substrate materials or complex substrate geometry.

Additional statistical considerations of the design philosophy include modeling error and establishing a probability index for the mechanical properties. Error is inherent when describing the physical world. In mathematical modeling of a well understood mechanical phenomenon, the error between the model and the true behavior is relatively negligible. Error increases when more assumptions are necessary to model a natural phenomenon. This error is accounted for in the report and the LFRD factors. The probability index is a measure of the likelihood of an event happening and is the standard variable of a normal distribution. The index, β, for the FRP design is 3.5. This value corresponds to a probability of .00023. This means that the probability of a failure event is assigned a low value.

A significant advantage of the LFRD design philosophy is the use of load and resistance factors. These factors create a rational and safe design while providing economical sections. Instead of recalculating the current LFRD factors, an additional FRP specific factor is calculated and incorporated. This factor is applicable only to FRP values. The resistance factors are calculated using adjusted AASHTO or ACI equations. A series of data was generated using Monte Carlo simulations. The nominal strengths of the FRP material are described using a Weibull distribution. The resistance factors

correspond to the failure probability defined by the probability index. A limit state of the design philosophy requires that each structural member must have some residual capacity before FRP application.

The guide concentrates on the analytical equations representing the mechanical behavior of FRP systems. Failure of any structural component of a member is considered as a limit state of the design. The three failure states considered in flexural bending are concrete crushing, debonding of the FPR material at locations of flexural cracks, and peeling of FRP reinforcement at its end. Each failure state has been observed in repeatable and verifiable research. Concrete crushing is the first failure state and is well understood.

The second failure mode is FRP laminate debonding at flexural cracks. This common failure mode was observed by several researchers and described above. Since fiber strain is an excellent indicator of debonding, the report uses fiber strain as a limit state of design. After examining the data of several experiments, it was determined that debonding failure happens between fiber strains of 0.003 to 0.008. The design equations suggested by the guide use a maximum allowable tensile fiber strain of 0.005. At this value, the strain experienced by concrete may not reach the conventional value of 0.003 commonly assumed in reinforced concrete beam design. Consequently a nonlinear model is adopted to describe the stress-strain nature of concrete. This relationship is explored later in this section.

The third and last failure mode, FRP peeling, occurs when the FRP composite end is subject to combined flexural and shear loading. This type of failure has several mechanisms: critical diagonal crack debonding with or without concrete cover separation,

concrete cover separation, and plate end interfacial debonding. These failures modes were discussed earlier. Critical diagonal crack debonding occurs in areas of high shear stresses, low steel shear reinforcement, and shear cracks. Shear cracks travel toward the end of the FRP laminate, effectively debonding it from the substrate. Critical diagonal crack debonding is restricted when the flexural strength of the beam is less than the shear capacity. Concrete cover separation arises when shear reinforcement is high, causing small cracks to develop near the end of the laminate. The high stress concentrations propagate cracks along the longitudinal steel. Plate debonding occurs when normal and interfacial shear stresses are higher than the strength of the weakest component of the system. The surface of the concrete is typically that weakest component. The FRP laminate will peel away from the surface, beginning at the end of the composite and moving inward until the separating stresses are inadequate to continue the debonding. Typically, this kind of failure mode happens when the FRP laminate width is significantly narrower than the width of the substrate.

The guide assumes the beam will contain adequate shear strength, which will prevent critical diagonal cracking. The other failure modes are mathematically described. A peeling stress model was chosen from previous analytical research and normalized with respect to interfacial stress transfer strength to form equation 19; where f_c' is in units of ksi. This equation is stated to be conservative.

$$\tau_{int} = 0.065\sqrt{f_c'} \qquad (19)$$

Shear failure modes include FRP laminate debonding before or after steel yielding, FRP fibers fracture following steel yielding, and diagonal concrete crushing.

The likelihood of steel yielding in combination with composite debonding is dependent on the amount of steel shear reinforcement. FRP fracture is unlikely since the fracture strength of the fibers is incredibly higher than resin strength. Diagonal concrete crushing can be avoided if the shear enforcement is limited, either in steel stirrups or FRP laminates.

The guide specifies several methods for providing FRP shear reinforcement. The techniques proposed are introduced in the research literature review but are explored in more depth here. The first of these is side bonding; which constitutes placing composite laminates on either side of the beam. This is the least effective method due to early laminate debonding from shear. The second application is U-jacketing. This solution provides FRP composites in the form of a "U", supplying reinforcement on both sides and beneath the structural member. This is the most common reinforcement and typically fails because of debonding. The third reinforcement type is U-jacketing with anchorage provided at the top of each "U" to help prevent premature debonding there. Completely wrapping the structural member is the last procedure. This method is rarely practical for beams, but provides the ultimate support, taking full advantage of the FRP composite capacity.

The guide proceeds further with exploring axial failure modes and FRP solutions. Conclusions, implementations, and recommendations bring the report to a close. The design equations are in the appendices, a section each for flexural design, shear, torsional, and axial design. The flexural design begins with a series of assumptions, including:

- The distribution of strains over the depth of the beam is linear

- Force equilibrium is satisfied
- Strain compatibility is satisfied
- The bond between the FRP composite and the substrate is perfect
- The tension strength of concrete is ignored
- Reinforcing steel behaves as elastic perfectly plastic
- The maximum strain of concrete is 0.003
- The maximum strain at the FRP/concrete interface is 0.005

When the concrete strain is below 0.003 under force equilibrium, the concrete compression stress distribution is modeled as a parabola described by equations 20 and 21.

$$f_c = \frac{2(.9f_c')\left(\varepsilon_c/\varepsilon_o\right)}{1+\left(\varepsilon_c/\varepsilon_o\right)^2} \qquad (20)$$

$$\varepsilon_o = 1.71\frac{f_c'}{E_c} \qquad (21)$$

The fatigue limit states define the concrete, steel, and FRP composite strain according to equations 22, 23, and 24. Limiting the strains to these values is considered to prevent fatigue failures. The variable η depends on the type of fiber. This value is 0.8, 0.5, and 0.3 for carbon, aramid, and glass fibers respectively.

$$\varepsilon_c \leq \frac{f_c'}{E_c} \qquad (22)$$

$$\varepsilon_s \leq 0.8\varepsilon_y \tag{23}$$

$$\varepsilon_{FRP} \leq \eta\varepsilon_{FRP}^{u} \tag{24}$$

The strength limit state for a rectangular reinforced concrete section is given by equation 25. The development length is given by equation 26.

$$M_r = 0.9[A_s f_s(d_s - k_2 c) + A'_s f'_s(k_2 c - d'_s)] + \phi_{FRP} T_{FRP}(h - k_2 c) \tag{25}$$

$$\text{where, } T_{FRP} = b_{FRP} N_b$$

$$\beta_2 = \frac{\ln\left(1 + \left(\varepsilon_c/\varepsilon_o\right)^2\right)}{\left(\varepsilon_c/\varepsilon_o\right)}$$

$$k_2 = 1 - \frac{2\left[\left(\varepsilon_c/\varepsilon_o\right) - \arctan\left(\varepsilon_c/\varepsilon_o\right)\right]}{\beta_2\left(\varepsilon_c/\varepsilon_o\right)^2}$$

$$L_d \geq \frac{T_{FRP}}{\tau_{int} b_{FRP}} \tag{26}$$

$$\text{where, } \tau_{int} = 0.065\sqrt{f'_c}$$

T_{FRP} is the FRP tensile reinforcement corresponding to an FRP strain of 0.005.

The reinforcement end peeling can be avoided if the peeling stress is limited, as described by equation 27. The peeling stress is given by equation 28.

$$\tau_{peeling} = 0.065\sqrt{f'_c} \tag{27}$$

$$f_{peel} = \tau_{av}\left[\left(\frac{3E_a}{E_{FRP}}\right)\frac{t_{FRP}}{t_a}\right]^{\left(\frac{1}{4}\right)} \tag{28}$$

$$\text{where, } \tau_{av} = \left[V_u + \left(\frac{G_a}{T_{FRP} t_{FRP} t_a} \right)^{\left(\frac{1}{2}\right)} M_u \right] \left(\frac{t_{FRP}(h-y)}{I_T} \right)$$

The shear capacity of a beam post strengthened with FRP composites is given by equation 29. ϕ_{FRP} is given in table 1.

$$V_r = 0.9\left(V_c + V_s + V_p\right) + \phi_{FRP} V_{FRP} \qquad (29)$$

Table 1. Reduction factor for FRP composite shear reinforcement

FRP shear application	Reduction Factor, ϕ_{FRP}
complete wrapping	0.65
U-jackets	0.55
U-jackets with Anchorage	0.60
Side plates	0.40

The shear strength of FRP composite reinforcement is given by equation 30 for intermittent reinforcing strips or equation 31 for a single continuous FRP reinforcement.

$$V_s = N_{FRP}^e d_{FRP} (\sin(\alpha) + \cos(\alpha)) \frac{w_{FRP}}{s_v} \qquad (30)$$

$$V_s = N_{FRP}^e (\sin(\alpha) + \cos(\alpha)) d_{FRP} \qquad (31)$$

The appendices of the guide are very helpful because it includes the equations above with commentary as well as example design problems.

The NCHRP created an additional report specific to the construction process of retrofitting concrete structures with carbon FRP composites (Mirmiran at al., 2004). The report addresses the care and precautions that must be taken in handling, storing, mixing,

applying, and curing of FRP materials. In addition, the document provides engineers and contractors with constructions specifications and insight into quality control and assurance of FRP applications. FRP manufactures often provide contractors with construction quality control measures, typically sending company representatives to job sites. This creates a dependency of engineers and contractors on FRP manufacturers. This report and others like it will serve to free the civil engineering community from that dependency.

Each FRP system, and the associated technologies, is unique. It is recommended that each retrofit job be planned well in advance in order to ensure that any unique equipment can be acquired and contractors and technicians can be properly trained. It is also recommended that each individual job be thoughtfully designed and discussed with the FRP manufacture or supplier.

Two important issues addressed in the report are FRP material handling and storage and worker safety. FRP materials are typically sensitive to shelf-time, humidity, and temperature. Engineers and technicians should be aware of storage and handling requirements prescribed by the manufactures. Most FRP resins and adhesives have specific shelf lives which are often dependent on temperature and humidity. Most adhesives are provided in two separate components, one is a resin and the other a hardening or curing agent. Adhesives must be correctly mixed; which may be proportioned by weight, volume, or in pre-measured batch amounts. Specific mixing speeds and durations should be strictly implemented to ensure the desired adhesive performance. Mixed resins and epoxies have limited pot lives, after which they become less effective and more difficult to work with. FRP materials are typically manufactured

in rolls. Care must be taken by technicians not to bend or fold the fiber material because this may cause damage and reduce composite capacity.

Each component of FRP systems is hazardous to some degree. The report suggests that appropriate Occupational Safety and Health Administration, OSHA, regulations be followed to ensure a healthy and safe workplace.

Proper installation is vital to the performance and durability of FRP composite systems. Substrate condition is critical to FRP performance. The type and extent of damage to the concrete and steel reinforcement must be considered first. The NCHRP report suggests the next field procedure is to create a suitable surface for the FRP composite to adhere. Concrete structural members must be cleaned to stringent requirements. Cleaning includes removing faulty concrete, replacing corroded reinforcing steel, renovating defective concrete, and preparing the final surface. Loose pieces of cement and aggregate should be removed and any concrete spalling or honeycombing repaired. Damage from corrosion or impact must be eliminated until only sound concrete remains. The entire substrate repair must be properly formed, placed, and waterproofed for the FRP application to be effective. Substrate repair may require sandblasting, power washing, epoxy or grout injection, and formwork. Correct surface preparation is critical to realize the desired FRP bond strength.

The guideline divides FRP systems into two categories; bond-critical and contact-critical. FRP repairs are bond critical if the bond between the structure and the composite laminate is the mechanism to transfer load. This type of application can be utilized for post strengthening of walls, slabs, beams, or columns. Composite action transferred by

physical contact of the FRP and substrate is considered contact-critical repairs. This type of bond is utilized to repair columns.

As stated before, FRP systems are applied by three methods; wet lay-ups, dry lay-ups, and near surface mounted. Near surface mounted FRP systems involve inserting FRP rods or strips into grooves cut into the structural member and is discussed in the research literature review. Wet lay-ups and precurred systems involve applying fibers or cured fiber laminates to substrates using adhesives. For applying epoxy to the surface, air voids must be removed, leaving a smooth layer of even thickness. Fibers should be correctly applied; incorrect fiber orientation will negatively affect the performance of the composite system. Lastly, the report suggests limiting FRP prestressing to no more than fifty percent of the ultimate strain. This limitation ensures conservatism.

As stated in the goals of the report, quality assurance is important to ensure effective FRP strengthening. Quality assurance begins with establishing the role and responsibilities of an inspector. State and Federal transportation departments should create a metric of satisfaction and identify items of inspection, including keeping detailed records and acquiring samples. FRP components need to be inspected as well as substrates and surface preparation, fiber orientation, epoxy and resin cure, final laminate thickness, and final glueline thickness. Recorded items should include environmental conditions, crack widths, surface profiles, batch numbers, mixing ratios and times. Observations should be quantitative and qualitative, noting the colors, consistencies, and appearances of the various FRP system components. Special care should be taken to note any debonding or delamination which may occur after the removal of jacking. The guide also points to a number of tests that may lead to understanding the state of the final

system, such as acoustic tap testing, core sampling, and direct pull-off tests. As a reference, the report supplies a table of applicable ASTM tests which are pertinent to assuring an effective and sound FRP composite repair system.

The report concludes by suggesting that proper installation by contractors should be an explicit contractual item. Quality control and assurance measures should be included in contractual obligations.

ACI Guidelines

There are distinct differences between the suggested design and application principles recommended by NCHRP and ACI. The differences that are most noticeable are found in the equations which drive the design of the FRP composite materials.

The ACI guide begins with general information, notation, and material overview (Busel, 2008). The guide was assembled from over 25 years of research into the performance of externally applied FRP composite systems. The research included analytical models, experimental studies, and long-term field applications. This conglomeration of research results in a detailed guide of construction and design practices for FRP composites externally bonded to concrete structures.

The guide explains that all FRP designs and applications begin with investigation of an existing member. A licensed engineer should, at a minimum, investigate the following items:

- Dimensions of existing structural members

- Location, size, and source of cracking and spalling
- Location and extent of steel reinforcement corrosion
- Location and quantity of steel reinforcement
- Incidence of active corrosion
- Strength of concrete
- The degree of soundness of concrete, especially concrete cover

The in-place capacity of the structural member should be calculated given this field inspection information. The licensed engineer should determine the scope and necessity of post strengthening, which is required by the desired service capacity. As a design philosophy, the guide adopts limits to post-strengthening structural members with FRP retrofitting systems. In the event of FRP loss, the existing member should not also fail at the same time.

An entire chapter of the guide is dedicated to the FRP materials. The first section revolves around resin materials; which includes putties, primers, saturating resins, epoxy adhesives, fibers, and protective coatings. There is a wide range of commercially available resin materials. FRP resins typically have the following qualities:

- Compatibility with concrete and FRP materials
- Resistant to many environmental factors, specifically moisture, salt water, extreme temperatures, and chemicals common to exposed concrete
- Ability to fill voids
- Workability

- Useful pot life
- Development of mechanical properties

Putties are used to fill holes in the substrate in order to achieve the required substrate profiles. Primers are used to penetrate concrete surfaces and provide an improved bonding surface for the resins or other adhesives. Saturating resins are used to impregnate the reinforcing fibers of the FRP system. The resins also work to fix fibers in place and create a load path to transfer stresses from the original structural member to the composite fibers. Adhesives, different from saturating resins, adhere cured FRP laminates to structural member substrates. Adhesives also create load paths. Protective coatings provide a manner of shielding FRP systems from ultraviolet light, fire, vandalism, impact, abrasion, chemical agents, and general wear.

FRP materials are characterized by physical and mechanical properties, time dependent behavior, and durability. The coefficients of thermal expansion are dependent on fiber type and fraction. The glass transition temperature is the temperature at which the fibers change phase from a hard material to a rubber-like material. This temperature typically ranges from 140° to 180° F. The temperature threshold at which composite fibers begin to degrade varies between fiber materials; for instance, carbon fibers can retain load capacity at temperatures exceeding 1800° F, aramid fibers have a threshold temperature around 350° F, and glass fibers are viable until temperatures around 530° F.

Tensile and compressive behaviors are the prime mechanical properties that characterize a FRP system. The tensile strength and stiffness are dependent upon several factors; including fiber type, orientation, and quantity. Unidirectional fibers loaded in

direct tension behave linear-elastically until rupture failure, which occurs abruptly. Fibers incorrectly oriented will reduce the capacity of the composite system. Composite production methods and conditions also play a role in tensile behavior and stiffness. The capacity reported by manufacturers is the average tensile strength less than three times the standard deviation of at least 20 test specimens. Appropriate methods for testing tensile strength include ASTM D3039, D7205, and ACI 440.3R. These test methods are also used to find the tensile modulus elasticity.

Creep rupture and fatigue are essential time dependent behaviors when considering FRP composites for civil engineering applications. Creep is caused by sustained loading over time. Certain loads have corresponding threshold times, at which the FRP fibers rupture. An increase of the ratio of long-term loading to short-term capacity causes a decrease in the threshold, or endurance, time. The endurance time also decreases under certain severe environmental conditions. Carbon fibers are the most resistant type of fibers to creep, and glass, being amorphous, is the most susceptible. Testing revealed a linear relationship exists between creep-rupture strength and the logarithm of time. Limit states have been developed for creep-rupture loads, under which creep is not a concern. Fatigue investigations by the aerospace industry lend themselves to civil engineering applications. Though the numerical results of such investigations are not applicable to FRP retrofitting of civil structural members, the qualitative observations are.

It is vital for any civil engineering material to be durable; this is no less true for FRP materials. Environmental conditions of high temperature, humidity, and chemical exposure are detrimental to FRP system performance. The mechanical properties

reported by manufacturers do not include the effects of weathering, and so special allowances should be made in the design. Such allowances are discussed in the following sections.

The general design philosophy proposed in the recommendation is similar to the limit states of ACI 318. FRP systems are designed according to the strength and serviceability requirements of ACI 318. Additional factors for the FRP components are incorporated, which produce reliability indexes equal to or above 3.5.

The first limit state imposed by the recommendation is that in the event of FRP failure, the remaining structure should not collapse. This limit state is controlled by equation 32.

$$(\phi R_n)_{existing} \geq (1.1S_{DL} + 0.75S_{LL})_{new} \qquad (32)$$

If the live loads are suspected to be sustained for a substantial amount of time, the live load coefficient should be changed from 0.75 to 1.0.

Environmental limit states are incorporated into the design with an additional set of coefficients. Equations 33and 34 demonstrate the inclusion of environmental factors. The factors are given in table 2.

$$f_{fu} = C_E f_{fu}^* \qquad (33)$$

$$\varepsilon_{fu} = C_E \varepsilon_{fu}^* \qquad (34)$$

$$E_f = \frac{f_{fu}}{\varepsilon_{fu}} \qquad (35)$$

Table 2. Environmental reduction factor C_E

Exposure Conditions	Fiber Type	C_E
Interior	Carbon	0.95
	Glass	0.75
	Aramid	0.85
Exterior	Carbon	0.85
	Glass	0.65
	Aramid	0.75
Aggressive	Carbon	0.85
	Glass	0.5
	Aramid	0.7

Common failure modes for FRP retrofitted structural members include:

- Concrete crushing in compression
- Yielding of steel reinforcement followed by FRP laminate rupture
- Yielding of steel reinforcement followed by concrete crushing
- Shear/torsion delamination of concrete cover
- Debonding of FRP from substrate

Some of these failure modes can be predicted and avoided. Limiting the strain of concrete will avoid concrete crushing and limiting FRP strain below the rupture strain is assumed to prevent FRP rupture. The rupture strain of the FRP composite is given by equation 36.

$$\varepsilon_{fd} = 0.083\sqrt{\frac{f'_c}{nE_f t_f}} \leq 0.9\varepsilon_{fu} \text{ in in.} - \text{lb units} \qquad (36)$$

For design of FRP systems applied to the tension face of reinforced concrete members, the following assumptions are necessary:

- Design calculations are based on member dimensions, internal reinforcing steel arrangement, and material properties of the existing member
- Concrete and reinforcing steel strains are directly proportional to their respective distances from the neutral axis, n
- No slippage occurs between the concrete surface and FRP laminate
- The adhesive layer is so thin that no shear deformation occurs
- The maximum compressive strain of concrete is taken as 0.003
- The tensile strength of concrete is ignored
- The FRP acts linear-elastically until failure

Some of the assumptions reflect the true nature and behavior of externally retrofitted steel reinforced concrete members, while others are included for computational ease. For increasing the strength of a member in flexure, the design engineer ensures that sufficient shear reinforcement is available to resist the increase in shear forces associated with such a flexural increase. Special considerations must be made if the superstructure is not jacked up before placing the FRP system. The strains present in a member not jacked are represented by the variable, ε_{bi}.

Finding the strain of the FRP fibers at ultimate load is important to ensure the rupture limit state stated above. The strain can be found using equation 37. The effective

depth of the FRP composite is not explicitly defined. The stress experienced by FRP composite is given equation 38.

$$\varepsilon_{fe} = \varepsilon_{cu}\left(\frac{d_f - c}{c}\right) - \varepsilon_{bi} \leq \varepsilon_{fd} \tag{37}$$

$$f_{fe} = E_f \varepsilon_{fe} \tag{38}$$

Applying an FRP system increases the stiffness of a member. Reduction factors based on steel strain will help enforce sufficient ductility in the member. This strength reduction factor is given by equation 39.

$$\phi = \left\{ \begin{array}{c} 0.90 \text{ for } \varepsilon_t \geq 0.005 \\ 0.65 + \dfrac{0.25(\varepsilon_t - \varepsilon_{sy})}{0.005 - \varepsilon_{sy}} \text{ for } \varepsilon_{sy} < \varepsilon_t < 0.005 \\ 0.65 \text{ for } \varepsilon_t \leq \varepsilon_{sy} \end{array} \right\} \tag{39}$$

Additional constraints ensure the serviceability requirements of ACI 318. To prevent inelastic deformations, the primary reinforcing steel of a concrete member externally retrofitted with an FRP composite should not be allowed to reach its yielding stress under service loads. This is especially vital for cyclically loaded members. Equation 40 enforces this steel stress limit. Concrete compressive stresses should also be limited under service loads. Equation 41 enforces this serviceability constraint.

$$f_{s,s} \leq 0.8 f_y \tag{40}$$

$$f_{c,s} \leq 0.45 f'_c \tag{41}$$

Limits are imposed on FRP composites to reduce the probability of creep-rupture failures. This failure mode is likely to occur when the member is subject to sustained or cyclic loading. Each fiber type responds to such loading conditions differently, and so different provisions are devised dependent on fiber type. Equation 42 illustrates the conclusion of research of FRP materials under such loading.

$$f_{f,s} = \begin{Bmatrix} 0.2f_{fu} \text{ for glass fibers} \\ 0.3f_{fu} \text{ for aramid fiber} \\ 0.5f5f_{fu} \text{ for carbon fibers} \end{Bmatrix} \quad (42)$$

The ultimate strength of a singly reinforced rectangular section is derived by the guide. The design procedure can be extended to include other beam types. The procedure uses an equivalent stress block to model the nonlinear compressive stress of concrete. The design utilizes force equilibrium and strain compatibility. A neutral axis depth is assumed and later checked. For the assumed neutral axis value, the strains of the FRP composite and reinforcing steel are calculated using equations 43 and 44. From these strain values, the FRP composite and steel stresses are found using equations 45 and 46.

$$\varepsilon_{fe} = (\varepsilon_{cu} = 0.003)\left(\frac{d_f - c}{c}\right) - \varepsilon_{bi} \leq \varepsilon_{fd} \quad (43)$$

$$\varepsilon_{fe} = (\varepsilon_{cu} = 0.003)\left(\frac{d_f - c}{c}\right) - \varepsilon_{bi} \leq \varepsilon_{fd} \quad (44)$$

$$f_{fe} = E_f \varepsilon_{fe} \quad (45)$$

$$f_s = E_s \varepsilon_s \leq f_y \quad (46)$$

Once these values have been determined, the depth of the neutral axis can be directly obtained by using equation 47. α_1 and β_1 are parameters defining the stress block and are found in ACI 318, section 10.2.7.3 (Busel, 2008).

$$c = \frac{A_s f_s + A_f f_{fe}}{\alpha_1 f_c' \beta_1 b} \tag{47}$$

An iterative process yields the true value of the neutral axis, and consequently, other desirable variables. The moment capacity of such a beam is given by equation 48. The resistance factor, $\psi_{f,}$ is usually taken as 0.85.

$$M_n = A_s f_s (d - 0.5\beta_1 c) + \psi_f A_f f_{fe} (d_f - 0.5\beta_1 c) \tag{48}$$

The service stresses of the reinforcing steel and FRP composite material are found using equations 49 and 50. These stresses should be compared to the limit states from above; kd is depth of the neutral axis under service loads.

$$f_{s,s} = \frac{\left[M_s + \varepsilon_{bi} A_f E_f \left(d_f - \frac{kd}{3}\right)\right](d - kd)E_s}{A_s E_s \left(d - \frac{kd}{3}\right)(d - kd) + A_f E_f \left(d_f - \frac{kd}{3}\right)(d_f - kd)} \tag{49}$$

$$f_{f,s} = f_{s,s}\left(\frac{E_f}{E_s}\right)\left[\frac{d_f - kd}{d - kd}\right] - \varepsilon_{bi} E_f \tag{50}$$

The next section focuses on retrofitting prestressed concrete beams. Again, the beam is rectangular and prestressed steel strands alone supply the tensile forces, though

the process is applicable to T and I beams with or without compression and mild steel. Several assumptions are necessary for the design procedure. These include:

- Strain compatibility can be used to find the strain of the composite materials, prestressing strands, and mild steel.
- Additional flexural limits should be considered
- For cases of draped prestressed strands, several sections should be evaluated for limit states
- Any initial strain of the concrete substrate should be calculated and then deducted from the effective strain of the FRP composite

The FRP composite strain is expressed in terms of the concrete strain, which governs the design process. Equation 51 gives the strain of the composite section for a concrete failure controlled design. If the design process is controlled by steel strand rupture, the value of the FRP composite strain is given by equation 52. For grades 270 and 250 ksi strands, ε_{pu} has a value of 0.035. ε_{pi} is given by equation 53.

$$\varepsilon_{fe} = (\varepsilon_{cu} = 0.003)\left(\frac{d_f - c}{c}\right) - \varepsilon_{bi} \leq \varepsilon_{fd} \qquad (51)$$

$$\varepsilon_{fe} = \left(\varepsilon_{pu} - \varepsilon_{pi}\right)\left(\frac{d_f - c}{d_p - c}\right) - \varepsilon_{bi} \leq \varepsilon_{fd} \qquad (52)$$

$$\varepsilon_{pi} = \frac{P_e}{A_p E_p} + \frac{P_e}{A_c E_c}\left(1 + \frac{e^2}{r^2}\right) \qquad (53)$$

The strength reduction factor is given by equation 54.

$$\phi = \left\{ \begin{array}{c} 0.90 \text{ for } \varepsilon_{ps} \geq 0.013 \\ 0.65 + \dfrac{0.25(\varepsilon_{ps} - 0.01)}{0.013 - 0.01} \text{ for } 0.01 < \varepsilon_{ps} < 0.013 \\ 0.65 \text{ for } \varepsilon_{ps} \leq 0.01 \end{array} \right\} \tag{54}$$

Additional limits of the stress of the prestressed steel strands are imposed to avoid excessive deformations. These constraints are expressed in equations 55 and 56.

$$f_{ps,s} \leq 0.82 f_{py} \tag{55}$$

$$f_{ps,s} \leq 0.74 f_{pu} \tag{56}$$

The nominal strength of the prestressed concrete beam with a FRP composite section externally bonded to its tensile face is found in a similar manner as in the case of reinforced concrete beam described above. The neutral axis is assumed and then applied to a series of equations, after which the neutral axis is calculated and the cycle is repeated iteratively until the true solution is found. If FRP composite rupture is the controlling failure mode, equation 57 drives the design. The strain of the prestressing steel is found using equation 58.

$$f_{fe} = E_f \varepsilon_{fe} \tag{57}$$

$$\varepsilon_{ps} = \varepsilon_{pe} + \frac{P_e}{A_c E_c}\left(1 + \frac{e^2}{r^2}\right) + \varepsilon_{pnet} \leq 0.035 \tag{58}$$

The value of ε_{pnet} depends on failure mode; equation 59 should be used if concrete crushing controls and equation 60 should be used if FRP rupture or debonding controls.

$$\varepsilon_{pnet} = 0.003\left(\frac{d_p - c}{d_f - c}\right) \tag{59}$$

$$\varepsilon_{pnet} = (\varepsilon_{fe} - \varepsilon_{bi})\left(\frac{d_p - c}{d_f - c}\right) \tag{60}$$

For typical seven strand low relaxation prestressing strand, the stress-strain curve can be found using the following equations in English units.

For grade 250 ksi steel:

$$f_{ps} = \begin{Bmatrix} 28{,}500\varepsilon_{ps} \text{ for } \varepsilon_{ps} \leq 0.0076 \\ 250 - \dfrac{0.04}{\varepsilon_{ps} - 0.0064} \text{ for } \varepsilon_{ps} > 0.0076 \end{Bmatrix} \tag{61}$$

For grade 270 ksi steel:

$$f_{ps} = \begin{Bmatrix} 28{,}500\varepsilon_{ps} \text{ for } \varepsilon_{ps} \leq 0.0086 \\ 250 - \dfrac{0.04}{\varepsilon_{ps} - 0.007} \text{ for } \varepsilon_{ps} > 0.0086 \end{Bmatrix} \tag{62}$$

Finally, the location of the neutral axis and nominal moment capacity can be calculated using equations 63 and 64.

$$c = \frac{A_p f_{ps} + A_f f_{fe}}{\alpha_1 f'_c \beta_1 b} \tag{63}$$

$$M_n = A_s f_s (d - 0.5\beta_1 c) + \psi_f A_f f_{fe} (d_f - 0.5\beta_1 c) \tag{64}$$

FRP composites are commonly used to provide additional shear capacity. Several common reinforcing schemes include complete wrapping, U-jackets, and side plates. The FRP reduction factor, ψ_f, varies according to the FRP scheme and is shown in table 3.

Table 3. FRP reduction factors for shear application

FRP Shear Application	Reduction Factor, ψ_f
complete wrapping	0.95
U-jackets	0.85
Side plates	0.85

The nominal shear capacity of a concrete member with FRP reinforcing is given by equation 65. V_c and V_s are calculated according to ACI 318. V_f is similar to the equations for V_s of ACI 318 Section 11.5.7.2, where reinforcement orientation and area are taken into consideration. Figure 15 shows a general diagram of FRP shear reinforcement. Equation 66 is used to calculate the shear capacity of the FRP composite.

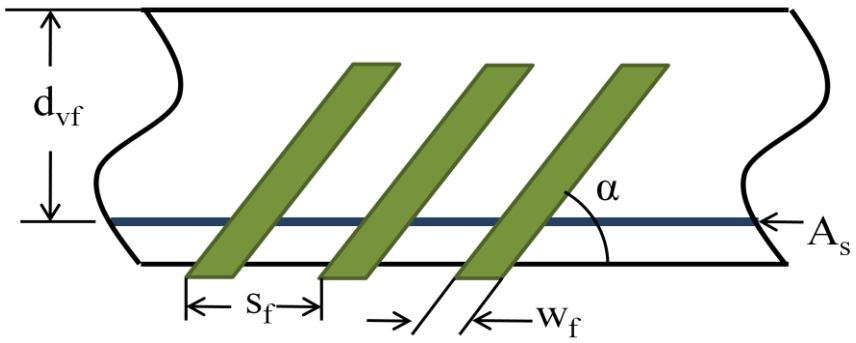

Figure 15. FRP shear reinforcement

$$V_n = (V_c + V_s + \psi_f V_f) \quad (65)$$

$$V_f = A_{fv} f_{fe} (\sin(\alpha) + \cos(\alpha)) \frac{d_{fv}}{s_f} \quad (66)$$

where, $V_f = 2nt_f w_f$

$f_{fe} = \varepsilon_{fe} E_f$

For completely wrapped FRP systems, ε_{fe} is easily calculated using equation 68. For other systems; ε_{fe} is calculated by applying a series of equations expressing active bond length, bond-reduction factors, and modification factors. Equation 69 through 72, are used to calculate ε_{fe} for side plates and U-jackets.

$$E_{fe} = 0.004 \leq 0.75\varepsilon_{fu} \quad (67)$$

$$\varepsilon_{fe} = \kappa_v \varepsilon_{fu} \leq 0.004 \quad (68)$$

$$\kappa_v = \frac{k_1 k_2 L_e}{468\varepsilon_{fu}} \leq 0.75 \quad (69)$$

$$L_e = \frac{2500}{(nt_f E_f)^{0.58}} \quad (70)$$

$$k_1 = \left(\frac{f'_c}{4000}\right)^{\frac{2}{3}} \quad (71)$$

$$k_2 = \begin{cases} \frac{d_{fv} - L_e}{d_{fv}} & \text{for U-wraps} \\ \frac{d_{fv} - 2L_e}{d_{fv}} & \text{for two sides bonded} \end{cases} \quad (72)$$

The methodology used to determine κ_v has been validated for regions of high shear and low moment. FRP shear spacing should follow the limits proposed by ACI 318

for internal shear stirrups. In order to reduce the FRP contributions, equation 73 was developed.

$$V_s + V_f \leq 8\sqrt{f'_c} b_w d \qquad (73)$$

ACI 440.2R has several construction recommendations for FRP applications. FRP materials should be stored according to the manufacturer specifications. Storage of materials should comply with OSHA regulations.

FRP materials are sensitive to handle. Material safety data sheets (MSDS) should be present at all construction sites where FRP materials are located. There are several handling hazards encountered when using thermosetting resins. Such resins include vinyl esters, polyurethane resins, unsaturated polyesters, and epoxies. Hardeners, curing agents, isocyanates, sillers, flexibilizers, and peroxide initiators are used in combination with thermosetting resins. The hazards associated with these chemical compounds include:

- Skin irritations including burns, rashes, and itching
- Skin sensitization, similar to the allergic reaction to poison ivy
- Breathing organic vapors
- Explosion or fire given conditions of chemical concentration and igniter
- Exothermic reactions resulting in fire or personal injury
- Nuisance dust from cutting and grinding FRP materials

Personal protection is the primary concern when handling FRP materials. Disposable gloves are strongly recommended. These gloves should be resistant to FRP resins and any cleaning solvents. Eye protection is also essential and protective shields or glasses should be worn whenever FRP materials are handled. In order to protect against hazardous fumes, dust masks or respirators should be worn whenever organic chemical compounds from resins and other agents are exposed or when dust from cutting fibers is in the air.

The guide stresses many points about FRP system field application: contractor competency, environmental conditions, equipment, substrate repair and preparation, resin mixture, composite application, alignment of fibers, curing of resins, and temporary protection. Any contractor working on FRP systems should have qualified their excellence on the subject, providing evidence of proficiency.

FRP performance can be adversely affected by several environmental conditions at the time of installation; specifically temperature, humidity, and surface moisture. The temperature and moisture of the concrete and FRP materials should be observed and recorded before and during installation. Many FRP components, such as primers, resins, and adhesives, should not be applied in cold or freezing temperatures. Additionally, such components should not be applied if the substrate surface is damp or wet unless stipulated otherwise by the manufacturer. Several FRP systems require specialized equipment, such as resin impregnators, sprayers, winding machines, and devices to position workers. Care should be taken when handling any equipment.

Substrate repair and surface preparation are critical to ensuring a sound FRP retrofitting solution. FRP systems must be applied to sound concrete with properly

prepared surfaces. ACI 546R and ICRI 03730 describe several methods to repair concrete substrates. Improper substrates will compromise FRP performance.

An additional consideration to ensure FRP performance is steel reinforcement corrosion. Such corrosion and its effects must be eliminated. Large cracks should be injected with epoxy. Cracks larger than 0.01 inches should be epoxy injected in accordance with ACI 224.1R, though more stringent constraints can be issued at the discretion of the design engineer. FRP systems which wrap around corners require that those corners be rounded to a minimum radius of 0.5 inches. This fillet prevents stress concentrates from forming in the FRP system. Surface preparation can be undertaken with pressure washing or abrasive methods. Laitance, dirt, dust, oil, filler and curing compounds should be removed from the surface. Small holes and voids should be filled and leveled off to the concrete surface and the entire surface profile should be thoroughly cleaned. The final profile should meet the concrete surface profile (CSP) 3 defined by the ICRI. Out of plane variations should not exceed $^{1}/_{32}$ of an inch.

Correct resin mixing is crucial for FRP performance. Resins should be correctly proportioned and thoroughly mixed. Mixed resins should be quickly applied to avoid exceeding the pot life. Once the pot life is reached, the resin should not be used as the viscosity of the resin increases; its ability to penetrate the concrete surface and impregnate the FRP fibers significantly is reduced.

There are two primary procedures to correctly apply FRP materials to the substrate surfaces. Wet layup systems involve applying dry fibers to substrate by hand with an impregnating resin. The saturating resin is first applied with a uniform thickness to the surface, and the composite fibers are then gently pressed into the resin. Before the

resin begins to cure, any air trapped between the composite and the substrate should be pushed or rolled out. Dry lay-ups usually involve precured FRP laminate, including shells, strips, and grids, and do not require an impregnating resin. Instead, the composites are bonded to the substrate with an epoxy adhesive. The adhesive should be applied to the concrete surface with a uniform thickness, and any trapped air should be expelled. Resins and adhesives are time and temperature dependent. Full curing can take several days under ambient conditions. Fluctuations in temperature will accelerate or retard curing times. Care must be taken to follow the manufacturer prescribed curing conditions and durations.

A plan of inspection, evaluation, and acceptance should be developed to satisfy the metrics of performance. Several inspection criteria need to be investigated, including:

- Date and time of installation
- Ambient temperature, relative humidity, and other weather observations
- Concrete surface temperature
- Concrete surface dryness defined by ACI 503.4
- Surface preparation methods/profile using ICRI guide
- Qualitative description of surface cleanliness
- Heat source types (if applicable)
- Catalog of cracks not injected with epoxy
- Fiber or procured laminate batch identification and location
- Batch identifications, mixing ratios, times, and descriptions of mixed resins

- Observations of cure progression
- Pull-off tests results; bond strength, failure mode, and location
- Locations and size of delaminations or air voids
- Progression of work

Tested properties should include tensile strength, infrared spectrum analysis, glass transition temperature, pot life, and adhesive strength. Resin samples should be taken during FRP installation, which are tested according to ASTM D3418. After completion, the work should be inspected, analyzing changes in color and observing debonding, blistering, cracking, debonding, deflections, or any other anomalies.

The previous design guides have many things in common, but also have distinct differences. For example, NCHRP report 655 bases flexural design on a tensile strain value of 0.005, whereas ACI 440.2R does not. Each system incorporates reduction and safety factors, but is nothing alike in value and sometimes application. The interfacial forces, which often drive design, are described with ambiguous equations which are not intuitive. This ambiguity can lead design engineers to use additional caution.

In order for FRP composite repairs to become a widely used repair option confidence in the system has to be developed to overcome the conservative ethos of the civil engineering community. This requires a clear, simple, and intuitive design and construction approaches. The better the understanding of FRP composite and their application, the more widely they are expected to be implemented. The research presented in this thesis develops intuitive and novel approaches to FRP design. The

concepts that drive the design and safeguard the results are instinctive to structural engineers.

Moreover, the sections designed by the procedure developed in this research effort successfully use significantly less material with complete satisfaction. For instance, the flexural composites are typically adhered to the tensile face and run the length of the structural member. This was obvious from the research reviewed in the last section; and the design guides discussed in this chapter also produce composites which run the length of the beams. The research presented in this manuscript shows that such reinforcing systems tend to waste composite materials. The design procedure developed in this research project is expected to allow design engineers to create economical, safe, and satisfactory FRP composite sections.

Objective and Scope of Study

The present study is focused on localized repair of bridge components using FRP composite laminates. All three types of common bridge materials, namely, reinforced concrete, prestressed concrete, and steel are considered. Localized damage types may be flexure, shear, or material loss due to corrosion in the case of steel components. The investigation identifies common FRP repair materials and studies their performance as patch material under laboratory conditions. Apart from identifying the optimum method to install the composite patches and testing performances through actual load testing, a mechanistic model predicts and verifies the observed performance in the laboratory. These objectives are realized by undertaking the following series of tasks:

1. Investigate FRP composite retrofitting application of in-place, damaged bridge girders.
2. Create an effective and simple procedure for designing FRP composite patches to increase the limit capacity and fatigue life of in-place, damaged bridge girders
3. Given Objective 2 above, develop economic use of FRP composite material
4. Develop a FRP composite patch application procedure to maximum quality control, worker safety, and patch effectiveness
5. Accurately model FRP composite reinforced damaged bridge girders behavior

The following methods and processes were implemented in undertaking the above tasks:

A. Performed two series of experiments on beam specimens representative of in-field, damaged bridge girders. The first series loads specimens to create damage and a benchmark of capacity. The second series loads FRP patched repaired specimens to verify effectiveness of post-strengthening.
B. Utilized several types of composite materials; exploring several composite materials not only led to greater understanding but will also empower design engineers.
C. Closely observed any failure patterns that emerge from experiments. Understanding how and why a beam fails is as important as the failure itself. Closely examined beams up to and during failure increased understanding and ensured conservative FRP composite patch design.

D. Developed a cost effective and field reproducible application process that manages the sensitive nature of composite materials. Implementing simple methods to correctly apply composite material increases the post-strengthening effectiveness.

E. Created an accurate model of the retrofitted in-field and damaged bridge girders in a scientifically sound manner; utilizing clear and simple mathematical derivations that may be used by engineers as a useful design aid.

Chapter II

EXPERIMENTAL SPECIMEN & FRP COMPOSITE CHARACTERIZATION

The primary emphasis of this research effort is experimental in nature to develop a clear understanding of the physical phenomena of damaged beams externally retrofitted with FRP composite patches. The tests provide qualitative and quantitative results and act as a source of validation of the composite patch design. The beams are representative of those designed by bridge engineers, specifically reinforced concrete, prestressed concrete, and steel I-beams. Each type of the beam was designed specifically for this research project. Design constraints include laboratory facilities, weight of test beams, construction feasibility, and associated costs. These are common limitations of civil engineering research, typically resulting in either a few large beams or many smaller beam specimens. In the context of the research presented here, 18 reinforced concrete beams, 3 prestressed concrete beams were designed and constructed. Additionally, 4 steel were beams purchased. All beams were tested in four point bending. Figure 16 shows a generic example of a beam under four point bending. The loads are placed symmetrically with respect to the center of the beam, consequently the value of the eccentricity, ‘e’, will vary according to the beams tested.

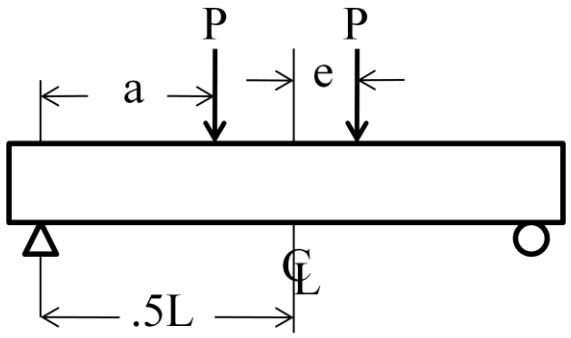

Figure 16. Typical four point loading scheme

Design Reinforced Concrete Beam Specimens

Reinforced concrete beams constitute the majority of the aging bridge superstructures. For this reason, several beams of this type were constructed to test a variety of FRP retrofitting solutions. 18 concrete beams were cast for the present study. Six of the beams were purposefully designed with insufficient shear reinforcing to create opportunity to study FRP repair solutions that enhance shear capacity. These beams were designed without shear reinforcement or stirrups to increase the probability of shear failure. Hereinafter, these beams will be referred as "shear beams". Likewise, 12 beams were intentionally designed to fail in flexure so the performance of FRP flexural post-strengthening could be studied. These beams are designated as "flexural beams". Flexural beams are deliberately over designed in shear to accomplish an increase in the probability of flexural failure.

Given the heavy weight of concrete structures, these beams were limited in size so the beams can be lifted and maneuvered by a single person of average strength. Consequently, the depth and width of the bean section were limited to 6 inches and 4 inches, respectively. To compliment this cross-section, the total length of the beam was

restricted to 42 inches, resulting in each beam weight roughly 88 lbs. Additionally, by constraining the size of the beam, the available resources are more efficiently utilized.

An additional limiting factor is the capacity of the available lab equipment, specifically the hydraulic cylinder, load cell, and load frame. Assuming a load eccentricity of 3 inches, the ultimate load was chosen as 2.5 kips. Given the geometry and a known load, the ultimate moment can easily be calculated. The design steps of the flexural beam are shown below. Figure 17 shows a generic beam cross-section.

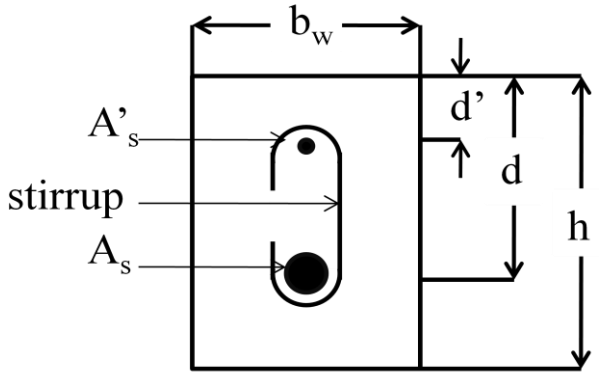

Figure 17. General cross-section detail of a reinforced concrete beam

Based on: $b_w = 4$"; $d = 4$", $P_u = 2.5$ kip; $f_y = 60$ ksi; $f_c' = 4$ ksi; $\lambda = 1$; $L = 36$"; $e = 3$"; $a = 15$", the ultimate applied moment and shear values are found.

$$M_u = Pa = (2.5 \text{ kips})(15") = 37.5 \text{ kip} - \text{in}$$
$$V_u = P = 2.5 \text{ kips}$$

Applying normal force and moment equilibrium conditions yields the following quadratic equation of steel ratio, ρ.

$$\frac{M_u}{b_w d^2} = \rho \phi f_y \left(1 - \frac{\rho f_y}{1.7 f_c'}\right)$$

Solving the equation produces the steel ratio and the required area of steel.

$$\rho = .012154$$
$$A_s = \rho b_w d = .1944 \text{ (in)}^2$$

This area is near that of a #4 reinforcing bar; which is chosen as the main reinforcing steel of the beam. The shear capacity of the beam is calculated according to ACI 319-18 as shown below (Busel, 2008).

$$\phi V_c = 2\lambda\phi\sqrt{f_c'} b_w d = 1.52 \text{ kips}$$
$$\phi V_c = 1.52 \text{ kips} \leq V_u = 2.5 \text{ kips}$$

Flexural beams need significant shear capacity to ensure that flexural bending is the primary failure mode. A #2 bar was chosen for the top hanger, similarly #2 bars were also chosen for the shear stirrups. The required stirrup size and spacing

$$\phi V_s = V_u - \phi V_c = .98 \text{ kips}$$
$$s_{theoretical} = \frac{A_v f_y d}{\phi V_s} = 9"$$
$$s_{max} = \frac{d}{2} = 2" \leftarrow \text{controls}$$

The spacing provided is 4" beginning with 5" from the end of the beam. Figure 18 shows the flexural beam details. Figure 19 shows the stirrup spacing.

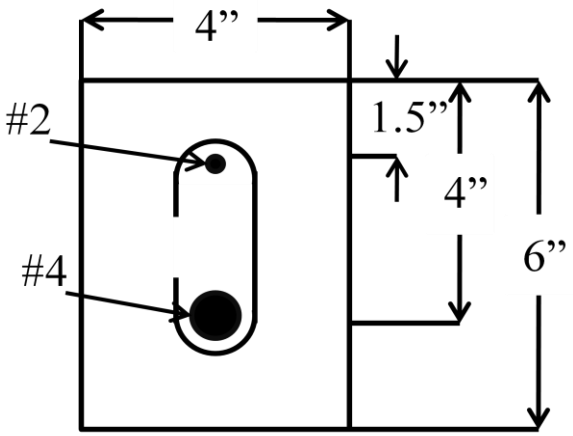

Figure 18. Reinforcing detail for concrete beam designed to fail in flexural bending

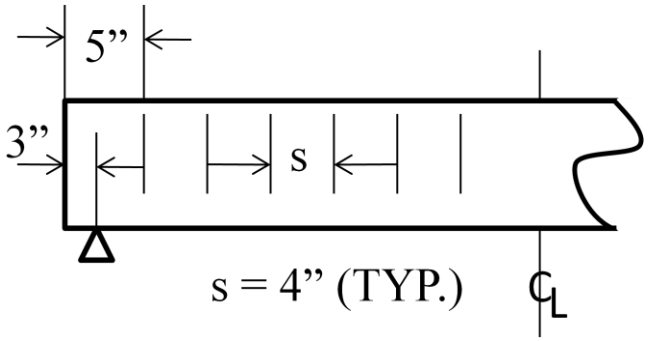

Figure 19. Shear stirrup spacing

Shear beams are provided with the same main flexural reinforcement of a #4 bar. Shear stirrups are not provided in order to ensure the beams fail in shear. The details of the shear beams are shown in figure 20.

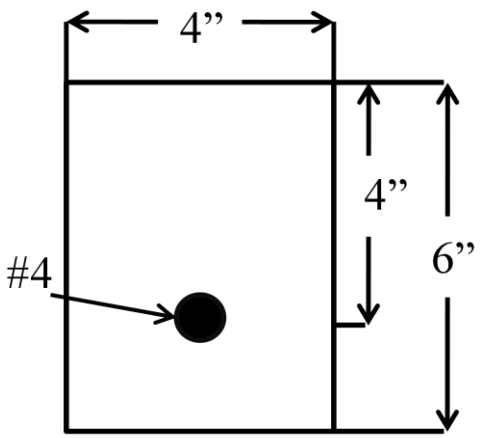

Figure 20. Reinforcing detail for concrete beams to fail in shear

Concrete is a complex, heterogeneous mixture, so great care was taken in both mixing and placing the concrete used to create the reinforced concrete specimens. The mix design utilized for the reinforced concrete beams was formulated by TDOT. The mix was originally designed for bridge substructures. The design compressive strength is 4000 psi. Table 4 describes the mix and the source of each material component. The course aggregate has a maximum size of ½ inch. The fine aggregate is fine sand.

Table 4. Concrete mix design and material source

Materials	Weight	Source
Fine Aggregate	1112 PCY	Ingram Materials, Nashville TN
Course Aggregate	1820 PCY	Vulcan Materials, Nashville TN
Cement Type I	465 PCY	Lafarge, Nashville TN
Flyash	115 PCY	Cooper Power Station, Somerset KY
Silicia Fume	25 PCY	Lafarge, Nashville TN
Water	30 Gal/CY	

The forms for the reinforced concrete beams were fabricated from Southern Pine for the sides and plywood for the bottom. The formwork was designed to easily fall away once the concrete set. Figure 21 and 22 show the assembled form with reinforcing bars in place. The stirrups were anchored with metal wire ties and were additionally held at the correct spacing with epoxy glue.

Figure 21. Forms for 6 shear beams and 3 flexural beams

Figure 22. Forms for remaining flexural beams

The forms were coated vegetable oil to prevent the concrete from adhering to the formwork. It was ensured that the reinforcing bars were free of oil, as such would be detrimental to developing necessary bond strength.

A 4.5 cubic-yard electric drum mixer was used to batch the concrete. The mixer could accommodate enough materials for two beams and two cylinders with relative ease or three beams and cylinders with more effort. Most materials were weighed out in five gallon buckets with a Toledo *True Weight* scale with accuracy to the nearest half pound. Given the required quantity of silica fume was small, a digital scale was used to measure its weight.

Once the concrete was thoroughly mixed, it was transferred from the mixer to the formwork with a shovel. The concrete was placed in three layers, each of which was thoroughly tamped with a rod. The concrete was then finished and covered with plastic

sheets for protection. For each beam, one 4 inch diameter by 8 inch tall test cylinder was made following standard procedures. Each cylinder was properly labeled to be identifiable with the respective beam. Given the large number of beams be produced and the relatively small batch sizes, maintaining proper uniformity would be difficult. Making the cylinders helps to account for variability between beams and batches. Figure 23 shows the beams being poured and finished. Table 5 provides the notes taken throughout the construction of the reinforced concrete beams.

Figure 23. Reinforced concrete beams being placed

Table 5. Notes on concrete mixture

Beam I.D.	Batch	Texture	Beam Type
1	1	good	flexure
2		good	flexure
3	2	sloppy	flexure
4		Fair	shear
5		fair/dry	shear
6	3	slightly sloppy	shear
7		slightly sloppy	shear
8	4	slightly sloppy	shear
9		slightly sloppy	shear
A	5	good	flexure
B		good	flexure
C	6	sloppy	flexure
D		sloppy	flexure
E	7	sloppy	flexure
F		sloppy	flexure
G	8	good	flexure
H		good	flexure
I	9	Fair	flexure

Notable exceptions in pouring the beam include:

- Batch 2 lost water, cement, silica fume, and fly ash during mixing process due to inadequate size of mixer
- Ran out of concrete for the fifth beam, and finished with concrete from the next batch
- Cylinders 1 through 5 and A through D were made immediately after beams were poured
- Cylinders 6 through 9 and E through I were made while beams were poured
- Batch 8 and 9 had reduced added water to compensate for moisture of aggregates

The beams were left to cure in the forms for 24 hours undisturbed, after which, they were placed in tanks and covered with water to properly cure for an additional 27 days. The tanks were covered with plastic sheets and undisturbed for this period. Figures 24 and 25 show the concrete beams before removal from formwork. Figures 26 and 27 depict the beams and cylinders in the tank being covered with water.

Figure 24. Flexural beams 24 hours after placement

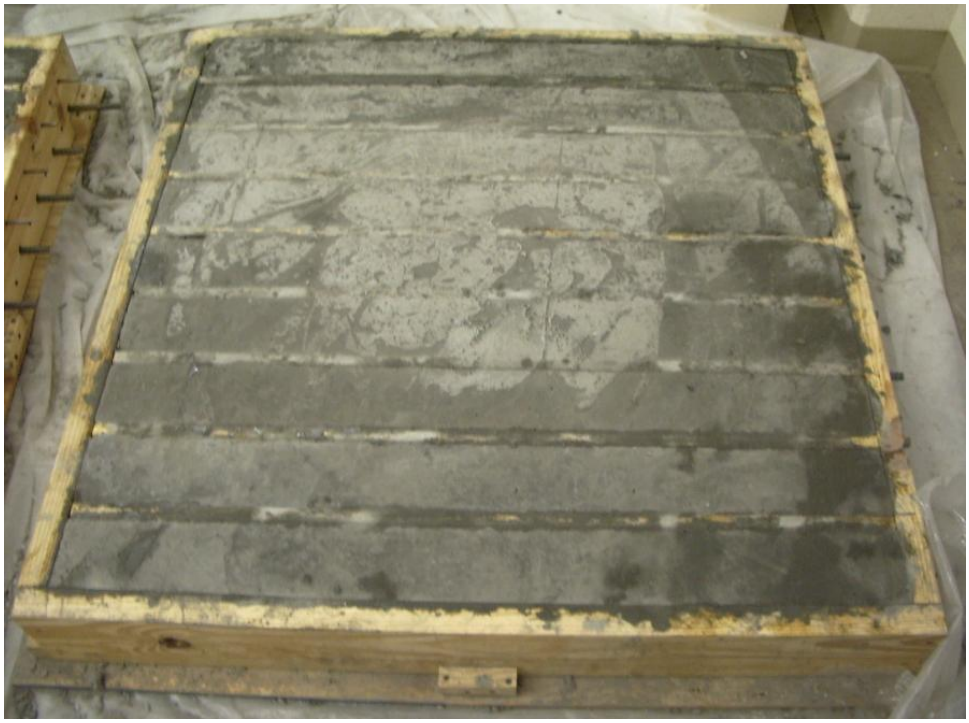

Figure 25. 3 flexural and 6 shear beams 24 hours after placement

Figure 26. Concrete beams and cylinders being submerged in water

Figure 27. Covered tanks holding concrete beams and cylinders in water

After 27 days of curing under water, the beams and cylinders were removed from the tanks and left to air dry thoroughly. Once completely dried, the cylinders were tested in compression according to ASTM C873 in a calibrated 500 kip Forney machine, as shown in Figure 28. Figure 29 shows a typical cylinder failure. The results of these tests are given in table 6.

Figure 28. Machine for testing concrete cylinders

Figure 29. Typical test cylinder failure

Table 6. Concrete cylinder results

Cylinder ID	Failure Load (lb)	Strength (psi)
1	88860	7071.25
2	90940	7236.78
3	85940	6838.89
4	79170	6300.15
5*	95190	7574.98
6	91910	7313.97
7**	93020	7402.3
8	83400	6636.76
9	81370	6475.22
A	85740	6822.97
B	79290	6309.7
C	62510	4974.39
D	61800	4917.89
E	72570	5774.94
F	71150	5661.94
G	89520	7123.78
H	89140	7093.54
I	87490	6962.23
* high loading rate		
** inaudible failure		

Selection of Steel Beam Specimens

It was concluded that the selection of a steel I-beam with overall width and depth dimensions similar to those of the reinforced concrete beams would optimize the use of the laboratory facilities and testing apparatus. Accordingly, a W6x12 was chosen and 4 beams, each 5.5 feet long, were purchased. The respective clear span is 5 feet.

In order to determine the limit capacity of the steel beams under the four point loading shown in figure 16, it is necessary to consider several flexural and shear limit states. For the sake of simplicity, the standard parameters of the beam from the AISC

design manual are used. Table 7 shows the AISC section properties of a W6x12, including necessary application parameters for determining the capacity of the beams (Thornton and Holland, 2007).

Table 7. Steel Properties from 2008 AISC Steel Manual

$A =$	3.55	$(in)^2$	$t_w =$	0.23	In	$k =$	0.53	In
$d =$	6.03	In	$t_f =$	0.28	In	$N =$	0.1	In
$Z =$	8.30	$(in)^3$	$h_o =$	5.75	In	$l_b =$	60	In
$S_x =$	7.31	$(in)^3$	$J =$	0.0903	$(in)^3$	$F_y =$	62.5	Ksi
$I_x =$	22.10	$(in)^4$	$r_{ts} =$	1.08	In	$E =$	29000	Ksi
$I_y =$	2.99	$(in)^4$	$r_y =$	1.08	In	$a =$	27	In

It is necessary to find the controlling limit state of the beams given the loading scenario of figure 16. In the following limit state calculations, the beams are assumed to be braced at the end support points.

Plastic Moment Capacity:

$$M_p = M_n = F_y Z_x = 518.75 \text{ kip} \cdot \text{in}$$

The corresponding values of the two symmetric point loads are easily calculated.

$$P = 19.21 \text{ kip}$$

Lateral Torsional Buckling:

$$l_p = 1.76 r_y \sqrt{\frac{E}{F_y}} = 34.8 \text{ in}$$

$$l_r = 1.95 r_{ts} \frac{E}{.7F_y} \sqrt{\frac{Jc}{S_x h_o}} \sqrt{1 + \sqrt{1 + 6.76 \left(\frac{.7F_y}{E} \frac{S_x h_o}{Jc} \right)^2}} = 102.6 \text{ in}$$

$$M_n = c_b \left[M_p - \left(M_p - .7F_y S_x \right) \left(\frac{l_b - l_p}{l_r - l_p} \right) \right] = 474.7 \text{ kip} - \text{in} \leq M_p$$

$$\Rightarrow P = 17.59 \text{ kip}$$

Compression Flange Local Buckling:

$$\lambda_p = 0.38 \sqrt{\frac{E}{f_y}} = 9.15$$

$$\lambda_r = 1.0 \sqrt{\frac{E}{f_y}} = 24.08$$

$$\lambda = \frac{b_f}{2t_f} = 7.14$$

$$k_c = \frac{4}{\sqrt{\frac{h}{t_w}}} = 0.76$$

$$M_n = \frac{0.9 E k_c S_x}{\lambda^2} = 2844.30 \text{ kip} - \text{in}$$

$$\Rightarrow P = 105.34 \text{ kip}$$

Web Local Yielding:

$$R_n = (5k + N) F_{yw} t_w = 29.22 \text{ kips}$$

$$\Rightarrow P = 29.22$$

Web Crippling:

$$R_n = 0.8t_w^2\left[1 + 3\left(\frac{N}{d}\right)\left(\frac{t_w}{t_f}\right)^{1.5}\right]\sqrt{\frac{Ef_{yw}t_f}{t_w}} = 36.23 \text{ kip}$$

$$\Rightarrow P = 36.23 \text{ kip}$$

Web Compression Buckling:

$$R_n = \frac{24t_w^2\sqrt{Ef_y}}{h} = 164.11 \text{ kip}$$

$$\Rightarrow P = 164.11 \text{ kip}$$

Based on the calculated values of applied load, P, the limit load of the W6x12 is 17.59 kips corresponding to a controlling failure mode of lateral torsional buckling.

Since the motif of this research project is to study the effectiveness of FRP repair of in situ bridge structures, the beams needed to be physically altered to simulate corrosion caused by environmental factors. Previous research showed that steel beam sections sustained a fifteen percent loss of section, a loss observed in both flanges and webs (Sirisak, 1996). To simulate the loss of section from corrosion, three beams were milled, while the fourth beam served as a control. The first case of corrosion resulted in removing fifteen percent of the bottom flange from one beam, beam SBI; the second case resulted in symmetrically milling fifteen percent of the web of a beam, beam SBII; and finally a third case resulted in removing fifteen percent of both the bottom flange and web, beam SBIII. Figures 31 though 34 show the milled beams.

Since, it is difficult to manufacture steel beams free of flaws; the beams had many small imperfections including: chambering, twisting, and variation in web and flange thicknesses. The presence of such irregularities made removing exactly fifteen percent of the surfaces difficult. The machine shop personnel who performed the milling were in

constant contact with the researcher to find the best solutions when encountering the flaws. Solutions often involved the use of wedges and shims.

After milling, each beam was weighed to the nearest pound and the length measured to the nearest $^1/_{16}$ of an inch. Assuming the density of steel to be 0.2836 pci, the areas of each beam can be determined. These areas are summarized in table 8, the difference of the milled beams to the control beam is given in the last column of the table. Table 9 shows the corresponding theoretical values for a perfect W6x12 beam.

The primary reason for the discrepancy between the values of tables 8 and 9 comes from the variations of the flange and web thicknesses of the manufactured beams. Measuring sample web and flange thicknesses demonstrates variability in the beams. Calipers of 0.01 inch accuracy were used to measure the beam thicknesses at distinct locations as shown in figure 30. Tables 10 and 11 give the results of these measurements.

Table 8. Results of milling on steel beam specimens

Beam	Weight (lbs)	Length (ft)	Area (in)2	% Difference
Control	66.8	5.50	3.57	
SBI	65.5	5.49	3.50	-1.76
SBII	65.0	5.50	3.47	-2.65
SBIII	63.0	5.50	3.37	-5.60

Table 9. Theoretical milling values

AISC Area (in)2	% difference
3.55	
3.38	-4.73
3.39	-4.37
3.23	-9.11

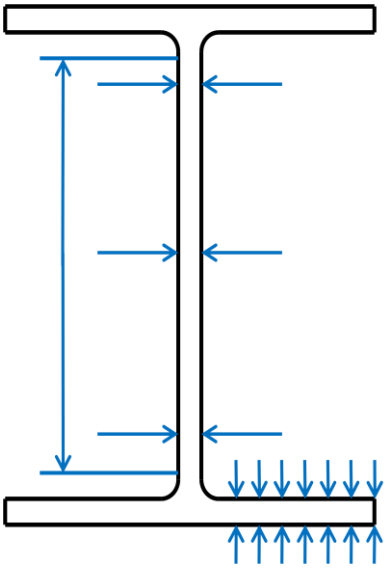

Figure 30. Measurement locations

Table 10. Measured flanges thicknesses

Distant from free edge (in)	0	0.2	0.4	0.6	0.8	1	1.2
Control	0.215	0.285	0.290	0.290	0.270	0.260	0.250
SBI	0.210	0.290	0.290	0.270	0.260	0.260	0.260
SBIII	0.220	0.255	0.250	0.250	0.250	0.250	0.245

Table 11. Measured web thicknesses in inches

	Top	Middle	Bottom	Height of Mill
Control	0.240	0.250	0.240	0.000
SBII	0.210	0.190	0.210	4.890
SBIII	0.210	0.190	0.200	4.695

Figure 31. Close up view of bottom flange of beam SBI

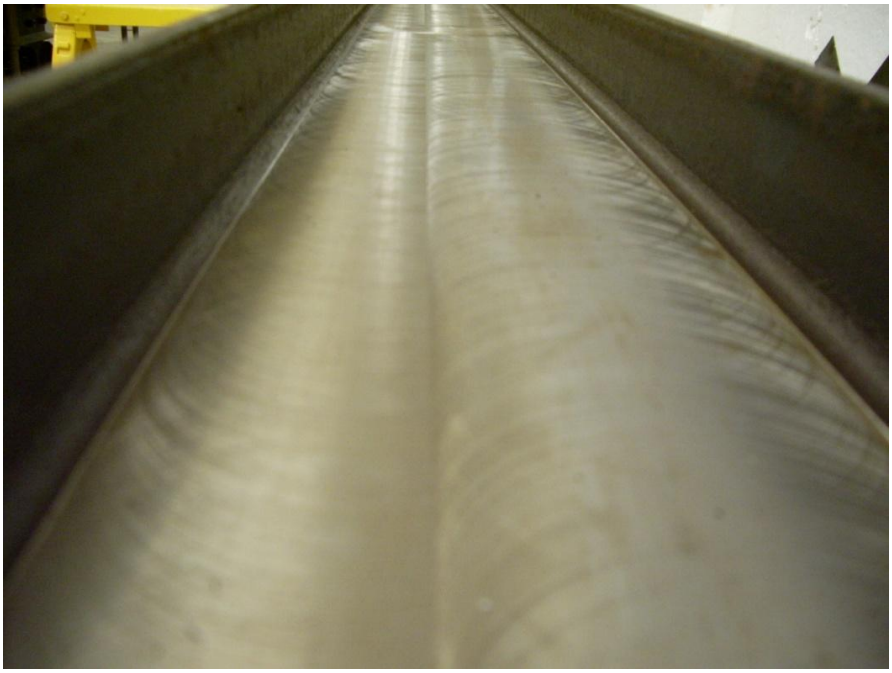

Figure 32. Close up view of milled web of beam SBII, side 1

Figure 33. Close up view of milled web of beam SBII, side 2

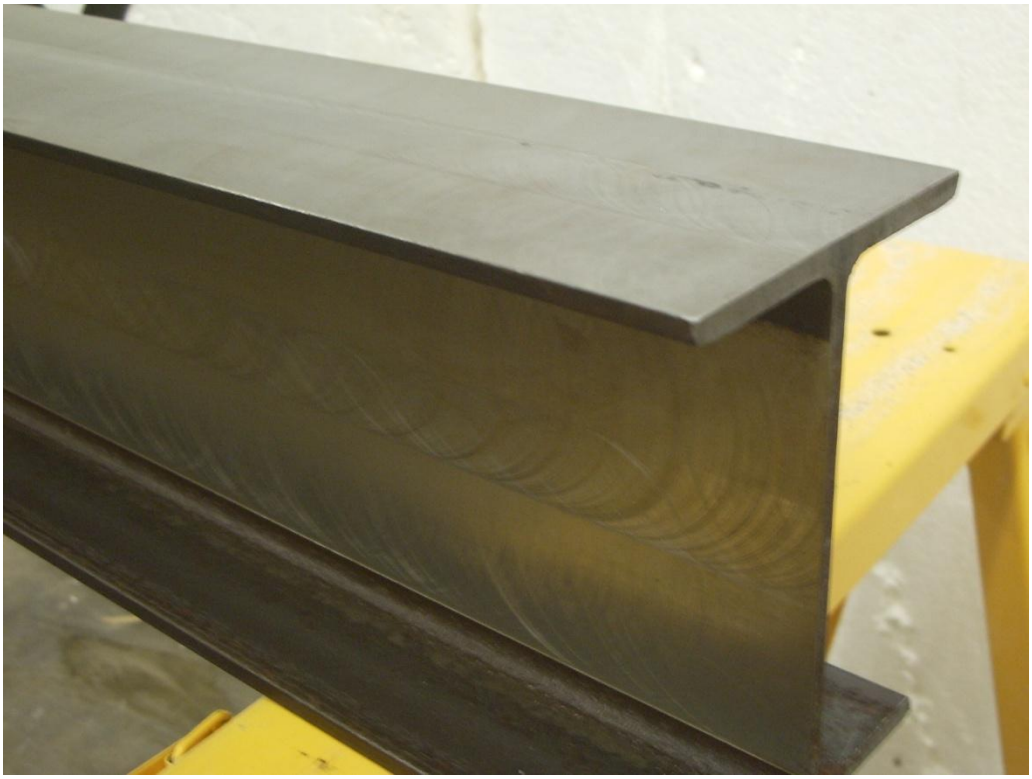

Figure 34. Milling marks show section loss of flange and web of beam SBIII

Design of Prestressed Concrete Beam Specimens

The prestressed concrete beam specimens were designed with the assistance of Adrian Bennett, a TDOT bridge design engineer. The design constraints were beam length and the upper limit of load capacity. A symmetric I cross-section was chosen for simplicity and is shown in Figure 35. Two one-half inch, low relaxation strands were placed at the bottom of the beam, and two #3 bars in the top. The length of the beam is determined by the distance required for the prestressing force to be effective. #3 stirrups were placed along the length. Figure 36 shows the spacing and Figure 37 shows the stirrup shape which alternates orientation, this is shown as dashed lines. Spacing A is three and one half inches, B is two and one half inches, and C is five inches. The total

length of the beam is 8 feet, 6 inches. Significant details of the prestressed beams are given in table 12.

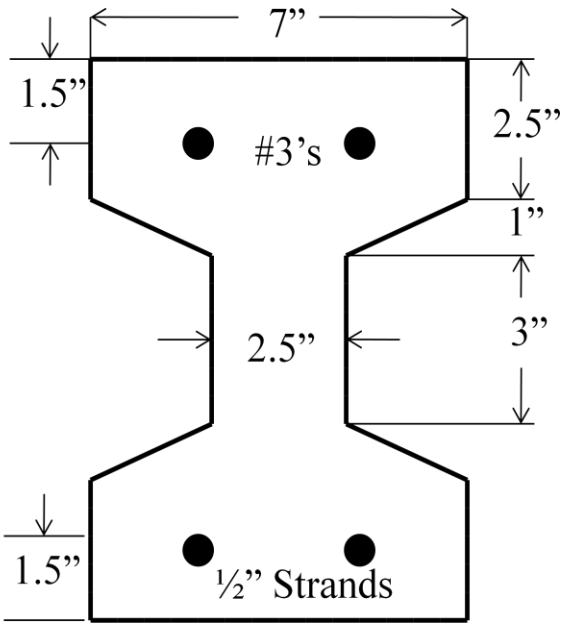

Figure 35. Cross-section of prestressed beam

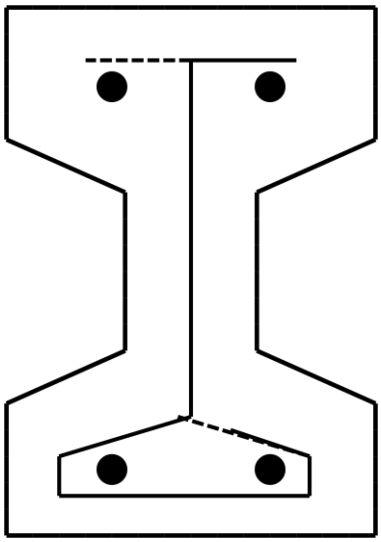

Figure 36. Detail of stirrup configuration

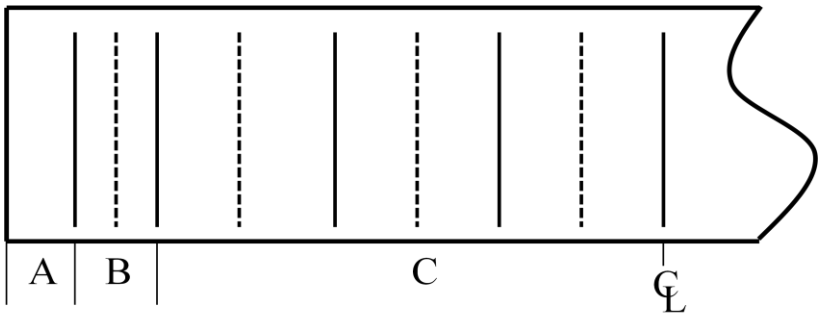

Figure 37. Stirrup spacing detail

Table 12. Relevant prestressed beam design parameters

f'_c =	5000	psi
f'_{ci} =	4000	psi
f_u =	270	ksi
Area =	52	$(in)^2$
Self Weight =	54.17	$^{lb}/_{ft}$
Length =	8.5	ft
I_x =	557.83	$(in)^4$
M_n =	38.98	kip-ft

The prestressed concrete beams utilized in the research presented in this manuscript were manufactured at Construction Products Incorporated in Jackson, Tennessee. The concrete mix was designed to have a minimum strength of 5000 psi. The results for concrete test cylinders are shown in table 13. The beams were cast one at a time in a row and were steam cured for 24 hours. Figure 38 shows the formwork in which the beams were cast. Figure 39 shows one of the beams before the high tensile steel strands were cut. Figure 40 shows the beam after the strands were torch cut and removed from the casting bed.

Given the relatively small size, it was not initially clear that the beams were effectively prestressed. This doubt was generated from a lack of visible upward camber

once the strands were cut. However, within days of stress transfer, tensile cracking was evident in the top of the beams. This tensile cracking, shown in figures 41 and 42, indicates that the prestress was sufficiently active.

Table 13. Prestressed concrete beam compressive strength

Beam ID	Failure Load (lb)	Strength (psi)
PSCB1	88500	7042.61
PSCB1	81500	6485.56
PSCB2	83000	6604.93
PSCB2	80000	6366.20

Figure 38. Formwork for prestressed concrete beams

Figure 39. End of prestressed beam before steel strands were torch cut

Figure 40. Prestressed beam before transportation to Vanderbilt laboratory facility

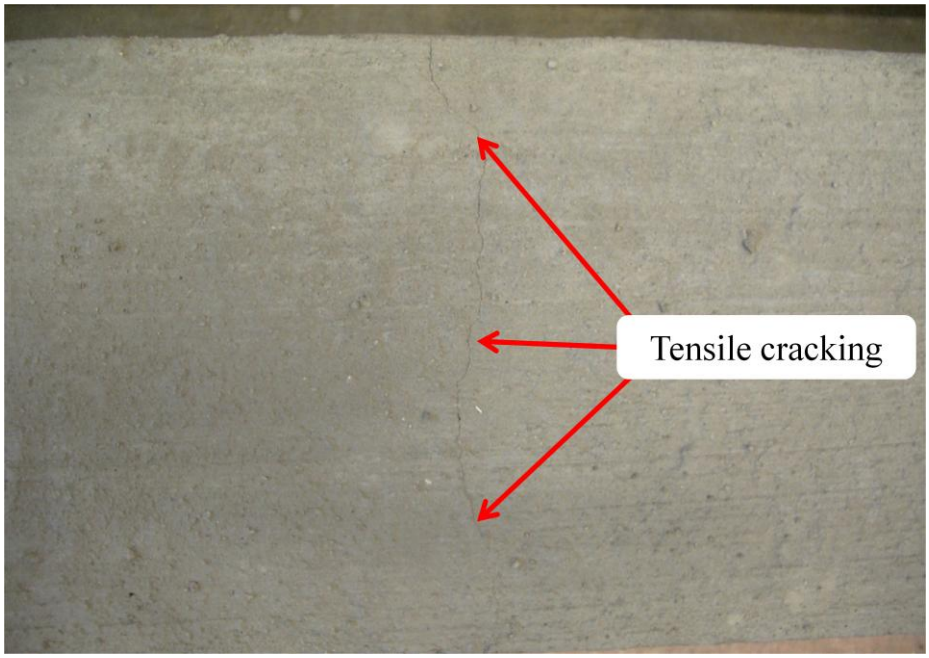

Figure 41. Tensile cracking in the top of PSCB1

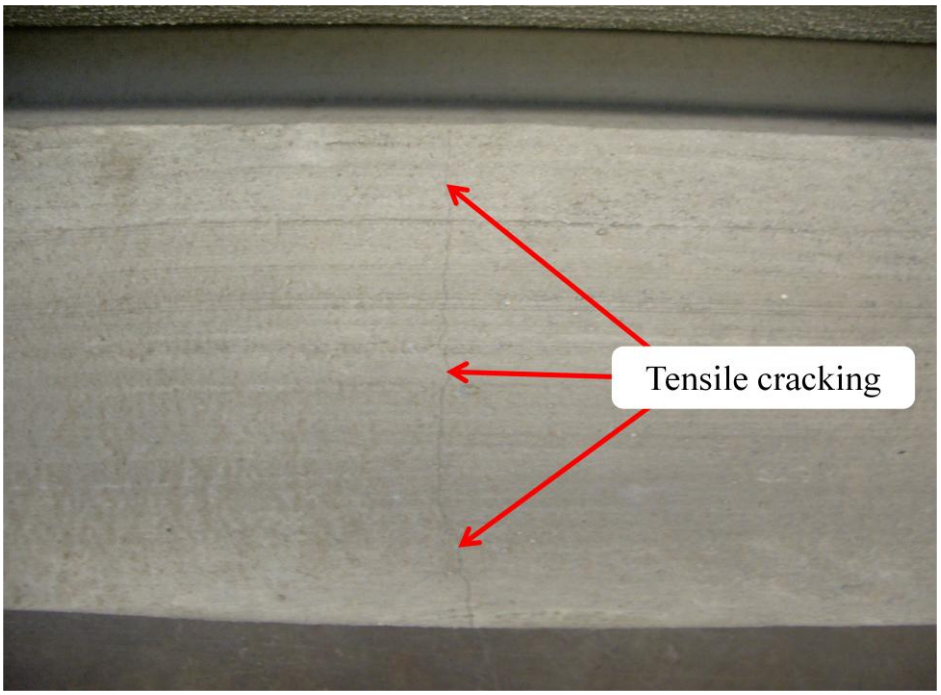

Figure 42. Tensile cracking in the top of PSCB2

Introduction to Composite Characterization

The civil engineering field currently revolves around systems of well known and defined materials. The primary systems of materials are similar to those just described. Steel quality is standardized, and concrete has become a relatively well understood material. For example, design engineers understand reinforcing steel bars will meet minimum material properties independent of the provider. The FRP industry is highly unique, and no standard exists for their application in the civil engineering community. FRP materials vary for several reasons, including manufacturer, fiber type, direction, prestressing, resin type and mixture, and matrix resin structure. Each composite system typically has two main components: fiber materials and resin matrix material. Each system of fibers is adhered to substrates with an adhesive; both have distinct mechanical, thermal, and chemical properties. The manufacturer provided technical and data sheets of all the FRP and adhesives used in this research project. They are available in Appendix A. Some significant mechanical properties of the composite fiber materials used in this project are provided in table 14.

Table 14. Comparison of physical and mechanical properties of composite

Material	Density ($^{lb}/_{in^3}$)	Tensile Strength (ksi)	Tensile Modulus (ksi)	Elongation %	Factory Thickness (in)
Grade 60 Steel	0.284	60	29000	10.00	Varies
SikaWrap Hex 230	0.064	624	34000	1.80	0.010
Sika CarboDur	0.058	449	23900	1.69	0.047
Newport LTC 4300		290	18700	1.44	0.010

Manufacturers currently provide a limited amount of mechanical, thermal, and chemical properties for adhesives used to adhere composite fibers. This information is not for engineers to design FRP composite systems. *A Model Specification for FRP Composites for Civil Engineering Structures* discussed in the literature review explains this general lack of standardization of FRP composites and adhesives for civil engineering and provides a basis for the process to begin (Bank, 2003). There is no set of standard tests which composite materials and adhesives must undergo to provide adequate mechanical information for engineers.

Experiments were developed in the context of this research to find adhesive properties, including; equivalent spring stiffness constants in both tension and shear for use in the mechanistic model, adhesive tensile and shear modulus, adhesive tensile and shear capacity, and the type of failure modes possible with adhesives. Appendix B describes adhesive testing and analysis. Table 15 shows the results of adhesive characterization.

Table 15. Adhesive properties

Adhesive	G (ksi)	E (ksi)	τ_u (ksi)	σ_u (ksi)	k_v ($^{kip}/_{in^3}$)	k_h ($^{kip}/_{in^3}$)
SikaDur 330	0.441	0.769	0.362	1.010	72.73	8.77
SikaDur 30	16.002	23.886	1.594	0.867	75.76	34.25
LTC 4300	0.079	0.769	0.089	0.846	58.56	4.28

SikaWrap Hex 230/Sikadur 330 System

The Sika Company manufactures innumerable composites; SikaWrap Hex 230, or Sikawrap for short, is a unidirectional carbon fiber fabric. The fabric, or sheet, is laminated to the structure substrate in the field to create a complete composite system. Sikawrap is high strength, light weight, conforms to complex shapes, is noncorrosive and alkali resistant. It can be employed to increase structural capacity, strengthen columns and walls for seismic loading, correct design or construction errors, renovate structural systems, and repair deficient members. The fabric is manufactured in 25-inch-wide rolls that can be up to 300 feet long. Such substantial lengths allow for application without concern for splicing.

Sikawrap is simple to handle as it is very similar to cotton cloth material. The carbon fibers run in one direction and are woven together with a white nylon thread every half inch. Sikawrap is very easy to measure and cut. The manufacturer prefers shearing the fibers with commercial heavy duty scissors. It is also recommended that the scissors be sharp to prevent damaging the fibers, which can lead to reduced capacity. Review of several manufacturers instructions show that shearing action is preferred above all other methods for partitioning fibrous composite materials. The primary reason for cutting the fibers with shears is to reduce the possibility of damaging or fraying the fibers. Another reason to shear composite fibers is to reduce the production of carbon dust. Carbon dust particles can be small enough to be considered a carcinogen. It is the manufactures' and author's recommendation to wear a National Institute for Occupational Safety and Health (NIOSH) approved respirator. Wearing protective gloves is also recommended. Gloves

protect the skin from contact with any loose carbon fibers or dust, which act as an irritant and can be difficult to wash. Gloves also protect the composite surface from oils, grease, or other contaminates residing on the user's hands.

Sikadur 330 US or Sikadur 330, was created to work in tandem with Sikawrap. It is a high strength, high modulus resin for impregnating the carbon fiber fabric. Positives include long shelf life, pot life, and exposure time. The adhesive is highly resistant to heat, abrasion, and shock, as well as being tolerant of environmental moisture at all curing stages. Sikadur 330 holds to most structural systems well, specifically concrete, steel, timber, and masonry. The shelf-life of each component is approximately 2 years and has a mixed pot life of 57 minutes.

Epoxy adhesives typically are two components; a curing agent and a hardening agent. It is beneficial to have either be different colors to ensure that either component is thoroughly combined. Streaks of either component's color indicate that the mixture requires additional mixing. As is typical of many adhesives, Sikadur 330 is supplied in two components which are mixed together in a specified proportion and mix rate. Four parts of component "A" should be mixed with one part of component "B" by weight. Each part is a different color, one gray, the other violet, and the final mixture should be a smooth combination of both colors. Sikadur 330 should be mixed thoroughly for 5 minutes with a drill mounted mixer at a low speed. In the research presented, the adhesive was mixed by hand with a wood or metal stirring rod for the full 5 minutes as prescribed at which time the mixture was closely examined for streaks of either component color.

In general, Sikadur 330 is a thin, runny adhesive. If pulled into the air, the adhesive will develop into thin strings. Each component produces noticeable fumes and proper protection should be taken. A 3M respirator mask was worn at all times when mixing and applying Sikadur 330.

Carbodur/Sikadur 30 System

An additional Sika product, Sika CarboDur or Carbodur for short, is a carbon fiber laminate. It is formed by curing protruded carbon fibers into laminate. It is designed to strengthen concrete, timber, and masonry structures. Carbodur is lightweight, incredibly strong, and has a high Young's modulus of elasticity. Additionally, it is alkali resistant, non-corrosive, and has excellent fatigue resistance. It is intended to aid in repairing damaged structures, increasing load capacity of structural members, renovating structural systems, and enhancing serviceability. It is available in widths of 2, 3, and 4 inches, and can be produced in lengths up to 820 feet.

Carbodur is the only composite material which is stiff enough to resist bending by itself. The laminate is very stiff in the longitudinal fiber direction. However, the material is easily snapped in the transverse direction. The material is similar to SikaWrap in that it is very light and easy to handle. The favored technique of cutting Carbodur is, again, to use heavy shearing scissors.

Sikadur 30 is designed to adhere Carbodur to structural members. Like Sikadur 330, it is a high strength, high modulus epoxy. The significant difference is that Sikadur

30 is an epoxy paste. This distinction means it is significantly thicker than Sikadur 330. The adhesive offers all the benefits mentioned above for Sikadur 330.

Like, Sikadur 330, Sikadur 30 is a two part adhesive. It is mixed at a ratio of 3 parts component 'A' to 1 part component 'B' by volume, at a slow rate for 3 minutes. Again, a uniform color should be achieved by proper mixing. In the research presented, the adhesive was weighed out in correct and accurate proportion and mixed by hand for the full prescribed duration. Sikadur 30 has the consistency of a fine aggregate-cement mixture or a grout. It appears that the adhesive has a fine sand mixed into the chemical components, resulting in a thick viscosity. Sikadur 30 can act as a grout material if oven dry fine aggregate is mixed into the adhesive. The manufacturer does not define the correct proportion of additional aggregate to add. This utility of the adhesive was also used in the research presented here. The respirator mask was worn at all times to limit exposure to chemical fumes. Image 43 shows a picture of Sikadur 30.

Figure 43. Sikadur 30

LTC 4300 Pre impregnated System

Pre-impregnated composite materials, commonly called prepregs, are composed of carbon fiber sheets manufactured with a resin system incorporated. Additional adhesives are not required to properly adhere the FRP system to the substrate. Instead, the composite material is pressed against the substrate with a uniform pressure, and the entire system is then heated to a prescribed temperature at a prescribed rate. The resin softens and adheres to the substrate. Newport Adhesives and Composites produces such a prepreg product, LTC 4300. LTC 4300 is a **L**ow **T**emperature **C**ured prepreg composite, requiring cure temperature range of 140 to 200˚F. The manufacturer supplies specific heating instructions to ensure curing the resin epoxy surrounding the fibers properly. The prescribed pressure is 1 atm. 1 atm is equal to 14.2 pounds per square

inches or roughly 2,045 pounds per square foot. Pressure is typically applied by vacuum bagging which easy supplies a uniform pressure that conforms to a variety of shapes. Prepreg materials usually have specified shelf lives, which are usually dependent on environmental conditions. The shelf life of LTC 4300 is 30 days at 70˚F. Finally, prepreg composites are usually manufactured at specific widths and onto rolls. Given that the adhesive is integral with the fibers, prepreg composites have a tacky feel, and the protective plastic sheets easily adhere. Typically, prepreg composites are tacky in nature because the resin is already present. Manufacturers protected prepreg composites from dirt, chemicals, and other containments with protective plastic sheeting. Plastic gloves were always worn when handling LTC 4300 in the event that the plastic sheeting should fall away, exposing the resin impregnated fibers.

LTC 4300 arrived from Newport Adhesives and Composites in late summer and was kept safely stored until patching in December. This time difference exceeds the recommended self-life, but due to budget and laboratory limitations, the material was utilized anyway. LTC 4300 was dimensioned and cut to length using the same razor blade technique described above for cutting the Sika products. Figure 44 shows a sample strip of LTC 4300.

Figure 44. 6” x 1.5” sample of LTC 4200

Chapter III

MECHANISTIC MODEL

Development of Elastic Model

Creating a scheme to find the interfacial stresses between beam substrates and composite patches is a prerequisite to using composite patches to repair localized damage of bridge superstructures. This requires the development of analytical models of the patched repaired beam systems, which are applicable to service and limit state situations. This chapter develops mechanistic models for steel and reinforced concrete beams which are used in the patch design process. The proposed models are an extension beyond existing models discussed in Chapter I because they are inadequate for this research project. The steel beam specialization is straight forward because steel poses ideal mechanical properties. Specialization of reinforced concrete beams is more complex due to the heterogeneous nature of the material; especially considering the low tensile strength of concrete which leads to cracking.

The general model of a patch repaired beam is based on the principle of minimum potential energy. Consider the total potential energy for a patch repaired beam shown in figure 45 with a composite patch bonded to the bottom face. The simply supported beam is subject to the distributed load of self weight and to a pair of concentrated loads placed as shown in the figure. The total potential energy of the beam-patch system is expressed

as the difference of the total strain energy and the potential energy of the applied loads, given by equation 74.

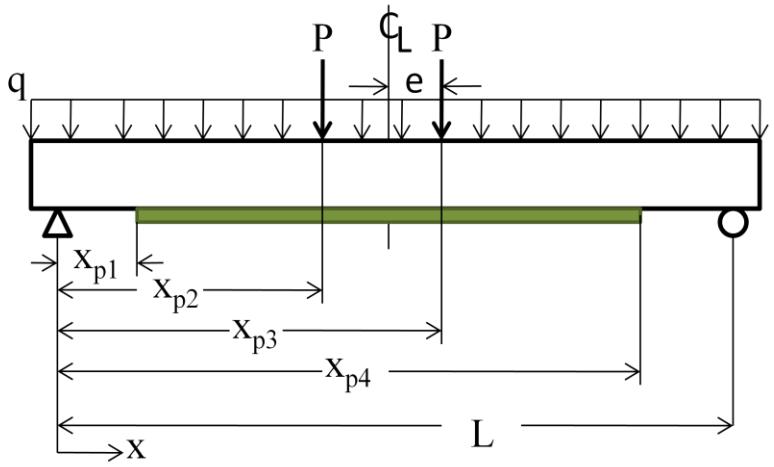

Figure 45. Generic beam with composite patch under four point loading and self weight

$$\Pi = U - V \tag{74}$$

The following assumptions are required to write the expressions of the strain energy of the beam and potential energy of applied loads:

1. All materials are linearly-elastic
2. Plane sections remain plane in the beam and patch, individually
3. No delamination occurs between the composite patch and substrate
4. Mechanical behavior of composite adhesives can be represented by a series of axial, or vertical, and shear, or horizontal, springs; shown in figure 44.
5. Springs characterizing the composite adhesives follow Hooke's Law

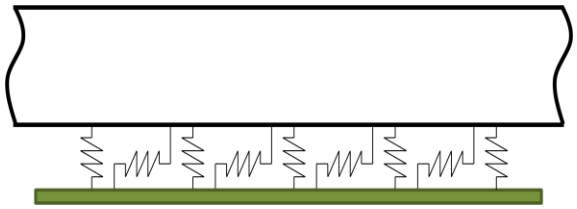

Figure 46. Adhesive layer modeled by spring system

The axial tensile force exhibited by the adhesive is represented by vertical springs; similarly the shear force is represented by horizontal springs. The intensity of these forces is expressed in terms of unit vertical and horizontal spring constants and associated vertical and horizontal displacements, given by equations 75 and 76.

$$F_v = k_v v \tag{75}$$

$$F_u = k_u u \tag{76}$$

The vertical spring extension is the difference of vertical displacements at a point between the beam and patch, as defined in equation 77. With this additional definition, equation 75 can be rewritten as equation 78. The horizontal spring extension is similarly defined, resulting in equations 76 and 80.

$$v = v_b - v_p \tag{77}$$

$$F_v = k_v(v_b - v_p) \tag{78}$$

$$u = u_b - u_p \tag{79}$$

$$F_h = k_h(u_b - u_p) \tag{80}$$

Enforcing compatibility conditions of the horizontal and vertical displacements at the beam and patch interface; the horizontal displacements can be expressed in terms of beam depth, patch thickness, and slope. This is illustrated in figure 47.

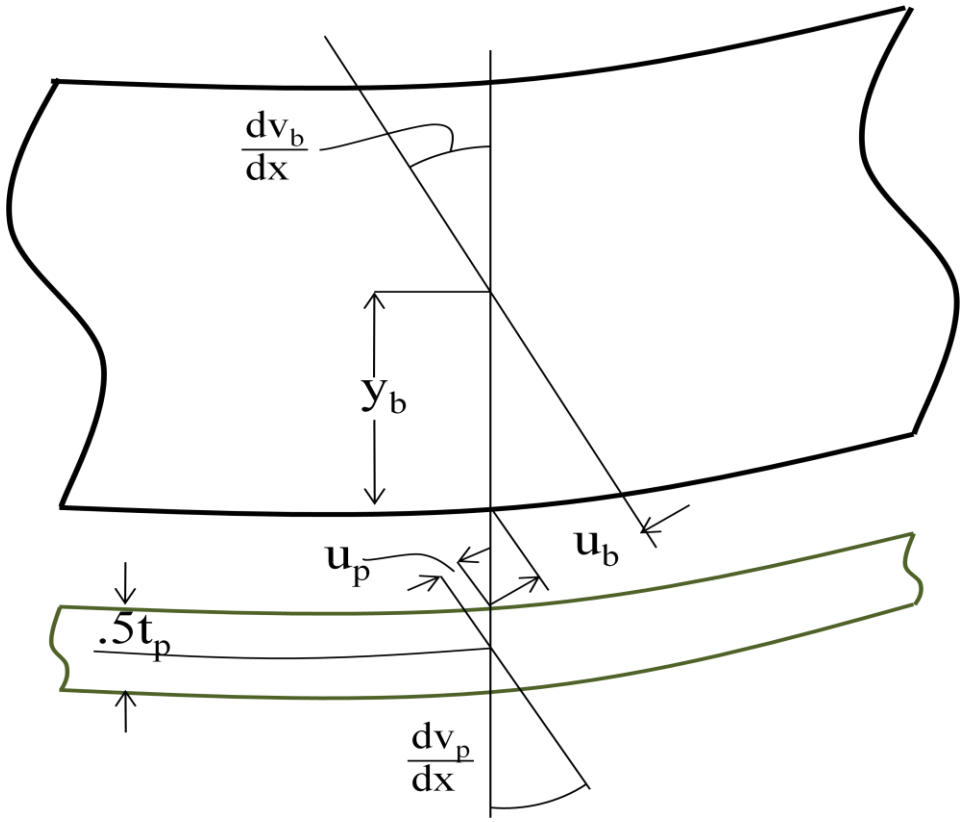

Figure 47. Compatibility relationship between vertical and horizontal displacements at beam-patch interface

For small displacements, the horizontal displacement can be redefined by equation 81 and 82. The application of these definitions yields an expression of horizontal spring extension, given by equation 83.

$$u_b = y_b \frac{dv_b}{dx} \tag{81}$$

$$u_p = -\frac{t_p}{2}\frac{dv_p}{dx} \tag{82}$$

$$\Rightarrow u_b - u_p = \left(y_b v_b' + \frac{t_p}{2} v_p'\right) \tag{83}$$

$$\text{where, } v_b' = \frac{dv_b}{dx} \text{ and } v_p' = \frac{dv_p}{dx}$$

For ease in expressing the strain energy, the beam-patch system is broken into three segments of different sectional properties, as shown in figure 48. Based on the contribution of each segment, the total potential energy can be stated as equation 84.

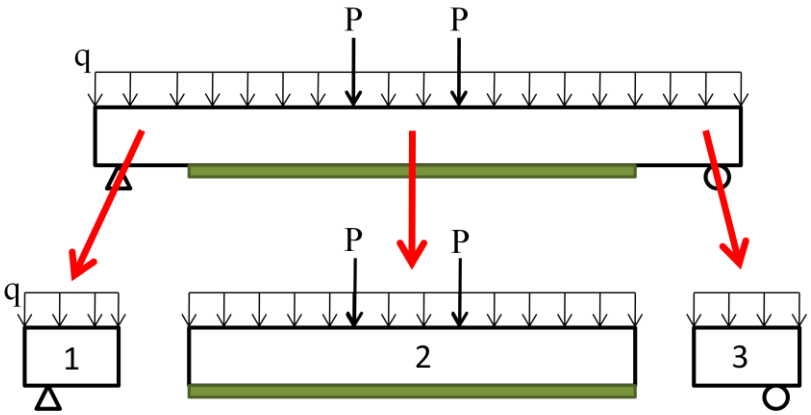

Figure 48. Beam separated into segments of similarity

$$\Pi = U_1 + U_2 + U_3 - V \tag{84}$$

The potential energy of the applied loads is composed of components due to the self weight and the concentrated loads; this is described in equation 85.

$$V = V_q + V_P \tag{85}$$

$$\text{where, } V_q = \int_0^L q v_b dx \tag{86}$$

$$V_P = P_{xp2}(v_b)_{xp2} + P_{xp3}(v_b)_{xp3} \tag{87}$$

The flexural energy of the beam and patch are given by equation 88 and 89. The strain energy from the extension of the spring systems is given by equation 90 and 91.

$$U_{beam} = \frac{1}{2}\int (EI)_b (v_b'')^2 \, dx \tag{88}$$

$$U_{patch} = \frac{1}{2}\int (EI)_p (v_p'')^2 \, dx \tag{89}$$

$$\text{where,} \qquad v_b'' = \frac{d^2 v_b}{dx^2} \text{ and } v_p'' = \frac{d^2 v_p}{dx^2}$$

$$U_{V.S.} = \frac{1}{2}\int F_v (v_b - v_p) dx \tag{90}$$

$$U_{H.S.} = \frac{1}{2}\int F_h \left(y_b v_b' + \frac{t_p}{2} v_p'\right) dx \tag{91}$$

From the expressions described above, the segmental strain energies can be expanded as given below.

$$U_1 = U_{beam} = \frac{1}{2}\int_0^{x_{p1}} (EI)_b (v_b'')^2 \, dx \tag{92}$$

$$U_2 = U_{beam} + U_{patch} + U_{V.S.} + U_{H.S.}$$

$$= \frac{1}{2}\int_{x_{p1}}^{x_{p4}} (EI)_b (v_b'')^2 \, dx + \frac{1}{2}\int_{x_{p1}}^{x_{p4}} (EI)_p \left(v_p''\right)^2 dx + \frac{1}{2}\int_{x_{p1}}^{x_{p4}} F_v (v_b - v_p) dx + \frac{1}{2}\int_{x_{p1}}^{x_{p4}} F_h \left(y_b v_b' + \frac{t_p}{2} v_p'\right) dx \quad (93)$$

$$U_3 = U_{beam} = \frac{1}{2}\int_{x_{p4}}^{L} (EI)_b (v_b'')^2 \, dx \quad (94)$$

The total potential energy of the beam-patch system is now written as equation 95.

$$\Pi_{beam} = U_1 + U_2 + U_3 - V_q - V_P \quad (95)$$

In the above equations, the vertical displacements of the beam and patch are unknown; these variables are functions of the location along the span of the beam, x. The variables can be expressed of a Fourier series expansion with unknown coefficients. The coefficients are determined by applying the principle of minimum potential energy. Given that the beam is simply supported, a sinusoidal series is appropriate considering the beam and patch deflections are symmetric about the center-line, only terms odd terms are considered. Generally, the first few terms are adequate to accurately describe such systems. This series is expressed by equation 96.

$$v_b = \sum_{i=1,3,5\ldots}^{i_b} A_i \sin\left(\frac{i\pi x}{L}\right) \quad (96)$$

The deflection of the patch may be different than that of the beam; consequently a correction function representing the difference of such displacements should be included. A parabolic function over the length of the patch with zero values at each end of the patch is a simple way to append the beam displacement, as given by equation 97.

$$v_p = B_0\left[\bar{x}\left(L_p - \bar{x}\right)\right] + \sum_{i=1,3,5\ldots}^{i_p} B_i \sin\left(\frac{i\pi x}{L_p}\right) \qquad (97)$$

$$\text{where,} \qquad \bar{x} = x - x_{p1}$$

From equations 96 and 97, the total number of unknown coefficient is: $i_b + i_p + 1$. Equation 98 shows the application of the principle of minimum potential energy. Satisfying the principle leads to equations 99 through 100.

$$\delta\Pi = \sum_{i=1,3,5\ldots}^{i_b} \frac{\delta\Pi}{\delta A_i}\delta A_i + \sum_{i=0,1,3,5\ldots}^{i_b} \frac{\delta\Pi}{\delta B_i}\delta B_i = 0 \qquad (98)$$

$$\frac{\delta\Pi}{\delta A_i} = 0, \text{for } i = 1,3,5 \ldots i_b \qquad (99)$$

$$\frac{\delta\Pi}{\delta B_i} = 0, \text{for } i = 0,1,3,5 \ldots i_b \qquad (100)$$

Equations 99 and 100 lead to as many equations as it does unknown coefficients, for which the equations are solved in order to find the values. Knowing the values of the Fourier series expansion coefficients allows for the solution of the beam and patch displacement at any given point along their length using equations 96 and 97, as well as the determination of the interfacial forces with equations 78 and 80.

Specialization for Steel Beams

The general model can be directly applied to steel beams with composite patches applied to the tensile flange as long as the beam behaves elastically. In the event of plastic flow, the model needs to be modified.

Considerations for Concrete Beams

Cracking of concrete in tension requires modification of the general model. Cracking causes a reduction of the effective moment of inertia, which affects the moment-curvature relationship given by equation 101. The curvature is the slope of the flexural strain diagram of a beam. Concrete cracks when the tensile strain exceeds the rupture strain as defined by ACI 318 in equation 102 (Busel, 2008). For tensile strains below this rupture value, concrete is assumed to develop tensile stresses; figure 47 shows the strain-stress-force diagrams of such a situation. Figure 48 shows similar diagrams for a cracked section.

$$M = (EI)\phi \tag{101}$$

$$\text{where, } \phi = \frac{\delta^2 v}{\delta x^2}$$

$$\varepsilon_{rup} = \frac{7.5\sqrt{f_c'}}{E_c} \tag{102}$$

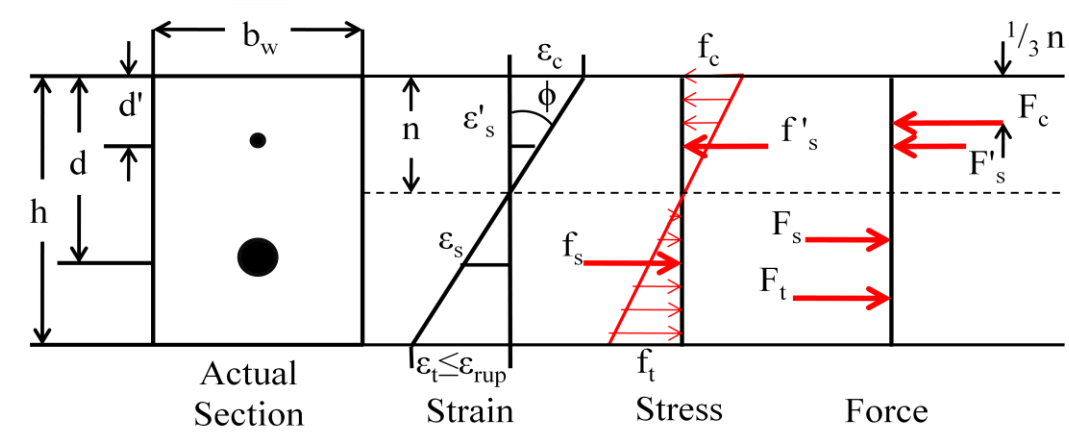

Figure 49. Strain-stress-force distribution of uncracked rectangular section

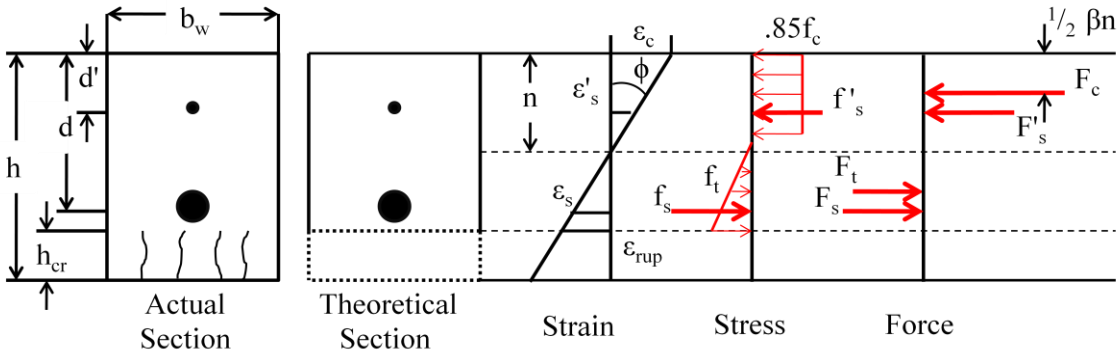

Figure 50. Strain-stress-force distribution of cracked rectangular section

In order to find the equivalent moment of inertia for any loading scheme, it is necessary to determine the relationship between applied moment and resulting beam curvature. In order to accomplish this, consider the beam section shown in figure 49.

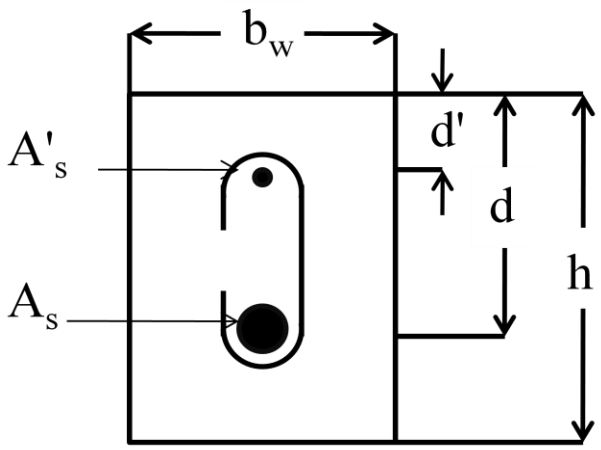

Figure 51. Typical rectangular section of flexural beam

The moment capacity and corresponding curvature of this section can determined for different loads. The first scenario occurs when cracking of the bottom face is imminent. The neutral axis is found using the transformed section of the uncracked section, expressed in equation 103. The strains of the concrete and reinforcing steel are found in terms of the rupture strain using linear variation, given below as equations 104 though 106.

$$n = \frac{A_c y_c + \frac{E_s}{E_c}(A_s y_s + A'_s y'_s)}{A_c + \frac{E_s}{E_c}(A_s + A'_s)} \tag{103}$$

$$\varepsilon_c = \varepsilon_{rup}\left(\frac{n}{h-n}\right) \tag{104}$$

$$\varepsilon_s = \varepsilon_{rup}\left(\frac{d-n}{h-n}\right) \tag{105}$$

$$\varepsilon'_s = \varepsilon_{rup}\left(\frac{n-d'}{h-n}\right) \tag{106}$$

Each stress component and respective resulting force are given by equations 107 through 112.

$$f_s = \varepsilon_s E_s \quad (107)$$

$$f_s' = \varepsilon_s' E_s \quad (108)$$

$$F_s = f_s A_s \quad (109)$$

$$F_s' = f_s' A_s' \quad (110)$$

$$F_t = \frac{1}{2} f_r b_w (h - n) \quad (111)$$

$$F_c = F_s + F_t - F_s' \quad (112)$$

The moment capacity and curvature of the uncracked section is expressed by equations 113 and 114, respectively.

$$M_n = F_c\left(h - \frac{n}{3}\right) + F_p\left(t_p + \frac{t_p}{2}\right) + F_s'(h - d') - F_t\left(\frac{h - n}{3}\right) - F_s(h - d) \quad (113)$$

$$\phi = \arctan\left(\frac{\varepsilon_s}{n}\right) \quad (114)$$

To find the moment, curvature, and effective moment of inertia values for cracked sections, the following strategy was followed:

Step 1 – Assume steel stress and crack height; use the assumed stress to find the resulting tensile force in the reinforcing steel. Using a relationship found using

linear variation, the strain of the top steel is expressed in terms of the depth of the neutral axis.

Step 2 – Define F_t and F_c; for any given loading, the tensile and compressive forces of the concrete are defined by equations 115 and 116.

$$F_t = \frac{1}{2} f_r b_w (h - n - h_{cr}) \qquad (115)$$

$$F_c = (.85 f_c') \beta n b_f \qquad (116)$$

Step 3 – Neutral axis solution; enforcing equilibrium of forces results in a polynomial equation from which the neutral axis depth is found.

Step 4 – Strain check; using linear variation relationships the strains of the top reinforcing steel and compressive strain of the concrete are found. If the strain of the reinforcing steel is greater than the value of yielding and/or the top strain of the beam is greater than the allowable value of 0.003, then the process is repeated again incorporating the yield strain of the top steel or crushing strain of the concrete.

Step 5 – Find crack height; the depth below the neutral axis at which the modulus of rupture is located using the linear variation relationship expressed in equation 117. The crack height is then calculated using equation 118.

$$d_{rup} = \frac{\varepsilon_r}{\varepsilon_c} n \quad (117)$$

$$h_{cr} = h - n - d_{rup} \quad (118)$$

Step 5 – Solution convergence; update concrete tensile equation with crack height value obtained and repeat the process from first step. Iteration continued until the percent difference of the crack height value between iterations is less than one percent.

Step 6 –Moment and curvature solution

Once the crack height is confidently determined, the moment capacity of the cracked section is found using equation 119, where β is defined by ACI 318 (Busel, 2008). The curvature of the deflected shape is calculated using equation 101.

$$M_n = F_c\left(h - \frac{\beta n}{2}\right) + F_p\left(t_p + \frac{t_p}{2}\right) + F_s'(h - d') - F_t\left(\frac{h - n}{3}\right) - F_s(h - d) \quad (119)$$

The moment curvature values obtained by the above scheme are a function of material properties. In the present study, the reinforcing steel was taken as Grade 60 and the concrete compressive strengths varied from 5 to 7 ksi, so as to capture the reinforced concrete beams cast for the research project. Three sets of moment-curvature plots were derived, corresponding to 5, 6, and 7 ksi. Tables 16 through 18 show the variation of the effective moment of inertia according to beam curvatures. Figures 52 and 53 show the

moment-curvature relationships and the effective moment of inertia-curvature relationships. Table 19 gives the best fit relationships between the effective moment of inertia and curvature.

Table 16. Moment-curvature relationship for flexural beam and f'c = 5000

n (in)	h_{cr} (in)	M_n (lb-in)	ϕ	EI_b (lb-in^2)	I (in)^4
3.0298	0.0000	0.0	0.0	259559750.3	81.94
3.0298	0.0000	12762	0.000043201	295409828.5	81.94
0.8710	4.930	33208	0.000661194	50224296.3	13.93
1.0224	4.9327	45184	0.002934264	15398751.4	4.27

Table 17. Moment-curvature relationship for flexural beam and f'_c = 6000

n (in)	h_{cr} (in)	M_n (lb-in)	ϕ	EI_b (lb-in^2)	I (in)^4
3.0269	0.0	0.0	0.0	259559750.3	72.00
3.0269	0.0	13895	0.000043247	321293962.6	89.12
0.7334	5.0588	34554	0.000633379	54555039.6	15.13
0.852	5.1068	46244	0.003169003	14592600.0	4.05
0.8518	5.1109	46242	0.003521939	13129699.5	3.64

Table 18. Moment-curvature relationship for flexural beam and f'_c = 7000

n (in)	h_{cr} (in)	M_n (lb-in)	ϕ	EI_b (lb-in^2)	I (in)^4
3.0247	0.0	0.0	0.0	259559750.3	72.00
3.0247	0.0	14937	0.000043283	345100847.9	95.73
0.6333	5.1526	35510	0.000614543	57782794.6	16.03
0.731	5.2201	47011	0.002735971	17182563.4	4.77
0.7299	5.2381	46998	0.004110129	11434677.8	3.17

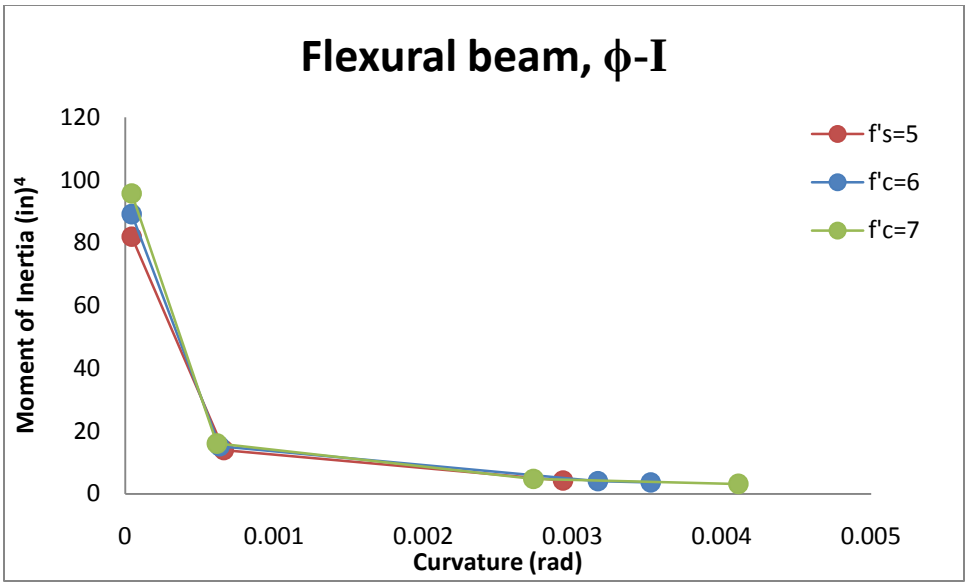

Figure 52. Relationship between curvature and moment of inertia

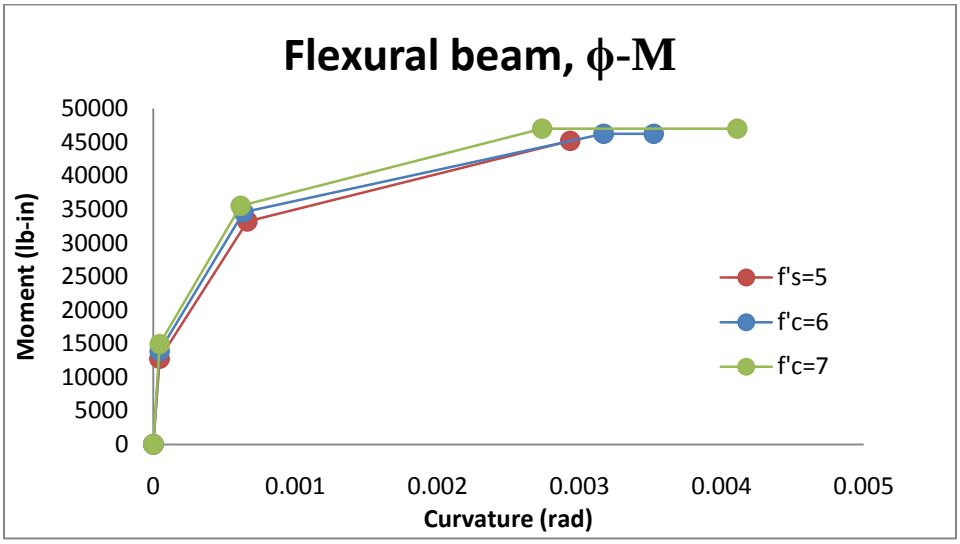

Figure 53. Relationship between curvature and moment

Table 19. Equations relating curvature and moment of inertia

Concrete Strength	5000 (psi)	6000 (psi)	7000 (psi)
Relationship	$I = 0.0791(\phi)^{-0.694}$	$I = 0.0637(\phi)^{-0.726}$	$I = 0.0592(\phi)^{-0.741}$
R^2	0.9972	0.9968	0.9962

Verification

Verifying the models is simple to accomplish; the mechanistic model is utilized to find the deflection of both a steel beam and reinforced concrete beam with no composite patch under an arbitrary load. The number of terms used to describe the deflection was varied from a one to three. The deflections of the same beams under similar loadings are calculated using Euler-Bernoulli beam theory. The results of both solution strategies are given in tables 20 and 21. Additionally, displayed in the table is the percent difference between the two solutions schemes.

Table 20. Verification of steel mechanistic model with Euler-Bernoulli beam theory

	Deflection	% difference
Beam Theory	0.1328270	
Mech. Model w/ 1 term	0.13188687	0.708
Mech. Model w/ 2 terms	0.13289007	-0.048
Mech. Model w/ 3 terms	0.13289015	-0.048

Table 21. Verification of reinforced mechanistic model with Euler-Bernoulli beam theory

	Deflection	% difference
Beam Theory	0.02356284	
Mech. Model w/ 1 term	0.02336633	0.834
Mech. Model w/ 2 terms	0.02357009	-0.031
Mech. Model w/ 3 terms	0.02358004	-0.073

The results show that the mechanistic model coincides well with Euler-Bernoulli beam theory. Defining the displacement variable with a single term for either steel or concrete models yields results within one percent of respective beam theory value.

Chapter IV

FRP DESIGN AND APPLICATION PROCEDURE

Design Philosophy

Currently, there is no accepted design code for retrofitting civil engineering structures externally with FRP composite materials. There are several guidelines developed by well-known and trusted civil engineering institutions. However, these preliminary guides require improvement. This research project is an attempt toward that goal.

Developing a design procedure in the practice of civil engineering bears the great responsibility of public well being. Given this burden, several important design considerations and recommendations are considered to avoid hubris while creating an effective and economic FRP composite solution. The considerations and recommendations are given as follows.

Considerations:

1. Identification and implementation of a series of coefficient resistance factors. Such factors account for uncertainties in physical and mechanical properties of the composite system materials, construction quality, and long-term performance. The ACI and NCHRP recommended design procedures discussed in Chapter I use resistance factors, but the values do not coincide. A scarcity of data and lack of manufacturing standardization are the main culprits that such factors have not

been confidently determined. Consequently, a value of 0.9 was chosen and implemented; this value was a discretionary choice. This effort was primarily made to create conservatism and confidence in composite patch design.

2. Retrofitting a structure presents the unique opportunity to restore, or even improve, the performance and capacity of existing structures. The motif of this research project is to investigate the value and performance of FRP composites to retrofit damaged bridge superstructures. With such a charge, the design procedure includes the ability for design engineers to increase the nominal capacity of the damaged structure with externally bonded composite systems. Given the task at hand, an increase of ten percent in capacity was chosen and implemented.
3. Previous research into composite patch repairs applied to the tensile face of beams typically applies the composite systems along the length of the beam substrate. In contrast, the design procedure presented in this research project provides composite material only where it is required because of inadequate moment capacity. The length of the composite patches is based on theoretical moment cut-off points and required stress capacity based development length. Limiting the length of composite materials avoids several common composite failure modes, including critical diagonal crack debonding with or without concrete separation, plate end interfacial debonding, and concrete cover separation at plate ends. These failure modes were discussed in chapter I.
4. Several empirical formulas and models have been developed to describe the shear behavior of composite adhesives (Teng and Cheng, 2009). Such characterizations

were seriously contemplated for use in this research project, but were ultimately abandoned for a more intuitive and reliable solution. The results of the adhesive testing explored in Appendix B were utilized to define the adhesive shear bond behavior and capacity.

5. Current design guidelines utilize semi-empirical formulas in the design process. The process developed for this research project is based solely on sound and well understood mechanics. Utilizing mechanics familiar to civil engineering creates confidence in the design results and is suitable for adoption in practice.
6. The design procedure presented in this research project does not consider layering the composite fibers or prestressing the fibers. This choice was made for the sake of simplicity.

In addition to the considerations implemented in the design procedure, several recommendations are suggested. These recommendations ensure conservatism in the designs and public safety. However, for the sake of research, these recommendations were examined

.

Recommendations:

1. Any member being reinforced with FRP composite should have some significant residual strength. This residual capacity should be sufficient to resist service loads so in the event of FRP composite system failure, the remaining existing structure will not fail in tandem. Any member, or more importantly structure system, should not fail in tandem or because of composite failure.

2. Development lengths calculated should be increased by some amount to account for long term creep and slippage. This is not implemented in the research presented for two specific reasons. The first being the experimental tests conducted in this research project are considered short term strengthening of beams with composites. The second is insufficient research into the nature of long term bond behavior so that a confident suggestion of elongation cannot be made. One paper of the research literature review investigates the effects of aging on the behavior and capacity of adhesives used to bond composites together (Diab and Zhishen, 2008).

The general design procedure uses the sum of forces and moment to find the force required of the composite patch resulting from the applied forces and moment. This force is then used to find the composite dimensions. In order to safely implement composite materials to strengthen in field civil super-structures, the existing, or residual capacity of the beam must be determined.

Flexural Composite Patch Procedure

In practice, the design engineer must determine the moment capacity of the beam in relationship to the ultimate applied moment from AASHTO bridge design code. If the existing bridge superstructure has occurred damaged, the purpose of composite patch retrofitting is to restore the capacity of the beam. When such damage is caused from

overloading or increased traffic use, the retrofitted beam capacity should exceed that of the original nominal capacity.

To investigate the ability of composite repair systems to proficiently restore and strengthen bridge superstructures, the nominal capacity of the retrofitted experimental beams was decided to be ten percent higher than the original capacity of the existing beam. This is demonstrated by equation 120.

$$1.1(M_n)_{original} = (M_n)_{repaired} \geq M_u \qquad (120)$$

The composite section is easily designed by first applying equilibrium of moments about the location of the force developed by the composite patch. This allows the designer to isolate and solve the resulting compression and tensile forces of the beam to be expressed in terms of applied moment. Then, applying equilibrium of forces allows the designer to solve for the force of the composite patch. The thickness of the composite patch is known in advanced and the width is found using the available capacity of the composite fibers. Design procedures for retrofitting beams with composite patches bonded to the tensile face of beams are illustrated for steel, reinforced concrete, and prestressed concrete beams in the following sections.

Steel Beams

The necessary assumptions before the beginning the design process includes:

- Beam has reached plastic moment capacity

- The loss of beam section is limited to either the flange or the web
- A perfect bond exists between the composite materials and steel substrate
- The same composite system is used for both web and flange repair as expressed in equation 121.

$$(t_p)_{web} = (t_p)_{flange} = t_p \qquad (121)$$

Consider the steel beam in figure 54. In the event of web, the composite patch is supplied symmetrically on either side of the web; similarly, flange loss is restored with composite patches placed on the bottom of the flange, the notation used in figure 54 is similar to that used by AISC.

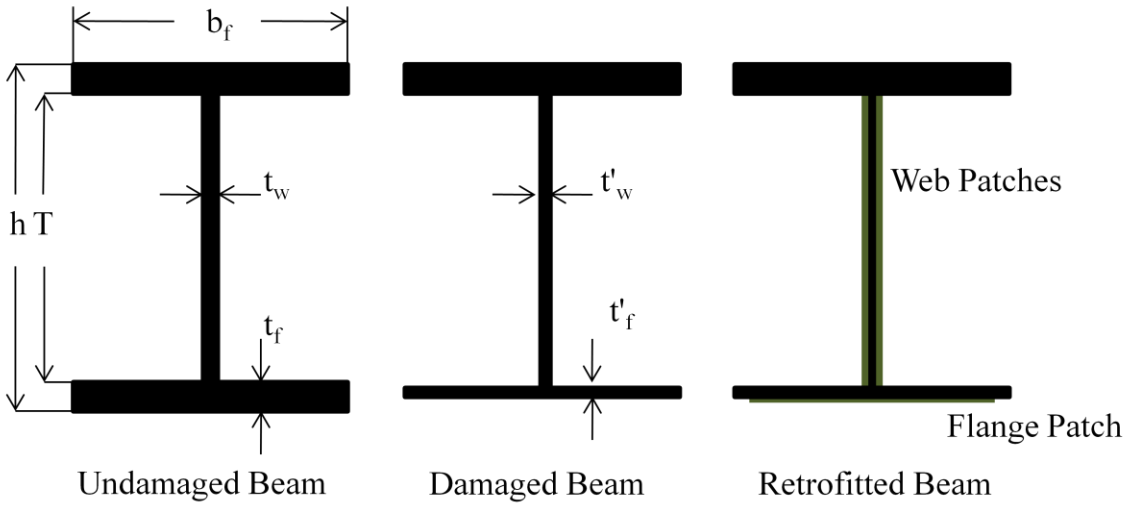

Figure 54. Steel beam section loss and repair

It is assumed that composite patches applied to the web will have a height equal to the distance between fillets, as shown in figure 55, so that the area of the two web patches is given by equation 122.

$$(A_p)_{web} = Tt_p \qquad (122)$$

Before applying equilibrium of moments, the retrofitted beam is decomposed into a series of expressions, from which the moment capacity can be defined, as illustrated in figure 55. Each case depicted has a respective moment capacity, given by equations 124 through 127, which the design engineer can add, subtract, or ignore in order to accurately describe the retrofitting scenario necessary. This is demonstrated by equation 123.

$$(M_n)_{repaired} = [(M_n)_I + (M_n)_{II} + (M_n)_{III} + (M_n)_{IV}] \quad (123)$$

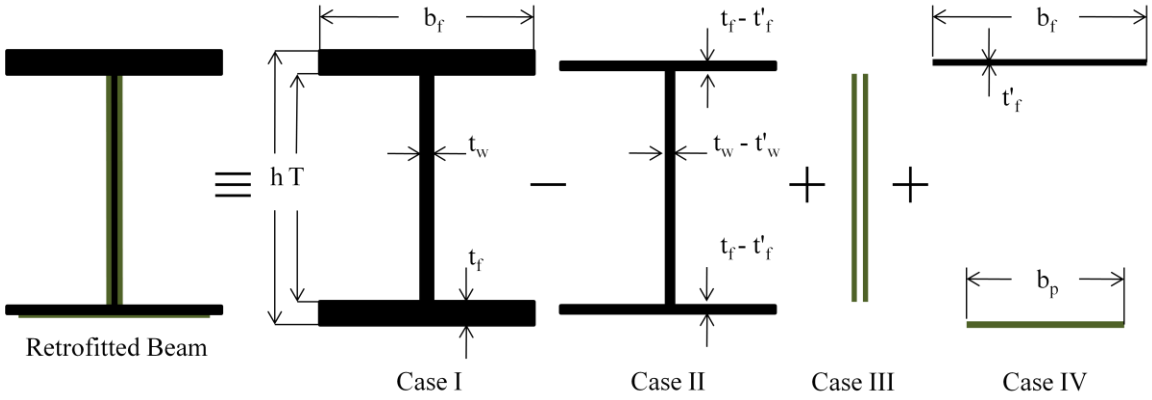

Figure 55. Case decomposition of moment capacity calculation

Case I: Moment capacity of originally undamaged steel beam

$$(M_n)_I = ZF_y \qquad (124)$$

Case II: Moment capacity of damaged beam. The thicknesses of both flanges and web have been reduced. For convenience, the top flange also has a reduced thickness, equal to that of the bottom flange.

$$(M_n)_{II} = \left[b_f(t_f - t_f') + \frac{1}{6}(t_w - t_w')T^2\right] \quad (125)$$

Case III: Moment capacity contributed by composite patch placed along web.

$$(M_n)_{III} = \frac{1}{3}t_p T^2 f_p \quad (126)$$

If the composite patch is considered thin, the moment resistance provided by the web patch can be ignored because the compression capacity and behavior of the fibers are not well established.

Case IV: Moment capacity contributed by composite patch bonded to tensile flange and replacement of top flange section removed for Case II.

$$(M_n)_{IV} = F_p\left[h - \frac{1}{2}\left((t_f - t_f') + t_p\right)\right] \quad (127)$$

The force of the patch can be solved for directly using equation 120. The patch dimensions are calculated using procedures detailed later in this chapter.

Reinforced Concrete Beams

A few assumptions concerning the beam and the composite materials are as follows:

- Tensile strength of concrete is ignored
- Concrete compressive stress is modeled with a Whitney stress block
- A perfect bond exists between the composite and steel substrate
- The stress experienced by the reinforcing steel may be one of the following possibilities:
    - Both top and primary reinforcing steel has yielded
    - Only primary reinforcing steel has yielded
    - Both top and primary reinforcing steel remain elastic

Consider a reinforced beam with both top and primary reinforcing steel. If the top and primary steel has yielded and concrete reached its crushing strain, as shown in figure 56, the forces acting on the section can be expressed as equations 128 through 130. The depth of the center of the patch is given by equation 131.

$$F_c = (0.85f_c')b_w\beta n \quad (128)$$

$$F_s = A_s f_y \quad (129)$$

$$F_s' = A_s' f_y \quad (130)$$

$$d_p = h + + \frac{t_p}{2} + t_a \quad (131)$$

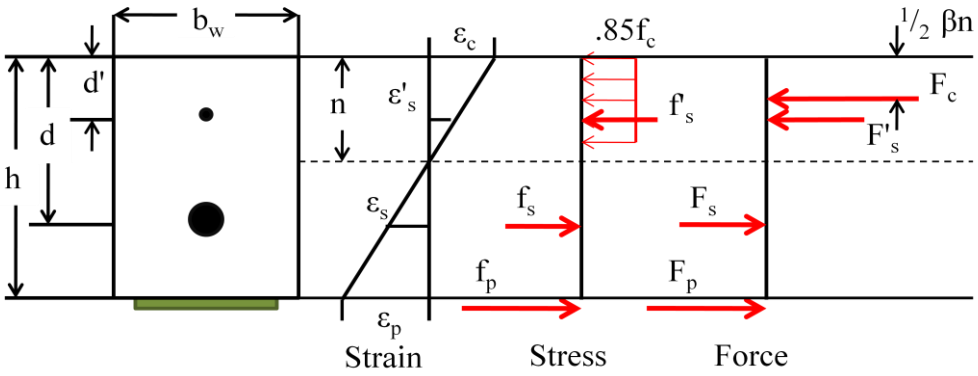

Figure 56. Strain, stress, and force diagram for patched flexural beam

Summing the internal forces about the center of the composite parch yields the nominal moment capacity, as expressed by equation 132.

$$(M_n)_{repaired} = F_c\left(d_p - \frac{\beta n}{2}\right) + F'_s(d_p - d') - F_s(d_p - d) \quad (132)$$

Substituting the definition of each force and rearranging the expression leads to equation 133 which is a simple quadratic expression for the neutral axis, as given by equation 134.

$$0 = n^2 - \frac{2d_p}{\beta}n + 2\left[\frac{M_u + A_s f_y(d_p - d) - A'_s f_y(d_p - d')}{0.85 f'_c b \beta^2}\right] \quad (133)$$

$$n = \frac{2d_p}{\beta}\left[1 - \sqrt{1 - \frac{M_u + A_s f_y(d_p - d) - A'_s f_y(d_p - d')}{0.85 f'_c b d_p^2}}\right] \quad (134)$$

With a known neutral axis location, the strains in the top and primary reinforcing steel can be calculated using equations 135 and 136 which are based on simple linear variation. If the strain values are not equal to or exceed yielding strain, the force

developed by the top and primary reinforcing steel can be calculated using 134 and 135. Substituting the force definitions of equations 137 and 138 yields a cubic equation which can similarly be solved for to find the depth of the neutral axis.

$$\varepsilon_s = 0.003\left(\frac{d - n}{n}\right) \tag{135}$$

$$\varepsilon_s' = 0.003\left(\frac{n - d'}{n}\right) \tag{136}$$

$$F_s = A_s E_s \varepsilon_s \tag{137}$$

$$F_s' = A_s' E_s \varepsilon_s \tag{138}$$

Once a neutral axis depth has been determined, the force required of the composite patch can be found enforcing equilibrium of forces, as given by equation 139. Dimensioning of the patch is described later in the chapter.

$$F_p = F_c + F_s' - F_s \tag{139}$$

Prestressed Concrete Beam

The same methods of summing moment and forces are used to find the load required of the patch. Consider the prestressed beam in figure 57, of which similar assumptions are made to those of the reinforced concrete beam.

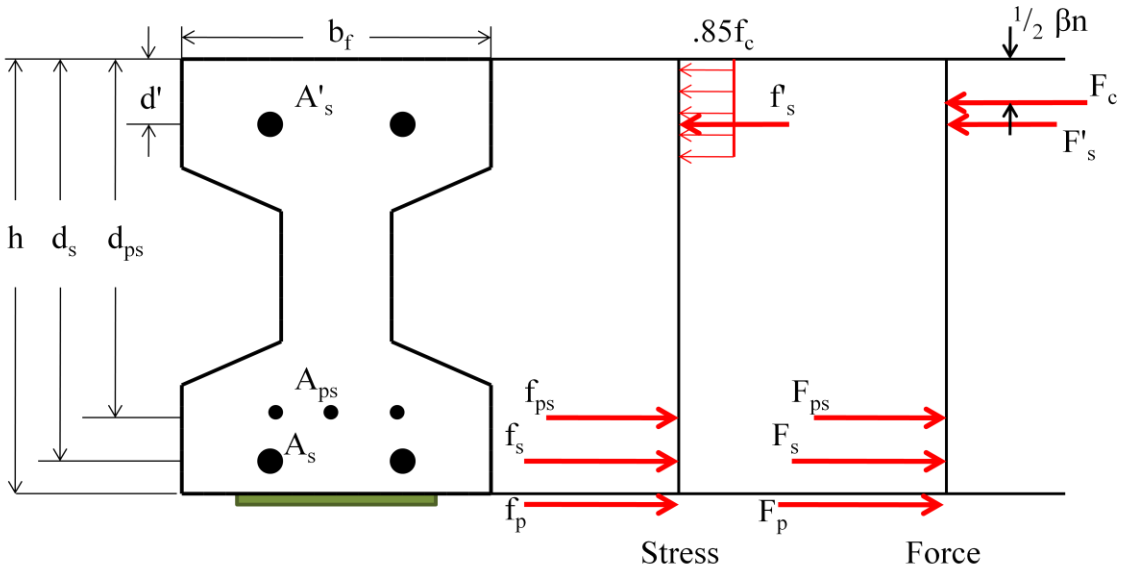

Figure 57. Stress and force diagrams for prestressed concrete beam

Examining the figure, it is obvious that the beam is composed of reinforcing steel both in the top and bottom flange in addition to the prestressing strands in the bottom flange. Equations 140 though 143 define the forces resulting from each component.

$$F_c = (0.85f'_c)b_f\beta n \quad (140)$$

$$F'_s = A'_s f'_s \quad (141)$$

$$F_s = A_s f_s \quad (142)$$

$$F_{ps} = A_{ps} f_{ps} \quad (143)$$

The depth of the neutral axis and the stress of the prestressing strands are found using an iterative process. This procedure detailed below is valid for rectangular, bulb tee, and T-beams when concrete compression is confined to the flange. A similar

procedure must be performed if the compression block exceeds the boundary of the flange.

1. Assume an initial value for the parameter α, which is simply the ratio of the prestressing stress to the mild steel yield stress, as defined in equation 144. A typical assumption is a between 3 or 4.

$$\gamma = \frac{f_{ps}}{f_y} \qquad (144)$$

2. Determine the depth of the centroid of the tensile steel areas, $\bar{d}$.

$$\bar{d} = \frac{\gamma A_{ps} d_{ps} + A_s d_s}{\alpha A_{ps} + A_s} \qquad (145)$$

3. Determine steel ratios and indices; assume yielding and verify later

$$\rho_{ps} = \frac{A_{ps}}{b\bar{d}} \Rightarrow \omega_{ps} = \rho_{ps} \frac{f_{ps}}{f'_c} \qquad (146), (147)$$

$$\rho_s = \frac{A_s}{b\bar{d}} \Rightarrow \omega_s = \rho_s \frac{f_s}{f'_c} \qquad (148), (149)$$

$$\rho'_s = \frac{A'_s}{b\bar{d}} \Rightarrow \omega'_s = \rho'_s \frac{f'_s}{f'_c} \qquad (150), (151)$$

4. Determine the prestressing strand stress

$$f_{ps} = f_{pu}\left\{1 - \frac{\gamma_{ps}}{\beta_1}\left[\rho_{ps}\frac{f_{pu}}{f'_c} + \frac{d}{d_p}(\omega_s - \omega'_s)\right]\right\} \qquad (152)$$

The force of prestressing force can be calculated using equations 152. The nominal moment expression can be written as equation 153.

$$\begin{aligned}(M_n)_{repaired} &= F_c\left(d_p - \frac{\beta n}{2}\right) + F'_s(d_p - d') - F_s(d_p - d_s) \\ &\quad - F_{ps}(d_p - d_{ps}) \qquad (153)\end{aligned}$$

Substituting the definition of each force and rearranging the equation in relationship to equation 154 leads to a simple quadratic expression for the neutral axis, as given by equation 155.

$$0 = n^2 - \frac{2d_p}{\beta}n + 2\left[\frac{M_u + A_s f_y(d_p - d) - A'_s f_y(d_p - d') - F_s(d_p - d_s)}{0.85 f'_c b \beta^2}\right] \qquad (154)$$

$$n = \frac{2d_p}{\beta}\left[1 - \sqrt{1 - \frac{M_u + A_s f_y(d_p - d) - A'_s f_y(d_p - d') - A_{ps} f_{ps}(d_p - d_s)}{0.85 f'_c b d_p^2}}\right] \qquad (155)$$

With a known neutral axis depth, the strain values of the steel reinforcement can be calculated using a linear variation similar to that derived in the reinforced concrete beam section based on the design strain of concrete crushing. If any strain values are not equal to the respective assumed values, the above process should be iterated until satisfactory convergence is accomplished.

With the converged solution of the neutral axis depth, the force of each component can be calculated using equilibrium of forces, specifically the magnitude of the force exerted by the composite patch.

$$F_p = F_c + F_s' - F_{ps} - F_s \tag{156}$$

Shear Composite Patch Procedure

FRP application for reinforcing beams in shear is unlike flexural reinforcing. There is no single course of action which can be repeated independent of the substrate materials. Shear deficiency is more common among concrete beams; subsequently significant attention has been paid to reinforcing concrete beams with externally bonded composite patches. In accordance with the first design consideration the final capacity of the member after composite application is ten percent greater than the original design strength, as demonstrated by equation 157.

$$1.1(V_n)_{original} = (V_n)_{repaired} \geq V_u \tag{157}$$

Steel Beams

The design procedure for shear reinforcement of steel beams was first discussed in the flexural design procedure and is expanded upon in more detail in this section. Similar to the analysis of steel, the shear strength of the composite patch is related to the

minimum tensile strength based on von Mises yield criterion, as expressed in equation 158.

$$f_p' = \frac{f_p}{\sqrt{3}} = 0.577 f_p \qquad (158)$$

As such, the shear capacity of the patch design from the flexural design section of steel can be shown as equation 159.

$$(V_n)_{repaired} = 0.6F_y[(dt_x) - (Tt_w')] + .577f_p'(2Tt_p) \quad (159)$$

Reinforced Concrete Beams

The design procedure presented is very similar to both the NCHRP and ACI design procedures outlined in Chapter I. Consider the shear reinforcing scheme shown in figure 58.

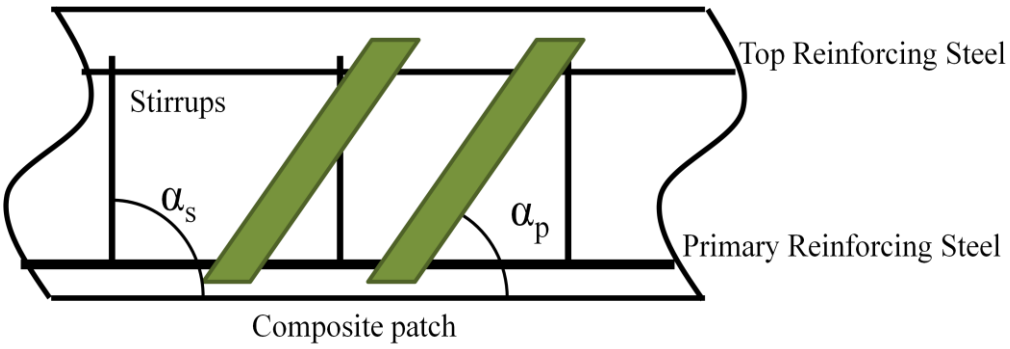

Figure 58. Typical shear reinforcing scheme

The resistance provided by the concrete and shear reinforcing stirrups is described by equations 161 and 162, which are similar to the definitions used by ACI 318 (Busel, 2008). The angle of traditional steel stirrup reinforcement is typically 90°.

$$V_u = V_c + V_s + V_p \tag{160}$$

$$V_c = 2\lambda\sqrt{f'_c}b_w d \tag{161}$$

$$V_s = A_v f_y(\sin(\alpha_s) + \cos(\alpha_s))\frac{d}{s} \tag{162}$$

The shear force required of the patch is found by applying the equilibrium of forces; demonstrated in equation 163.

$$V_p = V_u - (V_c + V_s) \tag{163}$$

For composite shear patch application with only a single strip on either side of the beam, the shear capacity is given by equation 164. If more than one strip of composite is placed along the beam, the capacity of those combined patches is expressed by equation 166. Rearranging the equations yields the force required of the patch, given by equations 165 and 167.

$$V_p = F_p \sin(\alpha_p) \tag{164}$$

$$\Rightarrow F_p = \frac{V_p}{\sin(\alpha_p)} \tag{165}$$

$$V_p = F_p\left(\sin\left(\alpha_p\right) + \cos\left(\alpha_p\right)\right)\left(\frac{d}{s}\right) \tag{166}$$

$$\Rightarrow F_p = \frac{V_p}{\left(\sin\left(\alpha_p\right) + \cos\left(\alpha_p\right)\right)}\left(\frac{s}{d}\right) \tag{167}$$

There is no distinction between the different reinforcing schemes, specifically wrapping, side plates, or U-jackets, in the above design procedure. Wrapping is not considered a suitable reinforcing scheme for two important reasons. First, completely wrapping a bridge beam may be impossible. Secondly, completely wrapped beams fail without warning, often explosively and catastrophically.

Both U-jackets and side plates are utilized in this research project, but no distinction is made between the schemes in design because of the symmetric nature of the applications. To expound on this, consider the cracked beam in figure 59 and the reinforcing schemes in figure 60.

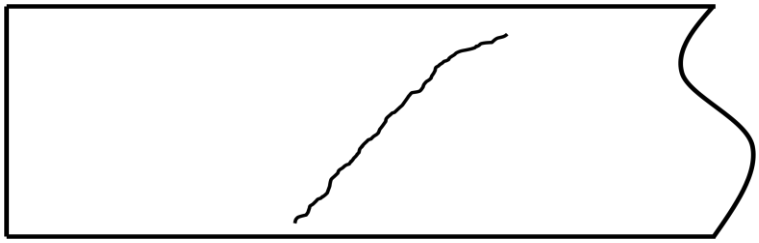

Figure 59. Typical concrete beam with shear crack

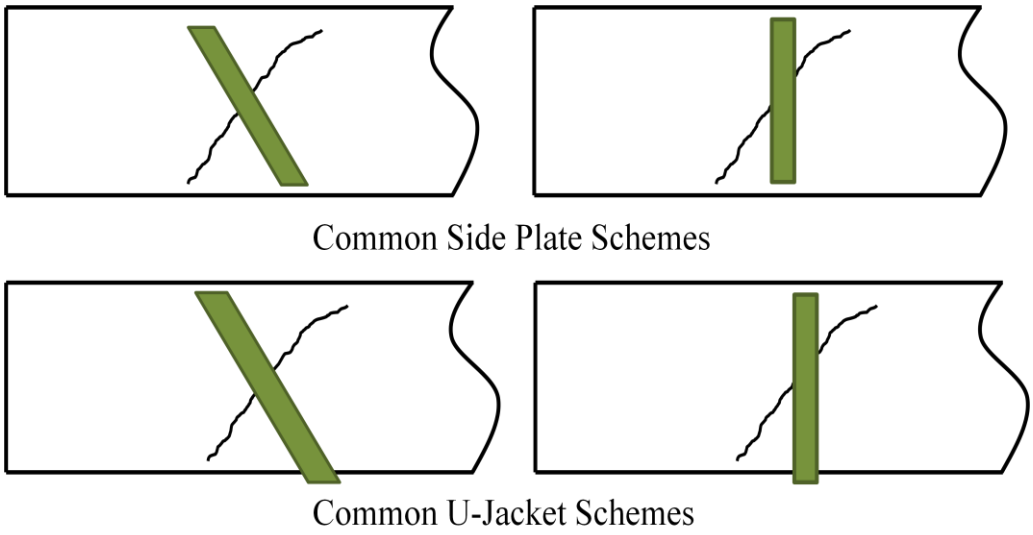

Figure 60. FRP composite reinforcing schemes

Debonding is the primary failure mode of side plate and U-jacket composite systems. Since the area of patch is equal on either side of the crack, it is equally probably that the patch area above or below the crack will debond. U-jacket applications extend the composite around the bottom of the beam, which decreases the likelihood of debonding failure by increasing the effective area of bond. This simply means that debonding is more likely to occur in the composite patch above the crack in the case of U-Jackets. However, having a higher probability of failure does not translate to a lower load carrying capacity. In this context, U-jacket and side-only applications of FRP composite can be considered as similar.

Prestressed Concrete Beams

The design procedure for prestressed beams is similar to that prescribed for reinforced concrete beams with the exception that the shear resistance of the concrete is defined in equation 168.

$$V_c = \left(.6\sqrt{f'_c} + 700\frac{V_u d}{M_u}\right) b_w d \qquad (168)$$

Dimensioning Composite Patch

The area and dimensions of the composite patch are easily found. The thickness dimension of the composite material is easily determined by simply measuring the material with accurate calipers or using the manufacturer supplied information.

The required width of the patch is determined using the tensile capacity of the composite fibers. The maximum tensile value is typically provided by the manufacturer, but can also be found through testing. For the sake of conservatism, only ninety percent of the ultimate tensile capacity of the composite is used. The required minimum width is determined using equation 169.

$$w_p = \frac{F_p}{(0.9f_{pu})t_p} \qquad (169)$$

For practical reasons, the width of the composite patch may be larger than that calculated using equation 169. Thin composite patches are prone to premature

debonding, but no detailed parametric research has been conducted into the composite patch proportions which result in such debonding. As such, the practical minimum width of two inches was chosen. The actual stress of the patch is calculated using equations 170.

$$f_p = \frac{F_p}{w_p t_p} \tag{170}$$

The length of the flexural composite patches is determined by the theoretical moment capacity requirements plus an additional development length to avoid delamination. The theoretical length is determined by the loss of moment capacity of the existing beam. The required length of the composite patch is based on the required moment based on the design moment envelop. Consider the beam shown in figure 61, subtracting the moment capacity of the loaded beam provides the underperformance of moment capacity. This loss must be compensated for by the patch.

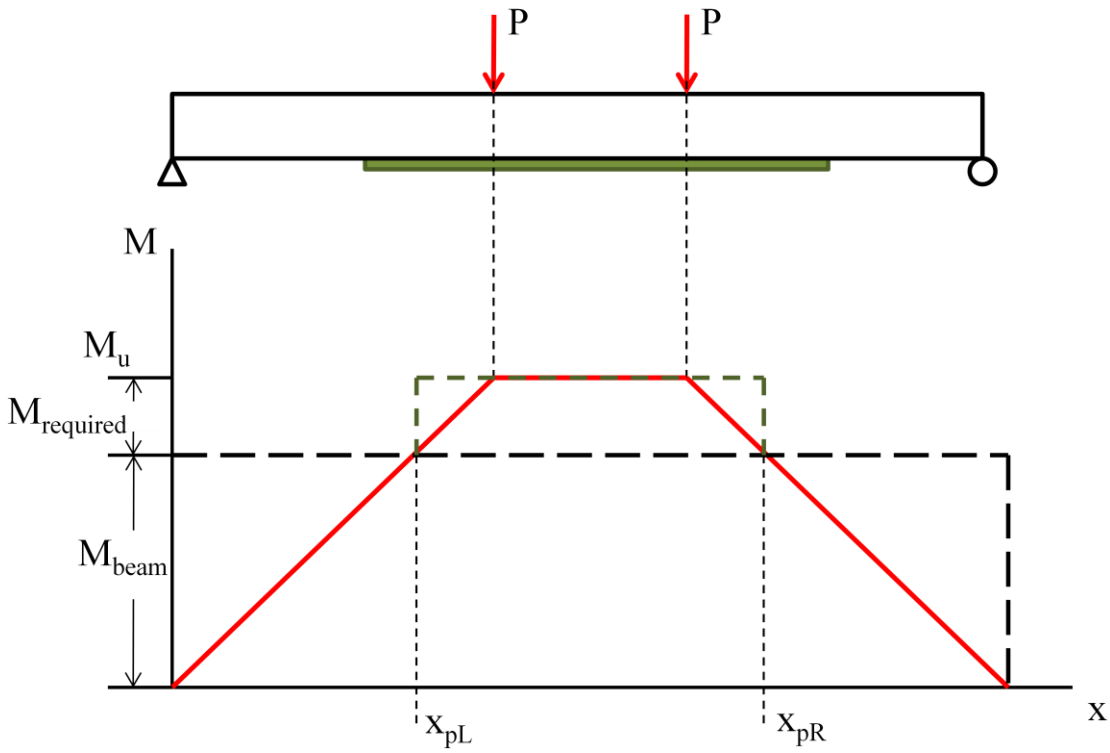

Figure 61. Required length of fully developed patch

From the diagram, the theoretical cut-off points are easily determined, as expressed in equation 171.

$$x_{pL} = \frac{M_{beam}}{P} \text{ and } x_{pL} = L - \frac{M_{beam}}{P} \qquad (171)$$

Reinforcement development is necessary of any reinforcing system. The development length is derived from equilibrium of forces which equates the force of the patch and the shear resistance of the adhesive. The bond stress distribution can be approximated with a triangle, as shown in figure 62.

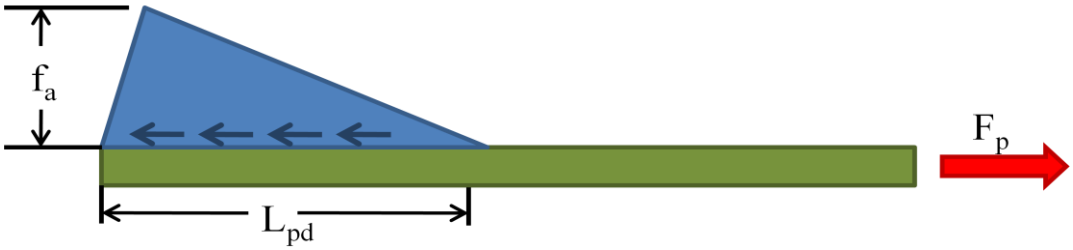

Figure 62. Stress distribution for developing composite force

The force of the adhesive is the product of the stress distribution and the area over which that distribution occurs. The adhesive strength is reduced by ten percent to be conservative in the design. The development length can be defined by equation 172.

$$L_{pd} = 2t_p\left(\frac{f_p}{0.9f_a}\right) \qquad (172)$$

Proper Composite Patch Application Procedure

The performance of FRP composite systems is dependent on the quality of workmanship in the application of the composite patch system. The unique nature of FRP composites results in several different applications procedures, which are typically supplied by the FRP composite manufacturers, see appendix A. Despite such variability, most application procedures can be separated into several common steps;

1. Surface preparation
2. Composite preparation
3. Adhesive mixing
4. Adhesive application

5. Composite application
6. Finishing

All the beam members were initially loaded before applying the composite patches. Pre-loading beams caused cracking and residual deformation. All the test beams were first flipped upside down to apply the composite system. This is analogous to jacking up bridge superstructures.

SikaWrap Hex 230/Sikadur 330

In the context of this research project, the sikawrap reinforcing systems were used to repair reinforced concrete beams in either flexure or shear, and prestressed concrete beams in shear. This composite system is an excellent choice for beams with unorthodox and complex geometries. Sikawrap is ideal for creating shear reinforcing wrapping and U-jackets schemes.

1. Surface Preparation

Sika prescribes a minimum surface concrete profile of 3 (CSP-3) defined by ICRI-surface-profile chips. Such specifications require that out of plane variations of the substrate surface should not exceed $^{1}/_{32}$ of an inch, and all contaminants should be removed, including dust, grease, oils, and waxes. The manufacturer suggests that substrates should be dry, but a saturated surface dry condition is acceptable.

Such strict guidelines can be accomplished in several ways. In the research project, the concrete surfaces were thoroughly brushed with a wire-hair brush. Both steel and brass wire brushes were used to accomplish a surface free of loose particles. Special attention was paid to cracks, pitts, and spalling and all loose materials surrounding such defects were carefully removed. Any sections that were suspect of being unsound were investigated by probing with a screwdriver.

After all the physical abrasion was completed, dust and any loose bits of material were brushed away. To ensure a particle free surface, a can of compressed air was used to blow any remaining undesirables free. Latex gloves were worn from this point on to protect the surface from oils and other contaminates that may be on the hands.

Figure 63 shows a concrete beam with several pits, cracks, and even light spalling. These defects caused out of plane variations of the substrate surface to be greater than $^{1}/_{32}$ of an inch, necessitating treatment. Such surfaces were treated with Sikadur 30, which when mixed with oven dry sands acts as a repair grout. Figure 64 shows the surface being filled with the epoxy grout.

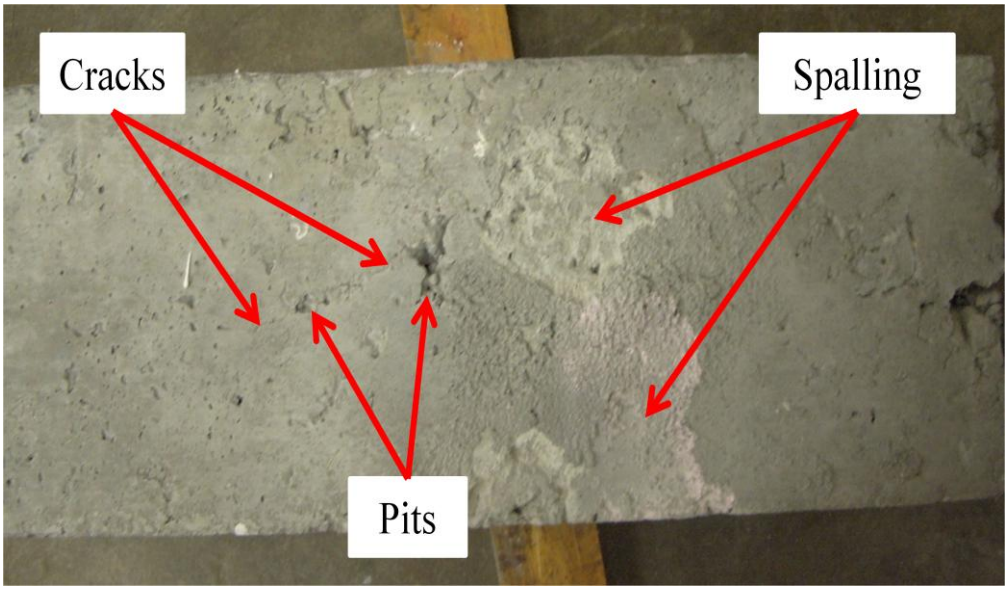

Figure 63. Inadequate concrete surface for composite application

Figure 64. Identical surface repaired with epoxy grout

2. Composite preparation

The composite material should also be clean before adhering it to the substrate surface. The best assurance that the fibers are clean is isolation from contaminants. In

this research project the fibers were kept stored in plastic until being cut, after which they were either kept in plastic or separated in a room away from all construction activities, including substrate preparation. The woven fibers were handled with gloved hands to prevent transferring oils, grease, or dirt.

In this research project, Sikawrap was cut by a utility knife with fresh, sharp blades. It is incredibly easy to cleanly cut the carbon fiber fabric with a sharp knife. A common problem when cutting Sikawrap is raveling of the fibers. A sharp edge will reduce the chance of damaging composite fibers when cutting them to correct dimension. In an effort to prevent this damage to the composite fibers, painters or masking tape was first placed along the center line of the proposed cut. This not only prevented the fibers from raveling, but also made accurate measurements simpler because the lines of the desired area are well defined. To achieve a clean cut, a steel ruler was placed along the length of the dimension lines to against which to rest the blade. Figure 65 shows all the tools used to cut Sikawrap. The white lines running perpendicular to the black carbon fibers are the nylon threads holding the fibers in place. Figure 66 shows the final product of two correctly dimensioned Sikawrap patches. Care was exercised when removing the tape from the fiber composite. If the tape is pulled haphazardly away, the fibers will fray very badly. Tape was pulled toward the edge of the fibers in the longitudinal direction. If removed properly, the tape will not affect the fiber direction or structure.

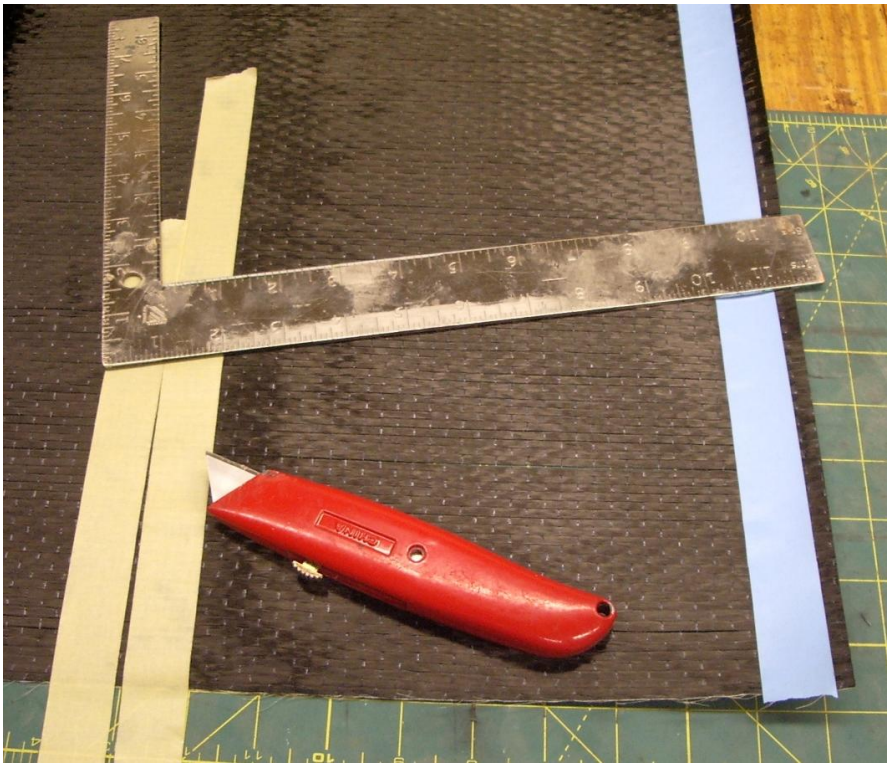

Figure 65. Tools used to cut Sikawrap

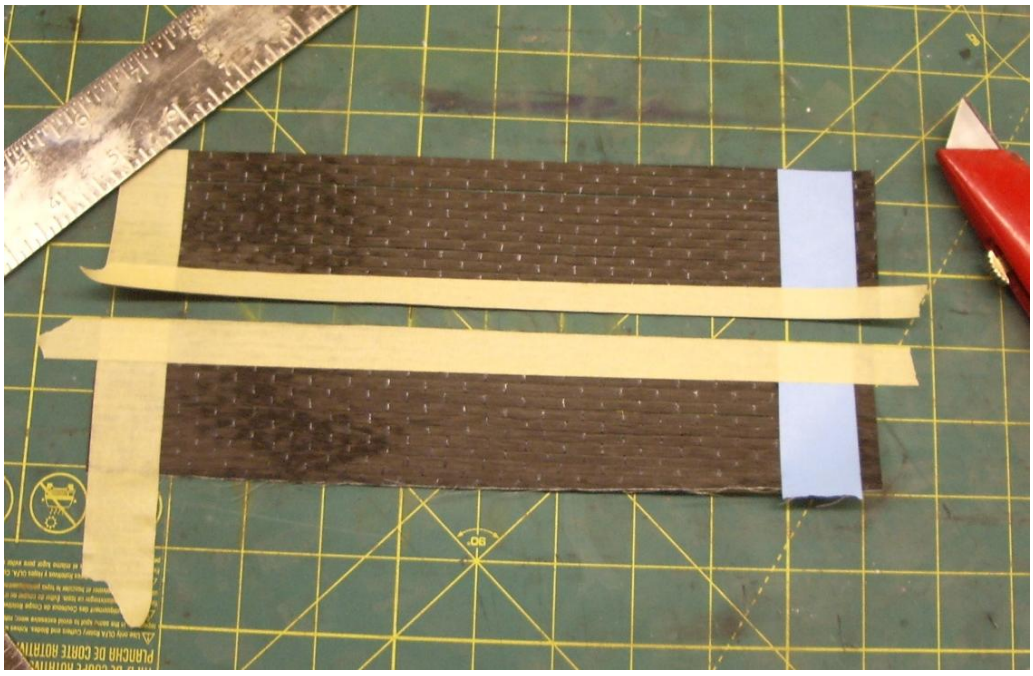

Figure 66. Final dimensioned Sikawrap patches

3. Adhesive Mixing

Sikawrap is a dry fiber system which requires impregnation of resin. The impregnating resin was measured and mixed according to the manufacturer instructions. Since composite adhesives and resin have a limited pot life, the adhesive was not mixed until the first two steps were completed and the job site was equipped with tools required by step 4.

4. Adhesive application

Before any adhesive was applied to the substrate, the surface was again blown free of any dust or dirt particles with a can of compressed air. The area of the patch was then outlined on the beam with a permanent marker. As discussed in Chapter II, Sikadur 330 is a low viscosity resin and was applied to the surface in small quantities to provide better control of the liquid. The manufacturer prescribed thickness of the adhesive is between 32 - 40 mils (0.032 - 0.04 inches). It is easily observed that the more thick the adhesive, the more opaque it appears. At a thickness of about 50 mils, about the thickness of a U.S. dime, the adhesive is nearly completely opaque. As a rule of thumb, the adhesive was applied to a thickness which retained some transparency. With a paddle like spatula as seen in figure 67, the adhesive was applied to an area slightly larger than the composite patch to ensure that the composite rested only on a bed of adhesive. The thin and runny nature of Sikadur 330 makes achieving a clean, uniform layer of adhesive very difficult. Figure 64 shows the adhesive being applied to the prestressed beam.

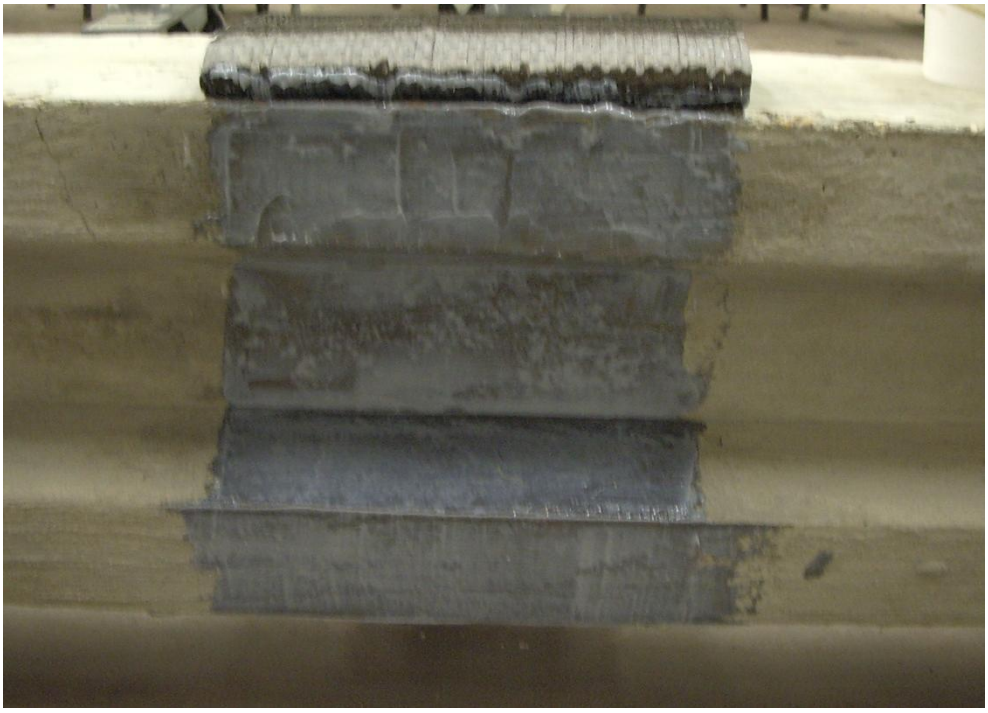

Figure 67. Applying Sikadur 330 to substrate

5. Composite application

Once a uniform layer of adhesive has been applied to the substrate, the composite fibers were placed. The fibers were carefully placed to ensure proper alignment within the desired borders and correct fiber orientation. Once the fibers were in the correct position on the substrate, they were gently embedded into the adhesive by hand, causing the resin to penetrate between the composite fibers. During this process, the adhesive may seep between the fibers, this is normal. A standard roller for such use was utilized to press the fibers further into the adhesive layer while also removing any trapped air. This will cause more adhesive to pass between the fibers to the surface. Figure 68 shows an example of the composite just after embedding the composite into the adhesive.

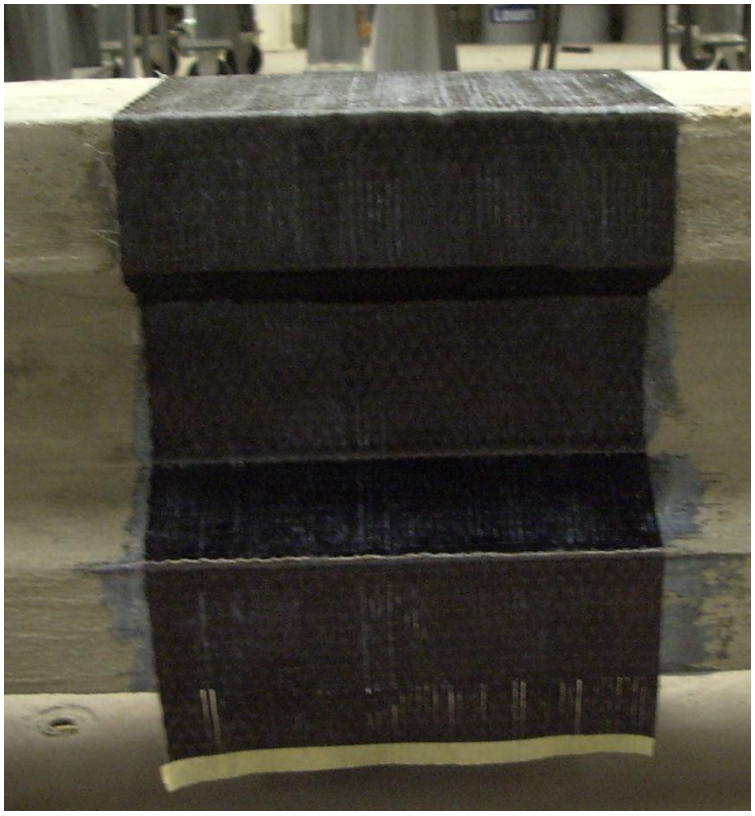

Figure 68. Composite fibers pressed into adhesive

6. Finishing

This step is required to properly secure the fibers to the substrate. Finishing also serves to protect the fibers from environmental corrosion and physical damage. This is achieved by simply applying a second layer of resin atop the woven fibers. This second layer should be relatively thin, about 10 mils (0.01 inches). It is very difficult to achieve a clean, uniform layer of adhesive because this protective layer is so thin. As a rule of thumb this layer should be thick enough to cover all the fibers and appear fairly transparent.

Figure 69 shows completed Sikawrap laminates applied to the tensile face of reinforced concrete beams. Note that the adhesive resin extends beyond the boundary of

the composite fibers. Observe that the finishing layer of resin is thin enough to see the fibers beneath it.

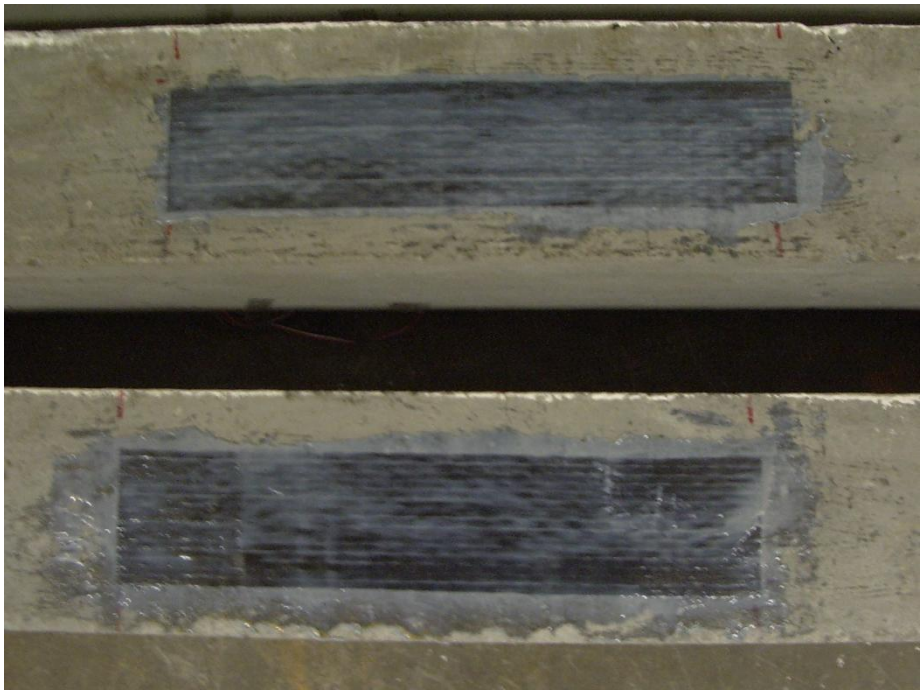

Figure 69. Completed Sikawrap composite patches

Figure 70 shows Sikawrap composites being used to strengthen a repair concrete beam in a U-jacket scheme. Figure 71 is a close up of the same patch crossing the shear cracks it bridges; the cracks are marked in green and red.

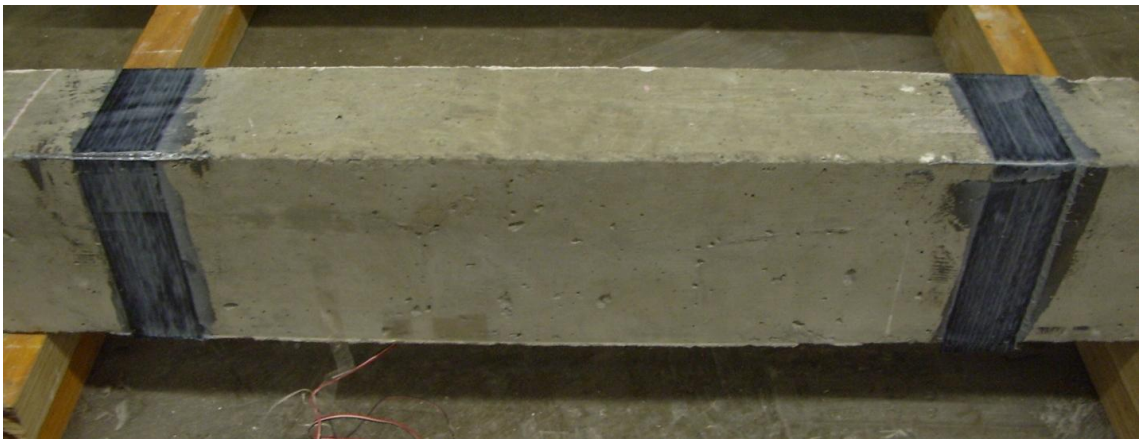

Figure 70. Example of Sikwrap as U-Jacket shear reinforcement

Figure 71. Close up view of Sikawrap reinforcement crossing shear cracks

Cardobur/Sikadur 30

Carbodur composite systems were used to repair reinforced concrete beams in flexure and shear, and prestressed concrete beams in flexure for this research effort. Figure 72 shows many of the necessary accessories to successfully apply a Carbodur

composite section. The can of compressed air removed any dust and dirt just before applying the adhesive and composite materials. The bottle of acetone was used to clean the composite patch just before applying epoxy.

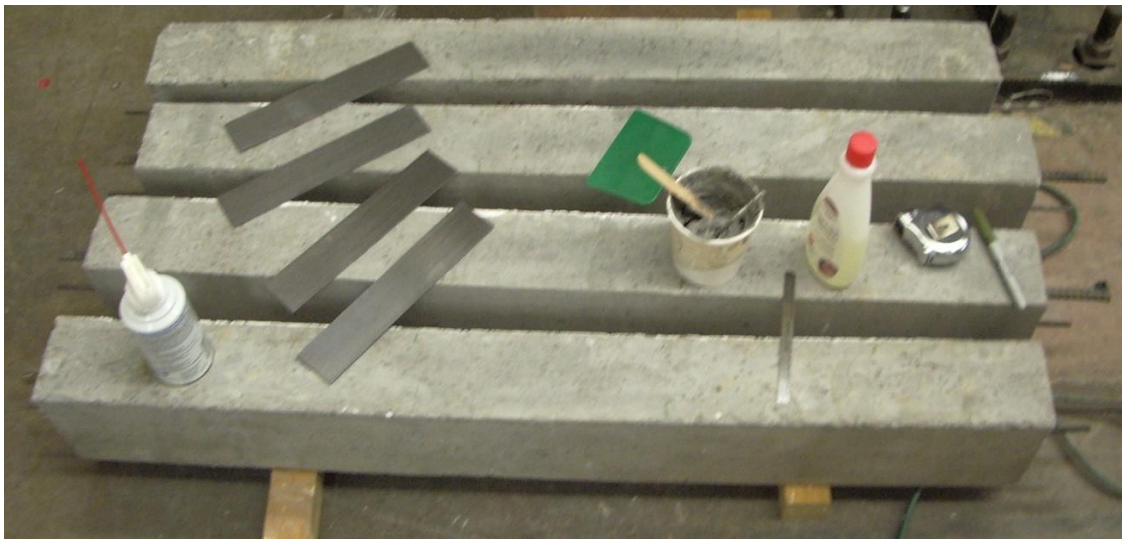

Figure 72. Necessary components to apply Carbodur composite patches

1. Surface preparation

The manufacturer suggests the same concrete surface preparation of CSP-3 for Sikadur 30. The procedures outlined in the above section were followed for the dry lay-up. One clear distinction between the systems is Sikadur 30 is moisture tolerant. Consequently, the substrate surface does not have to be dry. Despite this allowance, the test beams were prepared similarly to the Sikawrap specimens with the surface dry.

2. Composite preparation

Sika suggests cutting Carbodur with heavy shears, but purchasing heavy shears were not within the budget of the study, so alternative methods were implemented. The

first alternative attempted was to use a hacksaw as recommended by the manufacturer. Several different types of hacksaw blades were used; specifically blades with 18, 24, and 32 teeth per inch. Of these types, blades with 32 teeth per inch worked best at delivering clean and accurate cuts. As when sawing any fibrous material; special care must be taken not to fray the last fibers being sawed. A drawback to using a hacksaw to cut Carbodur is the carbon dust. As stated above, carbon dust should be avoided. Several methods were employed to contain or safely clean carbon dust. The best method was to use water to capture the dust and soak it up with paper towels, which were then disposed of in the trash. Gloves and long sleeves are suggested if a hacksaw is used, and additional measures should be taken to safely collect the dust after it is created. Ultimately, this technique was generally abandoned because containing the carbon dust was found to be too difficult.

A second alternative is similar to that utilized to cut Sikawrap. A utility knife was again used to cut the material to dimension. Carbodur is a tough, durable material and will dull razor blades very quickly. Several blades were required to effectively and cleanly cut a foot length section of Carbodur parallel to the fibers, and substantially more to cut perpendicular to the fibers. Figure 73 shows a Carbodur patch being cut to dimension. A silver permanent marker works well to mark the boundaries, and a stiff board or strip of metal ensures a clean edge to rest the utility blade against. It is tempting to simply snap Carbodur along the longitudinal direction to create the necessary width. This should be avoided because it will likely splinter the fibers chaotically. Splintered fibers will damage the laminate and reduce the capacity of the composite.

Figure 73. Typical cutting method for Carbodur patch

The specimens were cleaned with isopropanol and acetone, as prescribed by the manufacturer. Carbodur is manufactured to have a bonding surface on one side and a protective layer on the opposite. The bonding side of Carbodur is a flat, dull black color and the protective surface is a high gloss black, usually with white lettering. Latex gloves were worn at all times when handling the carbon composite laminate in an attempt to keep it as clean as possible.

3. Adhesive mixing

Carbodur is a pre-cured composite laminate, and only needs to be adhered to the substrate with epoxy adhesive. Since, Sikadur 30 has a limited pot life of 70 minutes; it was not mixed until necessary. The mixing details are detailed in Chapter II.

4. Adhesive application

As with Sikadur 330, the concrete surface was freed of any dust by using compressed air and the area in which to place the composite patch specified with permanent marker. The manufacturer recommends placing the epoxy adhesive on both the substrate and composite surfaces with a suggested thickness of $^{1}/_{16}$ of an inch. Since Sikadur 30 is relatively thick, it is possible to apply the necessary amount of adhesive to the substrate without fear of it running over the sides of the beam. It is also relatively easy to create a clean and uniform layer of epoxy adhesive.

The epoxy was applied to both surfaces with the paddle. Care was taken to place the adhesive uniformly over the composite patch. However, extra adhesive should be placed at the corners to ensure a proper bed of adhesive, as well as providing enough material to properly strike off the epoxy adhesive. The steel rule shown in figure 72 was used to measure the adhesive thickness throughout the application process.

5. Composite application

The Carbodur patches and respective adhesive were carefully placed onto the bed of adhesive applied to the substrate. Before applying the necessary pressure, care was taken to ensure proper alignment of the composite patch and orientation of the fibers. The composite was then gently pressed against the substrate. A roller was used to help remove air voids. It is not uncommon, nor a problem, for excess adhesive to push out from between the composite and substrate. The manufacturer suggests that the total thickness of the adhesive layer should not exceed $^{1}/_{8}$ of an inch. When the glue line was

measured and found to be too thick, the composite was simply pushed further toward the substrate, expelling the additional adhesive.

6. Finishing

Finishing Carbodur/Sikadur 30 composite systems is simpler than the Sikawrap/Sikadur 330 system. There is no need to apply a protective layer to the exposed composite face, as Carbodur is already cured with a protective surface. Correctly striking off excess adhesive is important. Samples of Carbodur/Sikadur 30 composite from the manufacturer have a 45 degree beveled edge along the length. This finish is simple to achieve with a trowel, spatula, or paddle. Figure 74 shows the beveled finishing of Sikadur 30. Figure 75 shows an example of a finished Carbodur composite system applied to the tensile face of several reinforced concrete beams. Note that the substrate surface of this beam was repaired earlier.

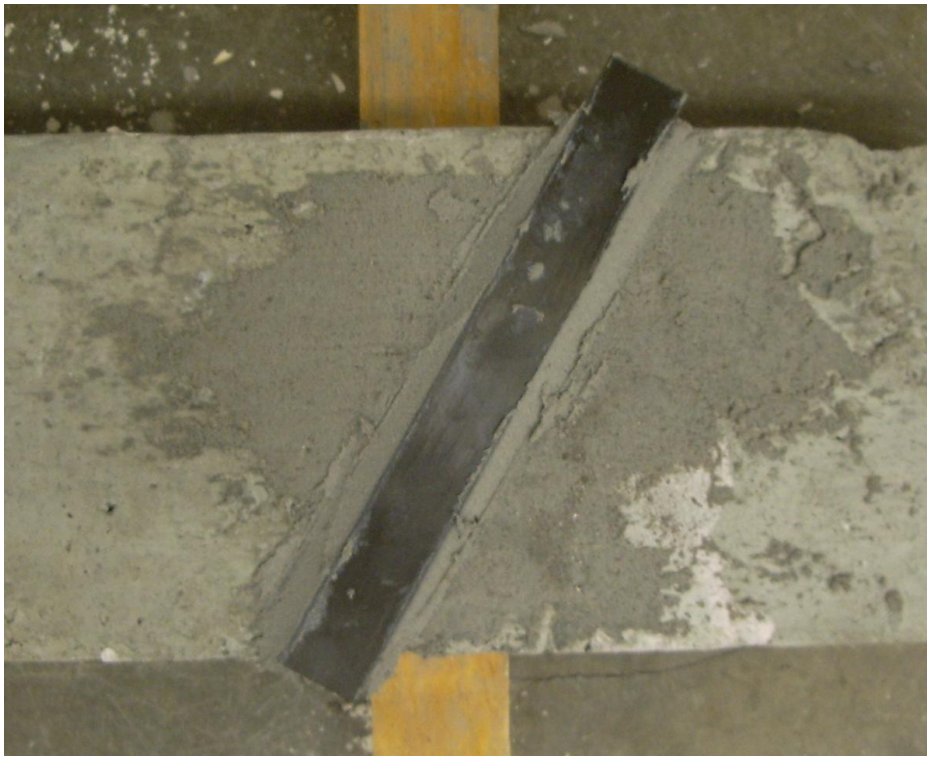

Figure 74. Completed Carbodur shear reinforcement

Figure 75. Completed Carbodur composite patch application

Prepreg reinforcing systems are the most involved FRP systems to apply, a fact likely to be exacerbated by typical civil engineering field conditions. The composition of prepreg composite systems is outlined in Chapter II. The resin impregnated system requires heat and pressure to properly adhere to substrate surfaces. Prepreg systems are usually cured in factory environments to create mass produced items, including automotive parts, golf clubs, and laptop computers. Recreating such a clean and controlled environment for civil engineering projects is difficult at best.

Ideally, prepreg composites are compressed into molds using vacuum bagging and cured in a temperature controlled oven. Each step of the prepreg application procedure is difficult in its own right; applying such practices to civil engineering superstructures in the field is difficult. The application procedure was developed in this research effort is both economical and effective. The procedure attempts to simplify the complex curing issues and provide the greatest quality control possible.

In the manufacturing setting, heat, pressure, and suction are critical for proper curing. Heat is required for curing the epoxy resin. Vacuum bagging creates a uniform pressure, consolidating the composite layers into a mold shape using atmospheric pressure. The vacuum suction also removes volatiles and trapped air. In a manufacturing setting, vacuum bagging creates a pressure of one atmosphere, which is equivalent to roughly 2000 psf. The composite system is then cured in an oven. The temperature varies in a controlled manner according to specific values unique to the prepreg composite system. The temperature of the oven rises at a controlled rate until

the gel temperature value is reached. The temperature is held constant for a specific time duration and then lowered at a prescribed rate.

In a civil engineering setting, vacuum bagging is impractical at best, and so an alternative system of applying the necessary pressure was developed using clamping. Metal C-clamps, or clamps, provide the required pressure. It was determined a successful clamping system must achieve the following:

- Resistance to high resin curing temperature
- Compressible to conform the composite system to substrate geometry
- Effective transfer of required pressure
- Economical

Of all the possibilities considered, rubber mats reinforced with lumber backing was considered. However, rubber mats cannot resist typical curing temperature. A second alternative uses silicon rubber mats, which is compressible to rubber, and have greater temperature resistance. A major drawback is that silicon rubber mats are expensive. The final acceptable clamping system chosen for the research uses foam insulating boards reinforced with a lumber backing. Foam insulation boards are available at most hardware stores at considerably low prices. A 4x8 square foot sheet of insulating foam is available for roughly ten U.S. dollars. Additional advantages of foam insulating boards are that they are light weight, simple to transport, and are easily cut into any desirable shape or size.

Experimental testing showed the foam can resist the required pressure of 1 atm without significant deformation. A one square inch section of foam insulation board and

loading was cut and then loaded in direct compression. The results revealed there is no observable deformation of the insulation board at 100 psi, or 144,000 psf; well within the pressure range necessary. In practice, the foam insulation board with lumber backing clamping system was tightened until noticeable deformation was achieved. This is a simple check, or rule of thumb, to ensure enough pressure is applied to the composite materials. Excessive pressure is not detrimental to the quality or performance of the cured prepreg composite.

The foam insulation boards have no flash point and cannot burn. However, if high temperatures are applied directly to the foam insulation board, it will melt. Melting only occurs under direct heat, an event which is easily avoidable. The fumes produced from melting the foam insulation boards are hazardous and have a distinct chemical smell. If a respirator was not worn, headaches quickly followed any melting of the foam insulation board. Figure 76 shows an example of some melted foam insulation board. The figure shows the LTC 4300 adhesive shear test specimens being cured.

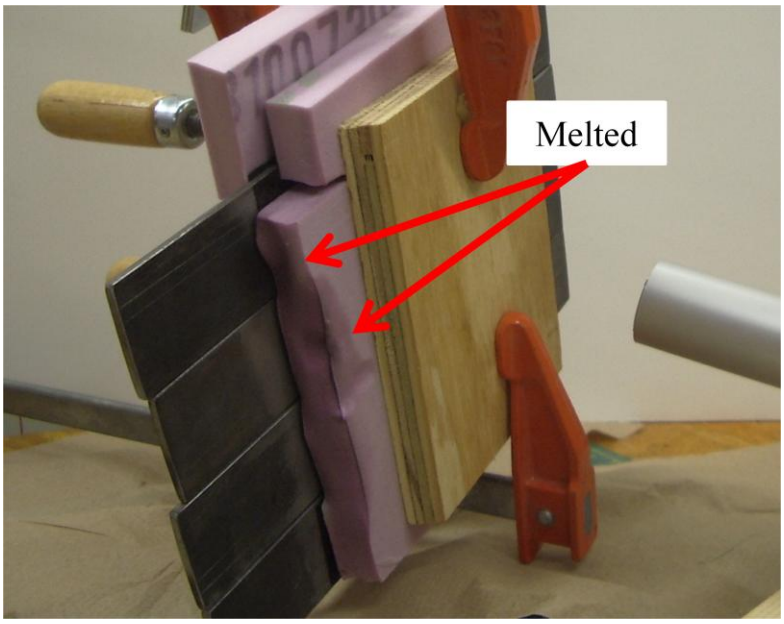

Figure 76. Melted foam insulation board

Considering the typical size, scope, and location of civil engineering structures, placing existing members into ovens for proper resin curing is not feasible. Likewise, encompassing structural members in field assembled ovens is not practical. Instead, heat sources must be brought to the members in the field to cure prepreg composites. For small beams or other projects, heat guns can supply temperatures well above the required maximum curing temperatures, are relatively inexpensive, and easy to handle. For the prepreg composite application in the context of this research project, a heat gun and an electric ceramic heater were utilized.

Several additional tools are required to apply prepreg composite systems. They are shown in figures 77 and 78. The essential tools include:

- Heat source (heat gun, ceramic heater, etc.)
- Mechanical clamps (C-clamps, F-clamps, pipe clamps, etc.)

- Insulating foam boards
- Hard surface rollers
- Release agent and agent application system (sprayer, brushes, etc)
- Temperature measurement device (thermocouple probes, infrared thermometer, etc)

Figure 77. Components used to apply LTC 4300 composite to coupons

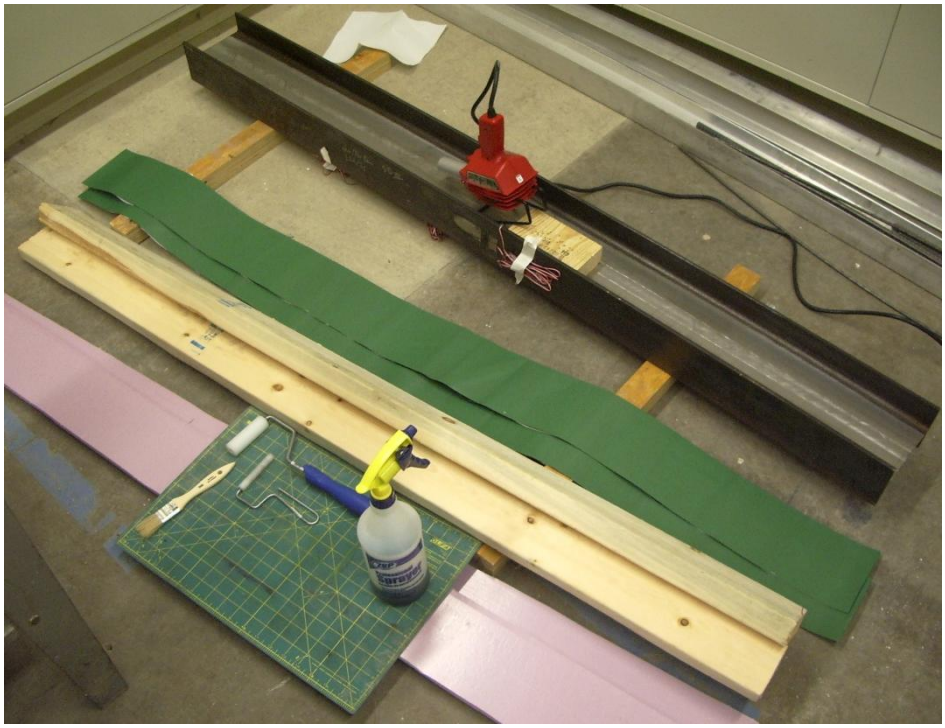

Figure 78. Tools for LTC 4300 application

To easily remove the foam boards from the prepreg composite, a release agent is commonly applied with a sprayer. Manufacturers typically supply purchasers with spray rates which produce ideal coverage. In the context of this research project, the release agent was applied with a spray bottle and a paint brush. A thin, even coat is desirable and will provide excellent results. The technical data of the release agent utilized in the research presented in this manuscript is located in Appendix A.

In the context of this research project, LTC 4300 was applied to the web and flange of steel beams. Additionally, it was utilized to strengthen reinforced concrete beams in shear and flexure. Each application is shown following the finishing step description at the end of this section.

1. Surface preparation

There are no specific surface preparation instructions available for LTC 4300 from the manufacturer, Newport Adhesives and Composites. In the absence of such information, the substrate surfaces were prepared to the specifications detailed for Sikawrap, since it is the more stringent. If the substrate surface is relatively cool to the touch, it can be difficult to secure the composite in place while compiling the clamping system around it. It was found that warming the substrate surface before composite application facilitated the clamping process. This practice of warming the surface can be seen in figure 78.

2. Composite preparation

A benefit of using pre-impregnated composites is that they are generally ready for application upon delivery from the manufacturer. There are no additional steps required to prepare the composite for adhesion. All that is necessary is to remove the protective plastic backing at the appropriate time.

3. Adhesive mixing

An advantage of pre-impregnated composite systems is that there is no need measure, combine, or mix adhesives. This eliminates operator mistakes, which may jeopardize the performance of the composite system. Since the resin adhesive is integrally manufactured with the composite fibers, there is no need to prepare any additional adhesives.

4. Adhesive application

As evident from the inherent nature of prepreg composites, no additional adhesive must be applied to the surface other than the resin of the composite itself.

5. Composite application

This step is the most complicated step when using prepreg composites. Figure 79 shows the general application scheme developed for use in this study. The release agent acts to prevent the prepreg composite from adhering to the foam board and was applied directly to the foam insulation boards. Figures 80 and 81 show LTC 4300 being clamped into place. Latex gloves were worn at all times when handling prepreg composites in order to protect the impregnated resins from possible dirt and oils on the hands.

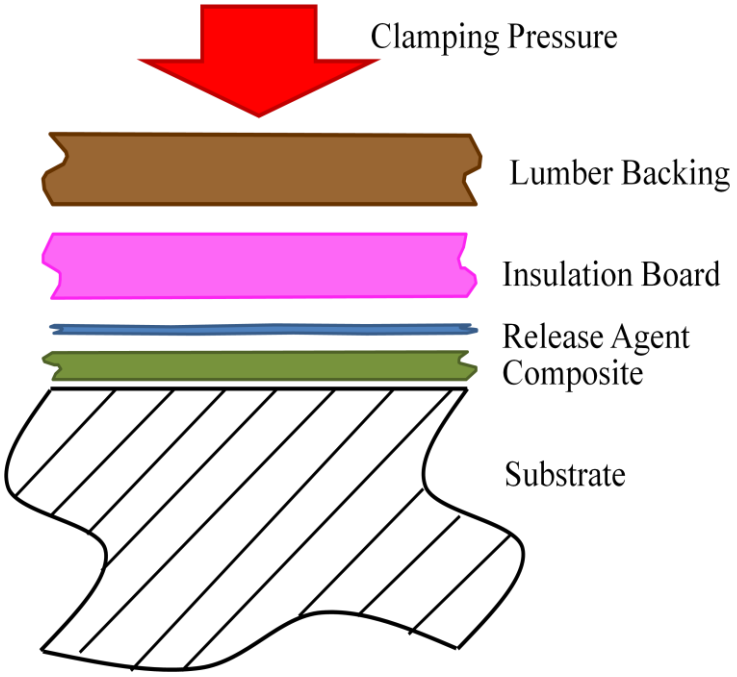

Figure 79. General LTC clamping order

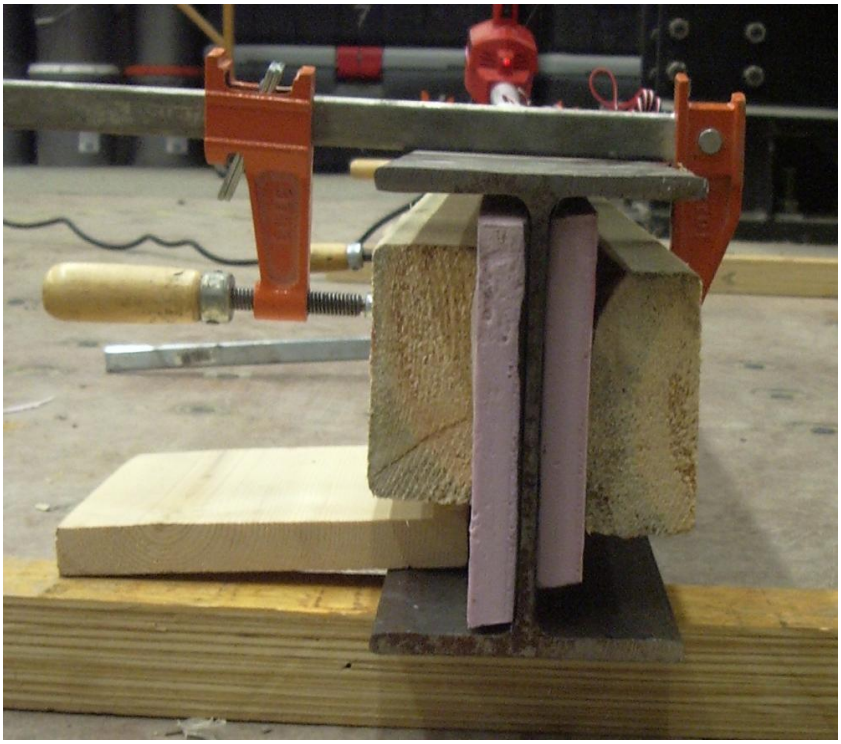

Figure 80. LTC 4300 clamped to web of SBII

Figure 81. LTC 4300 clamped to reinforced concrete beams

Once the composite was properly placed and clamped, heat was applied to the substrate to begin curing the resin. It is incredibly difficult to correctly heat the substrate to the prescribed heat at the required rate. The heating rates and holding temperatures for LTC 4300 are given in Appendix B. The substrate surface temperature was frequently measured in an attempt to control the heating rate. An additional difficulty encountered in the lab was maintaining the substrate temperature once the gel temperature of the resin was reached. A reason was the limitation of heat sources utilized in this research project, the other is that it is difficult to achieve such high temperature in an ambient environment.

In accordance with the recommendation of the manufacturer, LTC should be heated to 180 °F and kept at that temperature for 120 minutes. It is considerably difficult to accomplish proper curing in ambient environmental conditions. To overcome this difficulty and ensure the best possible resin cure, the heat sources remained on the substrates for typically six hours, and were left clamped for at least twelve hours. Figures 82 and 83 show several more examples of LTC 4300 composites being cured.

Figure 82. LTC 4300 cured to SBI with heat gun

Figure 83. LTC 4300 cured to concrete beams with ceramic heater (background)

6. Finishing

There are no protective coatings for LTC 4300 once it is cured. If the release agent is not properly applied to the foam insulating board, the protective plastic sheeting of the insulation foam board will adhere to the resin. If this happened, the thin plastic sheet would pull away from the insulation board. This is not considered a major issue of concern and is not detrimental to the performance of the prepreg composite. In fact, the plastic film may act to protect the prepreg composite, though this is a conjecture. Figures 84 through 88 show finished prepreg applications.

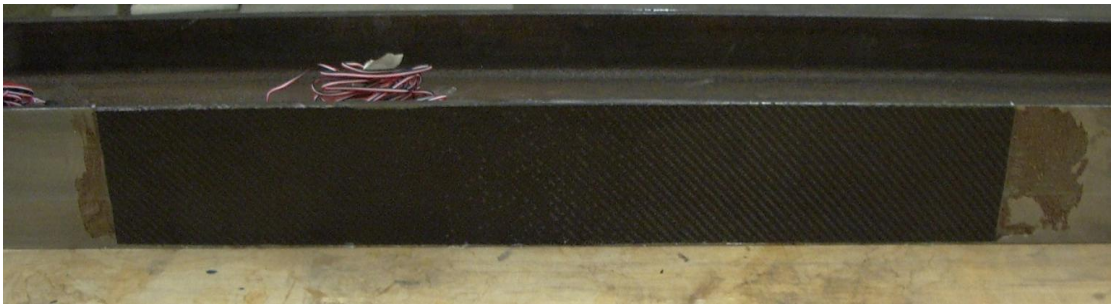

Figure 84. Completed LTC 4300 application to bottom flange

Figure 85. Completed steel web application of LTC 4300

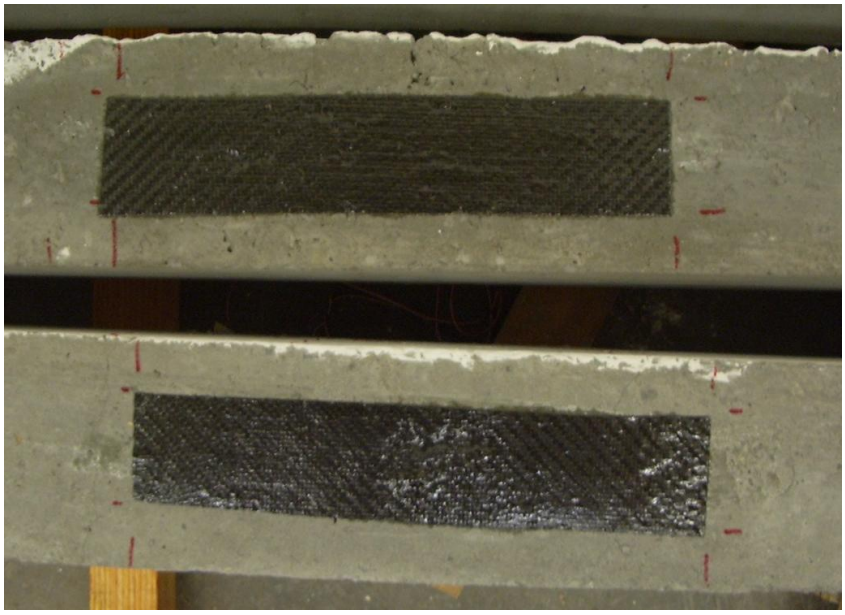

Figure 86. Completed application of LTC 4300 to tensile face of reinforced concrete beam

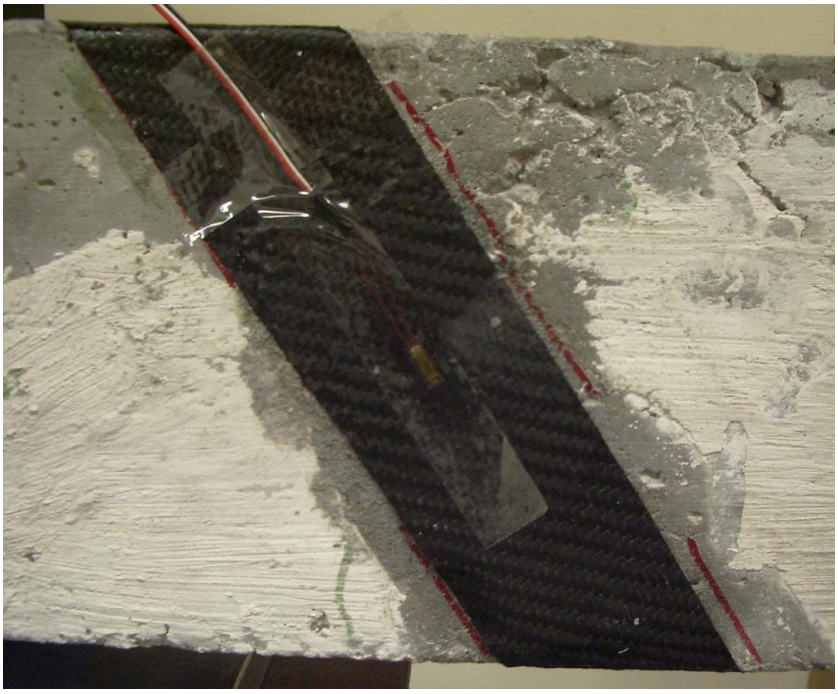

Figure 87. Completed LTC 4300 shear reinforcement with attached strain gage

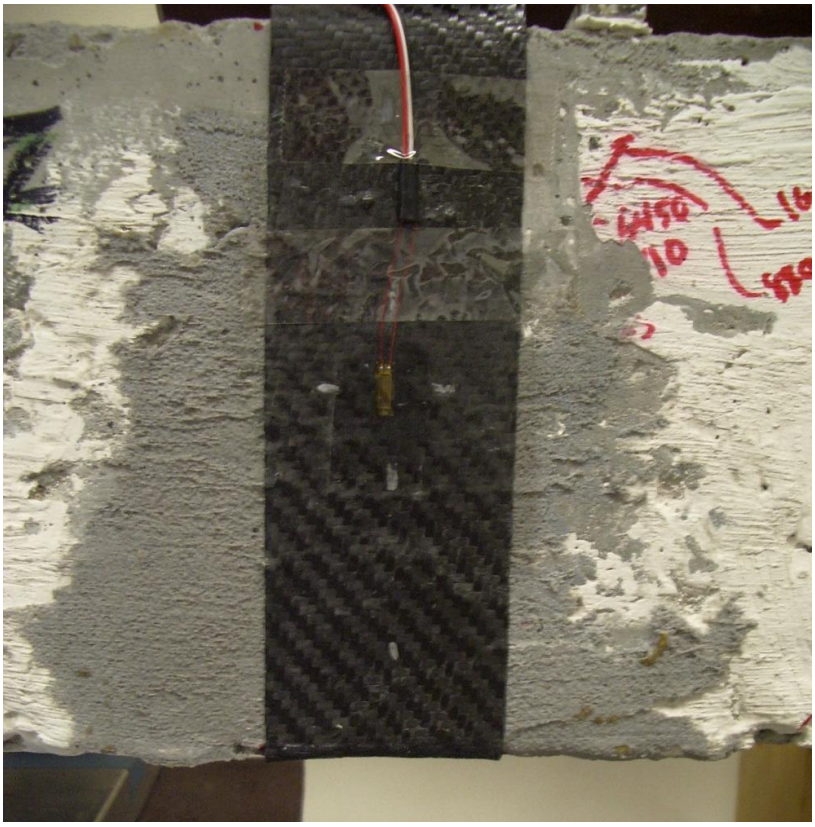

Figure 88. Completed LTC 4300 U-jacket with attached strain gage

Chapter V

EXPERIMENTAL WORK

The experimental work was conducted in the Vanderbilt University Structural Laboratory. The load testing was undertaken for this research project was conducted in four phases. Each phase is detailed in individual sections within this chapter. The first phase, Phase I, includes support, load, and data acquisition set-up, as well as specimen instrumentation. The second phase, Phase II, is comprised of predicting the nominal load capacity of the test beams followed by loading the beams to create initial and limited damage. Next, the third phase, Phase III, explores the repair strategy for each individual test beam, the limit states are determined; design is verified using the mechanistic model presented in Chapter III, and bonding the designed patches to the test beams. The last phase, Phase IV, includes additional instrumentation of the test beams and composite materials, and loading the test beams to ultimate failure.

Phase I: Equipment and Methods

As stated in chapter II, based on different considerations, the test beams were tested in four point bending. The loading was force controlled and response measurements of displacement, load, and strain values were recorded at several locations during each test. In order to achieve such quantities, several apparatuses are required to correctly test and evaluate the response of each test specimens, which include:

- Loading frame standing on a strong floor
- 50 kip load cell; figure 89
- linear variable differential transformer (LVDT); figures 90 and 91
- several dial gages;
- bearing pins, plates, and rollers; figures 92 through 94
- angle braces; figure 92
- hydraulic piston; figure 89
- hydraulic pump; figure 95
- data acquisitions software and hardware; figure 96

Figure 89. 50 kip load cell

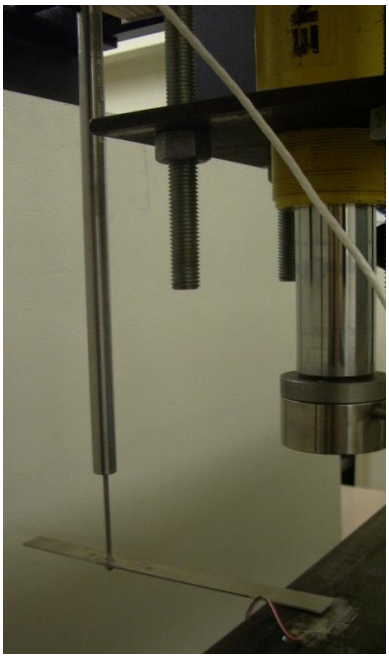

Figure 90. LVDT bridging to beam

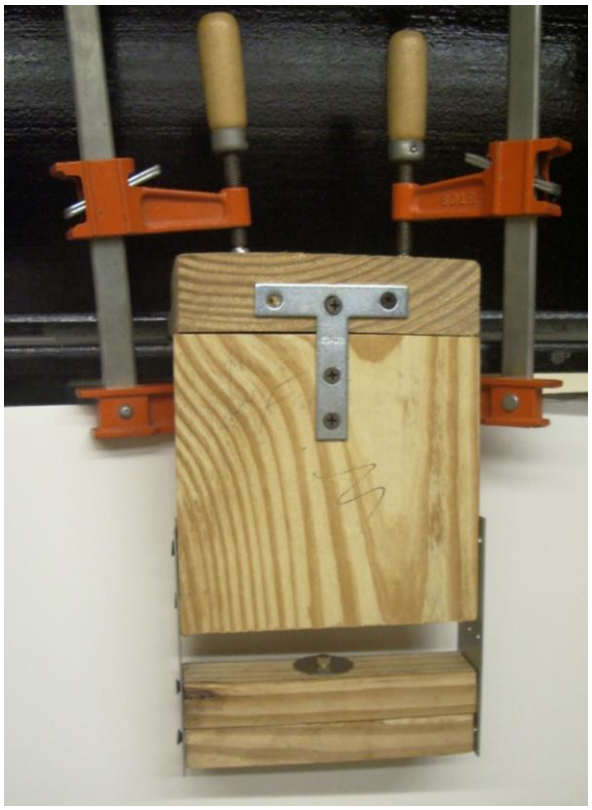

Figure 91. LVDT fixture attachment to strong frame

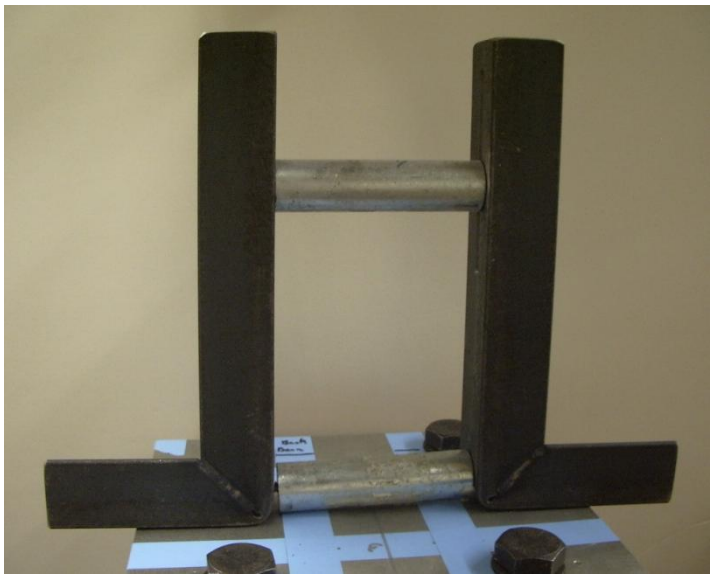

Figure 92. Support bearing pins and lateral braces

Figure 93. Exposed bearing pins with one lateral brace removed

Figure 94. Two point loading pins and attachments

Figure 95. Enerpac electric hydraulic pump

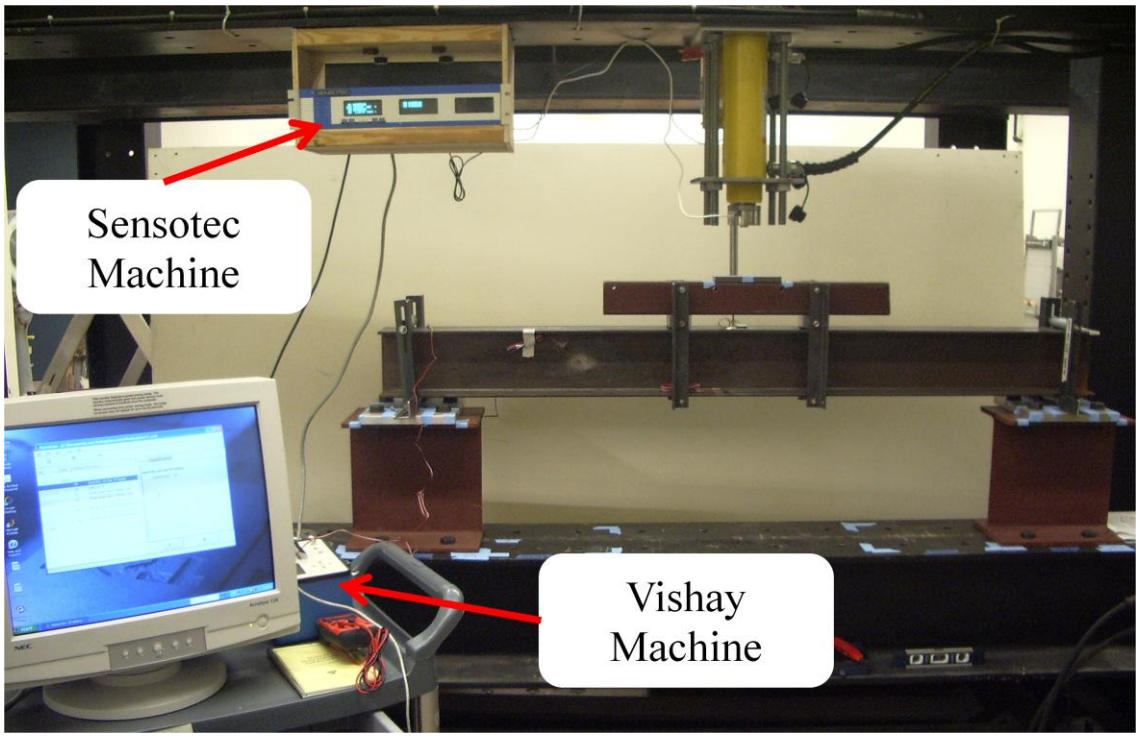

Figure 96. Test setup with data acquisition machines

Most of the testing apparatus utilized for the load testing were custom designed, machined, and assembled for this research project. The lateral supports are fabricated from angle brackets. The bearing plates are solid aluminum or steel. The loading pins are attached to a section of HSS 4x2x$^{3}/_{8,}$ and were milled from solid aluminum. The bearing pins are thick-wall galvanized steel pipe with aluminum fittings. The stub bearing I-beam sections were strengthened with symmetric half inch plates welded into place. To avoid stress concentrations at the load points of concrete beams, special measures were taken to distribute the applied load over steel strips over the width of the beam. These bearing strips were 4”x$^{1}/_{2}$”x$^{1}/_{4}$” steel plates and were set in a bed of gypsum plaster as shown in figure 97. All the hydraulic pieces were purchased from Enerpac®. The rate of pressure increase is driven by an electric motor and controlled with a T-screw

handle. The dial gages used in the load testing are accurate to 0.001 inches. The gage placed atop the strong frame above the hydraulic cylinder gave digital reading to an accuracy of 0.0001 inches.

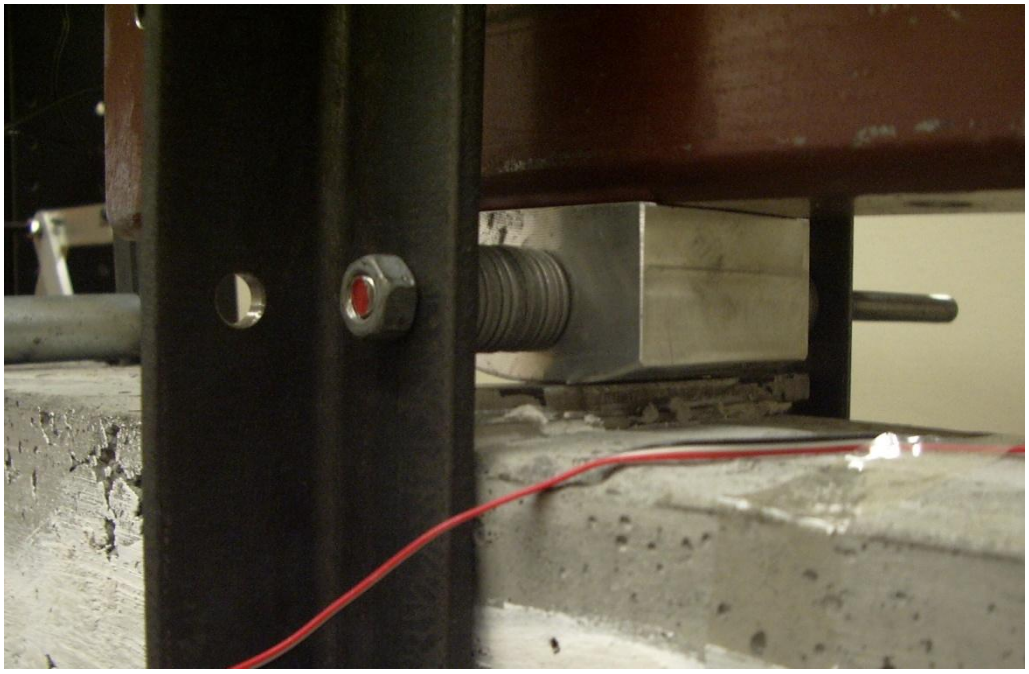

Figure 97. Bearing strip in bed of gypsum plaster under loading pin

Several data values were collected during the load testing experiments, including applied load, midspan beam deflection, strain values, and pertinent strong frame deflection. The load cell used is rated up to 50 kips with an accuracy to the nearest pound. The test beam deflection was captured with an LVDT mounted to the strong frame. The stroke of the LVDT is six inches and is accurate to 0.0001 inches. The load and beam deflection data were recorded by a Sensotec® machine, model SC3004, which was connected and controlled by a computer. The test beam strain values were captured with the strain gages, which were connected to a Vishay® strain indicator and recorder, model P3. These two data recording devices were independent of the other and were

synchronized to record respective data every second. The strong frame deflections were measured with dial gages and were recorded at the time of maximum load. Figure 98 shows a dial gage under the strong frame utilized to measure the deflection of the support beam under the left test beam support. Figure 99 shows the digital dial gage atop the strong frame. All the dial gages used to measure the upward deflection of the strong frame and were grounded to the strong floor, independent of the frame itself.

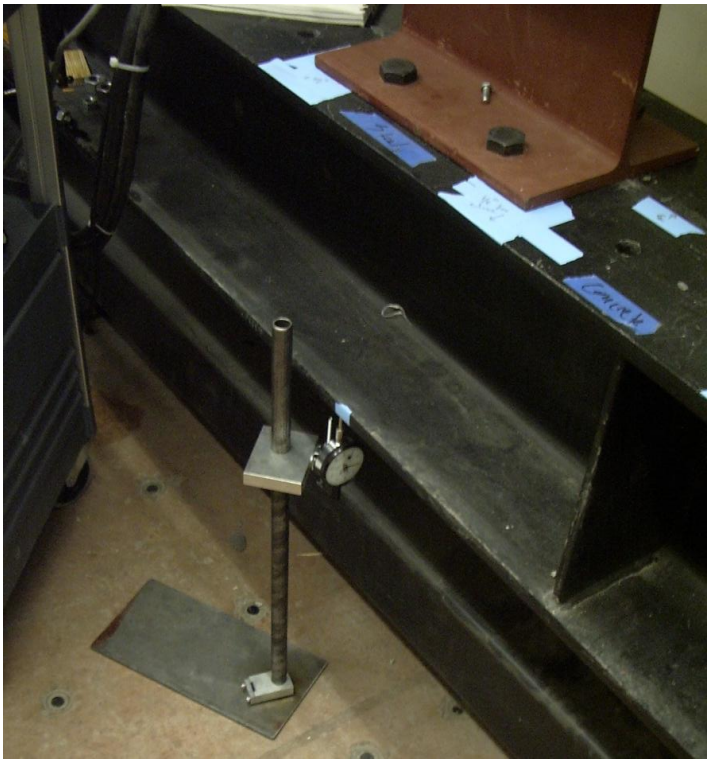

Figure 98. Dial gage under left test beam support

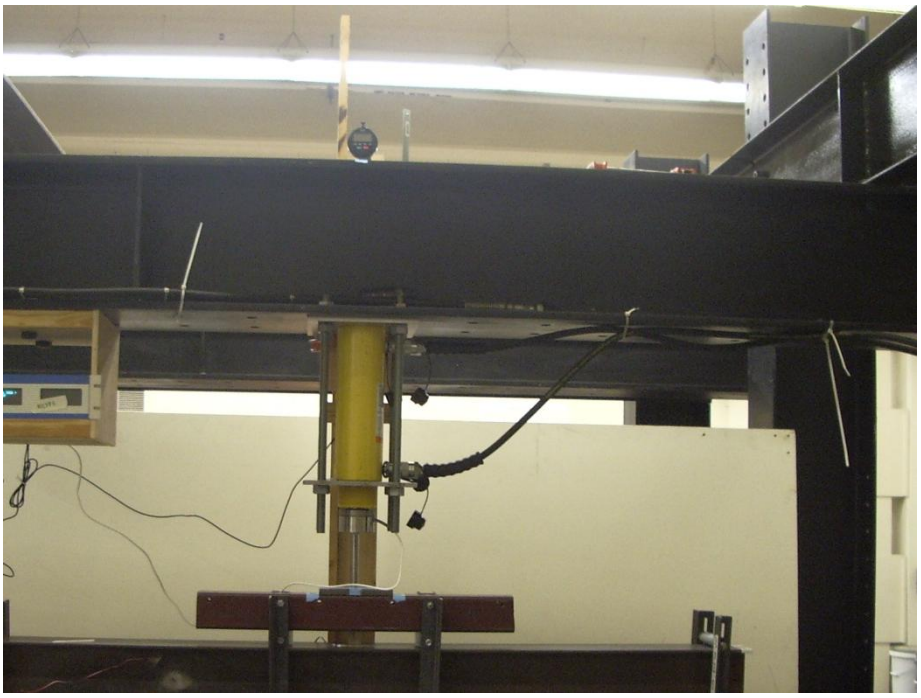

Figure 99. Digital gage atop strong frame to measure its deflection

Figure 100 depicts a schematic of the strong frame, several experimental apparatuses, and measurement devices. Note the location of dial gages necessary to correctly measure the strong frame deflection when testing the beams.

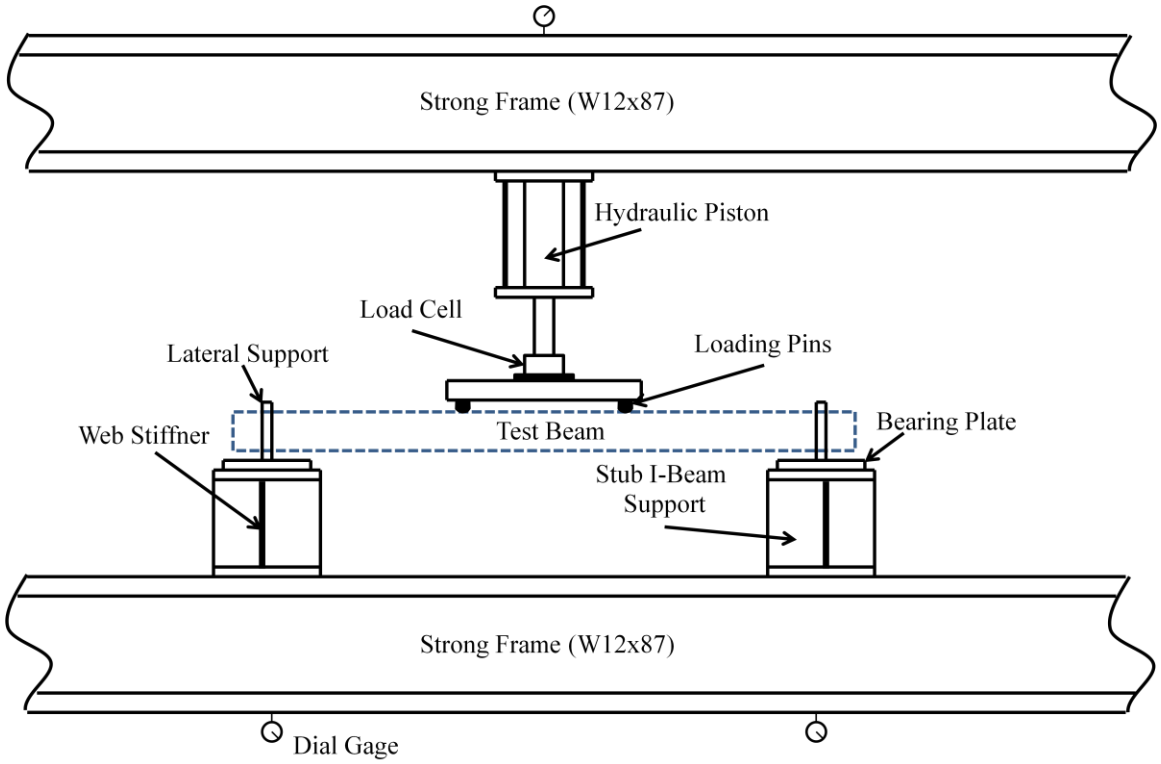

Figure 100. Libratory test setup

Each specimen was instrumented for strain measurement values. Steel beams were affixed with three separate gages. The first is located atop of the top flange to measure the normal compressive strain due to flexure, shown in figure 101. The second is on atop of the bottom flange, placed 0.75 inches from the edge of the flange at midspan, shown in figure 102. This location was chosen so the gages wouldn't interfere with composite patch application. The third, and final, strain gage affixed to steel beams was placed on the web, one quarter of the span from the edge of the beam span and placed at a 45° angle, oriented in the principle tensile direction; shown figure 103.

Figure 101. Typical strain gage instrumentation of top flange

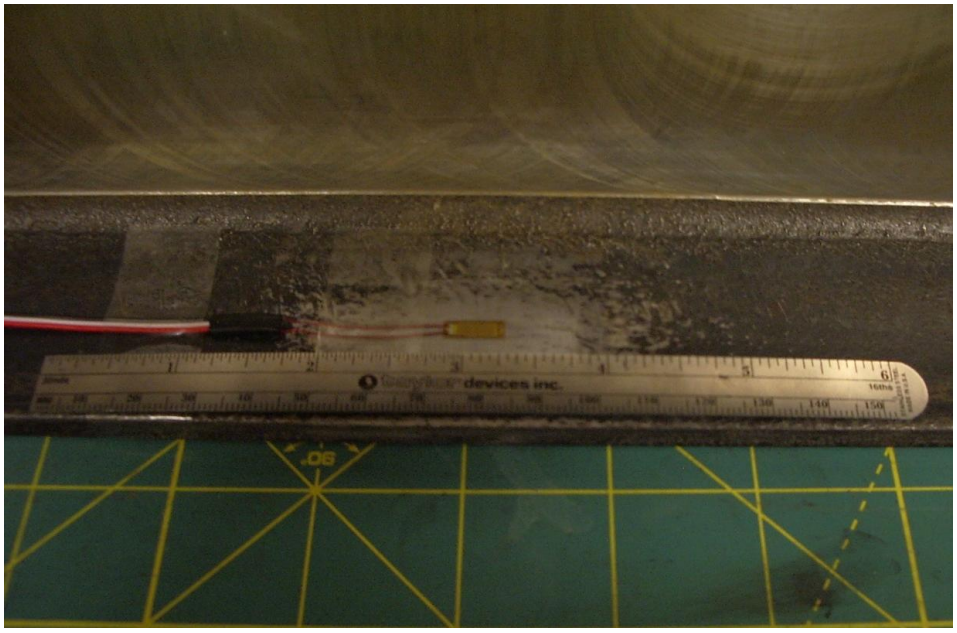

Figure 102. Typical instrumentation of the top of the bottom flange

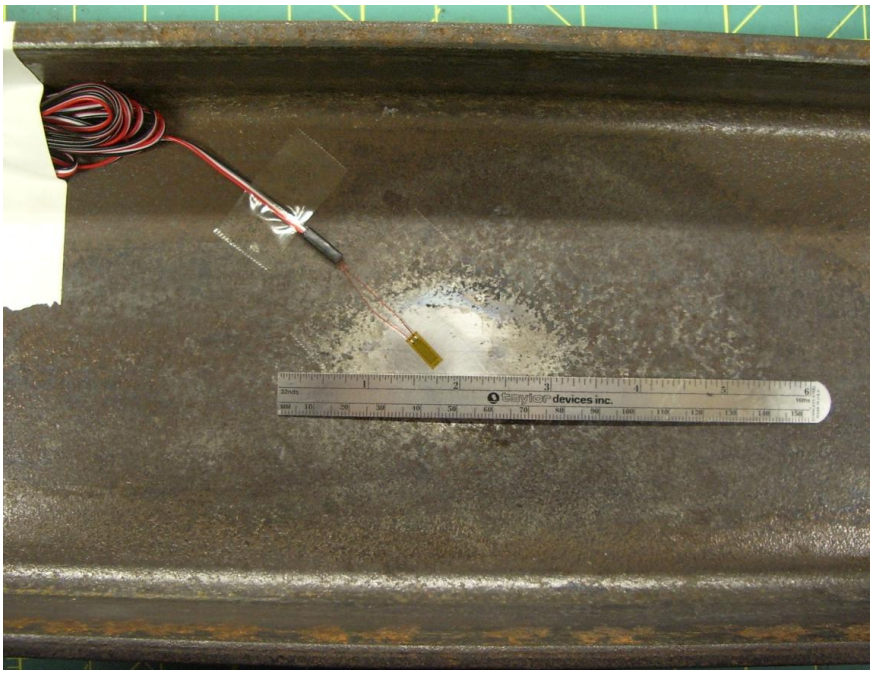

Figure 103. Typical strain gage instrumentation of web

Two different size gages were utilized; one being 0.125 inches long and the other 0.250 inches. These gages were placed with great care according to the manufacturers prescribed directions; including bringing the surface to a white finish with emory paper, preparing the gage location with several chemical cleaners, and adhering the gages with epoxy adhesive. The finished gages were tested for the correct resistance after placement, and all were within the manufacturer tolerance limits. Table 22 details the steel strain gage schedule, the more accurate 0.125 inch gages were utilized when it was pertinent to receive the most accurate results.

Table 22. Strain gage schedule

	Strain Gage Location		
Beam Type	Top FL	Web	Bottom FL
Control	.125"	.250"	.250"
SBI	.125"	.250"	.125"
SBII	.125"	.125"	.250"
SBIII	.125"	.125"	.125"

Each concrete test beam, both reinforced and prestressed, was also instrumented with a single strain gage to measure the compressive strain at midspan. The gages are one half inch in length; using a longer strain gage is necessary due to the heterogeneous nature of concrete. Correctly placing strain gages on concrete is more involved than steel, and is completed in several steps. The first step is to prepare the surface, requiring wire brushes and sand paper abrasion followed with cleaning the surface with acid and neutralizing chemical solutions. Epoxy was then placed on the cleaned area. Once cured, the epoxy surface was properly finished with further sanding and chemical treatments. An example of a finished epoxy site is shown in figure 104. The gages were then placed atop a thin bed of epoxy adhesive and left to cure under pressure to insure adherence; shown in figure 105. The gage lead wires were soldered to the gages and resistances checked to complete instrumentation.

To facilitate identification of crack growth of concrete test beams, the front of each beam was covered with a thin layer of gypsum plaster. During the initial loading, when a crack first appeared, it was traced in permanent marker and the load at which it occurred was recorded at the crack tip. This detailed recording of crack growth provides an accurate description of the beam damage as it was being loaded. When exceptionally wide cracks were observed, the width values were recorded separately.

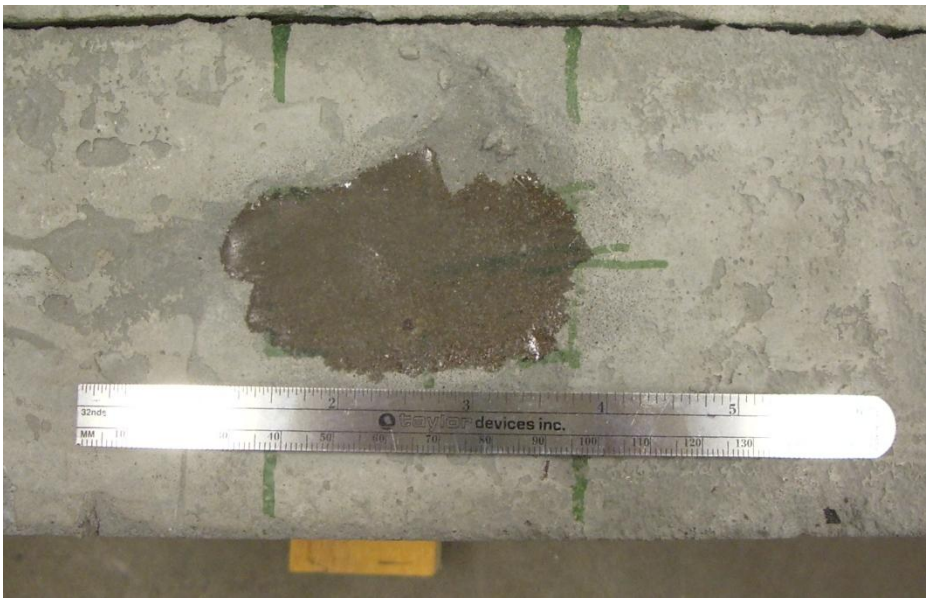

Figure 104. Cured epoxy finish of concrete surface

Figure 105. Concrete strain gages under pressure for proper epoxy adherence

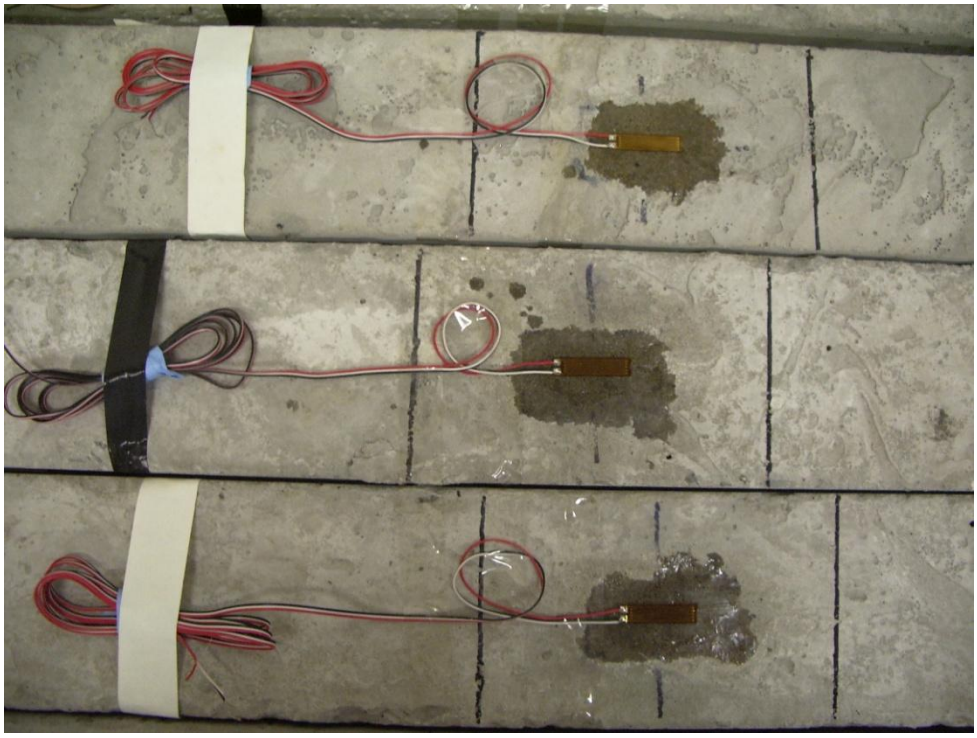

Figure 106. Finished strain gages with lead wires soldered in place

To provide a more detailed understanding of the behavior of the retrofitted beams and composite materials, strain gages were affixed to the bonded composite patches. Test beams with flexural composite patches were fitted with a single strain gage at the center of the patch in the principle tensile direction. Test beams with shear repair were instrumented with strain gages on either composite patch, oriented in the primary direction of the composite fibers.

Correctly applying strain gages to composite materials is difficult because of their unique nature. The wide spectrum of composite materials, weave configurations, and curing applications create numerous possibilities. The developers and manufacturers of strain gages have a difficult task of prescribing detailed application instructions to ensure gage performance.

The gage manufacturers only provided general suggestions for correct gage placement. These suggestions included surface preparation with appropriate chemical cleaners and degreasers and sanding away any adhesive or protective coating with Emory paper until the raw fibers are exposed. The application procedure followed to apply the strain gages to the composite materials is as follows:

- Surface thoroughly cleaned with isopropanol
- Adhesive lightly sanded with 400 grit Emory paper
- Surface thoroughly cleaned with isopropanol
- Gage outline marked
- Gage applied using instruction for steel surface application

The following figures show the applied strain gages to several specimens.

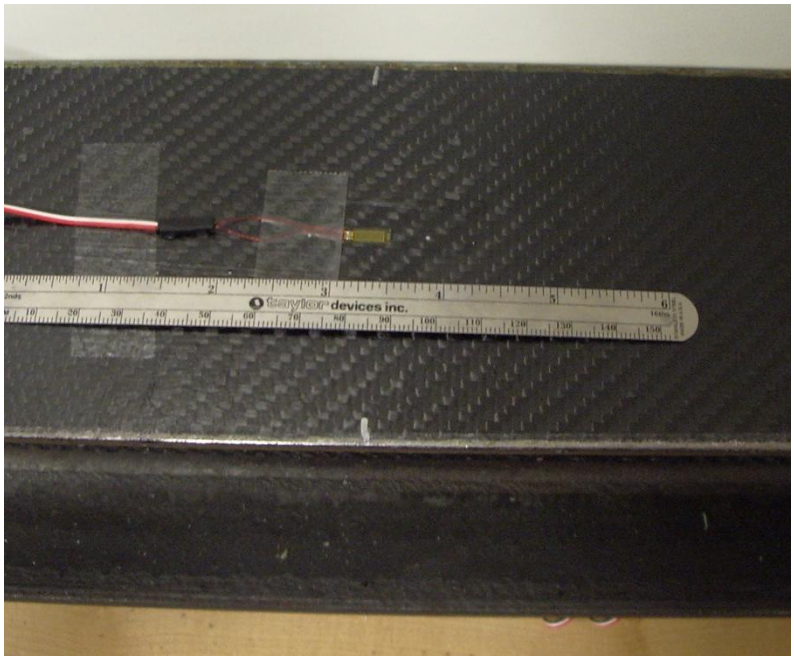

Figure 107. Strain gage applied to LTC 4300 composite material

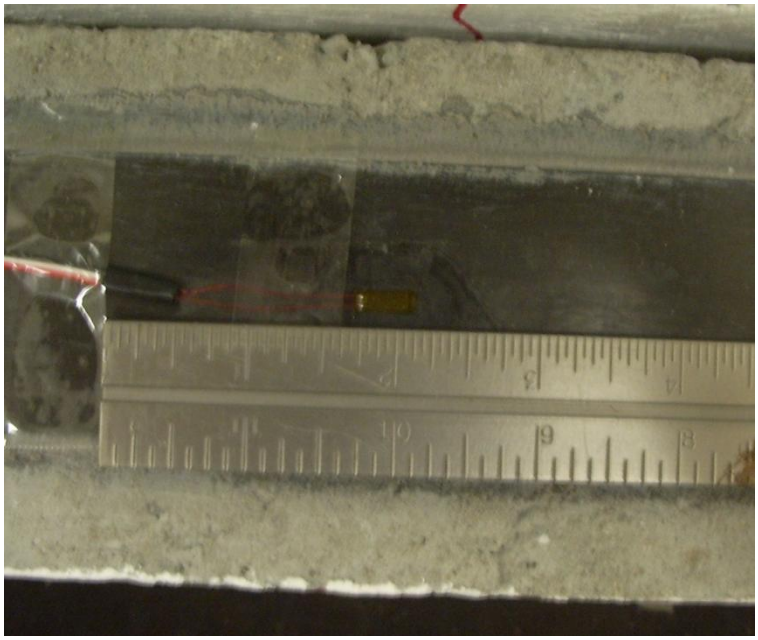

Figure 108. Strain gage applied to Carbodur composite material

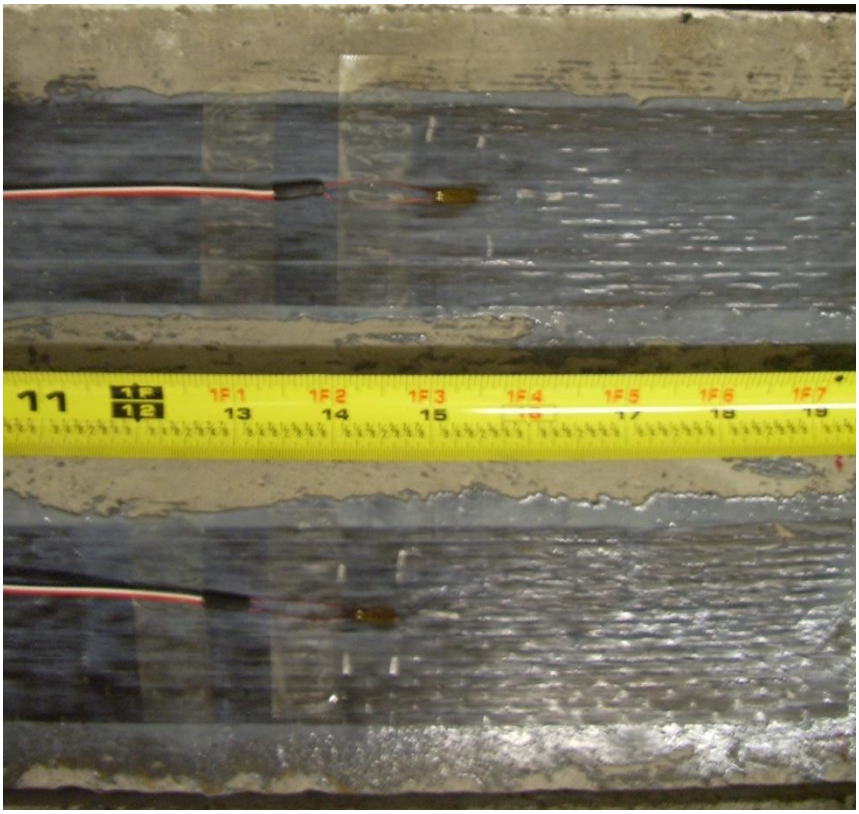

Figure 109. Strain gage applied to Sikawrap composite material

Phase II: Initial Loading to Create Damage

This phase includes loading the beams to establish a baseline of performance against which the repaired beams will be compared against in addition to creating sufficient initial damage. Before loading the test beams, it is necessary to predict their nominal load capacity.

Steel Beams

To determine the nominal capacity of the steel beams, the following equations were used. Local flange and web buckling are not controlling limit states.

$$(M_n)_{\text{Control Beam}} = ZF_y \tag{173}$$

$$(M_n)_{SBI} = ZF_y - \frac{1}{2}(t_f - t_f')b_f F_y\left[d + (t_f - t_f')\left(\frac{b_f}{t_f} - 1\right)\right] \tag{174}$$

$$(M_n)_{SBII} = ZF_y - \frac{1}{4}(t_w - t_w')^2 T^2 \tag{175}$$

$$\begin{aligned}(M_n)_{SBIII} &= ZF_y \\ &\quad - \frac{1}{2}(t_f - t_f')b_f F_y\left[d + (t_f - t_f')\left(\frac{b_f}{t_f} - 1\right)\right. \\ &\quad \left. - \frac{1}{4}(t_w - t_w')^2 T^2\right]\end{aligned} \tag{176}$$

$$(V_n)_{SBII} = (V_n)_{SBIII} = 0.6F_y[dt_w - T(t_w - t_w')] \tag{177}$$

Given the information of tables 6, 9, and 10, the nominal capacities of the steel test beams are easily calculated and given in table 23. Figure 110 shows the control test beam in the loading set-up and table 24 provides the loading rates of each test beams.

Table 23. Predicted nominal capacities of steel test beams

Beam ID	M_n (kip-in)	V_n (kip)
Control	498.00	49.93
SBI	495.92	49.93
SBII	497.75	45.23
SBIII	495.67	44.86

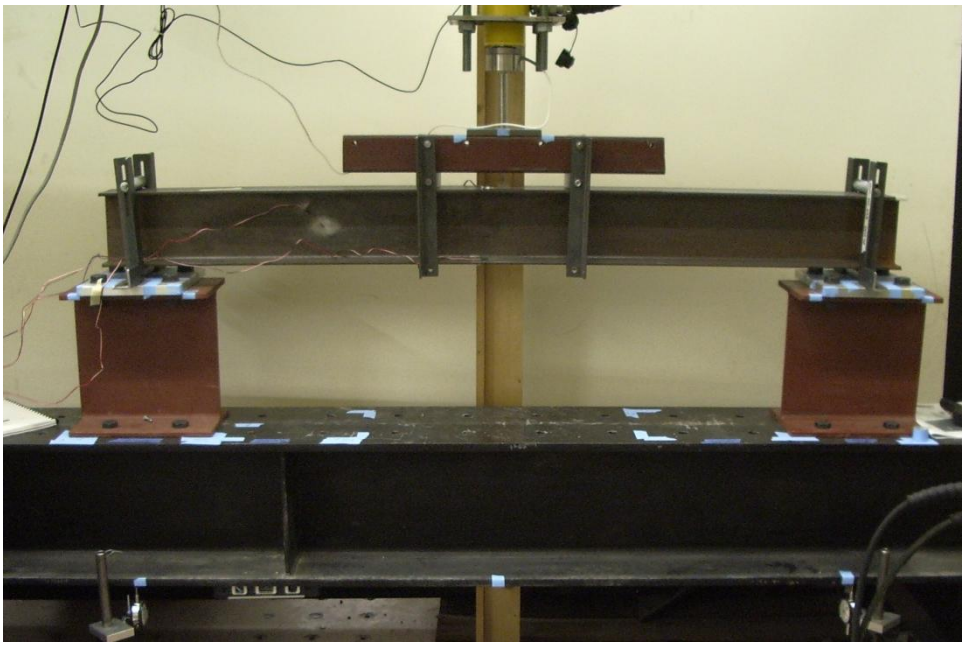

Figure 110. Control beam before initial loading

Table 24. Load rates of steel test beams during Phase II

Beam ID	Load Rate ($^{lb}/_{min}$)
Control	901.1
SBI	1226.2
SBII	1743.2
SBIII	1868.5

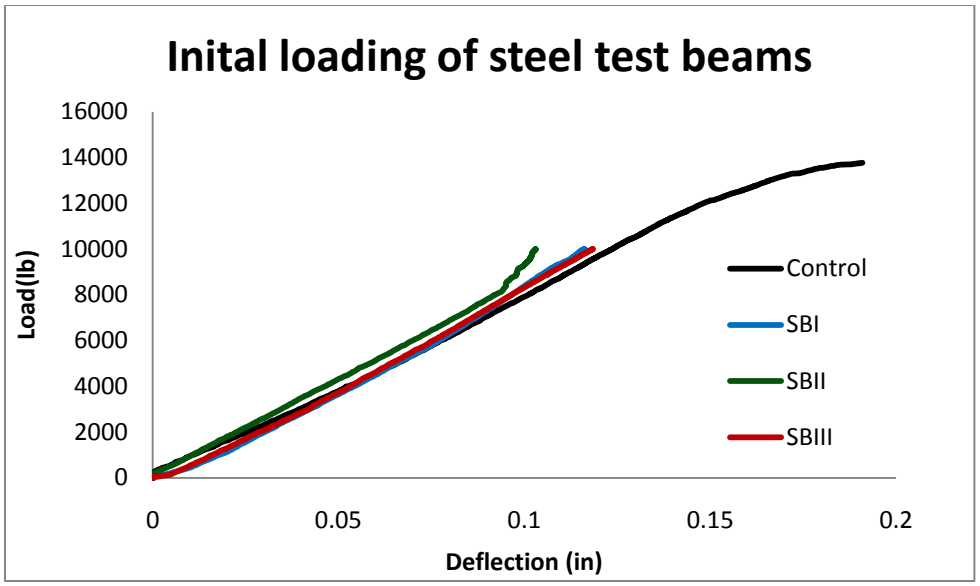

Figure 111. Load-displacement values from initial testing of steel test beams

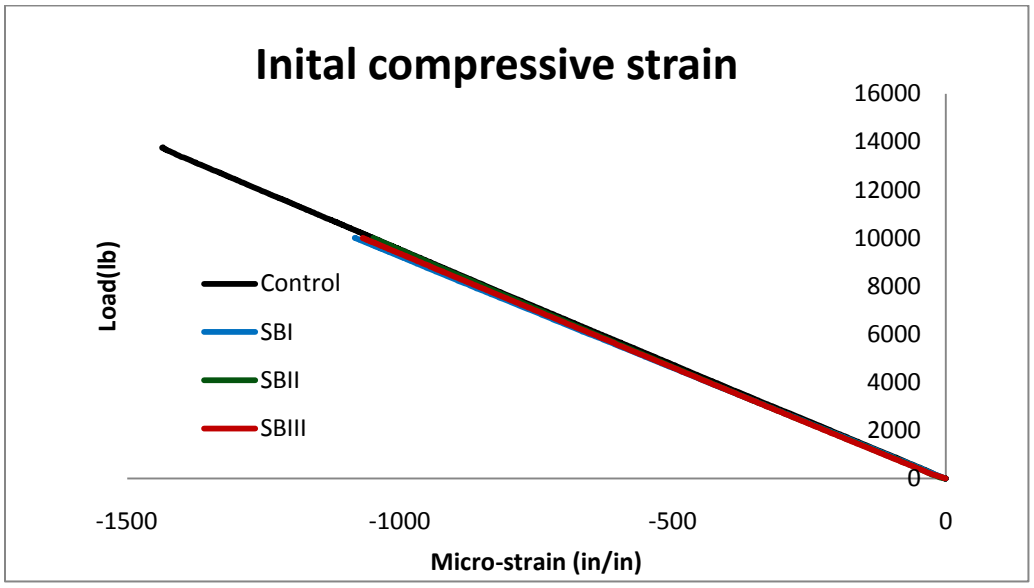

Figure 112. Load-strain values from top strain gage of steel test beams

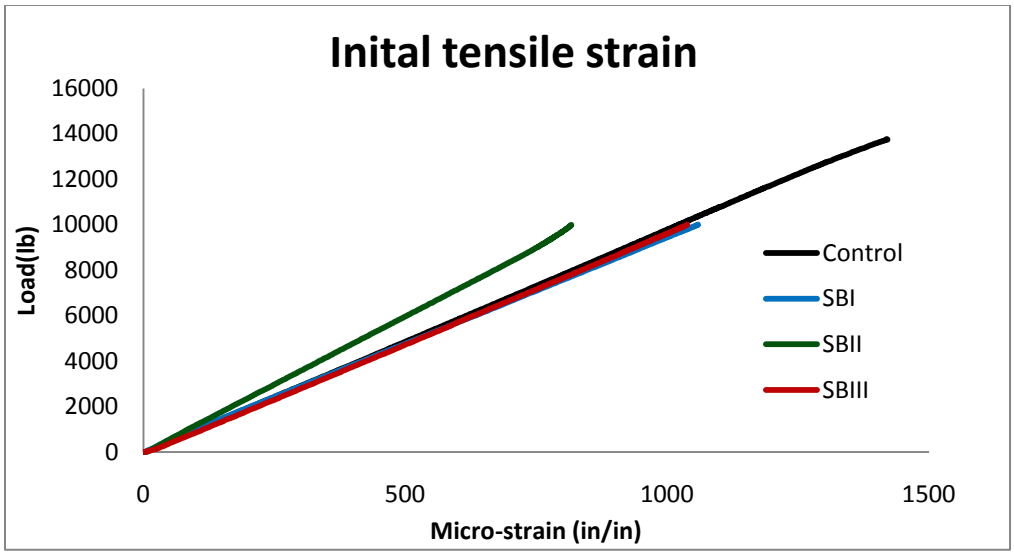

Figure 113. Load-strain values from bottom flange strain gage of steel test beams

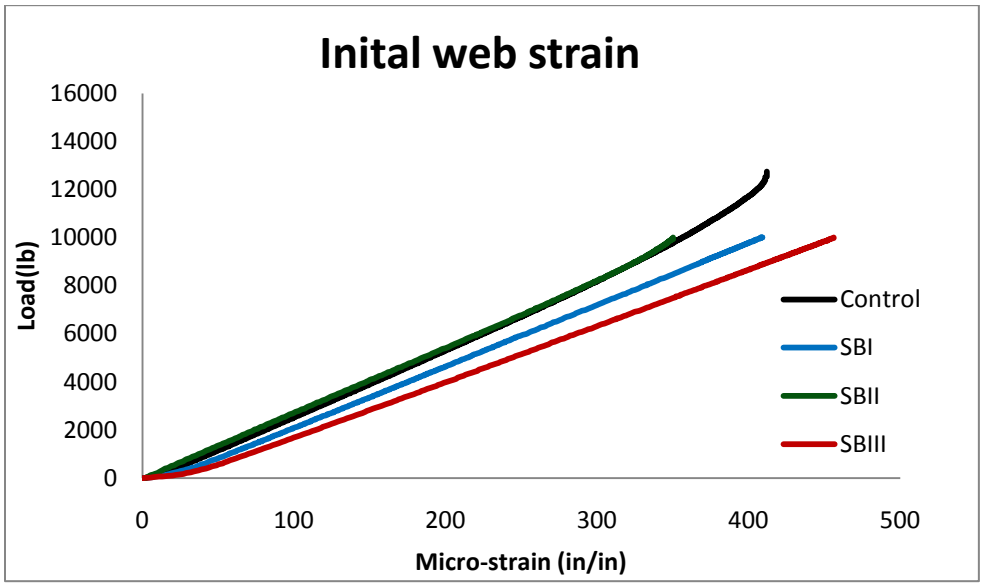

Figure 114. Load-strain values from the web strain gage of steel test beams

Reinforced Concrete Beams

The initial capacities of both the flexural and shear beams had to be determined in order to design the composite patch. The moment capacity of the test beams is calculated using equation 170; the capacity of the shear beams can be found by ignoring the top steel. The shear capacities of the beams can easily be determined using equation 160.

$$(M_n)_{flexure} = \begin{Bmatrix} A_s f_y \left(d - \frac{(A_s + A'_s)f_y}{2(0.85f'_c)b_w}\right) + A'_s f_y \left(d' - \frac{(A_s + A'_s)f_y}{2(0.85f'_c)b_w}\right), \text{if top steel yields} \\ A_s f_y \left(d - \frac{A_s f_y + A'_s f'_s}{2(0.85f'_c)b_w}\right) + A'_s f'_s \left(d' - \frac{A_s f_y + A'_s f'_s}{2(0.85f'_c)b_w}\right), \text{if top steel does not yield} \end{Bmatrix} \quad (178)$$

$$\text{where, } f'_s = E_s(\varepsilon_c = 0.003)A'_s\left(\frac{d' - n}{n}\right)$$

The results of utilizing equation 178 are given in tables 25 and 26.

Table 25. Capacities of shear test beams

Beam ID	f'$_c$ (psi)	β	n (in)	M_n (kip-in)	V_n (kip)
4	6300.15	0.735	0.748	43.88	2.54
5	7574.98	0.671	0.681	44.43	2.79
6	7313.97	0.684	0.692	44.33	2.74
7	7402.30	0.68	0.688	44.37	2.75
8	6636.76	0.718	0.727	44.05	2.61
9	6475.22	0.726	0.737	43.97	2.58

Table 26. Capacities of flexural test beams

Beam ID	f'_c (psi)	β	n (in)	M_n (kip-in)	V_n (kip)
1	7071.25	0.696	0.879	47.03	2.69
3	6838.89	0.708	0.894	46.88	2.65
A	6822.97	0.709	0.896	46.87	2.64
B	6309.7	0.735	0.935	46.49	2.54
C	4974.39	0.801	0.911	43.46	2.26
D	4917.89	0.804	0.916	43.39	2.24
E	5774.94	0.761	0.985	46.02	2.43
F	5661.94	0.767	0.997	45.91	2.41
G	7123.78	0.694	0.876	47.07	2.70
H	7093.54	0.695	0.878	47.05	2.70
I	6962.23	0.702	0.886	46.96	2.67

Figure 115 shows a typical concrete test beam in the strong frame before any loading. Appendix C is a collection of figures which show each concrete test beam before applying any load, after the initial loading, and a diagram with the resulting cracks clearly detailed.

The results of test beam C may not be reliable as it was accidently loaded while being properly aligned in the strong frame. This accidental load acted very quickly and caused several sudden cracks to appear; these cracks were noted and clearly marked before further loading.

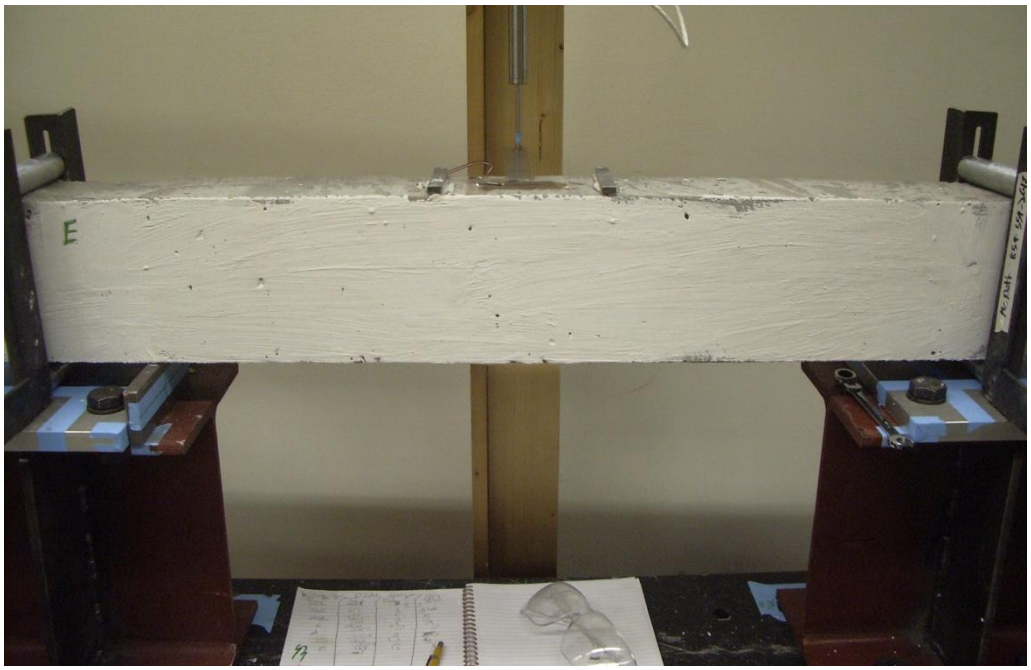

Figure 115. Typical concrete sample in loading devices

The load-displacement results of the flexural reinforced concrete test beam are given in figure 116. Additionally, plotted on the figure is the original design capacity first derived in chapter II and the average of the true capacities of the beams, given the compressive strength of each test beams. Figure 117 shows the compressive strain results of the flexural beam. The results of the shear beams are given in figure 118. Note that results are given in terms of moment and displacement instead of load and displacement; this is because the eccentricity of the symmetrically placed loads was symmetrically increased to encourage shear crack growth after loading two of the shear beams. The strain results of the shear test beams are provided in figure 119. The loading rates of the reinforced concrete test beams are given in table 27.

Table 27. Initial load rates for concrete beams

Beam ID	Load Rate ($^{lb}/_{min}$)	Beam ID	Load Rate ($^{lb}/_{min}$)
1	202.2	4	237.1
3	290.0	5	218.0
A	168.2	6	126.0
B	148.1	7	248.9
C	274.4	9	293.2
D	193.6		
E	251.0		
F	179.2		
G	312.0		
H	182.1		
I	156.7		

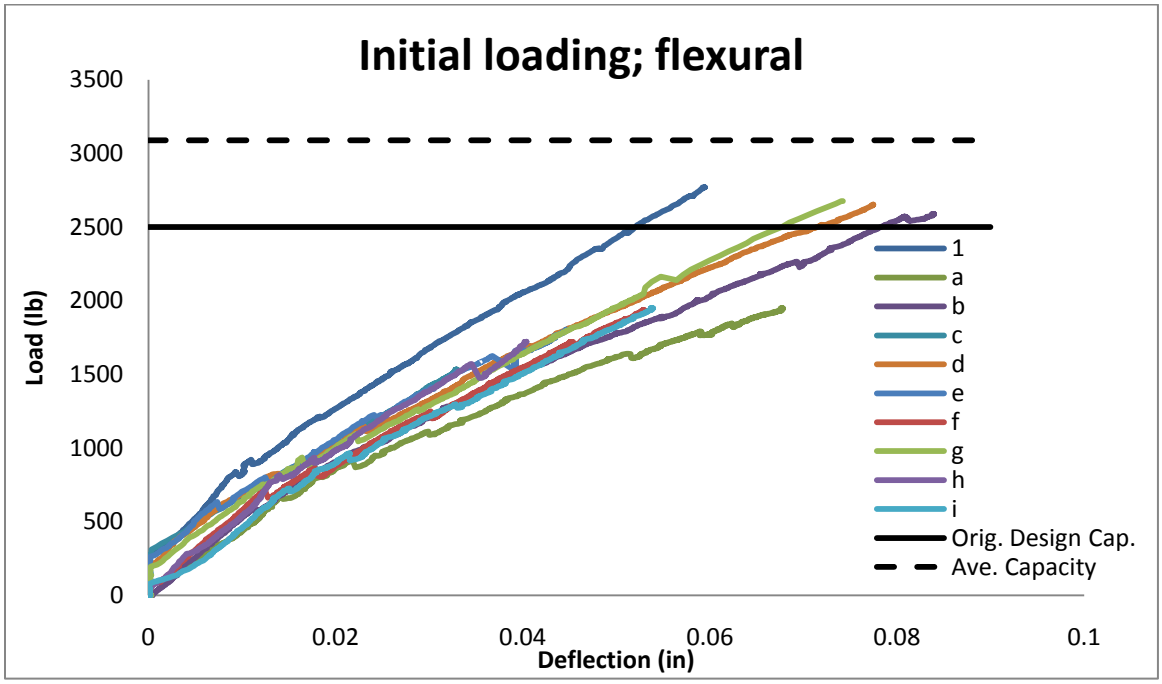

Figure 116. Load-displacement for the flexural test beams

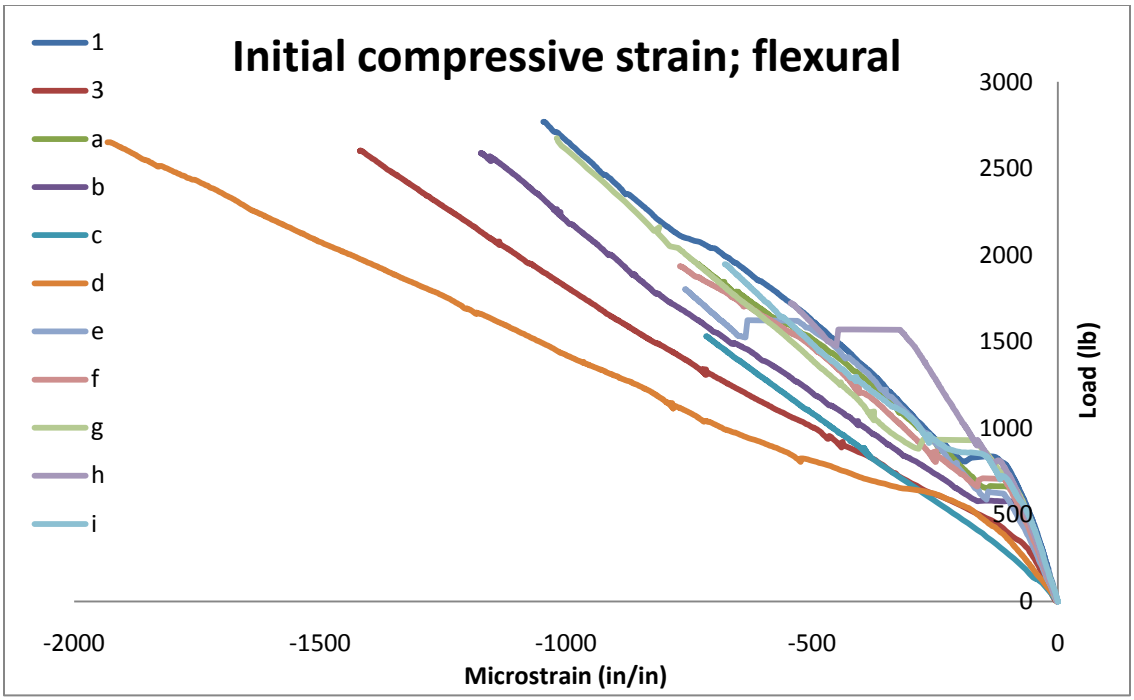

Figure 117. Load-strain values from top strain gage of flexural concrete test beams

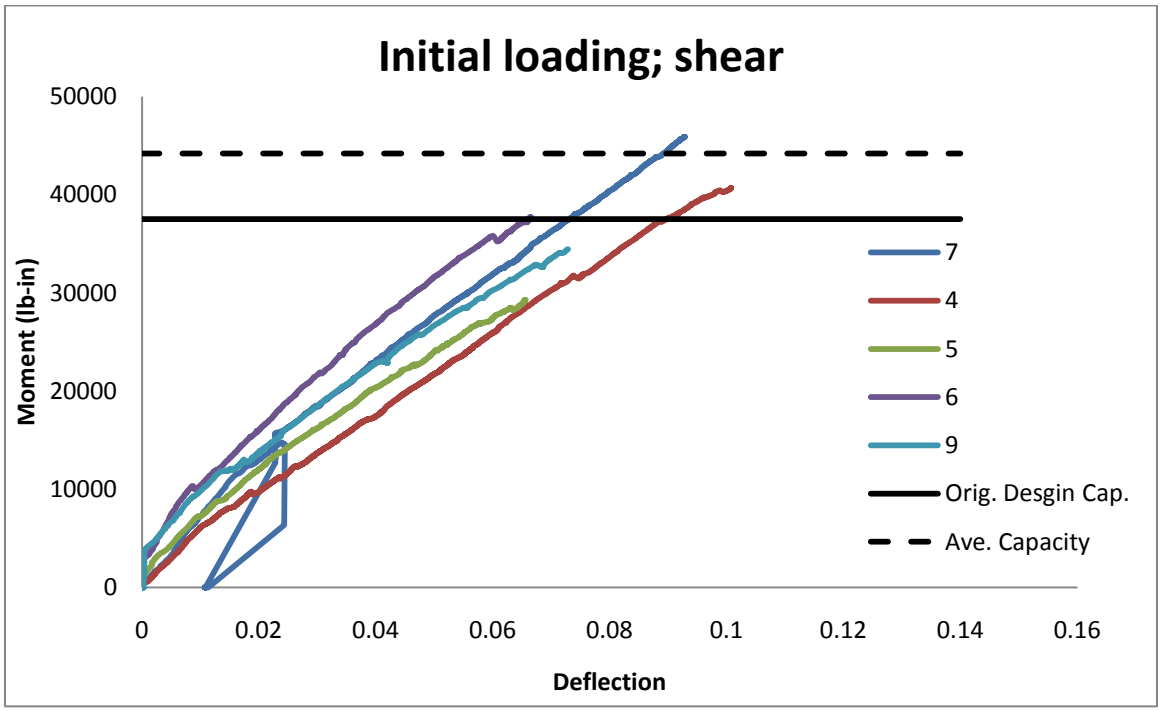

Figure 118. Moment-displacement results for shear test beams

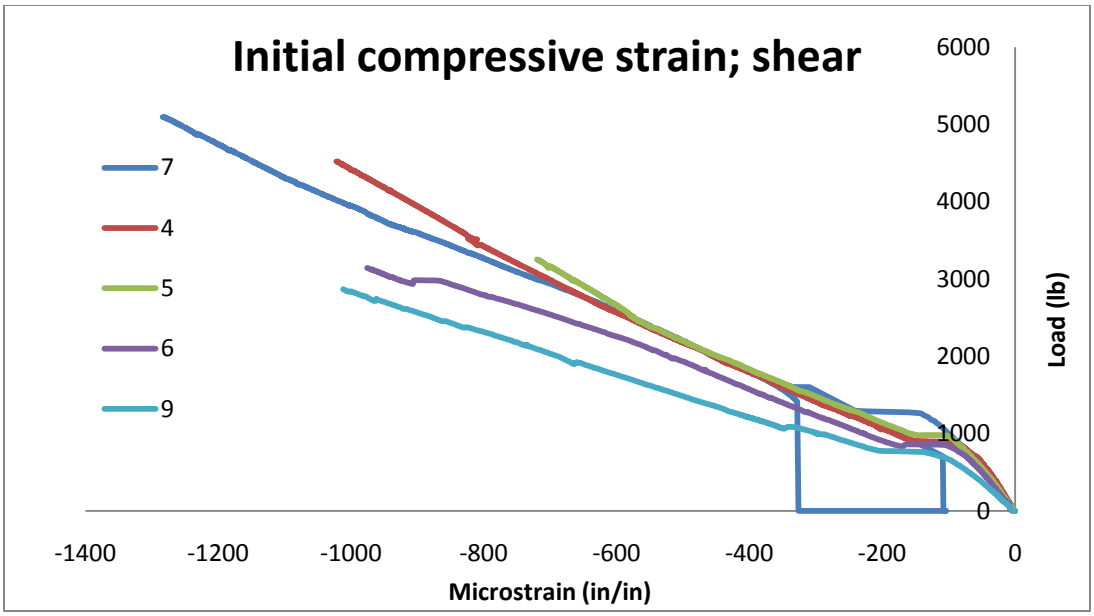

Figure 119. Load-strain values from top strain gage of flexural concrete test beams

Prestressed Concrete Beams

The initial loading of the prestressed beams, PSCB1 and PSCB2, revealed interesting details. PSCB1 developed large shear cracks on only one side of the beam, suggesting local deficiency of concrete strength or misplacement of shear stirrups. In contrast, PSCB2 developed flexural cracks concentrated near mid-span. Unfortunately, the complete initial loading information was not recorded by the data acquisition systems for either beam. The load data of the PSCB1 was captured, and as such figure 120 shows the load plotted as a function of time. Neither displacement nor load information was recorded; despite this the load values from crack growth show that the largest recorded load was 13.5 kips.

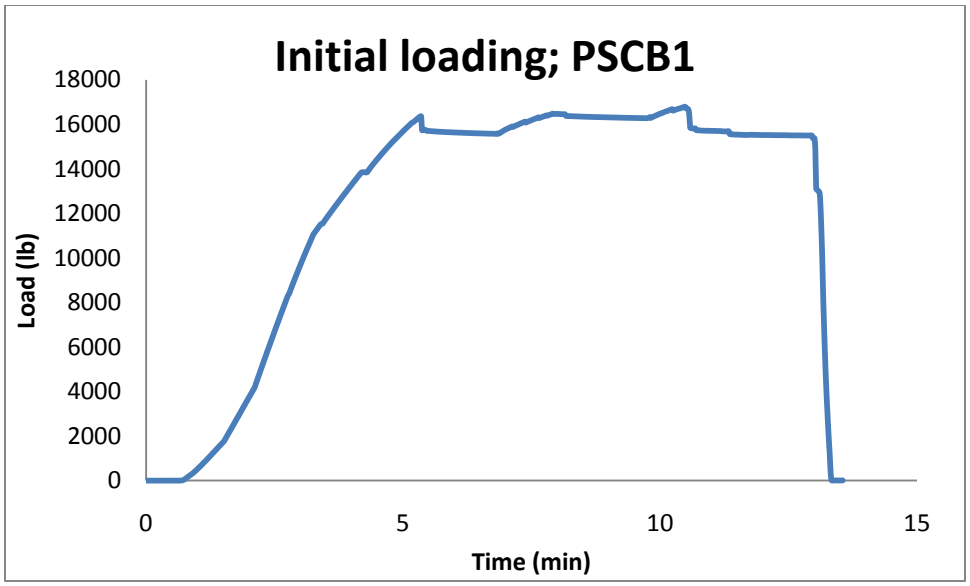

Figure 120. Load-time values from initial loading of PSCB1

Phase III: Patch Repair of Test Beams

Using the design procedure detailed in Chapter IV, the composite repair patches were found for each beam. The results are easily tabulated and presented below. The steel test beams were repaired, both in flexural and shear, with LTC 4300. The shear repair was provided along the entire length of the beam with a height of 4.5 inches.

The details of the flexural composite patches for repairing the flexural beams are provided in tables 29, 30, and 31. Each composite system was utilized and is presented in individual tables, respectively.

Table 28. Flexural composite patch design for test beams SBI and SBIII

Force, F_p (Kip)	Patch width, w_p (in)		Actual Stress, f_p (ksi)	Development Length, L_{pd} (in)	Patch Length, L_p (in)	
	Required	Provided			Theoretical	Provided
10.8	3.28	**3.75**	0.192	4.32	25.01	**26.00**

Table 29. Sikawrap patch design for flexural repair

Beam ID	Force, F_p (kip)	Patch width, w_p (in)		Actual Stress, f_p (ksi)	Development Length, L_{pd} (in)	Patch Length, L_p (in)	
		Required	Provided			Theoretical	Provided
3	0.876	0.10	**2.00**	29.20	0.44	9.61	**10.00**
B	0.864	0.10	**2.00**	28.81	0.43	9.59	**10.00**
D	0.523	0.06	**2.00**	17.43	0.26	9.25	**10.00**

Table 30. LTC 4300 patch design for flexural repair

Beam ID	Force, F_p (kip)	Patch width, w_p (in)		Actual Stress, f_p (ksi)	Development Length, L_{pd} (in)	Patch Length, L_p (in)	
		Required	Provided			Theoretical	Provided
1	0.696	0.22	**2.00**	29.13	0.44	9.60	**10.00**
A	0.709	0.22	**2.00**	29.22	0.44	9.61	**10.00**
G	0.694	0.22	**2.00**	29.21	0.44	9.61	**10.00**
H	0.695	0.22	**2.00**	29.21	0.44	9.61	**10.00**

Table 31. Carbodur patch design for flexural repair

Beam ID	Force, F_p (kip)	Patch width, w_p (in)		Actual Stress, f_p (ksi)	Development Length, L_{pd} (in)	Patch Length, L_p (in)	
		Required	Provided			Theoretical	Provided
C	0.515	0.03	**2**	5.48	0.16	9.05	**10**
E	0.865	0.05	**2**	9.2	0.27	9.27	**10**
F	0.866	0.05	**2**	9.21	0.27	9.27	**10**
I	0.876	0.07	**2**	9.31	0.27	9.28	**10**

A variety of shear composite reinforcing schemes were utilized in this research project to study the performance of each type. Table 32 shows the reinforcing scheme and respective composite material utilized for each beam, in addition to the applied shear for which the composite patches are designed. Test beams repaired with side plates of composite materials were placed at angles which best bridge the existing shear cracks. U-jacket reinforcing schemes were similarly placed at locations which best encompassed the existing shear cracks. Note that each beam has no residual shear capacity according to the design procedure detailed in Chapter IV, equation 160.

Table 32. Patch dimensions for reinforced concrete beams

Beam ID	Composite Material	Reinforcing Scheme	α_p (deg)	Force F_p, (kip)	Width, w_p (in)		Actual Stress, f_p
					Required	Provided	
4	Sikawrap	UJ	90.0	2.79	0.166	**2.00**	46.57
5	Carbodur	SP	60.0	3.54	0.904	**1.00**	37.63
6	LTC 4300	SP	55.0	3.67	0.469	**2.00**	61.25
7	LTC 4300	UJ	90.0	3.03	0.387	**2.00**	50.47
9	Carbodur	SP	45.0	4.01	0.233	**1.00**	42.61

SP = side plate
UJ = U-jacket

Absent from the tables are the values of the development length for the patches. These values were not neglected, but deemed irrelevant because the patches were applied along the height of the beam. In truth, the development lengths were fairly small, with maximum values of 0.25 inches.

The composite repair schemes for the prestressed concrete beams were designed using the procedures detailed in Chapter IV; PSCB1 required shear repair on one side of the beam and PSCB2 required flexural repair. The shear composite designs are given below in tables 33 and 34.

Table 33. PSCB1 composite repair patch dimensions

Composite Materials	Reinforcing Scheme	α_p (deg)	Force F_p, (kip)	Width, w_p (in)		Actual Stress, f_p
				Required	Provided	
Sikawrap	UJ	90	13.27	0.79	**8**	55.1

Table 34. PSCB2 composite repair patch dimensions

Force, F_p (kip)	Patch width, w_p (in)		Actual Stress, f_p (ksi)	Development Length, L_{pd} (in)	Patch Length, L_p (in)	
	Required	Provided			Theoretical	Provided
6.37	0.37	**4.0**	33.91	1.44	16.72	**18**

Before applying the composite patches, the interfacial stresses acting on the adhesives were determined with the mechanistic model. The model was programmed using the computational language MATLAB using the derivations of Chapter III. With the knowledge of the composite patch sizes, the stresses applied to the composite adhesive can be found using such a program.

The response of composite patches to a typical reinforced concrete beam is shown in figure 121. The figure was derived using a common compressive strength of concrete, common patch dimensions derived above, and an applied load of 1 kip. It is evident from the figure that beams repaired with Sikawrap and Carbodur patches are more stiff than those repaired with LTC 4300.

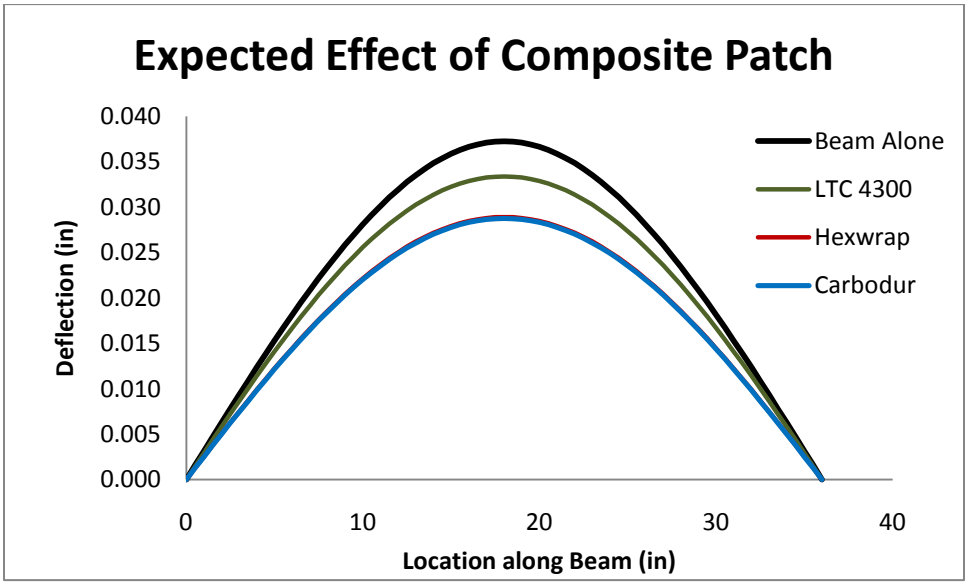

Figure 121. Deflection response of composite patched beams

The results of the mechanistic model according to each composite material type and desired capacity are given in tables 35 through 37. It is easily observed that the stresses applied to each composite system do not exceed the capacity of the adhesives.

The results of the model add confidence to the success of the composite reinforcing system.

Table 35. Mechanistic model results for Carbodur composite patches

Beam ID	Maximum Displacement (in)	Tension ($^{lb}/_{in^2}$)	Shear ($^{lb}/_{in^2}$)
B	0.1283	0.744	159.44
C	0.1400	0.81	173.94
E	0.1374	0.79	170.71
F	0.1398	0.81	173.66

Table 36. Mechanistic model results for Sikawrap composite patches

Beam ID	Maximum Displacement (in)	Tension ($^{lb}/_{in^2}$)	Shear ($^{lb}/_{in^2}$)
1	0.1158	0.18	141.71
H	0.1157	0.18	141.60
3	0.1193	0.18	145.99

Table 37. Mechanistic model results for LTC 4300 composite patches

Beam ID	Maximum Displacement (in)	Tension ($^{lb}/_{in^2}$)	Shear ($^{lb}/_{in^2}$)
A	0.1739	0.01	12.53
D	0.2192	0.01	15.79
G	0.1656	0.01	11.83
I	0.1720	0.01	12.39

With all the limit states checked and in compliance, the composite repair patches were applied to the test beams according to the procedures detailed in Chapter IV.

Phase IV: Load Testing of Patch Repaired Beams

Steel Beams

The steel beam specimens were loaded to similar values as in Phase II. The load rates for the beams are given in table 38. The results of the second loading are plotted in figure 122. Figures 123 through 125 show the strain results.

Table 38. Load rates of steel test beams during Phase IV

Beam ID	Load Rates ($^{lb}/_{min}$)
SBI	1504.8
SBII	1827.8
SBIII	1137.0

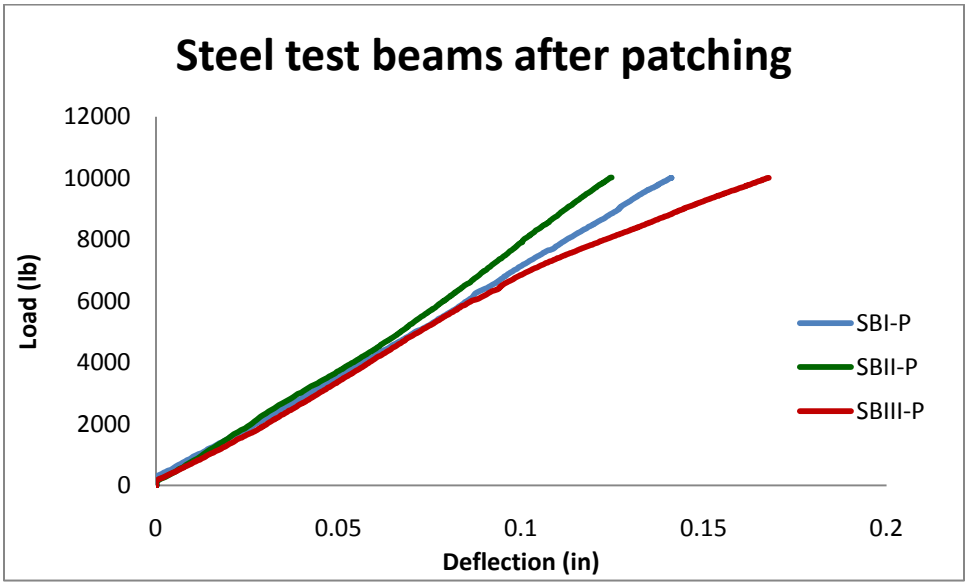

Figure 122. Load-displacement values of patched steel test beams

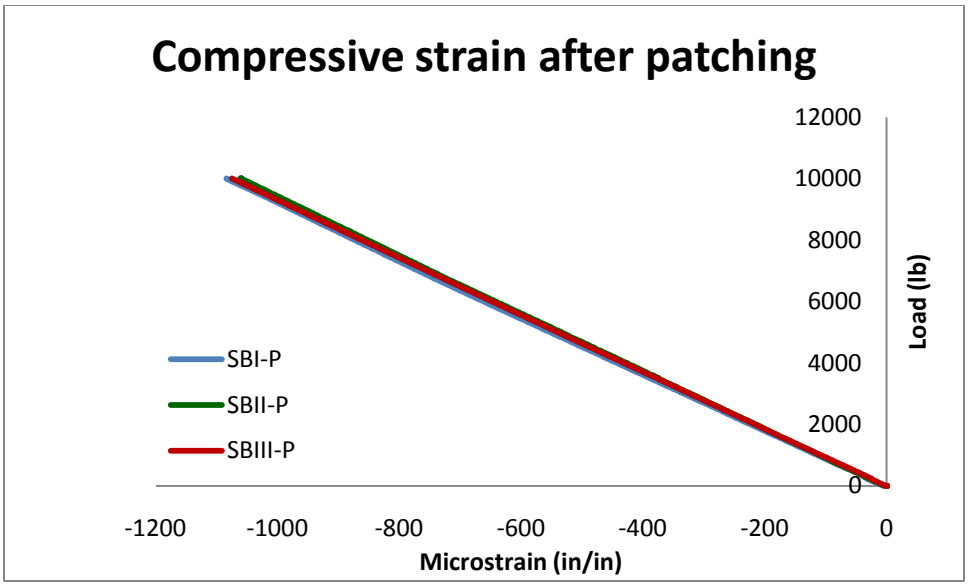

Figure 123. Load-strain values from top strain gage of steel test beams

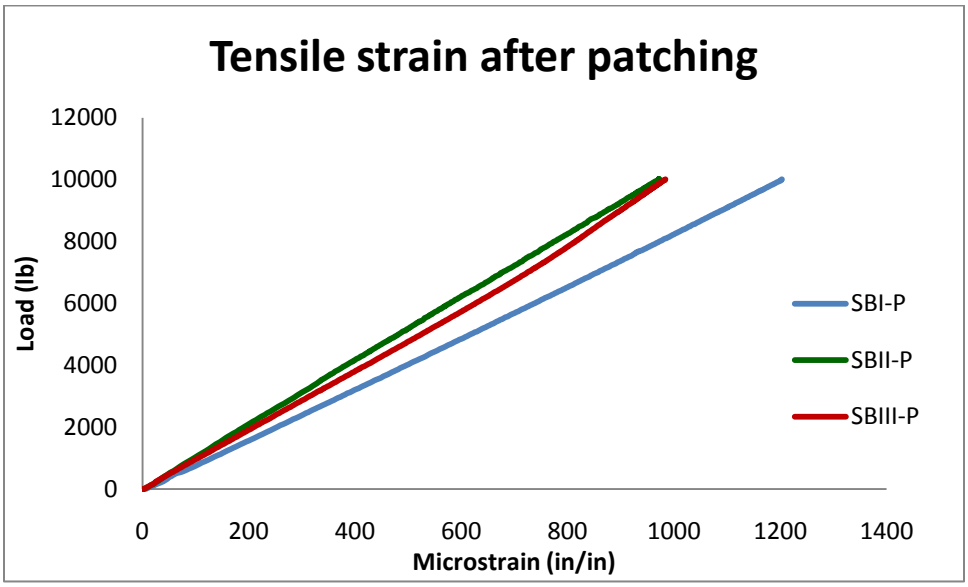

Figure 124. Load-strain values from bottom strain gage of steel test beams

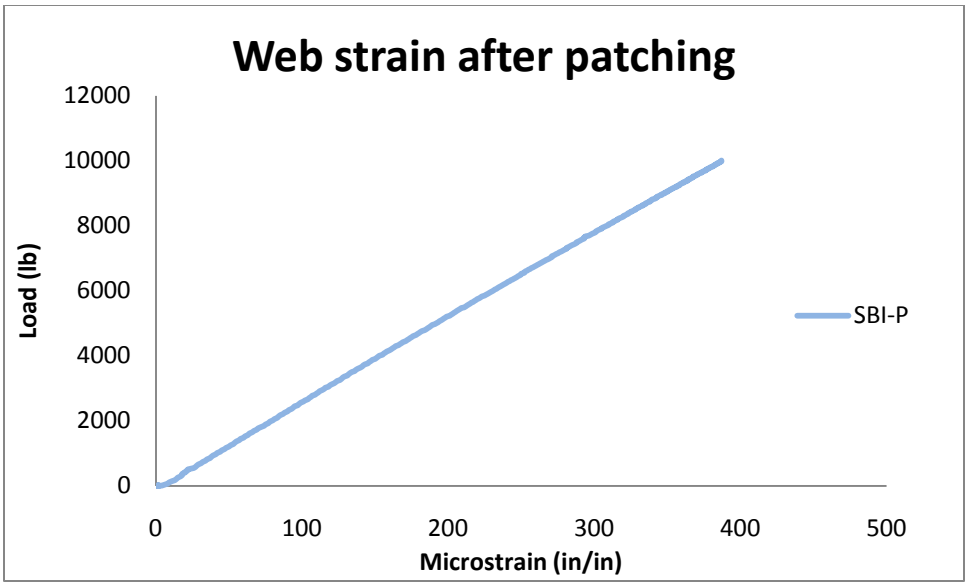

Figure 125. Load-strain values from web strain gage of steel test beams

Reinforced Concrete Beams

The composite patch repaired reinforced concrete beams were loaded until failure. In general, both the flexural and shear beams failed in shear. The cracking of test beams incurred during Phase IV were traced and recorded, similarly to that undertaken in Phase II testing, and are recorded in Appendix C. The loading rate of the patched flexural reinforced concrete test beams are provided in table 39 and the results of loading the composite patched flexural reinforced concrete beam specimens are given in figures 126 and 127. The next figures show the strain values experienced by the composite patched flexural beam specimens. The strains of the composite patches are plotted in figures 128 and 129. Two plots are provided given the incredible range of values recorded. Note the range of the microstrain of each figure and also the colors of the lines, which represent each patch type; blue for Sikawrap, green for LTC 4300, and orange for Carbodur.

Table 39. Load rate of patched flexural test beams during Phase IV

Beam ID	Load Rate ($^{lb}/_{min}$)
1	261.3
3	527.4
A	463.7
B	434.9
C	446.5
D	557.6
E	188.9
F	335.4
G	412.3
H	573.8
I	439.3

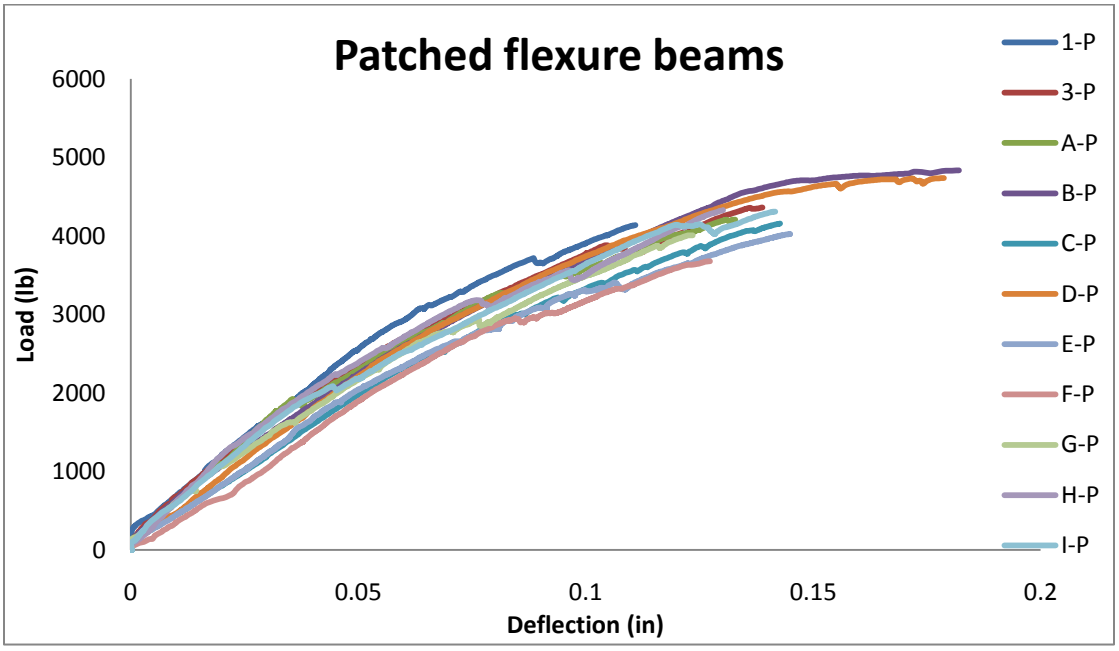

Figure 126. Load-displacement results of composite patched flexural beam

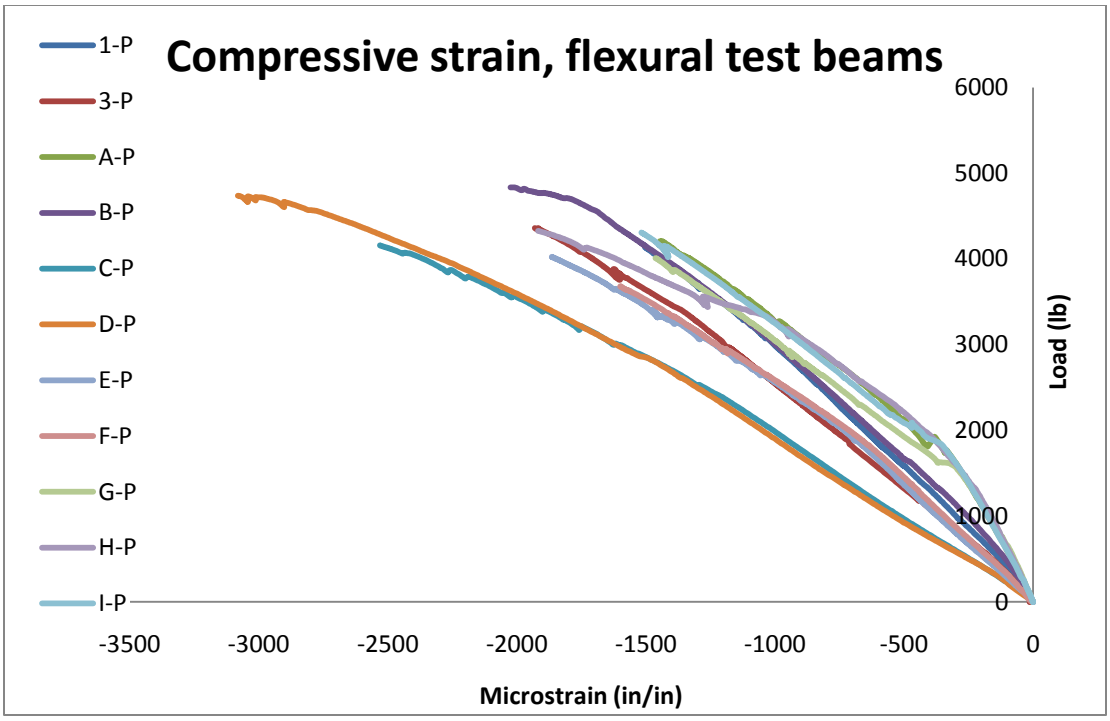

Figure 127. Load-strain values from top strain gage of flexural test beams

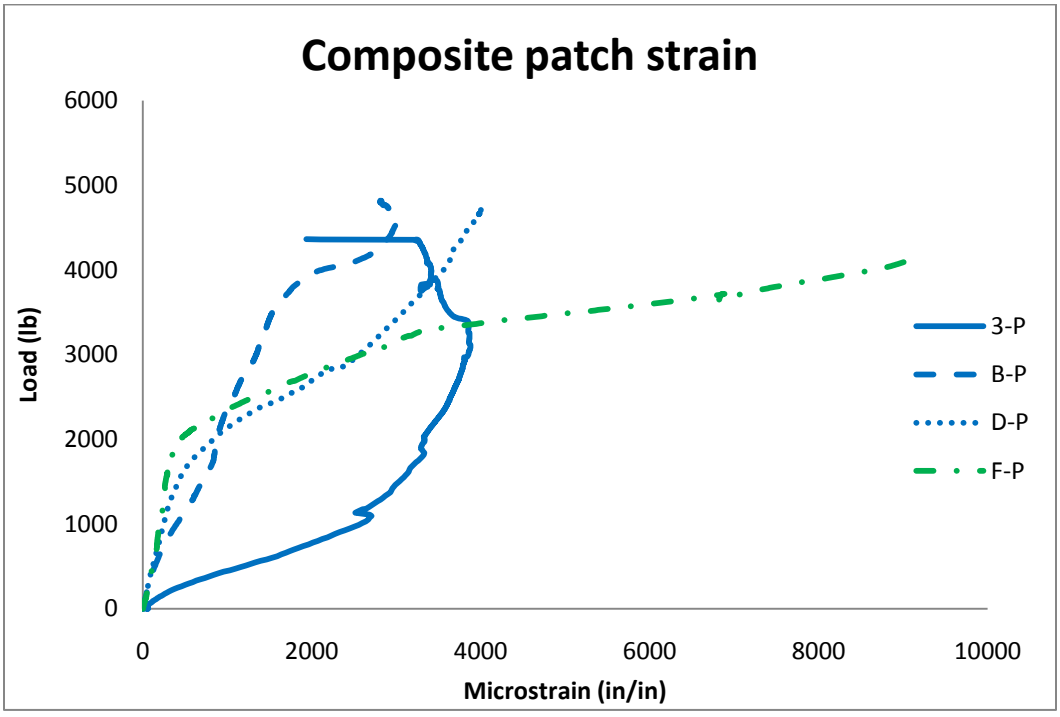

Figure 128. Strain measured from composite materials bonded to flexural test beams

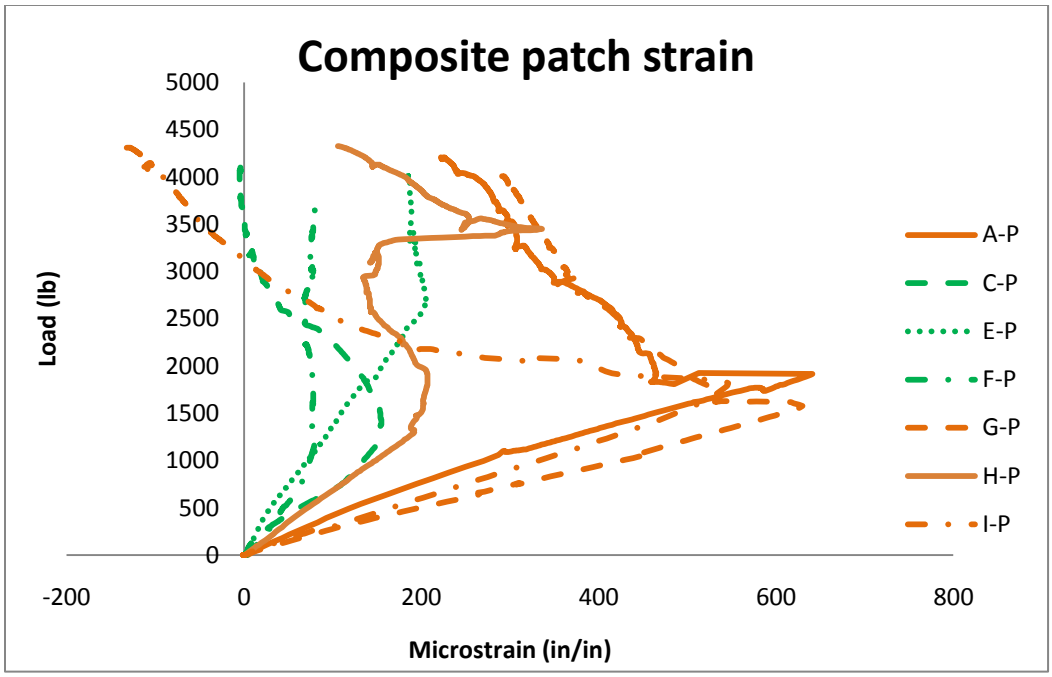

Figure 129. Strain measured from composite materials bonded to flexural test beams

The applied load data was not correctly recorded by the data acquisition system for the shear test beams. However, the largest recorded loads from the shear beam specimens crack records are given in table 40.

Table 40. Largest recorded load values of shear test beams

Beam ID	Maximum Load (lb)
4	5775.0
5	6400.5
6	3415.0
7	5230.0
9	4442.5

Prestressed Concrete Beams

The results of the final loading of the prestressed beams are as interesting as the initial loading of the prestressed beams. The data acquisition system was unable to capture any applied load data, but using the values recorded form crack growth and notes taken during the loading process, showed that the patch repaired PSCB1 had little to no increase in capacity. The reason for the stagnation of load is presented in Chapter VI. Despite the loss of load data, the strain values were properly recorded. Such strain values are given as functions of time and load in figures 130 and 131. The crack growth pattern is provided in Appendix C.

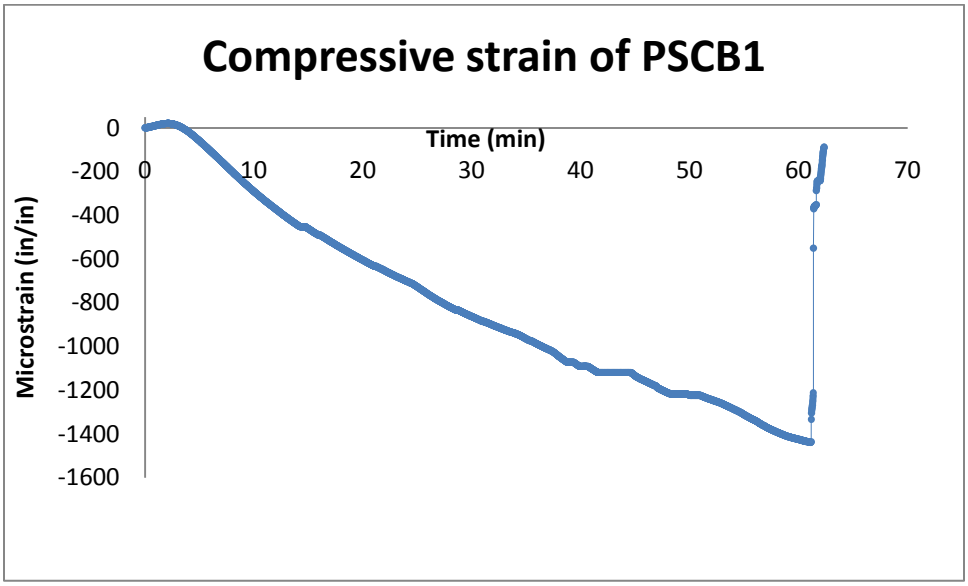

Figure 130. Strain measured from gage at midspan of beam

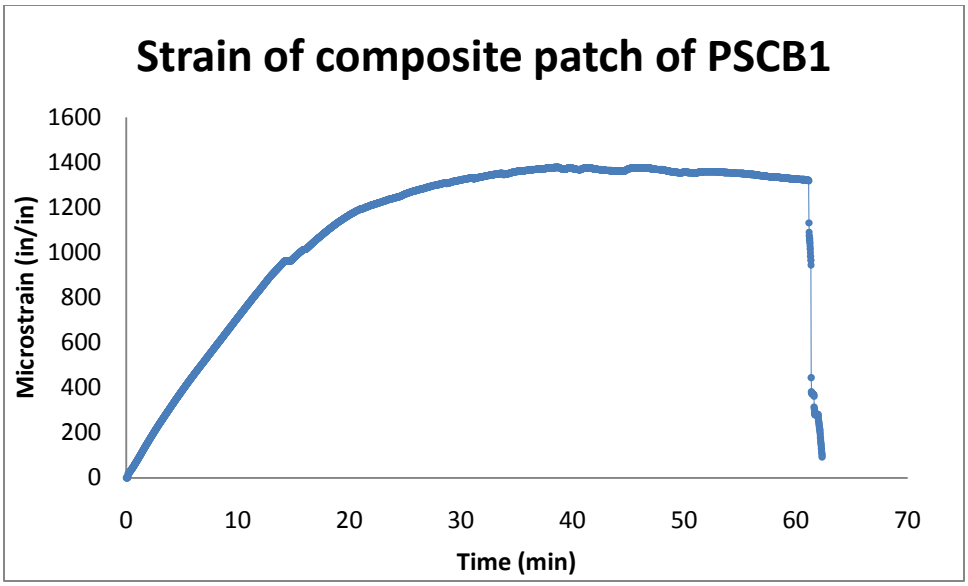

Figure 131. Strain measured from gage adhered to composite patch

The flexurally repaired PSCB2 test beam ultimately failed due to shear, as shown in figures 132 and 133. Since the data acquisition system failed to record the displacement information, only load and strain information are provided in the below figures.

Figure 132. Ultimate shear failure of PSCB2

Figure 133. Close up of shear failure of PSCB2, note rebar stirrup

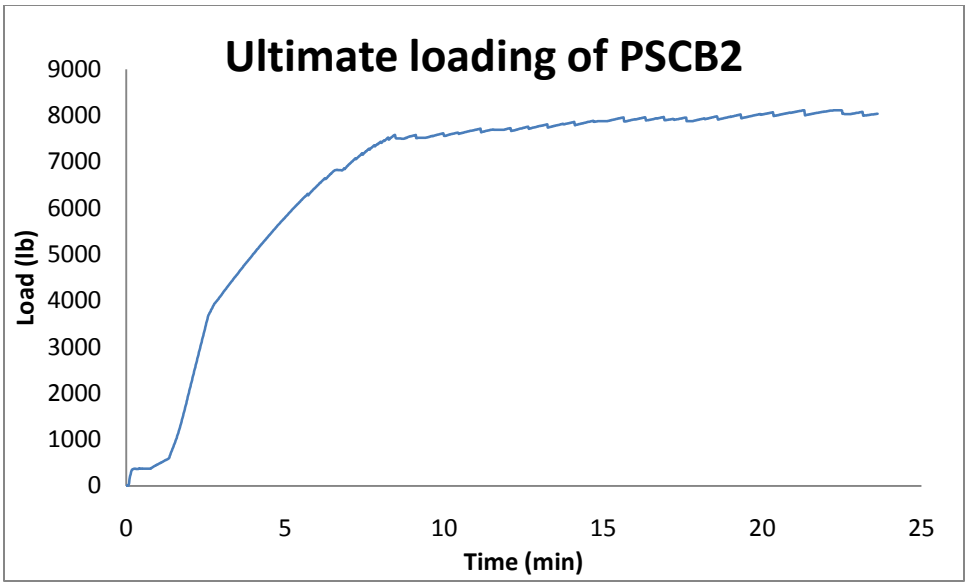

Figure 134. Loading of PSCB2 to failure

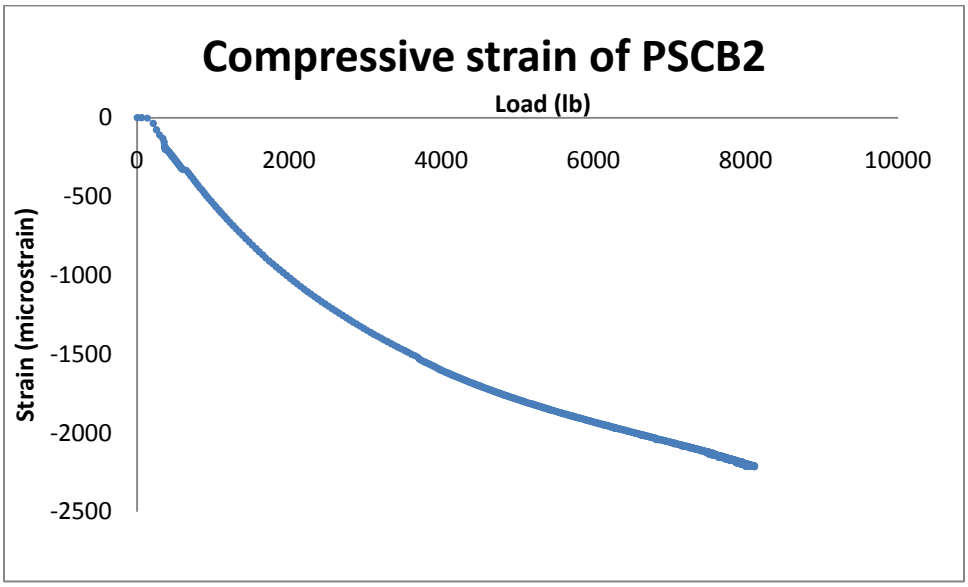

Figure 135. Load-strain values of top strain gage of PSCB2

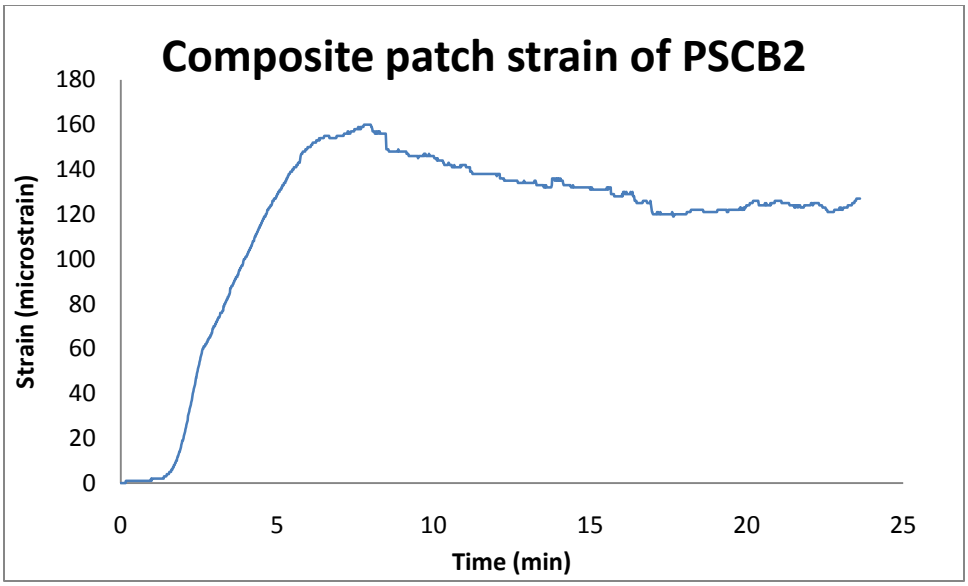

Figure 136. Tensile strain of composite patch as a function of time

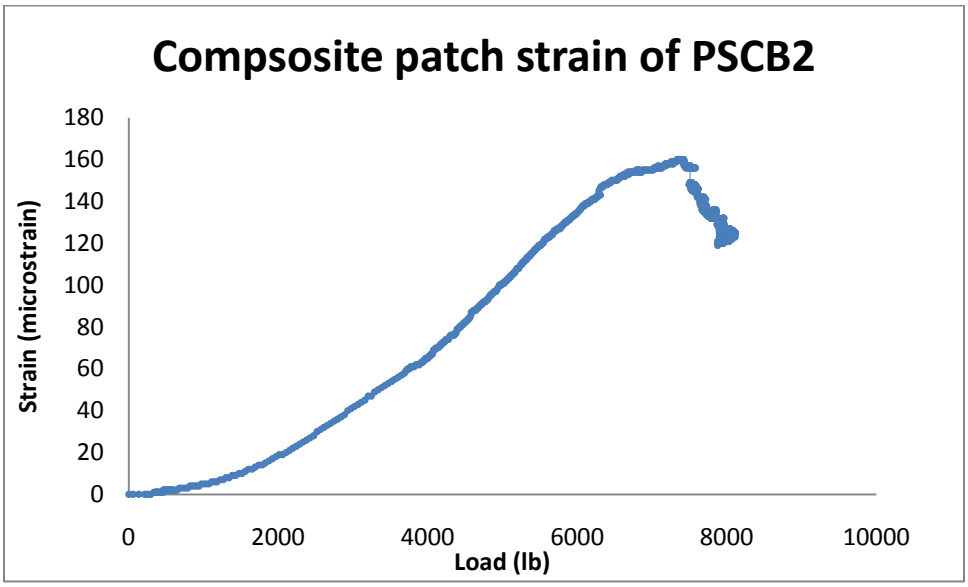

Figure 137. Tensile strain of composite patch as a function of applied load

Chapter VI

RESULTS, DISCUSSION, CONCLUSION

Effectiveness of Composite Patch Repair

There are several metrics of performance with which to evaluate the effectiveness of the composite patching scheme presented in the previous chapters. The critical metric is the increase in the load carrying capacity of a member. Other metrics include failure mode, nature of crack propagation, degree of increase in capacity compared with design capacity, and extent of strength recovery considering the initial damage.

Steel Beams

The steel beam results border between being intuitive and counter-intuitive. Considering the similarities of key material and mechanical properties, primarily the modulus of elasticity of steel and the composite fibers, shown in table 14, the increase in moment of inertia of the composite section is negligibly small. This minute difference suggests that the patched steel beams would behave essentially similarly to the unpatched beams in the elastic region. The increase in stiffness was almost negligible until the test beams reach the yielding limits of the beam. Consider that the thickness of the composite applied to the beam is roughly 0.01 inches and the modular ratio of the composite to steel is nearly 0.65. The addition of the composite is similar to adding an incredibly thin sheet of steel to the tensile flange or web. As illustrated in Chapter II, lateral torsional buckling

is the controlling limit state for the test beams; as such the composite patch provides little to no resistance to such behavior. This is confirmed in published research which found that composite applications to steel beams are only beneficial when yielding is the critical limit state (Colombi and Carlo, 2006). The test beams in the present study did not undergo either lateral torsional buckling or yielding. The effects of adding the composite patch did not exhibit noticeable gain in strength.

That being stated, the beams retrofitted with composite materials should show a difference in behavior: showing some increase in stiffness. Unfortunately, the deflections of the test beams seem to be inconsistent with expectations, thought the differences in values are within the margin of error of LVDT readings; found through calibration runs.

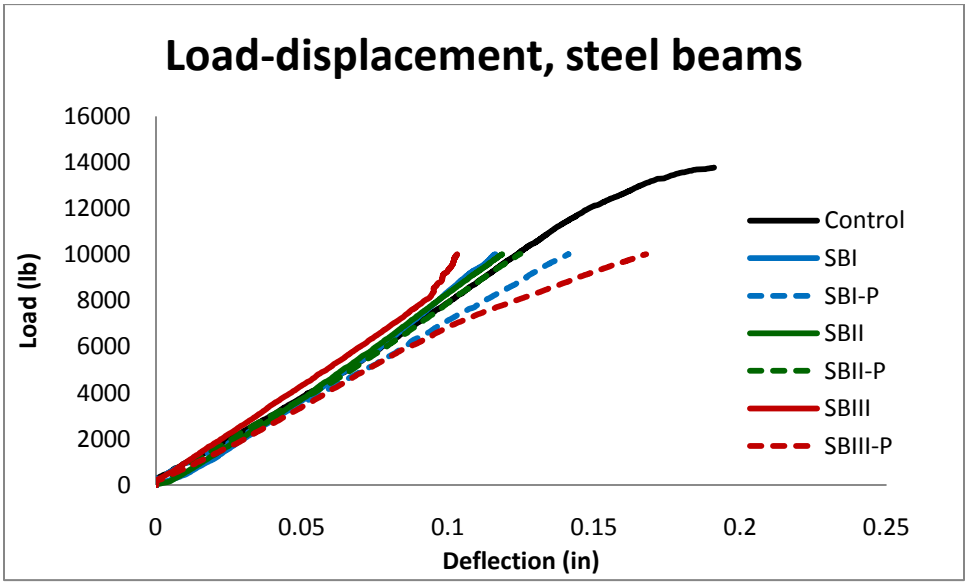

Figure 138. Load-displacement results for steel test beams

The recorded strain values also fall within the expected margin of error of measurement. The expected changes in strain values were small enough that the relative changes shown in the plots are indistinguishable. Figures 139 through 141 show the

measured strain results. The beams retrofitted with composite material along the bottom flange, SBI and SBIII, show greater strain in the bottom flange; while SBII, which only had composite materials placed along the length of the web, showed a decrease in the strain of the bottom flange. The diagonal web strain results from SBI show expected results; that the strain experienced by the web of a repaired beam is in fact smaller than the beam before the composite retrofit.

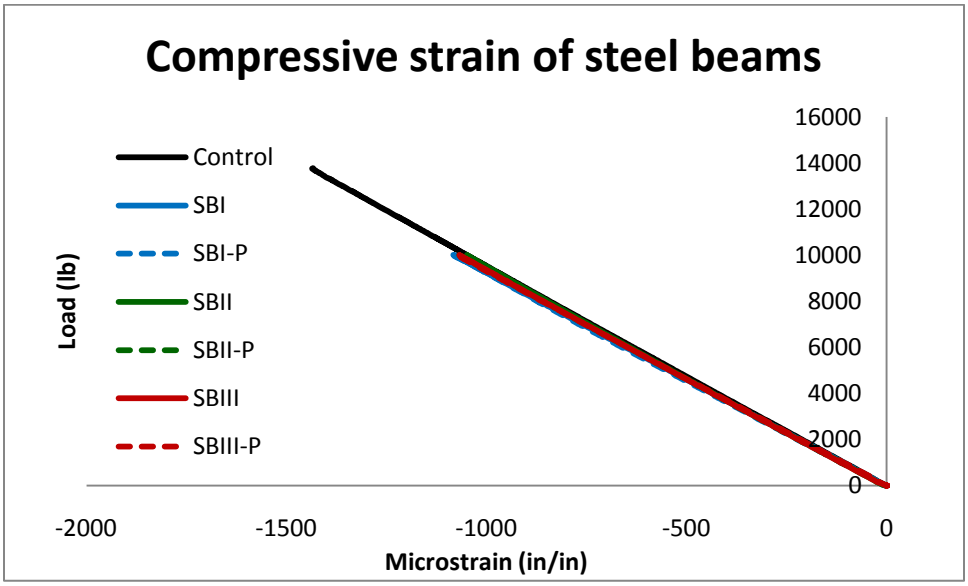

Figure 139. Load-strain values from top flange of steel test beam

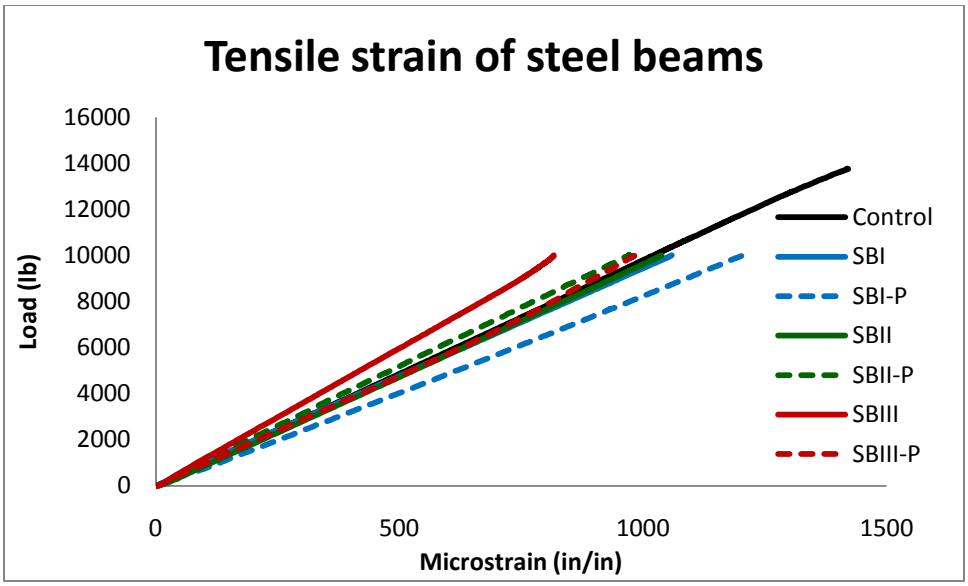

Figure 140. Load-strain values from bottom flange for steel test beam

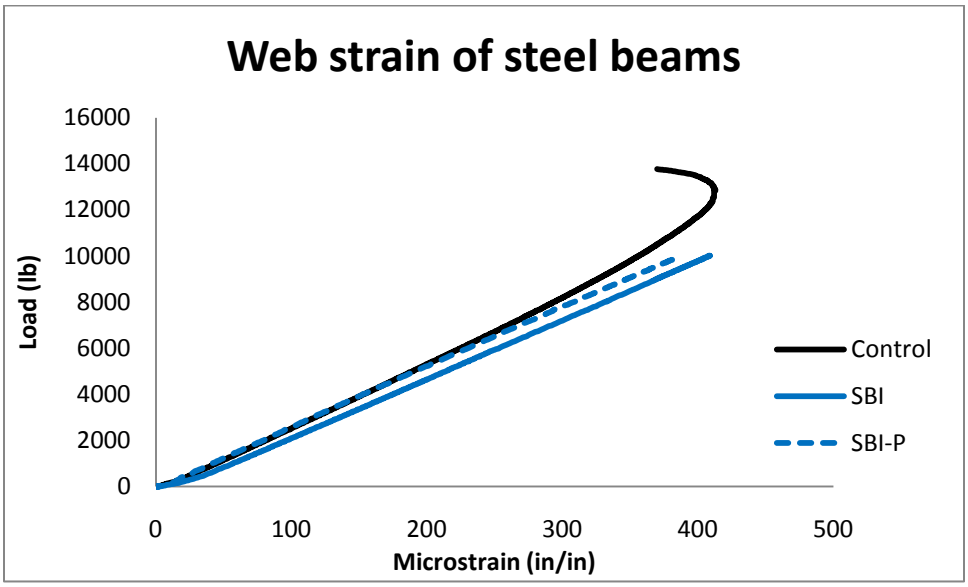

Figure 141. Load-strain values from the web of steel test beam

Reinforced Concrete Beams

The results from the concrete test beams show a much clearer understanding of the effectiveness of composite patching. The first metric examined is the effect of the composite patching on the shear or moment capacities of the beams. Figure 142 shows the load-displacement results of beam with flexural patches. Horizontal lines representing the original design capacity beam, the average value of the true capacity of the beams given the known compressive strength of the concrete, and, the average value of the patched beam design capacity. Note that all the test beams exceed these desired capacities of the patch design by a significant margin.

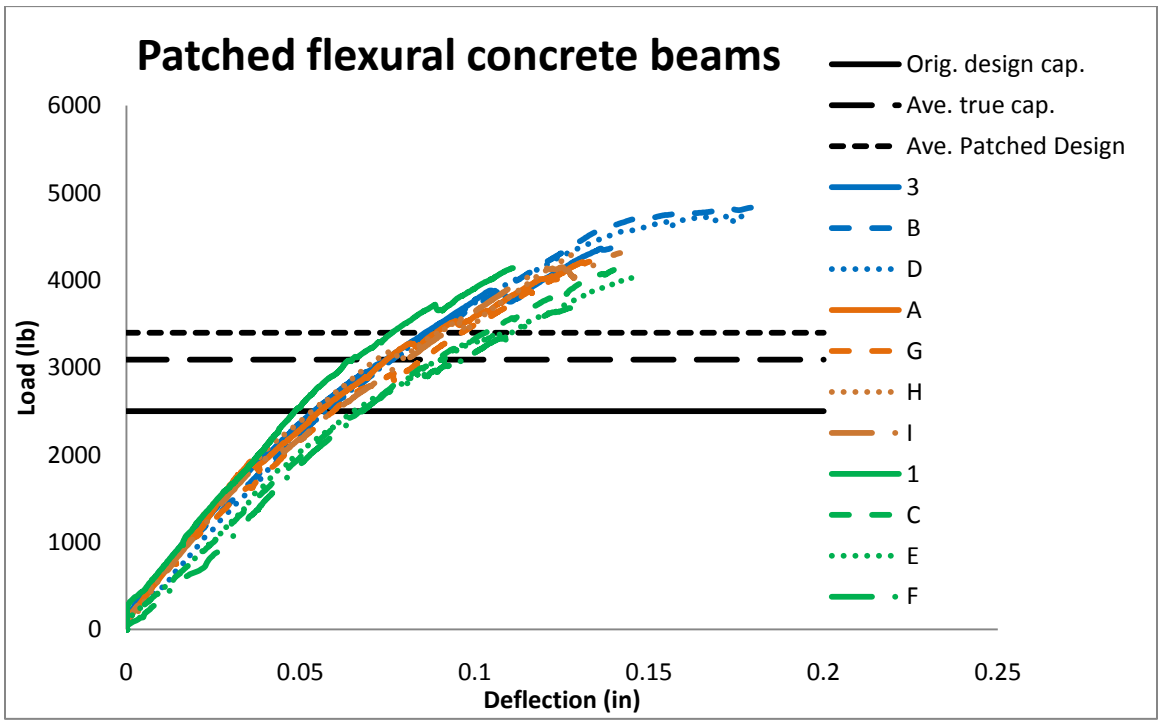

Figure 142. Final capacity of each flexural beam in reference to desired capacities

The shear span ratio of the beams varies from 3 to 3.75, so the failure of all the beams would be expected to be in shear or diagonal tension. The tests showed this was true. Within the shear span, diagonal cracks typically started from flexural cracks which gradually increased in inclination. Such cracks did not get into the imminent failure state initiated; as the crack path leveled, it approached the applied point load, culminating into a sudden compressive failure. This is illustrated with figures 143 and 144. Shear beams, failure tended to be shear compressive, with cracks extending from the applied load point to the support pins, as shown in figure 145 and 146. Some beams had distinct concrete crushing, while others did not. Others had significant crack propagation along the primary reinforcing steel.

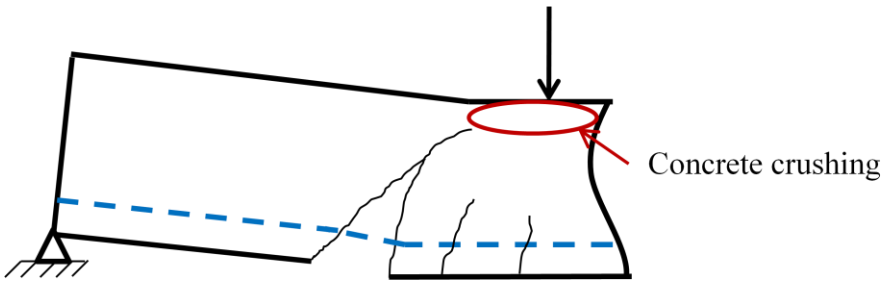

Figure 143. Failure modes of flexural beams repaired with composite systems

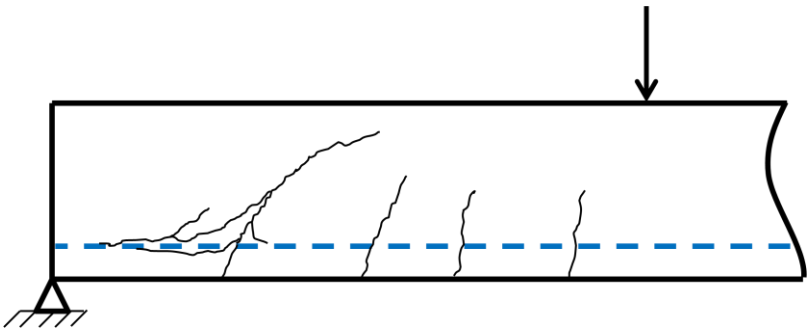

Figure 144. Failure modes of flexural beams repaired with composite systems

Figure 145. Top view of typical concrete crushing at point load application location

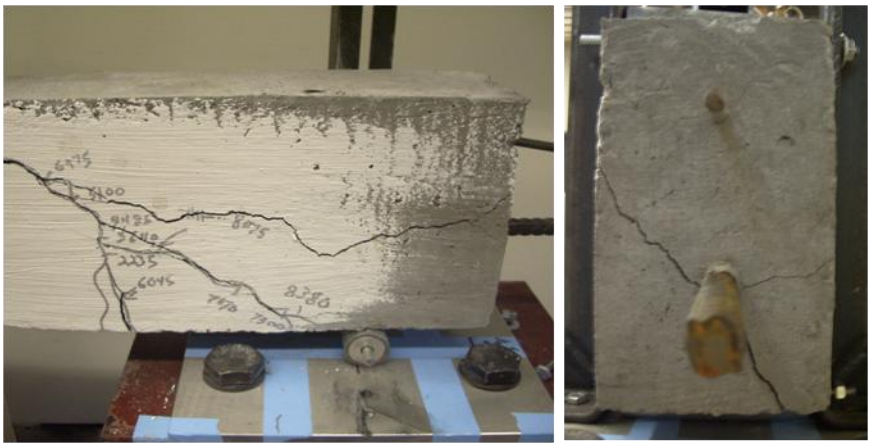

Figure 146. Cracking along primary reinforcing steel

Separating the results by type of composite system utilized reveals additional details. Figure 147 shows the results of retrofitting beams with Sikawrap composite fibers. Table 41 shows the individual performance of each beam retrofitted with Sikawrap and the increase in capacity over the design value. The noticeable drop in load capacity of beam 3 is the result of the sudden development of a diagonal shear crack;

which ultimately caused the failure of the beam in shear. On average, beams flexurally repaired with Sikawrap showed a 20% increase in capacity over the designed value. Overall, the beam capacity increased 32% over the original design capacity. At low loads, comparable to those in Phase II of testing discussed in Chapter V, beams retrofitted with Sikawrap composite systems were found to be considerably more stiff. At equal, or near equal, loads, the deflection of patched beams are nearly 25 percent smaller.

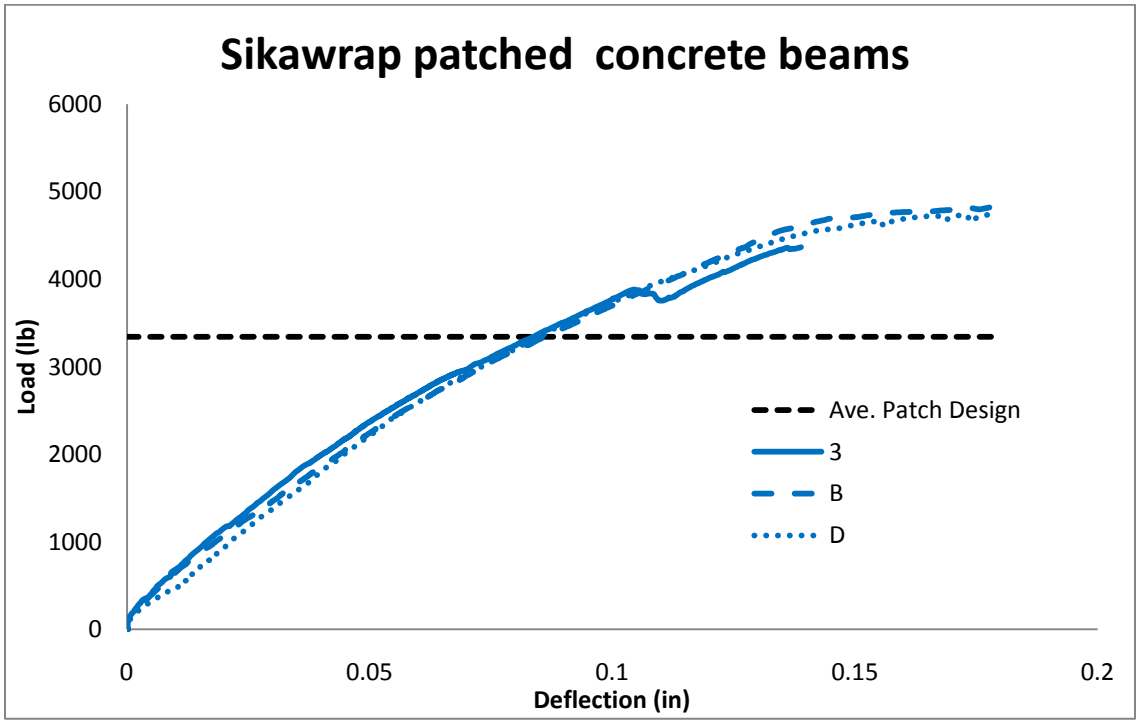

Figure 147. Final performance of flexural beams repaired with Sikawrap

Table 41. Individual results of flexural beams repaired with Sikawrap

Beam ID	Actual Patched Capacity (kip-in)	Patched Beam Design Capacity (kip-in)	Original Beam Design Capacity (kip-in)
3	62.05	51.57	46.88
B	55.19	51.14	46.49
D	62.36	47.73	43.39

Figure 144 shows the results of repairing reinforced concrete beams with LTC 4300 composite systems. Table 42 gives the individual moment capacities of each flexural beam retrofitted with LTC 4300. There is no obvious reason for beam 1to be stiffer than the other beams. On average, beams flexurally repaired with LTC 4300 showed a 26% increase in capacity over the expected patched design value. Additionally, the average beam capacity increased over 39% the original design capacity. At low loads, the displacement of the patched beam at equal, or near equal loads, is roughly 17 percent lower than the same beams when tested in Phase II.

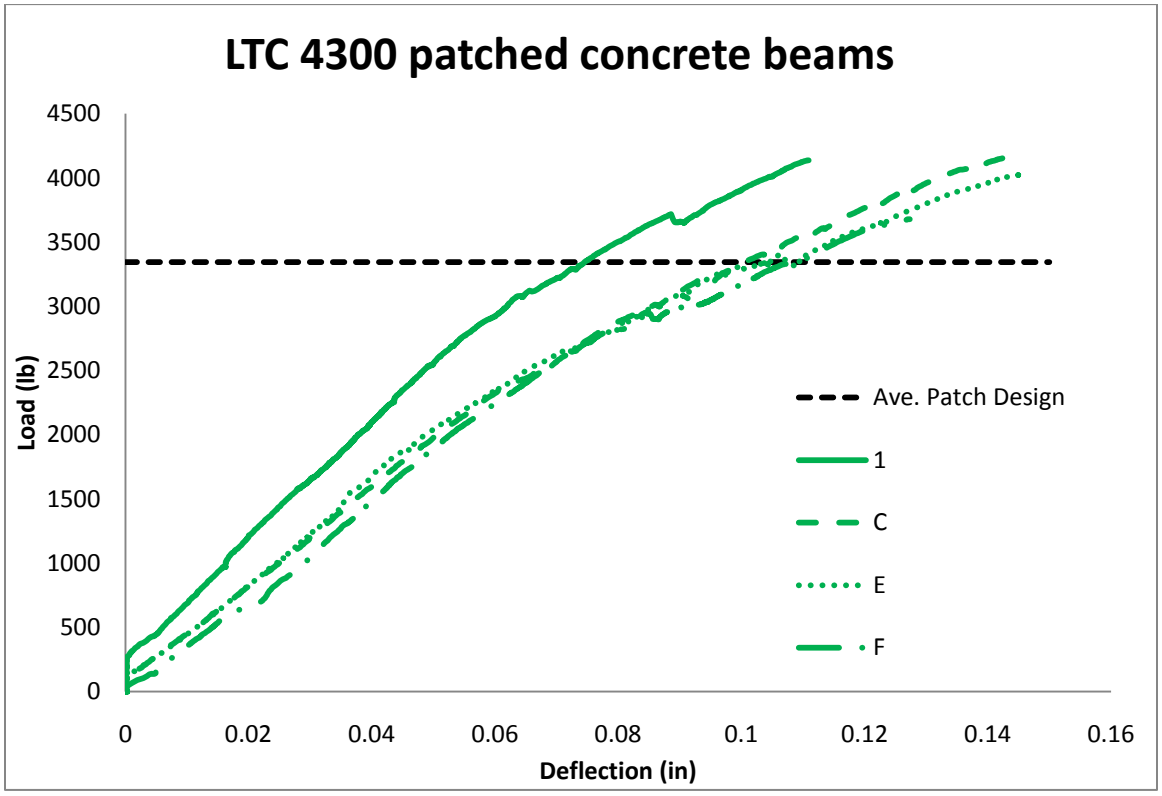

Figure 148. Load-displacement of flexural beams repaired with LTC 4300

Table 42. Individual results of flexural beams repaired with Carbodur

Beam ID	Actual Patched Capacity (kip-in)	Patched Beam Design Capacity (kip-in)	Original Beam Design Capacity (kip-in)
1	63.14	51.73	47.03
C	60.12	47.81	43.46
E	64.92	50.62	46.02
F	64.64	50.50	45.91

Figure 149 shows the results of repairing reinforced concrete beams with Carbodur composite systems. Table 43 gives the individual moment capacities of each beam retrofitted with Carbodur strips. On average, beams flexurally repaired with Carbodur showed a 31% increase in moment capacity over the expected patch design value. The average moment capacity increased 44% over the original design capacity. The displacements of flexural beams retrofitted with Carbodur composite systems are not significantly different than those with no composite repair.

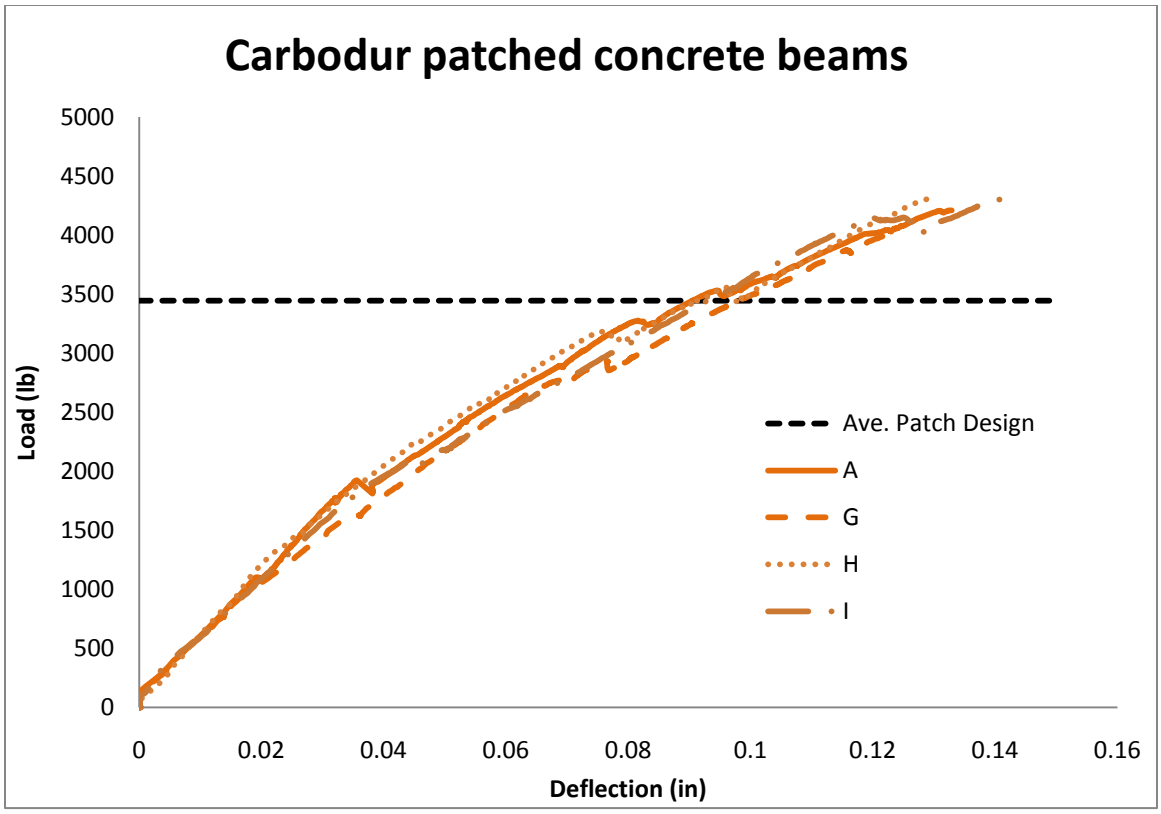

Figure 149. Final performance of flexural beams repaired with Carbodur

Table 43. Individual results of flexural beams repaired with LTC 4300

Beam ID	Final Capacity (kip-in)	Patch Design Capacity (kip-in)	Beam Design Capacity (kip-in)
A	72.50	51.56	46.87
G	71.36	51.78	47.07
H	65.46	51.76	47.05
I	60.35	51.66	46.96

The displacements of flexurally repaired beam with Sikawrap undergo the greatest deflection, despite resisting the lowest ultimate loads. The deflections of beams retrofitted with Sikawrap are 26% higher than those repaired with LTC 4300 and Carbodur. On the other hand, the deflection of beams repaired with LTC 4300 and

Carbodur are nearly the same. Increased deflection, or ductility, can serve as an additional source of warning of imminent beam failure.

The nature of crack propagation of the flexural test beams reveal insight into failure modes and patterns. General observations were documented throughout the fourth phase of the experimental work concerning the crack growth and behavior. The first observation is that crack growth is virtually halted in the region above the composite patch. This is especially true of Carbodur applications, possibly because of the high stiffness of this material. This is clearly visible in the figures of Appendix C.

The second observation is that stoppage of crack growth just above the patch causes stress to build in that region. This build up of stress caused flexural cracks at the boundary of the patch area to appear and travel inward, sometimes horizontally, bridging the existing flexural cracks in the patched region. Figures 150 through 154 shows several examples of cracks travelling inward to redistribute the flexural stress in the patched region

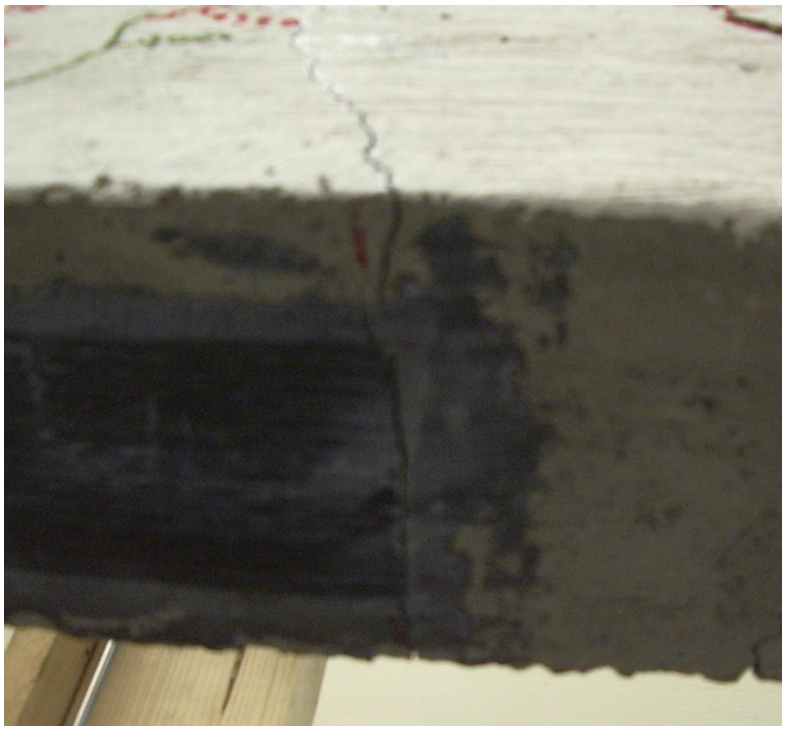

Figure 150. Crack development in the bottom of beam at Sikawrap edge

Figure 151, Crack development at the patch edge of a Carbodur patch

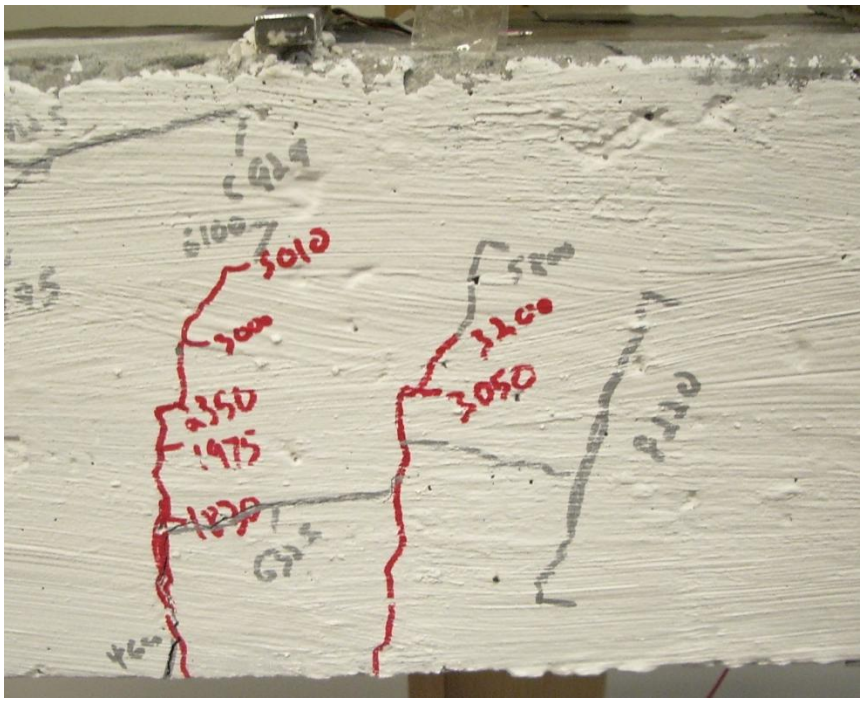

Figure 152. Horizontal cracks in beam H

Figure 153. Horizontal cracks in beam 3

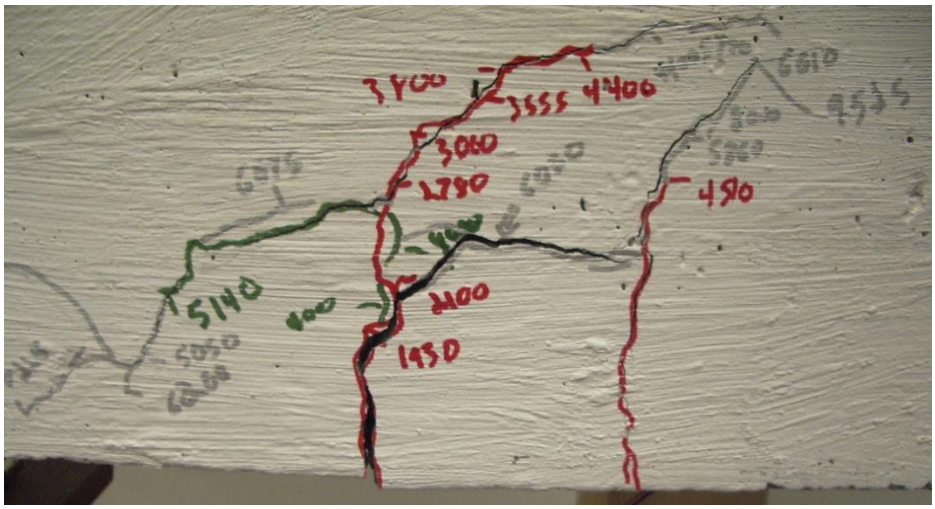

Figure 154. Horizontal cracking in beam B

Another general observation is that during loading, beams repaired with Sikawrap created audible noises, probably due to fibers separating from the resin and cracking. Beams repaired with Sikawrap produced the widest and most noticeable flexural cracks before failure. Such flexural cracks developed on either side of the composite patch, but did not cause failure. Such visual cracking may provide an excellent warning of imminent beam failure in field applications.

The strain information collected from the strain gages placed on top of the centerline of the beams show that only one actually reached the design crushing strain value of 0.003. However, crushing of concrete was observed in several beams near the load points during shear or shear-compression failure, as shown in figures 145 and 153.

Despite data acquisition problems, conclusions regarding the effectiveness of composite systems application to increase the shear capacity of damaged beams can still be drawn. Given the great variety of composite patching systems employed, it is not useful to separate the results according to composite system type or reinforcing scheme. As such, the shear capacity of patched beams is provided in table 44, the values of which

were collected from the records of crack propagation. Even without detailed load information, it is easily observed that repairing concrete beams with carbon fiber composites result in a minimum capacity gain of 35% over the original shear design capacity. All the shear beam failures were video recorded, and the film is available for review.

Table 44. Patch effectiveness in shear repair

Beam ID	Patch Design Capacity (lb)	Maximum Load (lb)	Percent Increase
4	2832	5775	103.9
5	3064	6400.5	108.9
6	2794	3415	22.2
7	3010	5230	73.7
9	3028	4442.5	46.7

A wide variety of failure modes were observed when loading the patched shear beams to failure. Each expected failure mode occurred: concrete crushing, composite debonding, concrete cover separation, and shear cracking. Several beams failed catastrophically, without warning and explosively. The crack growth of each beam is illustrated in Appendix C. What follows is an extensive portrait of each beam failure. Detailed investigation is needed given the complex failure of each beam.

Test beam 4 was retrofitted with Sikawrap U-jackets. Before failure, the patched beam sustained loads twice as large as the patch was designed for. The beam failed due to shear cracking in combination with concrete cover separation. Figure 155 shows the culprit shear crack after failure.

Figure 155. Shear crack in test beam 4

Figure 156. Concrete cover separation at patch location on the far side of beam 4

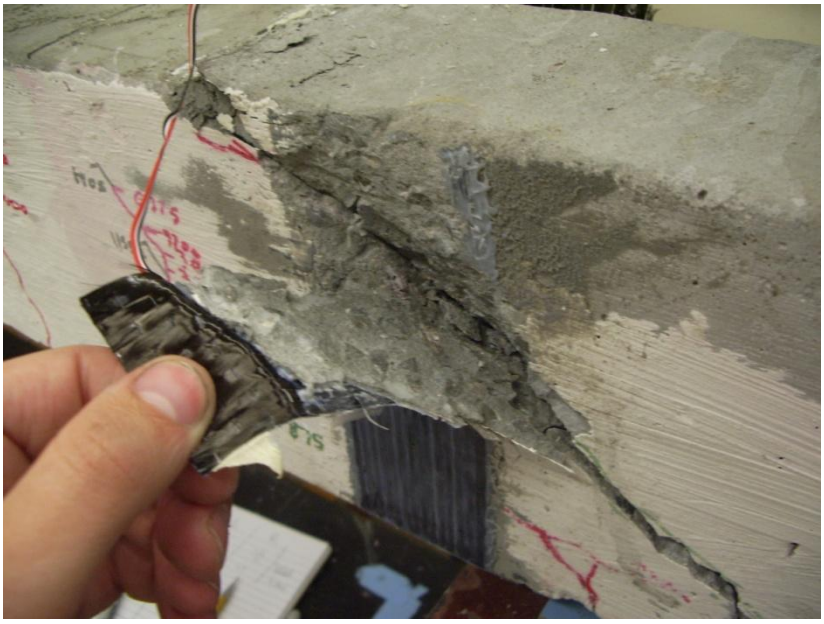

Figure 157. Close up of concrete cover separation of test beam 4

Test beam 7 was repaired with LTC 4300 U-jackets. Unlike beam 4, there was no concrete cover separation; instead the beam failed in a combination of shear cracking and composite debonding. Another dissimilarity between Sikawrap and LTC 4300 U-jacket reinforcing is that only one side of the patch failed; debonding from the beam substrate. The shear crack which caused the failure of the beam was not the same which initially dominated during the initial loading. Figure 158 shows the shear crack which caused the failure. Figure 159 shows the far side of the beam, from which the composite patch debonded. At failure, an entire section of the beam separated from rest, as shown in figure 160.

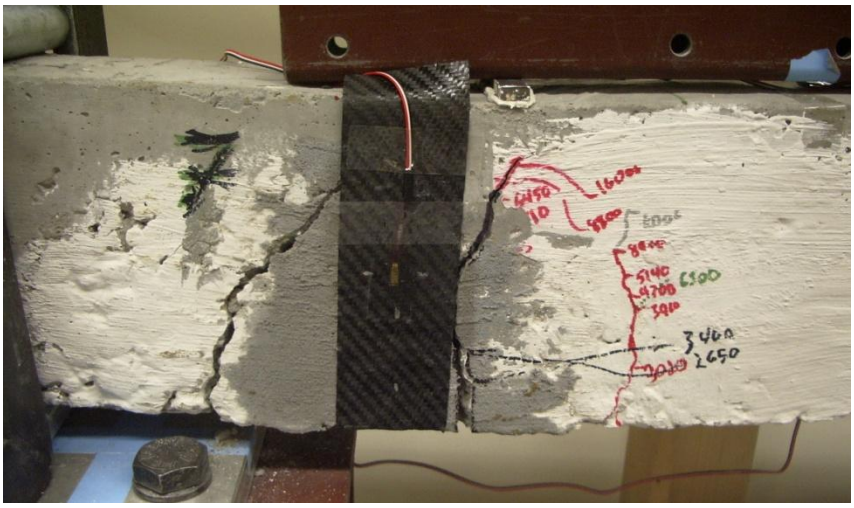

Figure 158. Failure of beam specimen 7

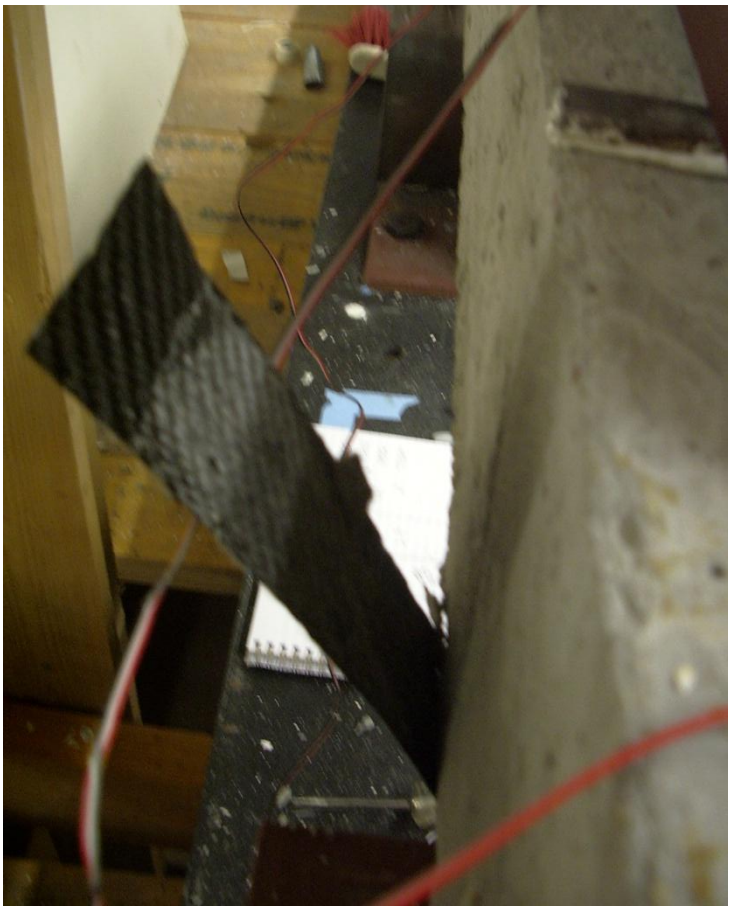

Figure 159. LTC 4300 debonding from concrete substrate

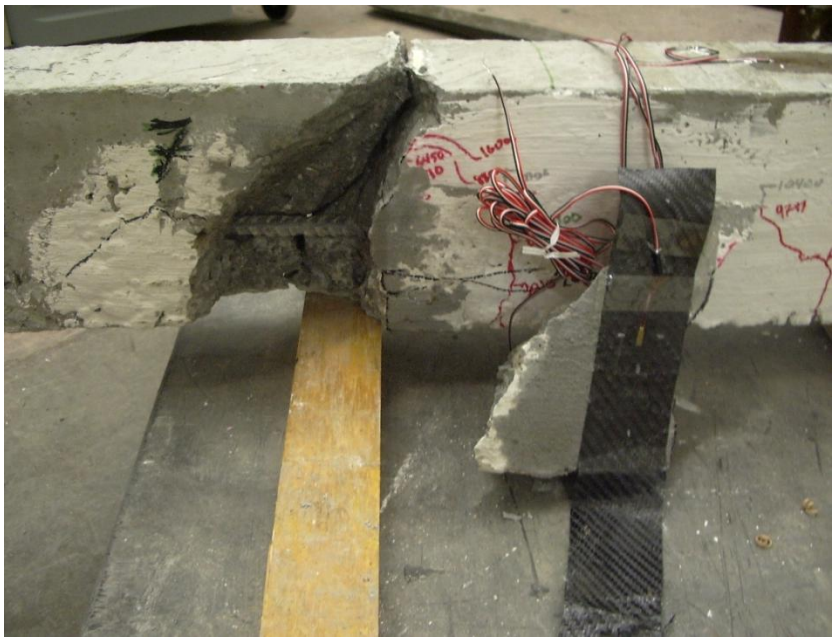

Figure 160. Final state of beam 7

Test beam specimen 6 showed the least increase in capacity, though the beam still withstood 24% more load than the patch design capacity. The beam was reinforced with LTC 4300 strips placed at 55 degree angles, which best opposed the initial shear cracking. The beam failed because of a combination of composite patch debonding, primary steel debonding, concrete crushing, and shear cracking. Figure 161 shows the beam after failure.

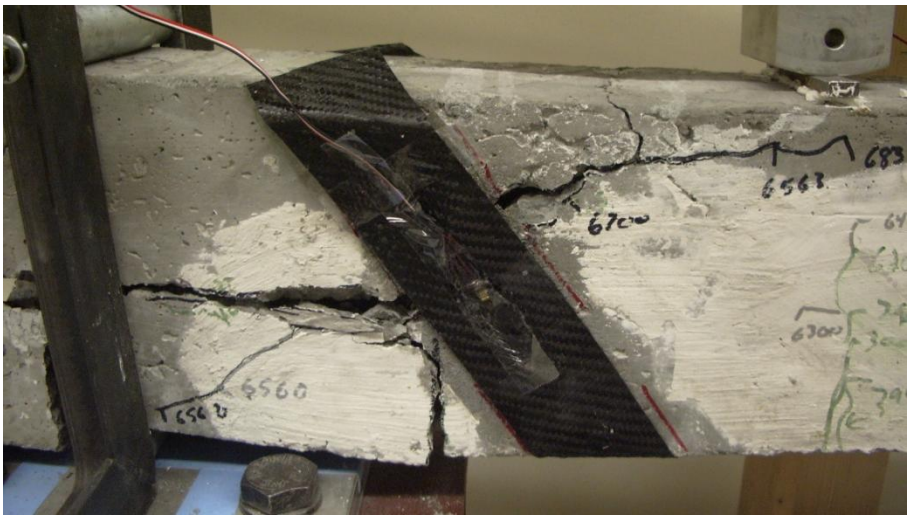

Figure 161. Failure of beam specimen 6

It can be easily seen that the shear crack extended from the point load end support, following along the primary reinforcing steel near the end of the beam. The composite patch debonded on both sides of the beam, as shown in figure 162. At the ultimate load, the beam essentially exploded under the high concentration of stresses. Figure 163 shows the final state of the beam; note that the beam did not fail along the original shear crack. Like test beam 5, a new shear crack developed. In practice, catastrophic failure is undesirable. Consequently, engineers must be careful when applying such a composite patch repair system.

Figure 162. Close up of LTC 4300 debonding

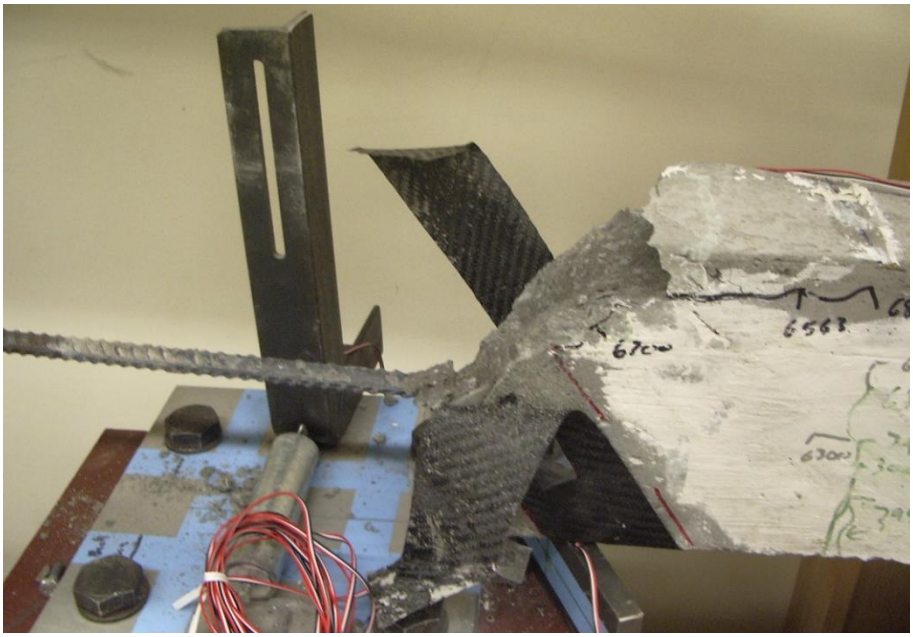

Figure 163. Final state of shear beam 6

Test beam 5 was retrofitted in shear with Carbodur strips placed at angles which provide best bridging across existing shear cracks. This reinforcing scheme withstood an incredible amount of load and failed by developing a large shear crack. Figure 164 shows this shear crack, the yellow line represents the approximate location of the original shear crack.

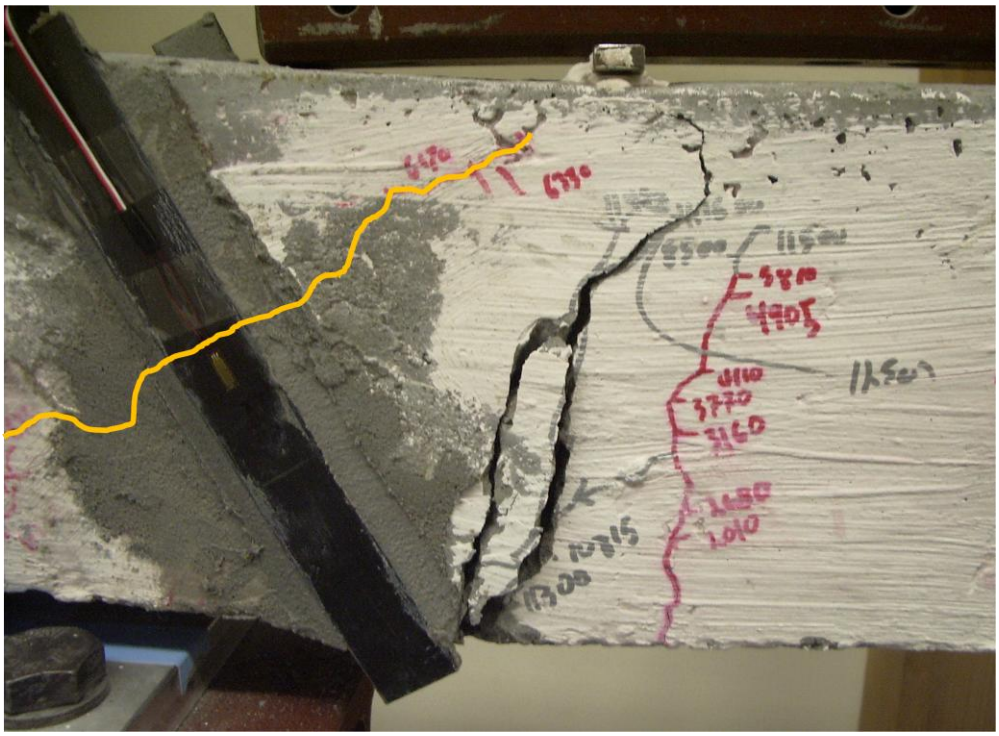

Figure 164. Failure crack of shear beam specimen 5

The new failure crack did not appear until the beam was loaded to 4250 pounds, over 66% of the total load. This composite reinforcing scheme essentially inhibited any further growth of the shear crack over which the strips were placed, prompting the beam to develop an entirely new shear crack adjacent to the patch.

Test beam 9 was repaired with Carbodur strips placed at 45 degree angle. One noticeable difference between the Carbodur reinforcing strips utilized to strengthen beam 9 from beam 5 is the length of the respective patches. The composite strips of beam 9 are shorter than those of beam 5, representing a practice feasible for field application. The beam failed due to concrete crushing, excessive cracking, concrete cover separation, and composite debonding. The failure of the beam was the most catastrophic of the shear beams, as evident from figures 165 and 167. Figure 168 shows the concrete cover separation and 169 shows the failed state of the beam.

Figure 165. Front side of beam 9 at time of failure

Figure 166. Far side of test beam 9 after failure

Figure 167. Concrete cover separation of test beam 9

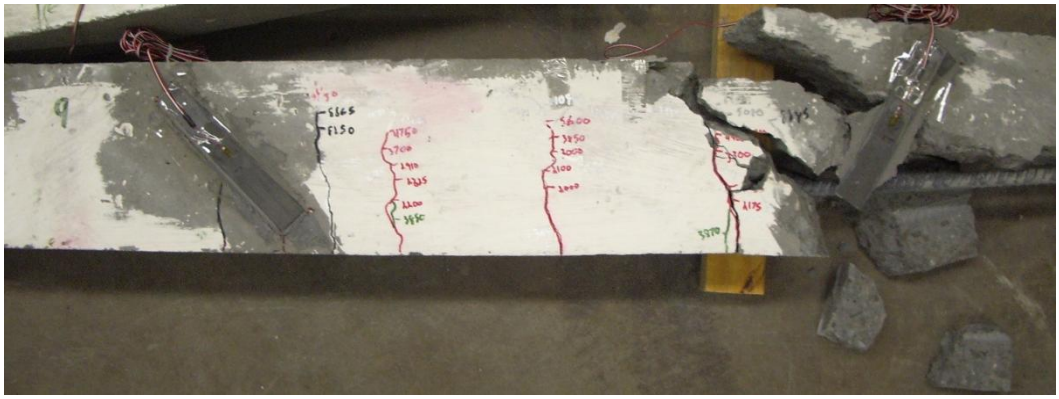

Figure 168. Final state of test beam 9

Prestressed Concrete Beams

The test results of the repaired prestressed concrete beams were interesting. PSCB1 was initially damaged in shear and repaired accordingly. The repair scheme was a pair of Sikawrap U-jackets which conformed to the parameter of the beam. The beam did not show any significant gain in strength once a threshold was reached. The reason for the stagnation of load capacity was troubling at first, until the patching system was closely examined. The reason can be attributed to the manner in which the composite patch was jacketed around the beam. Figure 169 shows the repair scheme of the test beam, and figure 170 shows the progressive debonding process the composite patch underwent.

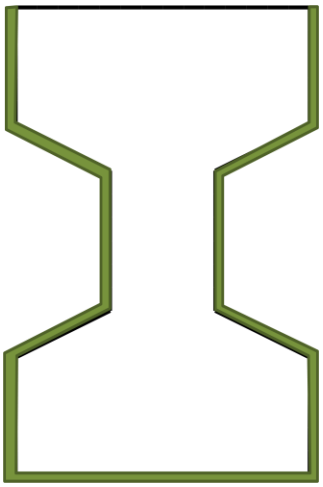

Figure 169. Conforming U-jacket reinforcing scheme of PSCB1

The application mistake of the repair scheme shown above occurs in the concave corners of the beam profile. As load increases, high stresses at the corners cause debonding, resulting in the composite patch moving away from the substrate. Given the inherent weakness of the adhesive to withstand tensile stresses; the composite pulls away from the concavity. This debonding action is aggravated by the presence of cracking at these corners. This is demonstrated by figure 170 and evident in figure 171.

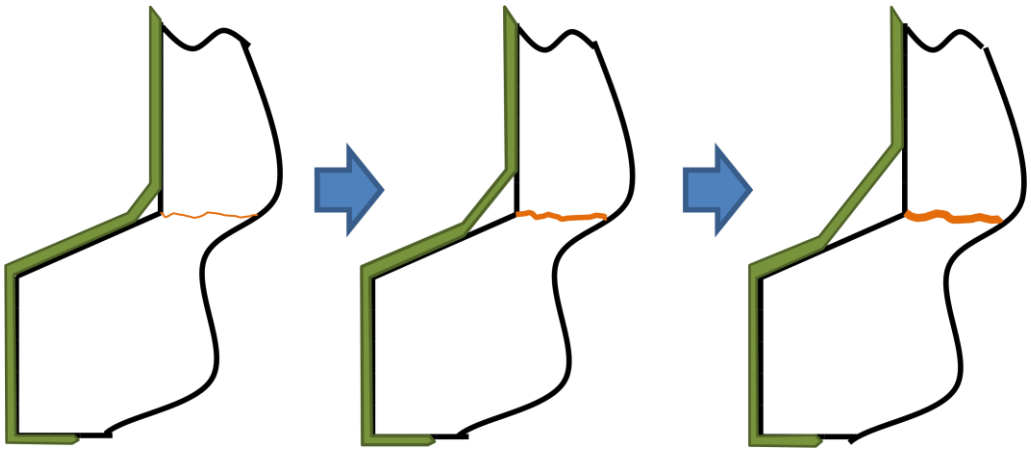

Figure 170. Debonding behavior of PSCB1 due to cracking and concavity

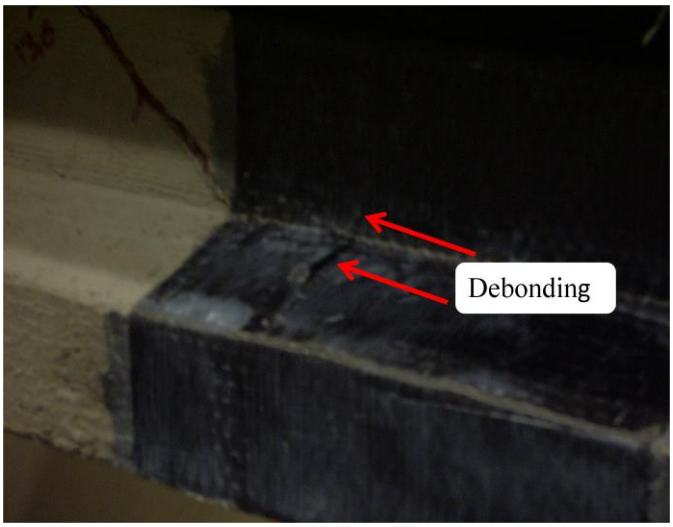

Figure 171. Debonding of composite patch along corner of PSCB1

The second prestressed concrete test beam, PSCB2, incurred flexural damage in the form of cracking and was repaired with a Carbodur composite patch placed on the bottom flange, symmetrically about the center span. The maximum load resisted by the beam was 30 kips. The beam was designed to withstand 39.98 kip-ft and the patched beam withstood roughly 105 kip-ft. This 168% increase of capacity is incredible. Despite showing only flexural cracking up to the limit load, the beam ultimately failed in shear and did so suddenly after being loaded for nearly an hour. The failures of both prestressed concrete beams were captured on video, which is available.

Discussion

Several observations are worthy of a detailed dialogue; such as the effectiveness of the composite patch design procedure, the value of the developed mechanistic model to design and prediction, the characterization and quality control of composite materials and repaired test beams, and the failure modes of concrete beams, and the need for further study.

The design procedure outlined and implemented in this research project sought to accurately and economically employs different FRP composite retrofitting systems to repair representative bridge superstructure elements. The procedure was straightforward and is easily understood. Given the results of the beams tested, it is safe to state that the design procedure succeeded in all aspects of its purpose. Moreover, confidence can be placed in the procedure given that most of the systems performed beyond the expectations of the designs, with the exception of the steel beams. The steel beam results were inconclusive at best, but given the nature of the limit state of the beams and the fact that the composite patches are most effective when the beam has reached its plastic limit, it is not strange that little effect from the composite patching was found in the elastic range. These additional capacities of the beams give a design engineers a margin of comfort when utilizing the limit state design procedure outlined in Chapter III.

The mechanistic model was used to predict first and foremost the shear and tensile stresses applied to the composite adhesive, though the model also predicted the displacement of beams retrofitted with composite systems. The assumptions made in developing the model were realistic. The model works best for steel beams loaded within

the elastic range; so the model is easily applicable for service load conditions. When modeling reinforced concrete beams, the model has to account for tension cracking which requires nonlinear analysis. For such phenomenon, the mechanistic model has been suitably modified; however, for highly accurate analysis, a comprehensive nonlinear analysis must be employed.

Utilizing the ultimate load values recorded from the experimental testing in tandem with the individual beam and composite system properties, provides the displacement values necessary for model validation. This validation showed that the mechanistic model consistently overestimates the displacement values, as shown in table 45.

Table 45. Validation of mechanistic model

Composite System	Beam ID	Model Displacement (in)	Experimental Displacement (in)	Percent Difference (%)
Carbodur	B	0.304	0.182	67
	C	0.254	0.143	78
	E	0.206	0.145	42
	F	0.171	0.127	34
Sikawrap	1	0.189	0.111	70
	3	0.224	0.139	61
	H	0.211	0.130	62
LTC 4300	A	0.348	0.133	162
	D	0.363	0.179	103
	G	0.250	0.124	102
	I	0.366	0.142	158
	SBI	0.141	0.136	4

The discrepancy between the model and the experimental results illustrates the limitations of the model given the assumptions required by it. The first limiting

assumption is how the energy of the system is calculated, more specifically, the neglect of an axial force term from the patch as illustrated in figure 172.

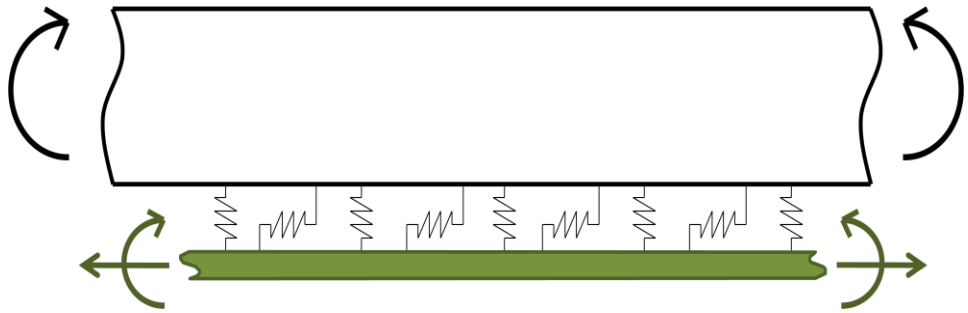

Figure 172. Proposed accounting of beam and patch resistance to applied forces

The current mechanistic model only accounts for bending resistance provided by the patch and as such an improvement to the current model would account for the axial contribution of the patch additionally. The ability of the composite system to resist axial loads is much greater than the ability to resist bending. Implementing the axial contribution of the composite patch system to the entire patched beam system is considered by the researchers and others in the research group to greatly improve the accuracy of the model.

The second limiting assumption of the mechanistic model is the assignment of the beam substrate moment of inertia, a limitation applicable to concrete beams. The current model uses the iterative process detailed in Chapter III to find the moment of inertia for a given beam, load, and modulus of elasticity and assigns that moment of inertia value to the entire span of the beam. In reality, the moment of inertia would vary along the beam according to the location of the tensile rupture stress of concrete. This limiting assumption and the more realistic truth are illustrated in figure 173.

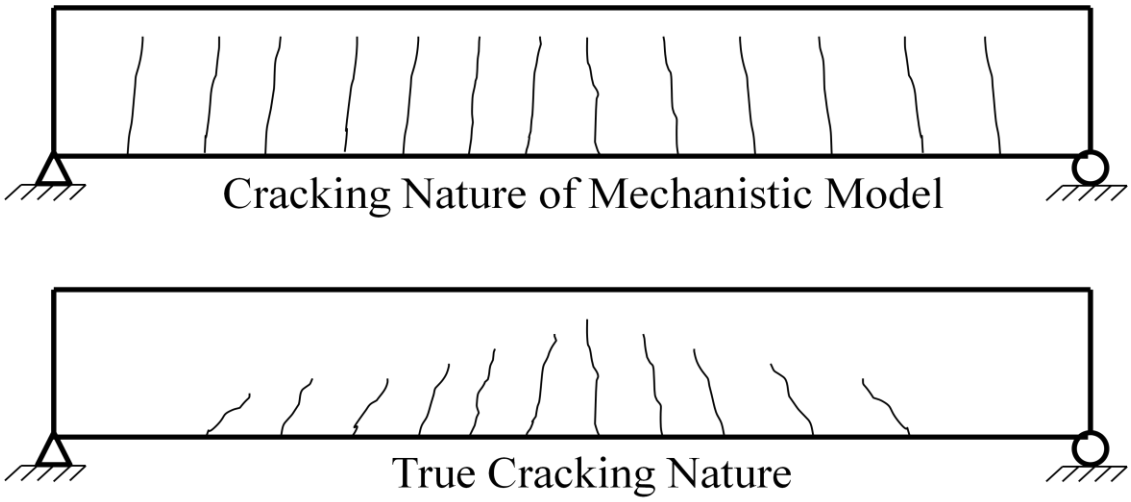

Figure 173. Assumed and realistic cracking phenomenon of concrete beams

A more complex model incorporating the fluctuating value of the moment of inertia of the beam would provide more accurate results. Note that the steel beam, SBI, did not suffer from the same order of inaccuracy as the concrete beams. This difference is due to the application error of moment of inertia.

The validation summarized in table 45 shows the model provides conservative displacement results, moreover adhesive tensile and shear stresses that are larger than expected in reality. The conservative nature of the mechanistic model verifies its use as a design tool, however inaccurate.

Another discussion point is the quality control of variability in the test beams and the testing process itself. Due to limitations of the laboratory facilities, casting the reinforced concrete beams in small batches created a large amount of variability in the composition of the test beams. This variability is most evident in table 45 of the concrete strengths. To reduce the effect of this expected source of error, each beam was cast with a representative test cylinder. The obvious ideal solution to reduce such variability would have been to cast all the beams from a single batch of concrete, from which several test

cylinders would be made. It is industry practice to use the average of two test cylinders to define a single compressive strength of concrete patch at a given point of pouring. Given this practice, if small batches were the necessary course of action, two test cylinders should have been made for each beam. However, given the constraints of the project, a relatively small concrete mixer was utilized to cast the beams. This small mixer allowed for a single test cylinder to be cast simultaneously with a beam without falling short on the concrete necessary to complete a beam.

There was additional variability in applying the FRP composite systems. To tackle this variability, all the composite patches were placed by the author who practiced the application process several times before working with the test beams. As stated before in Chapter II, significant difficulty was faced in correctly applying the prepreg composite system LTC 4300. Despite having a low gel temperature, it was very difficult to properly cure the composite. The precise need of heating and cooling the composite patch with specified temperature profiles and rates was difficult to produce in a field simulated condition. Proper curing of the resin dictates such specific temperature conditions, and improper heating and cooling of the beam results in insufficient resin curing, and consequently composite performance. Great pains were taken to properly cure the prepreg systems. In general, the flexural systems were the simplest to cure and the shear systems were the most difficult. Due to such limitations, the shear results of LTC 4300 patch repaired beams were less consistent than the other FRP composite systems.

It was observed in several flexurally tested concrete specimens that the failure mode of the beam changed once it was retrofitted with the composite system. It is clearly

stated in the design procedure that design engineers should check the limit states of the post-strengthened beams. It is vital for public safety that the design engineer is aware that any increase in either the shear or moment capacity of beam may cause the failure mode to change. During load testing, this was observed on several occasions, and was most pronounced when the moment capacity of beams were increased without corresponding increase in shear capacity.

It is critical for engineers to understand the brittle nature of many FRP composite materials, both fiber and adhesive. It is the wise tradition of civil engineers to avoid brittle failures in order to insure public safety. Moreover, it was observed countless times that FRP reinforced concrete beams failed catastrophically, sometimes explosively. However, careful observation of each composite system revealed that some systems are more prone to sudden failure. Additionally, conscientious study of crack patterns and crack growth revealed that some systems will provide enough warning before failure. In particular, concrete beams reinforced with Sikawrap rarely fail catastrophically without warning, usually in the form of large scale cracking. The reason for this most likely lies in the individual fibrous nature of the composite, which is prone to progressive failure. The system behaves like steel strands; when over stressed, individual fibers, or strands, will fail before the entire system will. This behavior of Sikawrap composite systems is a great advantage to engineers and the public at large.

Carbodur is by far the strongest and most stiff composite material tested in this research project. As such it was not uncommon for beams reinforced with Carbodur systems to develop complex cracking systems because the repaired cracks were tightly confined. This is best demonstrated by test beam 5 which underwent horizontal cracking

phenomenon observed in flexural beams. This information is vital to estimating the behavior of Carbodur system, which typically failed catastrophically. When employed in field applications, such systems should be regularly and keenly observed by knowledgeable technicians and engineers. Beams reinforced with the prepreg composite system LTC 4300 gave a mixed bag of warnings. This is probably because it is difficult to properly cure the system in general. As discussed before, this difficulty of achieving a consistent level of cure created high variability in the performance of LTC 4300 reinforcing systems. The flexural beams retrofitted with LTC 4300 did not show any behavior to signal the failure of the beam.

The results of reinforcing a prestressed beam with a FRP composite system in an attempt to increase the moment capacity of the beam was a great success, but it is important to note the rapid failure of the beam in shear without noticeable increase in capacity. There was no warning of the shear failure, and this should serve as a stark reminder to design engineers to check the limit states of the beam before implementing FRP repairs. The composite reinforcing of the second prestressed concrete beam revealed an important insight into the viable reinforcing scheme available to engineers. The concavity of the composite system led to an assumed early failure of the beam, resulting in a stagnation of capacity increase. With this understanding, the composite systems should have been placed in a discontinuous manner. An improved solution is provided below in figure 174. Note that the web portion of the composite system is a separate piece of composite section, which eliminates issues of concavity.

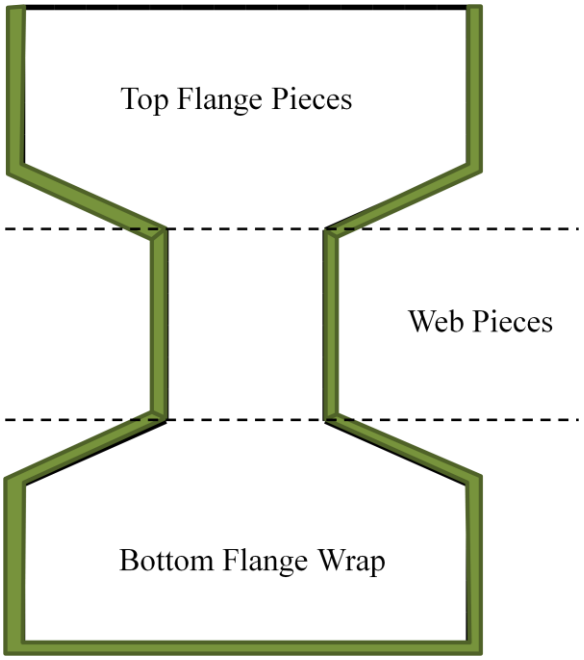

Figure 174. Improved conforming reinforcing system

Conclusion

Several broad conclusions arise from the previous discussion. The first is that the repair schemes developed by the design procedure are highly effective for increasing the capacity of damaged concrete beams. Both the flexural and shear repair patches serve to increase the capacity of the damaged members by a significant amount in accordance with the design philosophy. Designers and engineers should be aware of the shortcomings of the procedure, but should have confidence given the vast evidence previously presented in this manuscript.

The second conclusion is that the mechanistic model developed in the context of this research project serves to provide an excellent tool for checking the limiting adhesive capacities of the composite system. Designers and engineers should take comfort in the conservative nature of the model and feel comfortable in the results it produces.

The third conclusion is that the curing procedure for the preimpregnated FRP composite system was effective in sufficiently bonding the composite fibers to the substrate surface. Recreating the environment and procedures ideal for curing such composite products is incredibly difficult; however the techniques developed in this research project were not only successful, but also easily applicable to the constraints of typical civil engineering projects and field conditions.

A last conclusion derived from the research presented is that composite systems are not a highly effective retrofitting solution for steel beams. Given the discussion above, FRP composite repairs are only viable solutions for steel beams when the controlling limit state is yielding of the beam and the beam reaches yielding under the anticipated loads. The composite repair system under service loading requires additional considerations.

Recommendations

Given the considerable challenge of creating a comprehensive design, application, and analysis there is only so much any single research project can accomplish. There are several recommendations which accompany this work. The first recommendation is additional experimental testing; both in the adhesive and the patch repaired beam fields. The experimental work of the composite system adhesives creating an excellent foundation into discovering and modeling adhesive behavior and capacity, but additional efforts should be made to account for variability of each test specimen in addition to a variety of substrates.

Additionally tests of repaired beams should be conducted. Specifically, steel beams need to be repaired with a variety of composite systems; instead of a single composite type, preimpregnated, test beams should be retrofitted with both dry fiber and precurred systems. Additionally, steel beams should be loaded to ultimate capacity. The work presented above explores the ability of composite systems to restore and exceed the nominal behavior and capacity. Further testing of reinforced concrete test beams should be concluded, exploring the behavior of repaired beams of greater size, type, and span length. Given that all the reinforced concrete beams ultimately failed in a very similar shear manner. Increasing the shear span is a necessity of additional reinforced concrete testing. Given the limited number of prestressed beams, additional experimental work into the repaired response of composite patch repaired prestressed beams is necessary of future work. This is especially true, given the stagnation of capacity demonstrated by PSCB1.

A complete and exhaustive finite element modeling study should be conducted which can accurately predict the capacity and behavior of composite patch repaired beam systems. Finite element modeling will aid engineers and researchers into the effects diaphragms, abutments, and traffic will have on the repaired beams. Updating the mechanistic model to include nonlinear and plastic behavior should be completed in future work which will aid engineering is checking the patch design and serve as another tool which researchers can use in model validation.

Finally, implementation of the work presented here should begin. Field application of any research is a critical step. Given the positive results of the work and the significant conservatism present in the design procedure, execution of composite

patch repair on an appropriate bridge is realistic. A field application should be accomplished by a trained and skilled technician; the composite systems should also be carefully monitored for short and long term performance.

REFERENCES

Al-Emrani, M., and R. Kliger. "Analysis of Interfacial Shear Stresses in Beams Strengthened with Bonded Prestressed Laminates." *Composites Part B: Engineering* 37.4-5 (2006): 265-72. Print.

Bank, L. "A Model Specification for FRP Composites for Civil Engineearing Structures." *Construction and Building Materials* 17.6-7 (2003): 405-37. Print.

Benedetta, Joe. *AAHSTO Maintenance Manual for Roadways and Bridges*. Tech. 4th ed. 2007. Print.

Busel, John P. *Guide for the Design and Construction of Externally Bonded FRP Systems for Strengthening Concrete Structures*. ACI 440.2R-08. Michigan: American Concrete Institute, 2008. Print.

Colombi, P., A. Bassetti, and A. Nussbaumer. "Analysis of Cracked Steel Members Reinforced by Pre-Stress Composite Patch." *Fatigue Fracture Engineering Material Structures* 26 (2003): 59-66. Print.

Colombi, Pierluigi, and Carlo Poggi. "An Experimental, Analytical and Numerical Study of the Static Behavior of Steel Beams Reinforced by Pultruded CFRP Strips." *Composites Part B: Engineering* 37 (2006): 64-73. Print.

Chen, J. "Shear Capacity of FRP-strengthened RC Beams: FRP Debonding." *Construction and Building Materials* 17.1 (2003): 27-41. Print.

Diab, Hesham, and Zhishen Wu. "A Linear Viscoelastic Model for Interfacial Long-term Behavior of FRP–concrete Interface." *Composites Part B: Engineering* 39.4 (2008): 722-30. Print.

Ferracuti, B., M. Savoia, and C. Mazzotti. "A Numerical Model for FRP–concrete Delamination." *Composites Part B: Engineering* 37.4-5 (2006): 356-64. Print.

Gao, B., J. Kim, and C. Leung. "Strengthening Efficiency of Taper Ended FRP Strips Bonded to RC Beams." *Composites Science and Technology* 66.13 (2006): 2257-264. Print.

Gorji, Meisam S. "Analysis of FRP Stengthened Reinforced Concrete Beams Using Energy Variation Method." *World Applied Science Journal* 6.1 (2009): 105-11. Print.

Hart-Smith, L. J. "An Engineer's Viewpoint on Design and Analysis of Aircraft Structural Joints." *ARCHIVE: Proceedings of the Institution of Mechanical Engineers, Part*

G: Journal of Aerospace Engineering 1989-1996 (vols 203-210) 209.27 (1995): 105-29. Print.

Joshi, Bikram M. *Experimental Study on Repair and Strengthening of Reinforced*. Thesis. Hokkaido University, 2004. Print..

Jumaat, M. Z., M. H. Kabir, and M. Obaydullah. "A Review of the Repair of Reinforced Concrete Beams." *Journal of Applied Science Research* 2.6 (2006): 317-26. Print.

Kelly, Thomas D., and Grecia R. Matos. "Historical Statistics for Mineral Commodities in the United States, Data Series 2005-140." *USGS Mineral Resources Program*. Web. 05 Feb. 2011. <http://minerals.usgs.gov/ds/2005/140/>.

Lu, X. Z., J. G. Teng, L. P. Ye, and J. J. Jiang. "Intermediate Crack Debonding in FRP-Strengthened RC Beams: FE Analysis and Strength Model." *Journal of Composites for Construction* 11.2 (2007): 161. Print.

Meier, U. "Strengthening of Structures Using Carbon Fibre/Epoxy Composites." *Construction and Building Materials* 9.6 (1995): 341-51. Print.

Mirmiran, Amir, Mohsen Shahawy, Antonio Nanni, and Vistasp Karbhari. *Bonded Repair and Retrofit of Concrete Structures Using FRP Composite; Recommended Construction Specifications and Process Control Manual*. Rep. no. 514. Washington D.C.: National Cooperative Highway Research Program, 2004. Print.

Moy, S.S.J., and Hollaway, L.C. “Flexural Behavior of Steel Beams Reinforced with Carbon Fibre Reinforced Polymer Composite.” In: Shenoi, R.A., Moy, S.S.J., Hollaway, L.C., editors. Proceeding of the ACIC 2002, Advanced Polymer Coposites for Structural Applications in Construction. London: Thomas Telford (2002): 195-202. Print

Naaman, Antoine E. *Prestressed Concrete Analysis and Design: Fundamentals*. 2nd ed. Ann Arbor, MI: Techno 3000, 2004. Print.

Nanni, A. "North American Design Guidelines for Concrete Reinforcement and Strengthening Using FRP: Principles, Applications and Unresolved Issues." *Construction and Building Materials* 17.6-7 (2003): 439-46. Print.

American Association of State Highway and Transportation Officials. *$140 Billion Price Tag to Repair and Modernize America's Bridges*. *AASHTO Press Release*. 28 July 2008. Web. <http://news.transportation.org/press_release.aspx?Action=ViewNews&NewsID=184>.

Sena-Cruz, J.M., J.A.O. Barros, and A.F.M Azevedo. "Analysis of the Bond Between Near-Surface Mounted CFRP Laminate Strips and Concrete." *Computers and Structures* 82.17 (2004): 1513-1521. Print.

Sirisak, Suphasit. *Structural Integrity Evaluation of Truss Bridges*. Diss. Vanderbilt University, 1996. Print.

Soutis, C., and F. Hu. "Design and Erformance of Bonded Patch Repairs of Composite Structures." *Proceedings of the Institution of Mechanical Engineers, Part G: Journal of Aerospace Engineering* 211.4 (1997): 263-71. Print.

Spiegel, Leonard, and George F. Limbrunner. *Reinforced Concrete Design*. Englewood Cliffs, NJ: Prentice-Hall, 1986. Print.

Täljsten Björn. "Strengthening of Beams by Plate Bonding." *Journal of Materials in Civil Engineering* 9.4 (1997): 206-12. Print.

Teng, J. G., and J. F. Cheng. "Mechanics of Debonding in FRP-Plated RC Beams." *Preceedings of the Institute of Civil Engineers* SBS Oct. (2009): 335-345. Print.

Thornton, William A., and Mark V. Holland. *Steel Construction Manual*. 13th ed. Chicago, IL: American Institute of Steel Construction, 2007. Print.

Zureick, Abdul-Hamid, Bruce R. Ellingwood, Andrzej S. Nowak, Dennis R. Mertz, and Thanasis C. Triantafillou. *Recommended Guide Specification for the Design of Externally Bonded FRP Systems for Repair and Strengthening of Concrete Bridge Elements*. Rep. no. 655. Washington D.C.: National Cooperative Highway Research Program, 2010. Print.

Newport LTC 4300

Description:

LTC 4300 is a 140°F to 200°F low temperature cure, controlled flow epoxy resin system. Versatile processing, excellent mechanical properties, and long out-life make LTC 4300 especially suited for the wind energy and marine markets.

Application:

The long out-time and excellent mechanical properties of LTC 4300 make it an ideal product for use in the wind energy and marine markets where very large structures may take several days to lay-up, and may need to be cured at low temperatures.

LTC4300 can be supplied with commercially available fiber in both woven as well as unidirectional tape prepreg form, including:

Carbon
Quartz
Aramid
S-glass
E-glass
Other specialty fibers and fabrics

Woven fabrics are available in standard commercial widths up to 60 inches. Tape widths up to 39 inches (1M) are available in standard fiber weights ranging from 90 to 300 gsm.

Benefits/Features:

- Low Temperature Cure (from 140°F)
- Co-curable film adhesive version available (LTC 3300)
- Controlled flow
- 30 days out-life at 70°F
- Available on most commercial woven fabric
- Available on a wide range of unidirectional fibers

Recommended Processing Conditions:

LTC 4300 can be cured at temperatures from 140°F to 200°F, depending on service temperature requirements. Low, medium, and high pressure molding techniques may be used to cure LTC 4300. Recommended cure cycle is vacuum bag pressure, 3°F/min ramp to 180°F, hold for 120 minutes, cool to <140°F.

1822 Reynolds Avenue •Irvine, CA 92614 • (949) 253-5680 • FAX (949) 253-5692

Physical Properties:

Gel Time (200°F):	10-12 min
Specific Gravity:	1.18 ± 0.02
Tg (DMA,E'):	185° F
CTE (ppm/°C):	60 ± 10 (below Tg)

Mechanical Properties:

7781 E-Glass reinforcement

The mechanical property data supplied in the following table are average values obtained from LTC-4300 with style 7781 woven fiberglass. All values are based using an "in-hot out-hot" press cure at 180° F for 3 hours.

	Test Method	RT*
Tensile strength, ksi	ASTMD-638 Type I	60
Tensile modulus, Msi		3.5
Compression strength, ksi	SACMA SRM 1R-94	70
Compression modulus, Msi		3.3
Flexural strength, ksi	ASTMD-790	92
Flexural modulus, Msi	ASTMD-790	3.5
Short Beam Shear strength, ksi	ASTMD-2344	9.4
In-Plane Shear strength, ksi	ASTM-D3846	9.0
Mode I Fracture Toughness in-lb/in^2	ASTM-D-5528	2.4

** Values are average and do not constitute a specification*

34-700 (G300) Standard Modulus Uni-directional Carbon Fiber tape reinforcement

The mechanical property data supplied in the following table are average values obtained from LTC-4300 with 34-700 carbon fiber at 35% RC, using a vacuum bag cure at 160°F with a 6 hour hold. All values, except for SBS are normalized to a fiber volume of 60%.

	Test Method	RT*
0° Tensile strength, ksi	ASTM-D3039	290
0° Tensile modulus, Msi		18.7
Strain, %		1.44
Poisson's Ratio		0.31
0° Compression strength, ksi	SACMA SRM 1R-94	210
0° Compression modulus, Msi		17.5
0° Short Beam Shear strength, ksi	ASTM-D2344	10.8

** Values are average and do not constitute a specification*

Sandwich panel data

Data collected on 4-ply [0/90, ±45, 0/90, ±45] skinned sandwich panels of LTC 4300 EDB625 32%RC with LTC 3300HC 0.060psf film adhesive on foam core 0.6 inch thick cured under vacuum bag pressure with a 6 hour hold at 160°F and a final cure of 3 hours at 180°F.

Property	Baltek C71.75 PVC Foam Core Data*	Core-Cell A500 SAN Foam Core Data*	Core-Cell P500 SAN Foam Core Data*
Core Shear Stress at Yield, ASTM C 393, lbs/in²	150	140	160
Load at Yield, ASTM C 393, lbs	600	560	650
Deflection at Yield, ASTM C 393, in	0.26	0.22	0.23
Core Shear Stress at Maximum Load, ASTM C 393, lbs/in²	205	200	205
Maximum Load, ASTM C 393 lbs	830	790	830
Deflection at Maximum Load, ASTM C 393, in	0.83	1.10	0.78

Failure modes for all panels were a combination foam crush and skin deformation. No delamination was observed between skins and foam cores.

** Values are average and do not constitute a specification*

Gel Curve Profile of LTC-4300

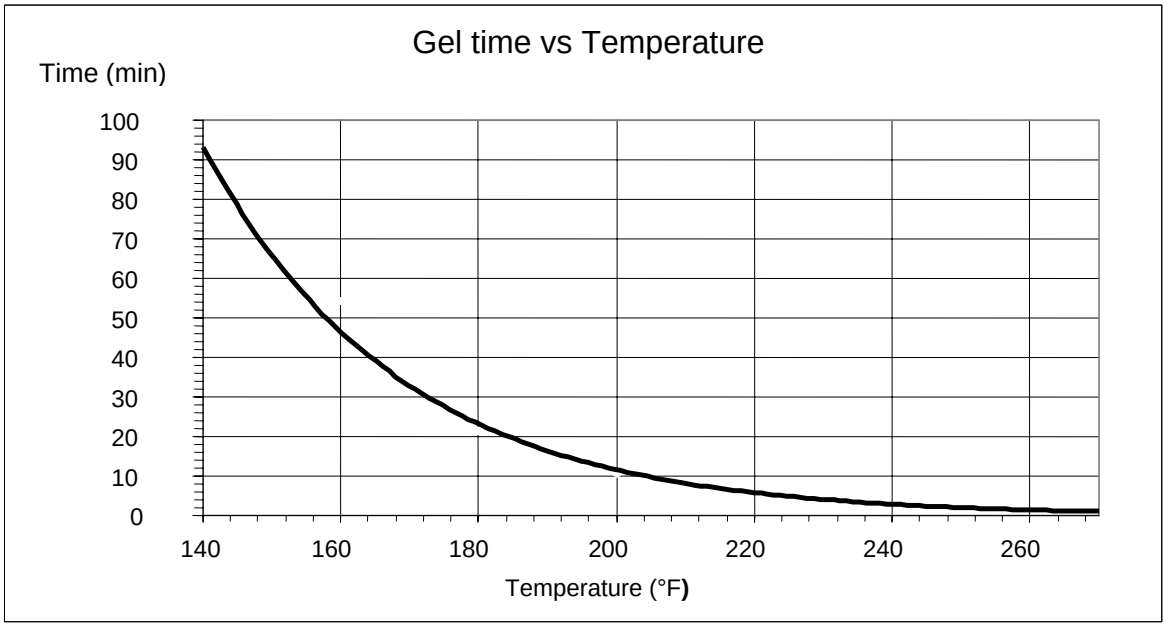

Melt Viscosity Profile of LTC 4300

A TA (model AR2000) parallel plate rheometer was used to determine the melt viscosity profile of the neat resin system.

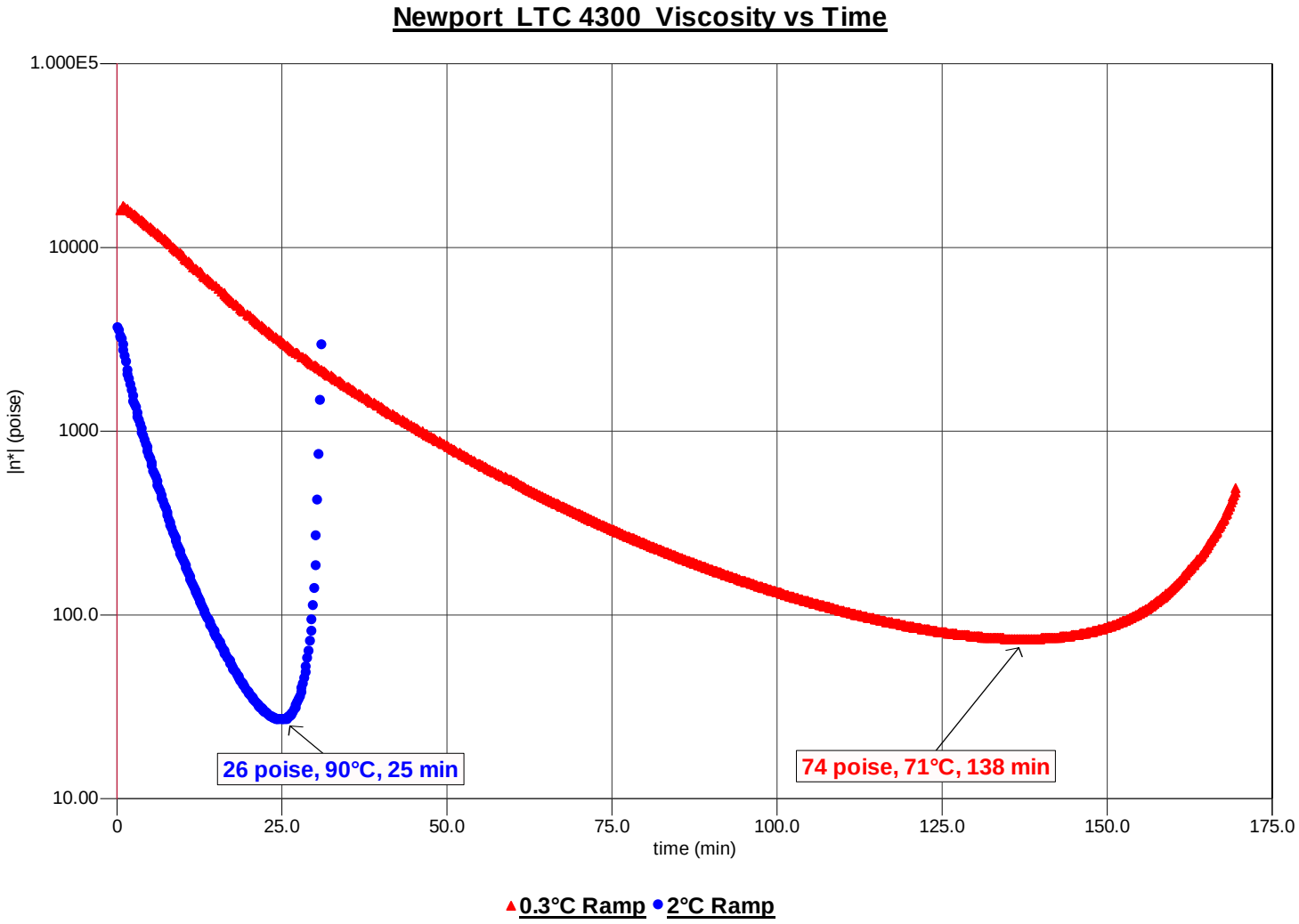

Prepreg Storage:

Material can be stored at 40°F for 3 months, or 0°F for 6 months.

Availability:

LTC 4300 is available on a wide variety of woven fabrics and unidirectional tapes including aramid, E-glass, S-glass, carbon, and other fibers. Tack, flow and other properties can be tailored to meet your specific requirements. Contact Newport about any specialty fibers or requirements

For orders, pricing, availability, technical assistance or other inquiries please contact:

CORPORATE OFFICES
Newport Adhesives and Composites
1822 Reynolds Ave,
Irvine, CA 92614
Tel: (949) 253-5680
Fax: (949) 253-5692
Sales@newportad.com
http://www.newportad.com

Construction

SikaWrap®-230 C/45

Woven carbon fiber fabric for structural strengthening

Product Description	SikaWrap®-230 C/45 is a unidirectional woven carbon fiber fabric for the dry application process. 
Uses	Strengthening of reinforced concrete structures, brickwork and timber in case of flexural and shear load due to: n Improved seismic performance of masonry walls n Substitute missing rebars n Strength and ductility of columns n Increasing loading capacity of structural elements n Changes of building utilisation n Structural design construction defects n Seismic movement n Improved serviceability n Structural upgrading to comply with current standards
Characteristics / Advantages	n Manufactured with weft fibers to keep the fabric stable (heat-set process) n Multifunctional use for every kind of strengthening requirement n Flexibility of surface geometry (Beams, columns, chimneys, piles, walls, silos) n Fabric available in several widths for optimum utilisation n Low density for minimal additional weight n Economical compared to traditional techniques

Tests

Approval / Standards	France: CSTB - Avis Technique 3/07-502, SIKA CARBODUR SIKA WRAP USA: ACI 440.2R-08, Guide for the Design and construction of Externally Bonded FRP Systems for strengthening concrete structures, July 2008 UK: Concrete Society Technical Report No. 55, Design guidance for strengthening concrete structures using fiber composite material, 2000 Italy: CNR-DT 200/2004 - Guide for the Design and Construction of Externally Bonded FRP Systems for Strengthening Existing Structures

Product Data

Form

Fiber Type

Mid strength carbon fibers.

Fabric Construction

Fiber orientation: 0° (unidirectional).

Warp: black carbon fibers (99% of total areal weight).

Weft: white thermoplastic heat-set fibers (1% of total areal weight).

Packaging

	Fabric length / roll	Fabric width
1 roll in cardboard box	≥ 50 m	300 / 600 mm

Storage

Storage Conditions / Shelf Life

24 months from date of production if stored properly in undamaged original sealed packaging in dry conditions at temperatures between +5°C and +35°C.
Protect from direct sunlight.

Technical Data

Areal Weight

230 g/m^2 ± 10 g/m^2

Fabric Design Thickness

0.131 mm (based on fiber content).

Fiber Density

1.76 g/cm^3

Mechanical / Physical Properties

Dry Fiber Properties

Tensile strength:
4'300 N/mm^2 (nominal).

Tensile E-modulus:
234'000 N/mm^2 (nominal).

Elongation at break:
1.8% (nominal).

Laminate Properties

Laminate thickness:
1.0 mm per layer (impregnated with Sikadur®-330).

Ultimate load:
350 kN/m width per layer

Tensile E-modulus:
25.0 kN/mm^2 (based on typical laminate thickness of 1.0 mm).

Note:
The above values are typical and indicative only.
The achievable laminate properties obtained from tensile test are dependant on the impregnating/laminating resin used and the type of tensile testing procedure.
Apply material reduction factors according to the relevant design standard.

Design

Design strain:
Max. 0.6% (this value is dependent on the type of loading and must be adapted according to the relevant local design standards)

Tensile strength: (theoretical tensile strength for the design):

- at elongation 0.4%: 100 kN/m width (= 30 kN / 30 cm)
  (= 60 kN / 60 cm)
- at elongation 0.6%: 150 kN/m width (= 45 kN / 30 cm)
  (= 90 kN / 60 cm)

System Information

System Structure	The system configuration as described must be fully complied with and may not be changed. Concrete primer - Sikadur®-330. Impregnating / laminating resin - Sikadur®-330. Structural strengthening fabric - SikaWrap®-230 C/45. For detailed resin properties, fabric application details and general information, refer to Sikadur®-330 Product Data Sheet.

Application Details

Consumption	Depending on the roughness of the substrate. - Impregnating of the first layer incl. primer: ~ 0.7 - 1.2 kg/m^2 (Sikadur®-330). - Impregnating of the following layers: ~ 0.5 kg/m^2 (Sikadur®-330).
Substrate Quality	Specific requirements: Minimal substrate tensile strength: 1.0 N/mm^2 or as specified in the strengthening design.
Substrate Preparation	*Concrete and masonry:* Substrates must be sound, dry, clean and free from laitance, ice, standing water, grease, oils, old surface treatments or coatings and any loosely adhering particles. Concrete must be cleaned and prepared to achieve a laitance and contaminant free, open textured surface. Repairs and levelling: If carbonised or weak concrete cover has to be removed or levelling of uneven surfaces is needed, the following systems can be applied: (Details on application and limitation see the relevant Product Data Sheets) • Protection of corroded rebars: SikaTop® Armatec® 110 EpoCem® • Structural repair materials: Sikadur®-41 epoxy repair mortar, Sikadur®-30 adhesive or cementitious Sika® MonoTop®-412 (horizontal, vertical, overhead) or Sika® MonoTop®-438 (horizontal, top-side) range.

Application Instructions

Application Method / Tools	The fabric can be cut with special scissors or razor knife. Never fold the fabric! Refer to Sikadur®-330 Product Data Sheet for impregnating / laminating procedure.
Notes on Application / Limitations	This product may only be used by experienced professionals. Minimum radius required for application around corners: > 10 mm. Grinding edges or building up with Sikadur® mortars may be necessary. In fiber direction, overlapping of the fabric must be at least 100 mm depending on SikaWrap® type or as specified in the strengthening design. For side-by-side application, no overlapping length in the weft direction is required. Overlaps of additional layers must be distributed over the column circumference. The strengthening application is inherently structural and great care must be taken when choosing suitably experienced contractors. The SikaWrap®-230 C/45 fabric is coated to ensure maximum bond and durability with the Sikadur® impregnating/laminating resins. To maintain system compatibility do not interchange system parts. The SikaWrap®-230 C/45 may be / must be coated with a cementitious overlay or coatings for aesthetic and/or protective purposes. Selection will be dependent on exposure requirements. For basic UV protection use Sikagard®-550 W Elastic, Sikagard® ElastoColor-675 W or Sikagard®-680 S.

Construction

Value Base	All technical data stated in this Product Data Sheet are based on laboratory tests. Actual measured data may vary due to circumstances beyond our control.
Local Restrictions	Please note that as a result of specific local regulations the performance of this product may vary from country to country. Please consult the local Product Data Sheet for the exact description of the application fields.
Health and Safety Information	For information and advice on the safe handling, storage and disposal of chemical products, users shall refer to the most recent Material Safety Data Sheet containing physical, ecological, toxicological and other safety-related data.
Legal Notes	The information, and, in particular, the recommendations relating to the application and end-use of Sika products, are given in good faith based on Sika's current knowledge and experience of the products when properly stored, handled and applied under normal conditions in accordance with Sika's recommendations. In practice, the differences in materials, substrates and actual site conditions are such that no warranty in respect of merchantability or of fitness for a particular purpose, nor any liability arising out of any legal relationship whatsoever, can be inferred either from this information, or from any written recommendations, or from any other advice offered. The user of the product must test the product's suitability for the intended application and purpose. Sika reserves the right to change the properties of its products. The proprietary rights of third parties must be observed. All orders are accepted subject to our current terms of sale and delivery. Users must always refer to the most recent issue of the local Product Data Sheet for the product concerned, copies of which will be supplied on request.

Sika Yapı Kimyasalları A.Ş.
Deri Org. San. Böl. 2. Yol J–7
Parsel, Aydınlı, Orhanlı Mevkii,
34957 Tuzla, İstanbul, Türkiye

Çağrı Merkezi
Telefon
Faks
bilgi@tr.sika.com

+90 216 444 74 52
+90 216 581 06 00
+90 216 581 06 99
www.sika.com.tr

Construction

Sika CarboDur®

Carbon fiber laminate for structural strengthening

Description

Sika CarboDur is a pultruded carbon fiber reinforced polymer (CFRP) laminate designed for strengthening concrete, timber and masonry structures. Sika CarboDur is bonded onto the structure as external reinforcement using Sikadur 30 epoxy resin as the adhesive.

Where to Use

Load increases
- Increased live loads in warehouses
- Increased traffic volumes on bridges
- Installation of heavy machinery in industrial buildings
- Vibrating structures
- Changes of building utilization

Damage to structural parts
- Aging of construction materials
- Steel reinforcement corrosion
- Vehicle impact
- Fire

Serviceability improvements
- Decrease in deformation
- Stress reduction in steel reinforcement
- Crack width reduction

Change in structural system
- Removal of walls or columns
- Removal of slab sections for openings

Design or construction defects
- Insufficient reinforcements
- Insufficient structural depth

Advantages
- Very high strength
- Lightweight
- Non-corrosive
- Unlimited lengths
- Minimal preparation of laminates
- Very easy to install, especially overhead
- High modulus of elasticity
- Outstanding fatigue resistance
- Alkali resistant
- Simple laminate intersections or crossings

Typical Data

Base	Carbon fiber reinforced polymer with an epoxy resin matrix.
Shelf Life	Unlimited (no exposure to direct sunlight).
Color	Black
Tensile Strength	
Mean Value	4.49 x 10^5 psi (3,100 MPa)
Design Value	4.06 x 10^5 psi (2,800 MPa)
Modulus of Elasticity	
Mean Value	23.9 x 10^6 psi (165,000 MPa)
Design Value	23.2 x 10^6 psi (160,000 MPa)
Elongation at Break	1.69%
Design Strain	0.85%
Thickness	0.047 in. (1.2 mm)
Temperature Resistance	>300°F (>150°C)
Fiber Volumetric Content	>68%
Density	0.058 lbs./in^3 (1.60 g/cm^3)

Physical Properties

Product	*Thickness (mils)*	*Width (inches)*	*Cross Sectional Area*	*Tensile Strength*
Type S 512	47.2 (1.2 mm)	1.97 (50 mm)	0.093 sq. in. (60 mm^2)	37.8 x 10^3 lbs. (168 kN)
Type S 812	47.2 (1.2 mm)	3.15 (80 mm)	0.149 sq. in. (96 mm^2)	60.4 x 10^3 lbs. (269 kN)
Type S 1012	47.2 (1.2 mm)	3.94 (100 mm)	0.186 sq. in. (120 mm^2)	75.5 x 10^3 lbs. (336 kN)

Construction

Coverage	Coverage of Sikadur 30 epoxy resin with CarboDur: Type S 512: approx. 50 LF/gallon. Type S 812: approx. 32 LF/gallon. Type S 1012: approx. 22 LF/gallon.
Packaging	Available in any length up to 250 m (820 ft.). Type S 512 width 50 mm (approx. 2”). Type S 812 width 80 mm (approx. 3”). Type S 1012 width 100 mm (approx. 4”).

How to Use

Surface Preparation

Surface must be clean and sound. It may be dry or damp, but free of standing water and frost. Remove dust, laitance, grease, curing compounds, impregnations, waxes, foreign particles, disintegrated materials and other bond inhibiting materials from the surface. Existing uneven surfaces must be filled with an appropriate repair mortar (e.g. mixed Sikadur 30 epoxy with the addition of 1 part oven-dried sand). The adhesive strength of the concrete must be verified after surface preparation by random pull-off testing (ACI 503R) at the discretion of the engineer. Minimum tensile strength, 200 psi (1.4 MPa) with concrete substrate failure.

Surface Levelness/Irregularities: Maximum allowable deviation in 6 ft. shall be limited to 1/4” (6 mm) but no greater than 1/8” (3 mm) per foot. Any sharp edges (i.e. fins, form-marks, etc.) must be ground smooth and flush.

Preparation Work: Concrete - Blast clean, shotblast or use other approved mechanical means to provide an open roughened texture.

CarboDur - Wipe clean with appropriate cleaner (e.g. MEK).

Cutting the CarboDur Laminate:

Preferred: CarboDur laminates should be cut with tools using a “shearing” force (e.g. guillotine or heavy duty shears). Care must be taken to support both sides of the CarboDur laminate to avoid splintering.

Alternate: A hack saw or other abrasive cutting method may be used. However, extra care must be taken to support the CarboDur laminate on both sides to avoid splintering. In addition, extra care must be taken to avoid exposure to carbon dust **(see Caution)**.

Mixing

Consult Sikadur 30 technical data sheet for information on epoxy resin.

Application

Apply the neat mixed Sikadur 30 epoxy onto the concrete with a trowel or spatula to a nominal thickness of 1/16” (1.5 mm). Apply the mixed Sikadur 30 epoxy onto the CarboDur laminate with a “roof-shaped” spatula to a nominal thickness of 1/16” (1.5 mm). Within the open time of the epoxy, depending on the temperature, place the CarboDur laminate onto the concrete surface. Using a hard rubber roller, press the laminate into the epoxy resin until the adhesive is forced out on both sides. Remove excess adhesive. Glue line should not exceed 1/8 inch (3 mm). The external reinforcement must not be disturbed for a minimum of 24 hours. The epoxy will reach its design strength after 7 days.

Limitations

Design calculations must be made and certified by an independent licensed professional engineer. Design guidelines are available from Sika Corporation.

Caution

CarboDur strips are non-reactive and fully cured. They do not require a material safety data sheet. However, caution must be used when handling the CFRP laminates since a fine “carbon dust” may be present on the strips. Gloves must therefore be worn to protect against skin irritation.

Caution must also be used when cutting CarboDur laminates to protect against airborne carbon dust generated by the cutting procedure. Use of an appropriate, properly fitted NIOSH approved respirator is recommended.

KEEP CONTAINER TIGHTLY CLOSED
NOT FOR INTERNAL CONSUMPTION
KEEP OUT OF REACH OF CHILDREN
FOR INDUSTRIAL USE ONLY
CONSULT MATERIAL SAFETY DATA SHEET FOR MORE INFORMATION

Visit our website at www.sikaconstruction.com **1-800-933-SIKA NATIONWIDE**

Regional Information and Sales Centers. For the location of your nearest Sika sales office, contact your regional center.

Sika Corporation
201 Polito Avenue
Lyndhurst, NJ 07071
Phone: 800-933-7452
Fax: 201-933-6225

Sika Canada Inc.
601 Delmar Avenue
Pointe Claire
Quebec H9R 4A9
Phone: 514-697-2610
Fax: 514-694-2792

Sika Mexicana S.A. de C.V.
Carretera Libre Celaya Km. 8.5
Corregidora, Queretaro
C.P. 76920 A.P. 136
Phone: 52 42 25 0122
Fax: 52 42 25 0537

QUALITY ISO 9001 9002 ACHIEVEMENT

Quality Certification Numbers: Lyndhurst: FM 69711 (ISO 9000), FM 70421 (QS 9000), Marion: FM 69715, Kansas City: FM 69107, Santa Fe Springs: FM 69408

Edition 7.1.2008
Identification no. 332-15
Sikadur 30

Construction

Sikadur® 30

High-modulus, high-strength, structural epoxy paste adhesive for use with Sika CarboDur® reinforcement.

Description

Sikadur 30 is a 2-component, 100% solids, moisture-tolerant, high-modulus, high-strength, structural epoxy paste adhesive. It conforms to the current ASTM C-881 and AASHTO M-235 specifications.

Where to use

- Adhesive for bonding external reinforcement to concrete, masonry, steel, wood, stone, etc.
- Structural bonding of composite laminates (Sika CarboDur CFRP) to concrete.
- Structural bonding of steel plates to concrete.
- Suitable for use in vertical and overhead configurations.
- As a binder for epoxy mortar repairs.

Advantages

- Long pot life.
- Long open time.
- Tolerant of moisture before, during and after cure.
- High strength, high modulus, structural paste adhesive.
- Excellent adhesion to concrete, masonry, metals, wood and most structural materials.
- Fully compatible and excellent adhesion to Sika CarboDur CFRP composite laminate.
- Paste consistency ideal for vertical and overhead applications of Sika CarboDur.
- High abrasion and shock resistance.
- Convenient easy mix ratio A:B=3:1 by volume.
- Solvent-free.
- Color-coded components to ensure proper mixing control.

Coverage

Type S 512 CarboDur: approx. 50 LF/gal.; Type S 812 CarboDur: approx. 32 LF/gal.; Type S 1012 CarboDur: approx. 22 LF/gal.

Packaging

1 gal. units.

Typical Data *(Material and curing conditions @ 73°F {23°C} and 50% R.H.)*

Shelf Life: 2 years in original, unopened containers.

Storage Conditions: Store dry at 40°-95°F (4°-35°C). **Condition material to 65°-85°F (18°-29°C) before using**.

Color: Light gray

Mixing Ratio: Component 'A': Component 'B' = 3:1 by volume.

Consistency: Non-sag paste.

Pot Life: Approximately 70 minutes @ 73°F (23°C) (1 qt.)

Tensile Properties (ASTM D-638)

7 day	Tensile Strength	3,600 psi (24.8 MPa)
	Elongation at Break	1%
	Modulus of Elasticity	6.5 X 10^5 psi (4,482 MPa)

Flexural Properties (ASTM D-790)

14 day	Flexural Strength (Modulus of Rupture)	6,800 psi (46.8 MPa)
	Tangent Modulus of Elasticity in Bending	1.7 X 10^6 psi (11,721 MPa)

Shear Strength (ASTM D-732) **14 day** Shear Strength 3,600 psi (24.8 MPa)

Bond Strength (ASTM C-882): Hardened Concrete to Hardened Concrete

2 day (moist cure)	Bond Strength	2,700 psi (18.6 MPa)
2 day (dry cure)	Bond Strength	3,200 psi (22.0 MPa)
14 day (moist cure)	Bond Strength	3,100 psi (21.3 MPa)
	Hardened Concrete to Steel	2,600 psi (17.9 MPa)
2 day (moist cure)	Bond Strength	3,000 psi (20.6 MPa)
2 day (dry cure)	Bond Strength	2,600 psi (17.9 MPa)
14 day (moist cure)	Bond Strength	

Heat Deflection Temperature (ASTM D-648)

7 day [fiber stress loading=264 psi (1.8 MPa)] 118°F (47°C)

Water Absorption (ASTM D-570) **7 day** (24 hour immersion) 0.03%

Compressive Properties (ASTM D-695) - Compressive Strength, psi (MPa)

	40°F* (4°C)	73°F* (23°C)	90°F* (32°C)
4 hour	-	-	5,500 (37.9)
8 hour	-	3,500 (24.1)	6,700 (46.2)
16 hour	-	6,700 (46.2)	7,400 (51.0)
1 day	750 (5.1)	7,800 (53.7)	7,800 (53.7)
3 day	6,800 (46.8)	8,300 (57.2)	8,300 (57.2)
7 day	8,000 (55.1)	8,600 (59.3)	8,600 (59.3)
14 day	8,500 (58.6)	8,600 (59.3)	8,900 (61.3)
28 day	8,500 (58.6)	8,600 (59.3)	9,000 (62.0)

Compressive Modulus **7 day** 3.9 x 10^5 psi (2,689 MPa)

*Material cured and tested at the temperatures indicated.

Construction

How to Use

Surface Preparation

The concrete surface should be prepared to a minimum concrete surface profile (CSP) 3 defined by the ICRI surface-profile chips. Localized out-of-plane variations, including form lines, should not exceed 1/32 in. (1 mm). Surface must be clean and sound. It may be dry or damp, but free of standing water and frost. Remove dust, laitance, grease, curing compounds, impregnations, waxes, foreign particles, disintegrated materials, and other bond inhibiting materials from the surface. Existing uneven surfaces must be filled with an appropriate repair mortar (e.g., Sikadur 30 with the addition of 1 part oven-dried sand). The adhesive strength of the concrete must be verified after surface preparation by random pull-off testing (ACI 503R) at the discretion of the engineer. Minimum tensile strength, 200 psi (1.4 MPa) with concrete substrate failure.

Preparation work

Concrete - Blast clean, shotblast or use other approved mechanical means to provide an open roughened texture.

Steel - Should be cleaned and prepared thoroughly by blastcleaning to a white metal finish.

CarboDur - Wipe clean with appropriate cleaner (e.g. MEK).

Mixing

Pre-mix each component. Proportion 1 part Component 'B' to 3 parts Component 'A' by volume into a clean pail. Mix thoroughly for 3 minutes with Sika paddle on low-speed (400-600 rpm) drill until uniform in color. Mix only that quantity which can be used within its pot life.

To prepare an epoxy mortar: slowly add up to 1 part by loose volume of an oven-dried aggregate to 1 part of the mixed Sikadur 30 and mix until uniform in consistency.

Application

For bonded, external reinforcement:

Apply the neat mixed Sikadur 30 onto the concrete with a trowel or spatula to a nominal thickness of 1/16" (1.5 mm). Apply the mixed Sikadur 30 onto the CarboDur laminate with a "roof-shaped" spatula to a nominal thickness of 1/16" (1.5 mm). Within the open time of the epoxy, depending on the temperature, place the CarboDur laminate onto the concrete surface. Using a hard rubber roller, press the laminate into the epoxy resin until the adhesive is forced out on both sides. Remove excess adhesive. Glue line should not exceed 1/8 inch (3 mm). The external reinforcement must not be disturbed for a minimum of 24 hours. The epoxy will reach its design strength after 7 days.

For interior vertical and overhead patching: Work the material into the prepared substrate, filling the cavity. Strike off level. Lifts should not exceed 1 inch (25 mm).

Limitations

- Minimum substrate and ambient temperature is 40°F (4°C).
- Do not thin. Addition of solvents will prevent proper cure.
- Use oven-dried aggregate only.
- Maximum glue line of neat epoxy is 1/8 inch (3 mm).
- Maximum epoxy mortar thickness is 1 inch (25 mm) per lift.
- Minimum age of concrete must be 21-28 days, depending upon curing and drying conditions.
- Porous substrates must be tested for moisture vapor transmission prior to mortar applications.
- Not an aesthetic product. Color may alter due to variations in lighting and/or UV exposure.

Warning

Component 'A' - IRRITANT; SENSITIZER - Contains epoxy resin, calcium carbonate, and silica (quartz). Can cause skin sensitization after prolonged or repeated contact. Eye irritant. High concentrations of vapor may cause skin/respiratory irritation. Harmful if swallowed.

Component 'B' - CORROSIVE; SENSITIZER - Contains amines, calcium carbonate, and silica (quartz). Contact with eyes or skin causes severe burns. Can cause skin sensitization after prolonged or repeated contact. Eye irritant. May cause respiratory/skin irritation. Sanding of cured product may result in exposure to a chemical known in the state of California to cause cancer.

First Aid

Eyes: Hold eyelids apart and flush thoroughly with water for 15 minutes. **Skin:** Remove contaminated clothing. Wash skin thoroughly for 15 minutes with soap and water. **Inhalation:** Remove person to fresh air. **Ingestion:** Do not induce vomiting. **In all cases, contact a physician immediately if symptoms persist.**

Clean Up

In case of spills or leaks, wear suitable chemical resistant gloves/goggles/clothing, contain spill, collect with absorbent material, and transfer to suitable container. Ventilate area. Avoid contact. Dispose of in accordance with current, applicable local, state and federal regulations. Uncured material can be removed with solvent. Strictly follow manufacturer's warnings and instructions for use. Cured material can only be removed mechanically.

Handling & Storage

Avoid direct contact with skin and eyes. Wear chemical resistant gloves/goggles/clothing. Use only with adequate ventilation. In absence of adequate general and local exhaust ventilation, use a properly filled NIOSH respirator. Wash thoroughly after handling product. Launder clothing before reuse. Store in a cool dry well ventilated area.

Visit our website at www.sikaconstruction.com **1-800-933-SIKA NATIONWIDE**

Regional Information and Sales Centers. For the location of your nearest Sika sales office, contact your regional center.

Sika Corporation
201 Polito Avenue
Lyndhurst, NJ 07071
Phone: 800-933-7452
Fax: 201-933-6225

Sika Canada Inc.
601 Delmar Avenue
Pointe Claire
Quebec H9R 4A9
Phone: 514-697-2610
Fax: 514-694-2792

Sika Mexicana S.A. de C.V.
Carretera Libre Celaya Km. 8.5
Fracc. Industrial Balvanera
Corregidora, Queretaro
C.P. 76920
Phone: 52 442 2385800
Fax: 52 442 2250537

Product Data Sheet
Edition 7.1.2008
Identification no.
Sikadur 330 US

Sikadur® 330 US

High-modulus, high-strength, impregnating resin

Description	Sikadur 330 is a two-component , solvent-free, moisture-tolerant, high strength, high modulus structural epoxy adhesive.
Where to Use	For use as an impregnating resin with the SikaWrap Hex 106G, 113C, 117C, 230C and 430G Structural Strengthening Systems.
Advantages	■ Long pot life. ■ Long open time. ■ Easy to mix. ■ Tolerant of moisture before, during and after cure. ■ High strength, high modulus adhesive. ■ Excellent adhesion to concrete, masonry, metals, wood and most structural materials. ■ Fully compatible and developed specifically for the SikaWrap Systems. ■ High temperature resistance. ■ High abrasion and shock resistance. ■ Solvent-free, VOC compliant.
Coverage	First coat: 40-50 sq.ft./gal.; Additional coats: 100 sq.ft./gal.; Final coat: 160 sq.ft./gal.
Packaging	3 gal. kit (two 1.25 gal. component 'A' pails, two 0.35 gal. component 'B' pails)

How to Use

Surface Preparation

The concrete surface should be prepared to a minimum concrete surface profile (CSP-3) as defined by the ICRI-surface-profile chips. Localized out-of-plane variations, including form lines, should not exceed 1/32 in. (1 mm).

Substrate must be clean, sound, and free of surface moisture. Remove dust, laitance, grease, oils, curing compounds, waxes, impregnations, foreign particles, coatings and disintegrated materials by mechanical means (i.e. sandblasting). For best results, substrate should be dry. However, a saturated surface dry condition is acceptable.

Mixing

Pre-mix each component. **Mix entire unit, do not batch.** Pour contents of part B to part A. Mix thoroughly for 5 minutes with a 1/2 inch "Jiffy" mixer mounted on a rotary drill and set at a slow speed (400-600 rpm) until uniformly blended. Mix only that quantity that can be used within its pot life.

Typical Data *(Material and curing conditions @ 73°F (23°C) and 50% R.H.)*

Shelf Life	2 years in original, unopened container.
Storage Conditions	Store dry at 40°-95°F (4°-35°C). **Condition material to 65°-75°F (18°-24°C) before using.**
Color	Light gray.
Mixing Ratio	Component 'A' : Component 'B' = 4 : 1 by weight
Consistency	Non-sag paste.
Pot Life	57 minutes (325 ml)
Tack Free Time	4-5 hours

Heat Deflection Temperature (ASTM D-648)

7 day [fiber stress loading=264 psi (1.8 MPa) 120°F (50°C)

Mechanical Properties

Compressive Properties (ASTM D-695), psi (MPa)

	40°F (4°C)	60°F (16°C)	73°F (23°C)	90°F (32°C)
8 hour	-	-	-	8,000 (55.2)
1 day	-	8,100 (55.8)	10,700 (73.7)	10,600 (73.1)
3 day	8,100 (55.8)	11,200 (77.2)	11,100 (76.5)	11,000 (75.8)
7 day	11,200 (77.2)	11,600 (80.0)	11,200 (77.2)	11,800 (81.3)
14 day	12,500 (86.2)	12,400 (85.5)	11,800 (81.3)	11,900 (82.0)

Tensile Strength (ASTM D-638)	**7 day**	4,900 psi (33.8 MPa)
Elongation @ Break (ASTM D-638)	**7 day**	1.2%
Flexural Strength (ASTM D-790)	**7 day**	8,800 psi (60.6 MPa)
Flexural Modulus (ASTM D-790)	**7 day**	5.06 x 10^5 psi (3,489 MPa)

Construction

Application

Dry Lay-Up: When installing a SikaWrap Hex fabric in the dry lay-up process apply the mixed Sikadur 330 epoxy resin directly onto the substrate at a rate of 40-50 ft.²/gal. (0.95-1.18 m²/L). Coverage rate will depend on the actual surface profile. This equates to a thickness of approximately 32-40 mils. Carefully place the fabric into the applied resin with gloved hands and smooth out. Work out any irregularities or air pockets with a plastic laminating roller. Let the resin squeeze out between the rovings of the fabric. If more than one layer of fabric is required, apply additional Sikadur 330 US at a rate of 100 ft.²/gal. (2.37 m²/L) and repeat as described above. This equates to a thickness of approximately 16 mils. Add a final layer of Sikadur 330 US onto the exposed surface at a rate of 160 ft²/gal. (3.79 m²/L). This equates to a thickness of approximately 10 mils.

Wet Lay-Up: When installing a SikaWrap Hex fabric vertically or overhead in the wet lay-up process, mixed Sikadur 330 can be applied to the substrate as a primer/tack coat to prevent the impregnated fabric from sliding down the concrete. Due to its mixed viscosity, do not use Sikadur 330 US with an automatic fabric saturating device. Consult the SikaWrap Hex fabric technical data sheet for information on saturating/impregnating fabric in a wet lay-up installation.

Limitations

- Minimum age of concrete is 21-28 days, depending on curing and drying conditions.
- All repairs required to achieve a level surface must be performed prior to application.
- Do not apply or cure Sikadur 330 US in direct sunlight.
- Minimum substrate temperature 40°F (4°C). Maximum application temperature 95°C (35°C)
- Do not thin with solvents.
- Material is a vapor barrier after cure.
- Do not encapsulate saturated concrete in areas of freezing and thawing.
- Color of Sikadur 330 US may alter due to variations in lighting and/or UV exposure.
- Due to its mixed viscosity, do not use Sikadur 330 US with an automatic saturating device. Fabric must be saturated/impregnated manually when the wet lay-up process is used.
- At low temperatures and/or high relative humidity, a slight oily residue (blush) may form on the surface of the cured epoxy. If an additional layer of fabric, or a coating is to be applied onto the cured epoxy. This residue must first be removed to ensure adequate bond. The residue can be removed with either a solvent wipe (e.g. MEK) or with water and detergent. In both cases, the surface should be wiped dry prior to application of the next layer or coating.
- Not an aesthetic product. Color may alter due to variations in lighting and/or UV exposure.

Warning

Component 'A' - IRRITANT, SENSITIZER: Contains Modified Epoxy Resin (CAS 25068-38-6) and Aromatic Hydrocarbon Blend (Mixture). Causes eye irritation. May cause skin/respiratory irritations. Prolonged and/or repeated contact with skin may result in allergic reaction/sensitization. Harmful if swallowed. **Deliberate concentration of vapors for purposes of inhalation is harmful and can be fatal.**

Component 'B' - CORROSIVE, IRRITANT, SENSITIZER: Contains Amines. Contact with skin and eyes causes severe burns. Causes eye/skin/respiratory irritations. Prolonged and/or repeated contact may cause allergic reaction/sensitization. Harmful if swallowed. **Deliberate concentration of vapors for purposes of inhalation is harmful and can be fatal.**

First Aid

Eyes: Hold eyelids apart and flush thoroughly with water for 15 minutes. **Skin:** Remove contaminated clothing. Wash skin thoroughly for 15 minutes with soap and water. **Inhalation:** Remove person to fresh air. **Ingestion:** Do not induce vomiting. **In all cases, contact a physician immediately if symptoms persist.**

Handling & Storage

Avoid direct contact with eyes and skin. Wear chemical resistant gloves/goggles/clothing. Avoid breathing vapors. Use with adequate general and local ventilation. In absence of adequate ventilation, use properly fitted NIOSH approved respirator. Wash thoroughly after handling product. Remove contaminated clothing and launder before reuse. Store product in closed container in a cool dry place 40° – 95°F (4° – 35°C). Condition material to 65° – 75°F (18° – 24°C) before using.

Clean Up

Ventilate area. Confine spill. Collect with absorbent material. Dispose of in accordance with current, applicable local, state and federal regulations. Uncured material can be removed with approved solvent. Cured material can only be removed mechanically.

Visit our website at www.sikaconstruction.com **1-800-933-SIKA NATIONWIDE**

Regional Information and Sales Centers. For the location of your nearest Sika sales office, contact your regional center.

Sika Corporation
201 Polito Avenue
Lyndhurst, NJ 07071
Phone: 800-933-7452
Fax: 201-933-6225

Sika Canada Inc.
601 Delmar Avenue
Pointe Claire
Quebec H9R 4A9
Phone: 514-697-2610
Fax: 514-694-2792

Sika Mexicana S.A. de C.V.
Carretera Libre Celaya Km. 8.5
Fracc. Industrial Balvanera
Corregidora, Queretaro
C.P. 76920
Phone: 52 442 2385800
Fax: 52 442 2250537

ISO 9000:2000

APPENDIX B

COMPOSITE ADHESIVE TESTING

Experimental tests to find similar adhesive properties were discussed in the journal article *Analysis of Bond between Near-Surface Mounted CRP Laminates and Concrete* (Diab, 2008). Those tests were very complex and required extensive set up and instrumentation. Experiments of such high complication make such a method difficult to implement on an industry scale. In contrast, the adhesive tests created for this research project are simple in concept and set-up and easy to perform. This simplicity increases confidence in results by avoiding multiple sources of possible error. Such a series of experiments lends itself to industry and research adoption.

To test adhesive shear properties, an experimental test involving two plates, adhesive, and the composite fiber material associated with the respective adhesive. These plates are placed end to end and connected by composite patches on either side by adhesive. Figure B1 illustrates the adhesive test specimen. Figure B2 shows the application of the spring assumption. The experiment works by pulling the two plates apart in the longitudinal direction. By measuring the displacement, load, and area of failure and application, all the desired adhesive properties stated above can be found. The shear stiffness of the adhesive is equal to the slope of the load displacement curve, which is normalized by dividing the slope by the area over which the adhesive is applied.

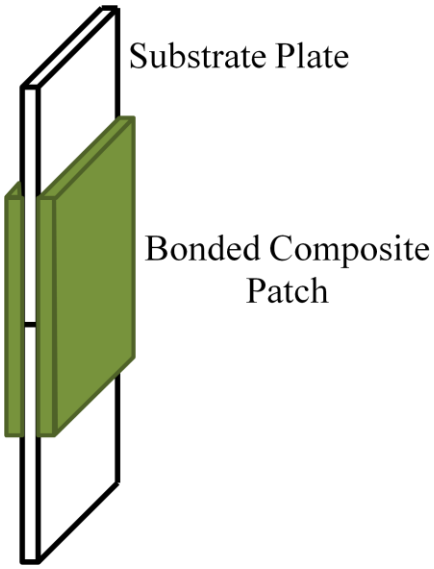

Figure B1. Adhesive tensile test specimen

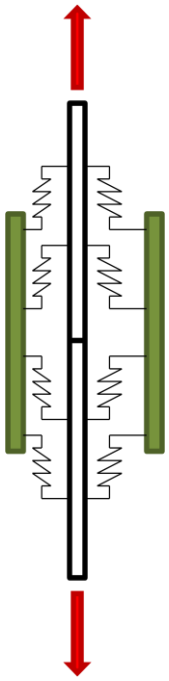

Figure B2. Application of spring theory to adhesive

The plates used in this research experiment are steel. They were bead blasted to a white finish, degreased, and cleaned. Such extensive surface preparation ensures an excellent bonding surface and eliminates any error that may have resulted from a dirt

substrate. The composite materials were included to observe if failure of the specimens might lie in the fibers. Figure B3 shows the cleaned plates before being used as specimens.

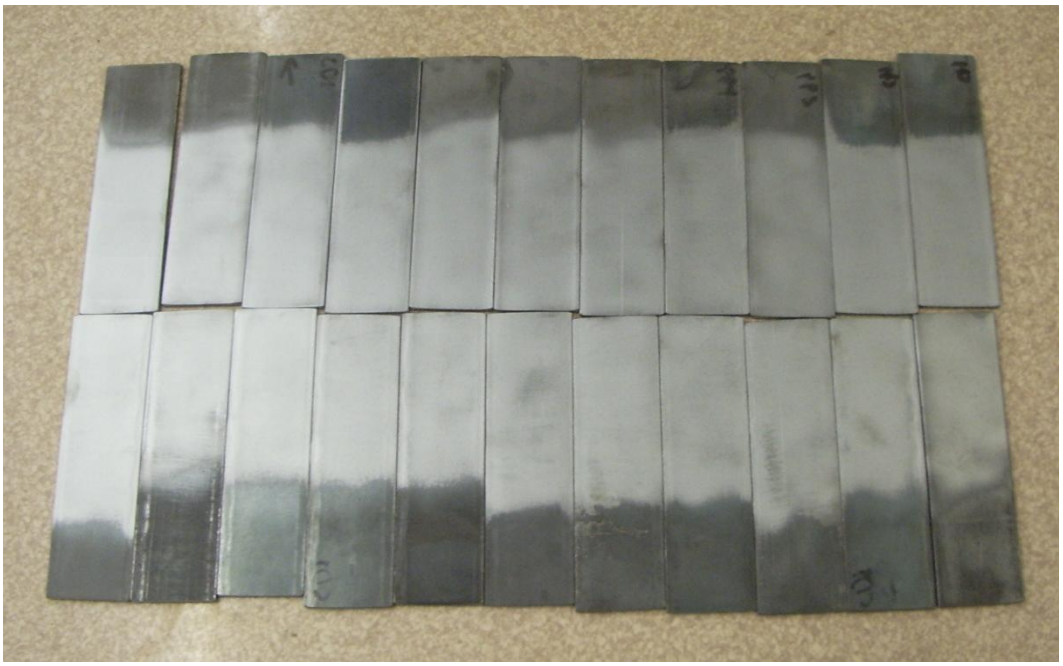

Figure B3. Plates for adhesive shear testing after bead blasting

Figure B4 shows all the types of specimens produced. Refer to Chapter IV for application of composite materials. In total, three specimens were produced with Carbodur composite patches, four with Sikawrap, and four LTC 4300 specimens.

Figure B4. Finished LTC 4300 (left), Sikadur 30 (center), and Sikadur 330 (right) specimens

A similar testing philosophy was adopted to find the tensile mechanical properties of each adhesive. The tests reveal the tensile spring constant, young's modulus, and tensile capacity of each adhesive. The specimens were created from an aluminum I-beam. The beam was cut along the web, creating two "T" shapes. As with the shear test plates, the surface of the aluminum T shapes was brought to a proper white finish, degreased, and cleaned, typically with acetone and isopropanol. The "T"'s adhered together by sandwiching a piece of composite fibers between two layers of adhesive. Figure B5 shows a typical example of a test specimen. Figure B6 illustrates the concept

of representing the adhesive as a series of spring. Since the tensile "springs" act in series, the tensile stiffness is found by dividing the slope of the load-displacement curve by two times the area of application.

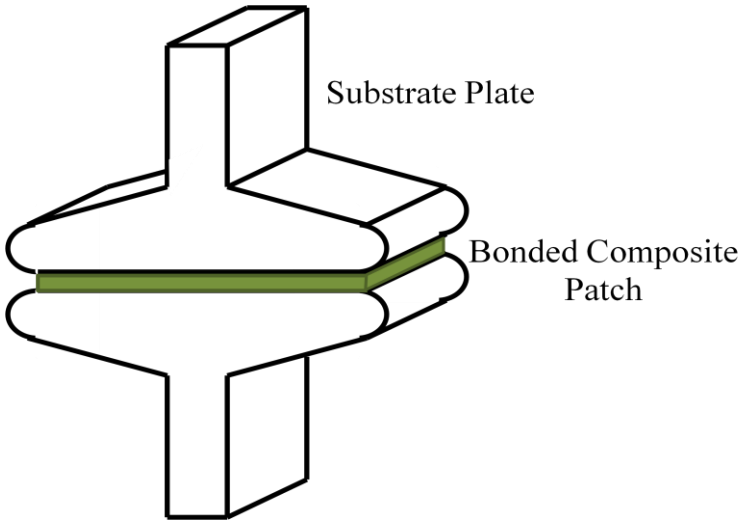

Figure B5. Adhesive tensile specimen

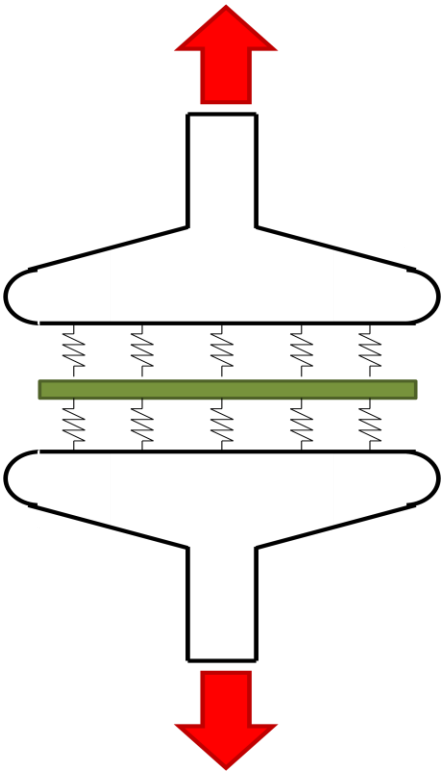

Figure B6. Spring representation of adhesive tensile strength

Manufacturers rarely provide information into the time necessary for adhesives to reach full strength, however, Sika suggests that seven days are necessary for the adhesive to reach full strength. Several weeks passed between when the specimens were created and tested in a MTS 810 universal testing machine.

The testing procedure is described below:

1. Specimen was placed into the machine
2. The data acquisition system was zeroed
3. Plates were separated at a rate of one millimeter per second
4. Specimen pieces were collected after failure

Misalignment of the plates caused the initial load to be measured before the data collection software was tared. This force measured was caused by the testing machine forcing the plates into alignment. The value of these misalignment stresses ranged from ten to fifteen percent of the maximum force calculated.

Once the experiments were completed, the area of failure was measured to the nearest sixteenth inch. The stress values of the adhesives were obtained by dividing the load values by the respective failure areas. The strain values of the shear specimens were obtained by dividing one-half of measured displacement at that load level with the thickness of the adhesive. The difference of measured displacements was used to find the strain values of the tensile specimens.

There are several methods to find the slope of the respective set of data. Two very similar methods were used to analyze the results and find the desired physical properties. The methods for finding linear lines of best fit involve several steps., which are described below.

Method A

1. Locate the point of maximum load before the first failure for each specimen
2. Eliminate all data following that value
3. Combine similarly processed test results from other test specimens to form single series of data points
4. Find line of best fit which begins at the origin and terminates at the average final value of each specimen

5. Find R^2 value of the trend line

An additional method utilized involved similar steps, yielding fit criteria, and is as follows:

Method B

1. Locate the point of maximum load before the first failure for each specimen
2. Eliminate all data following that value
3. Find trend line which begins at the origin
4. Average desired values of the slope for the lines
5. Find R^2 value, standard deviation, and coefficient of variation

The second method allows the researcher to find the standard deviation and coefficient of variation for each data set. These statistical measures provide a greater insight into how well the trend line fits the data beside the coefficient of determination, or R^2.

Given the limited number of specimens for each adhesive type adhered to only one type of substrate, it would be unwise to use the maximum value obtained from either Method A or B in design. Consequently, in an effort to be conservative, additional trend lines were found corresponding to percentages of the maximum load value; these percentages include 95, 90, 85, and 80 percent. In cases of percentages below 100, the adhesive it considered to be elastic-perfectly plastic. A product from Method A or B is

that the shear and tensile capacities of the adhesive are easily found by averaging the maximum capacity of each specimen.

Shear Adhesive Characterization

Sikadur 330

Figure B7 shows a typical Sikadur 330/Sikawrap specimen in the universal testing machine before loading began. Figures B8 and B9 show the specimens after failure. Note that the failure of the specimen occurs at the adhesive level. There were no signs of fibers ruptured. The only mode of failure is adhesive debonding. The surfaces of the plates where the debonding occurred are almost clean of adhesive. The only material left on the steel plate is adhesive in small quantities. The small dots of adhesives on the substrate coincide with the location of the white nylon thread weaving through the carbon fibers. This is the reason the specs of adhesive occur in linear patterns. There is no misunderstanding that the weakest of component of the FRP composite is the adhesive, which debonded at the substrate surface.

Figure B7. Sikadur 330/Sikawrap shear specimen before loading

Figure B8. Sikadur 330 adhesive shear specimens, side a

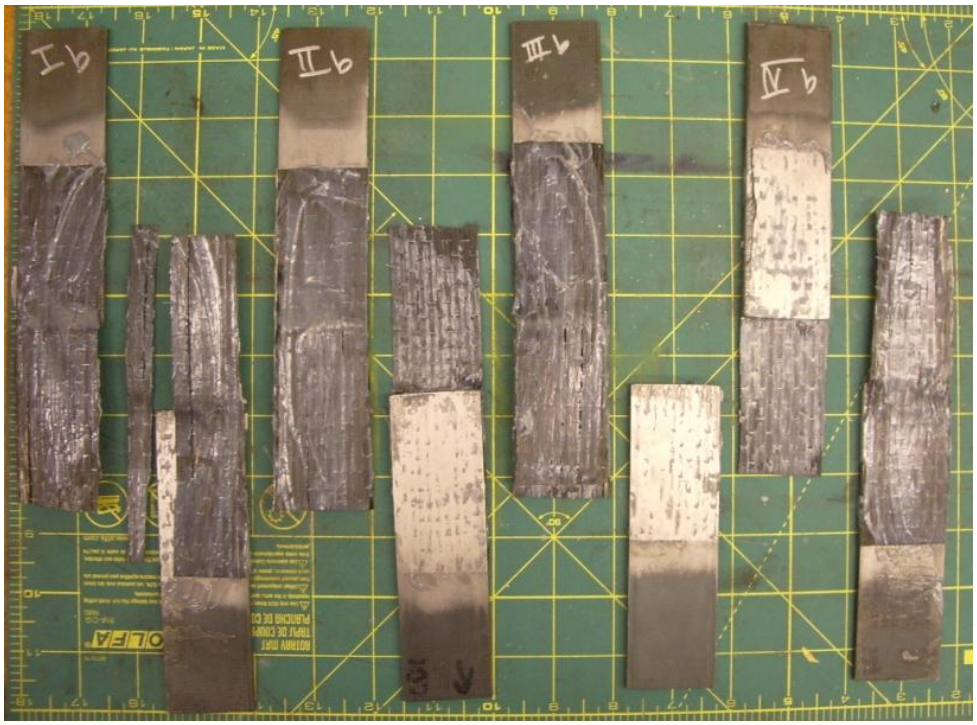

Figure B9. Sikadur 330 adhesive shear specimens, side b

The experimental results of the Sikadur 330 adhesive shear tests are in Figure B10. The results show that the adhesive progressively failed.

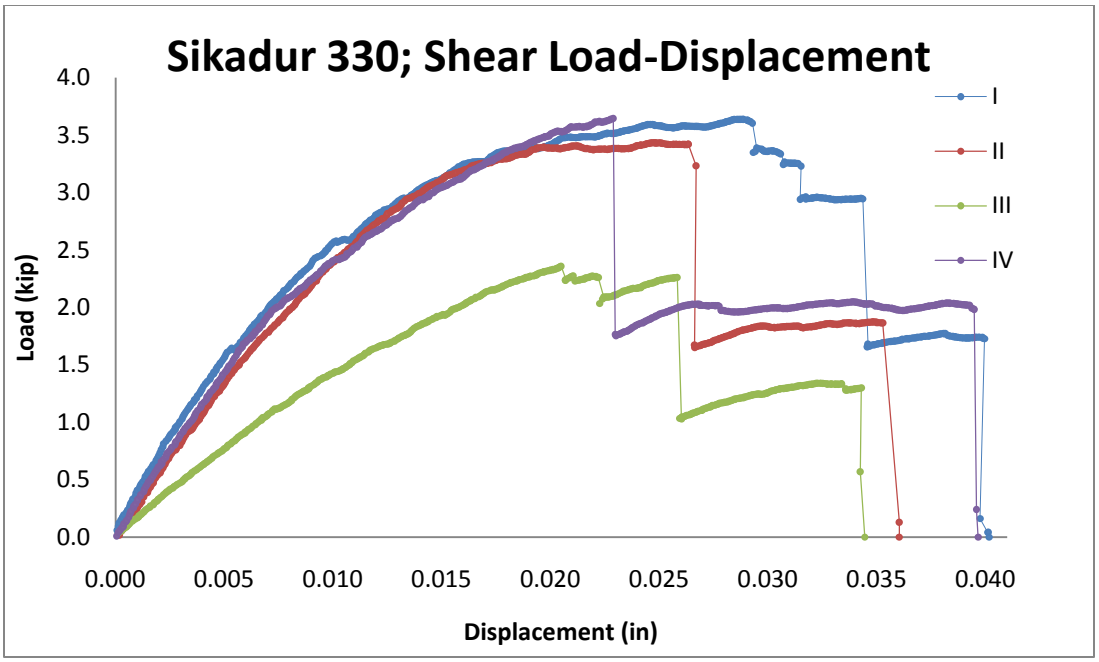

Figure B10. Sikadur 330 shear load-displacement results

The results of the first method for the spring stiffness and shear modulus respectively are shown in figure B11; both methods were used. The third specimen results were ignored in the analyses. The results of these analyses are tabulated in Tables B1 and B2 for the shear spring constant and Tables B3 and B4 for the shear modulus. The shear capacity of the adhesive is given in Table B5.

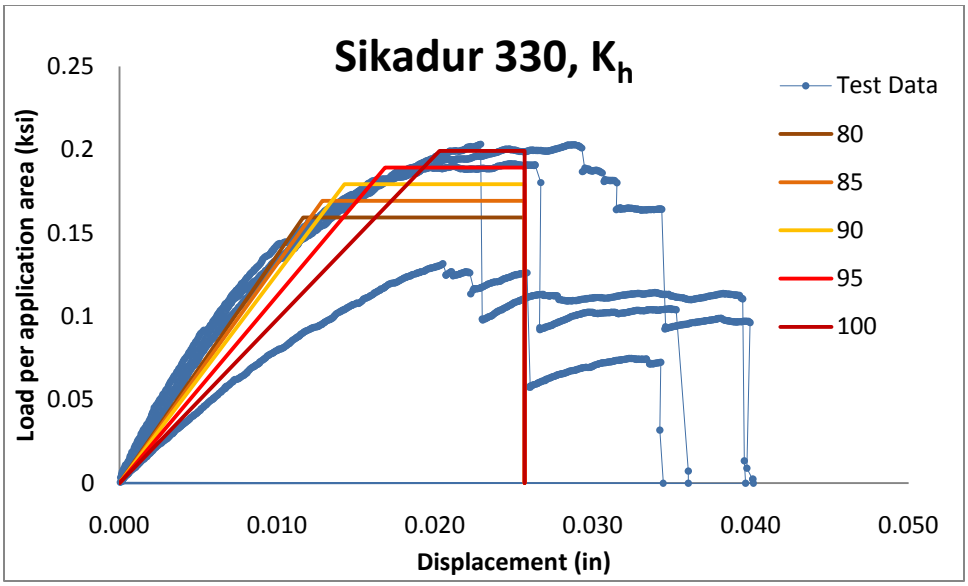

Figure B11. Shear spring constant trend lines of Sikadur 330

Table B1. Method A analysis of shear spring constant for Sikadur 330

Method A	k	R^2
100%	9.837	.7192
95%	11.257	.8433
90%	12.594	.924
85%	13.195	.9395
80%	13.709	.95

Table B2. Method B analysis of shear spring constant for Sikadur 330

Method B					
	Specimen	k	R^2		
100%	1	9.2574	0.5999	Ave. =	10.002
	2	10.018	0.7971	Std. Dev. =	0.736
	3 (exclude)	7.1397	0.9702	Cov =	0.0736
	4	10.73	0.8662	Ave R^2=	0.754
95%	1	10.654	0.759	Ave. =	11.488
	2	12.212	0.9581	Std. Dev. =	0.785
	3 (exclude)	7.3761	0.9786	Cov =	0.0683
	4	11.599	0.9071	Ave R^2=	0.875
90%	1	12.787	0.8944	Ave. =	12.601
	2	12.862	0.9781	Std. Dev. =	0.390
	3 (exclude)	7.5114	0.9816	Cov =	0.0309
	4	12.153	0.9242	Ave R^2=	0.932
85%	1	13.666	0.9221	Ave. =	13.192
	2	13.243	0.9855	Std. Dev. =	0.502
	3 (exclude)	7.6394	0.9843	Cov =	0.0381
	4	12.666	0.9381	Ave R^2=	0.949
80%	1	14.342	0.9386	Ave. =	13.681
	2	13.507	0.9891	Std. Dev. =	0.593
	3 (exclude)	7.775	0.9874	Cov =	0.0433
	4	13.195	0.95	Ave R^2=	0.959

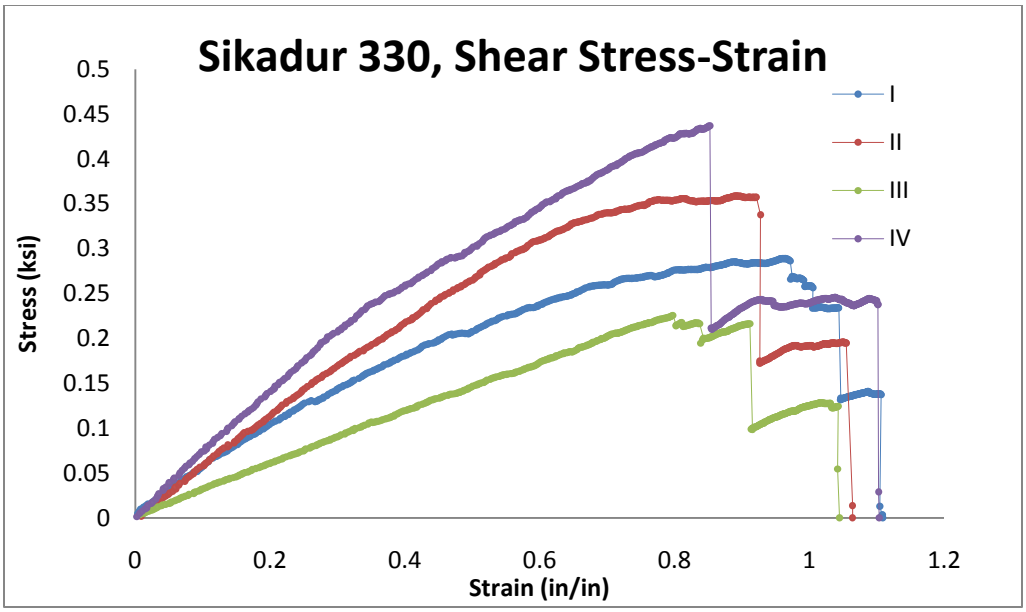

Figure B12. Sikadur 330 shear stress-strain results

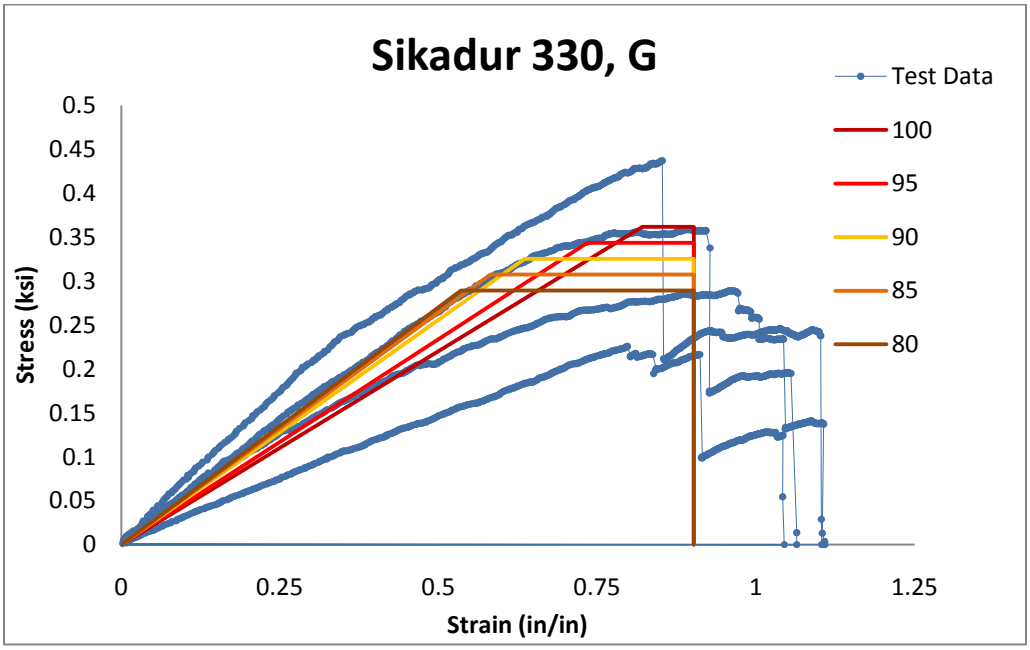

Figure B13. Shear modulus trend lines for Sikadur 330

Table B3. Method A analysis of shear modulus for Sikadur 330

Method A	G	R^2
100%	0.4406	0.7059
95%	0.4678	0.7557
90%	0.5121	0.8629
85%	0.5286	0.8842
80%	0.5405	0.8944

Table B4. Method B analysis of shear modulus for Sikadur 330

Method B	Specimen	G	R^2		
100%	1	0.3497	0.8666	Ave. =	0.461
	2	0.4699	0.9348	Std. Dev. =	0.107
	3(excluded)	0.2893	0.9982	Cov =	0.2321
	4	0.5631	0.9613	Ave R^2=	0.461
95%	1	0.374	0.9118	Ave. =	0.492
	2	0.5198	0.9894	Std. Dev. =	0.107
	3(excluded)	0.2909	0.9984	Cov =	0.2172
	4	0.5822	0.9683	Ave R^2=	0.492
90%	1	0.412	0.9539	Ave. =	0.513
	2	0.5326	0.9447	Std. Dev. =	0.093
	3(excluded)	0.2916	0.9982	Cov =	0.1811
	4	0.5947	0.9705	Ave R^2=	0.513
85%	1	0.4278	0.9619	Ave. =	0.525
	2	0.5396	0.9963	Std. Dev. =	0.091
	3(excluded)	0.2915	0.998	Cov =	0.1727
	4	0.6073	0.973	Ave R^2=	0.525
80%	1	0.4407	0.9673	Ave. =	0.535
	2	0.5442	0.9969	Std. Dev. =	0.091
	3(excluded)	0.2937	0.998	Cov =	0.1691
	4	0.6211	0.9756	Ave R^2=	0.535

Table B5. Sikadur 330 shear stress capacity

Shear Capacity Percentage	τ (ksi)
100	0.362
95	0.344
90	0.325
85	0.307
50	0.289

Sikadur 30

Figure B14 shows a shear specimen of Sikadur30/Carbodur loaded in the testing apparatus. Figures B15 and B16 shows the final results of the tests. Each specimen suddenly failed with no warning. In one test, failure caused the composite patch to fly off the specimen. Like Sikadur 330 before it, the failure of the specimen is caused by the adhesive. However, there is no adhesive left on the plates except for a portion of the fillet.

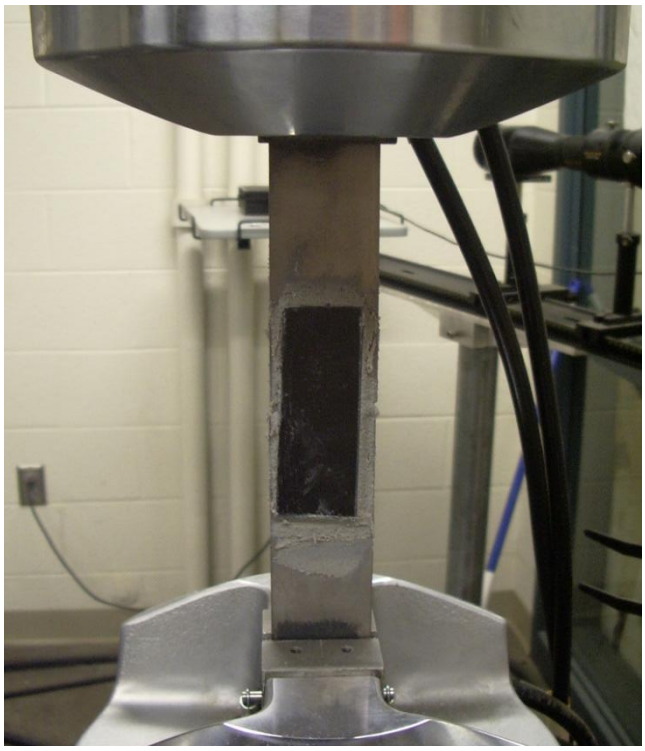

Figure B14. Sikadur 30/Carbodur specimen before loading

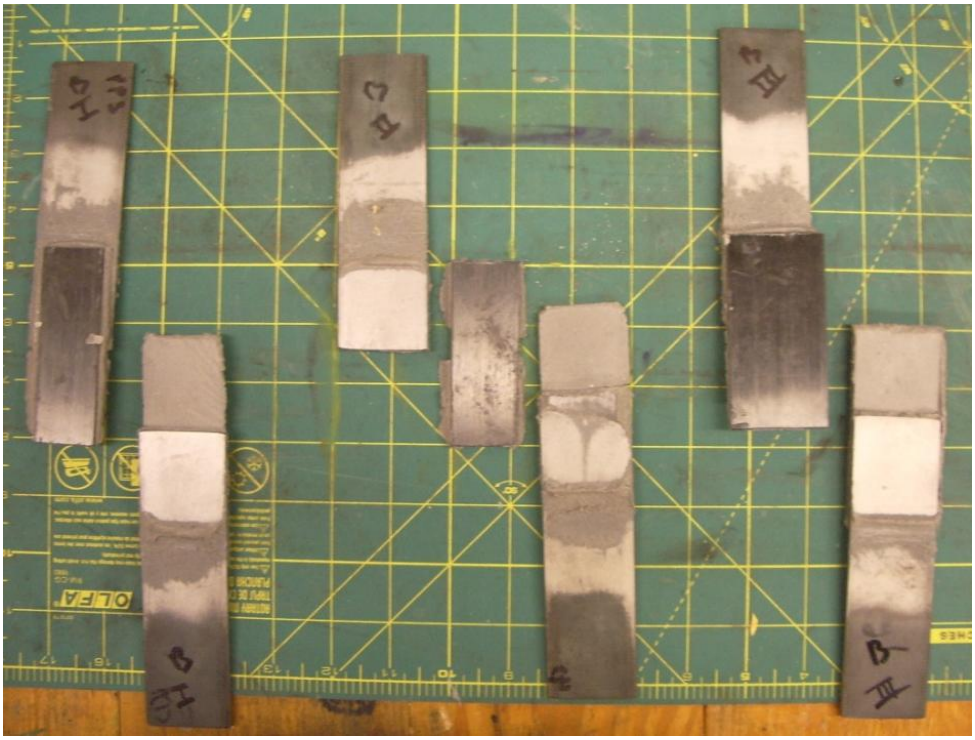

Figure B15. Sikadur 30 shear specimens after failure, side a

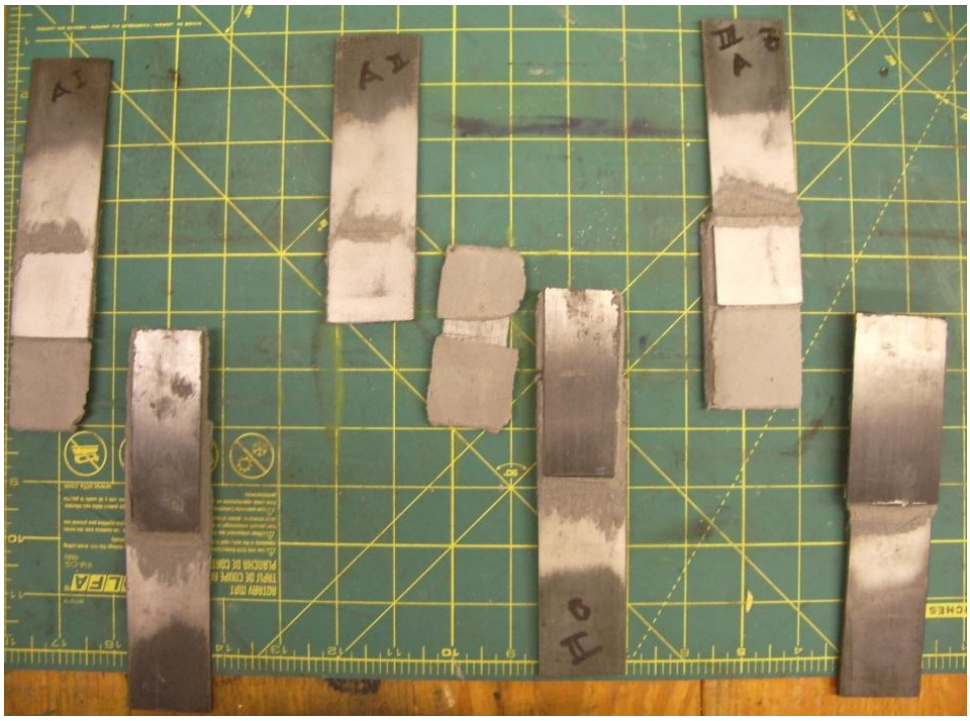

Figure B16. Sikadur 30 shear specimens after failure, side b

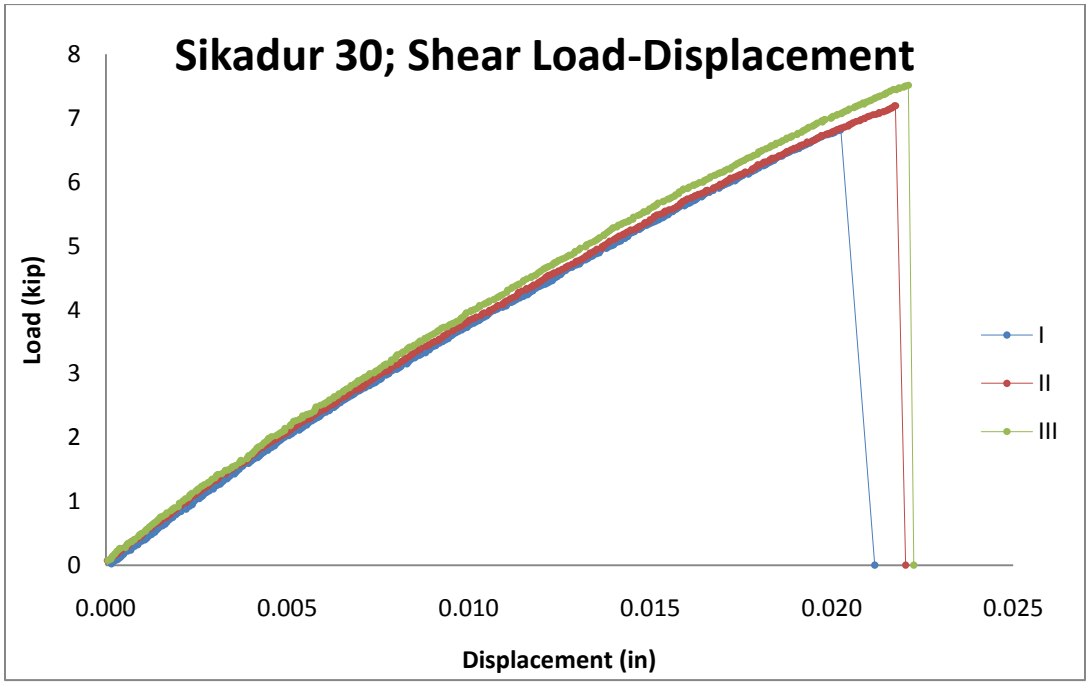

Figure B17. Sikadur 330 load-displacement results

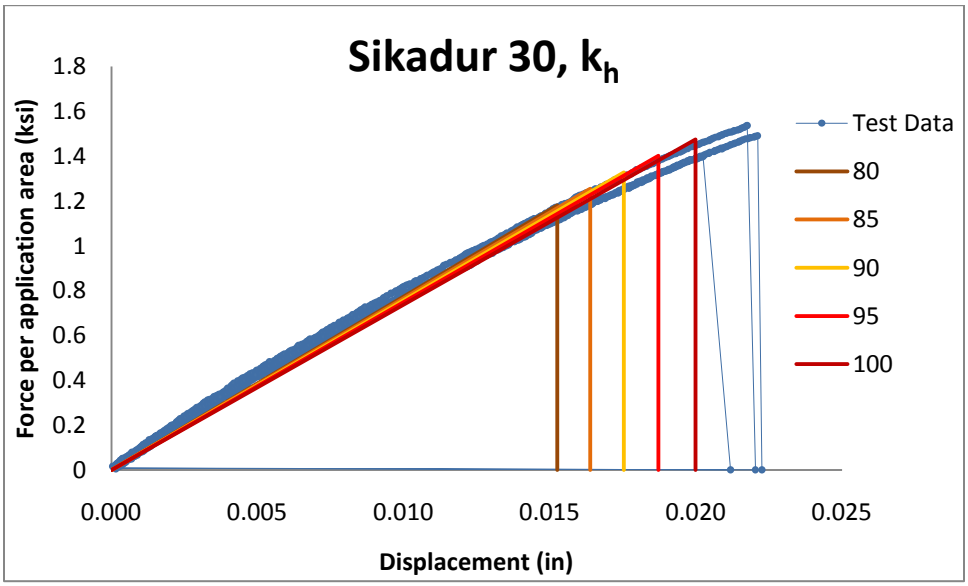

Figure B18. Trendlines for Sikadur 330 spring constant

Table B6. Method A analysis of shear spring constant for Sikadur 30

Method A		
	k	R^2
100%	73.846	0.9856
95%	74.879	0.9872
90%	75.736	9882
85%	76.553	0.9888
80%	77.377	0.9893

Table B7. Method B analysis of shear spring constant for Sikadur 30

Method B	Specimen	k	R^2		
100%	1	73.047	0.992	Ave. =	73.811
	2	75.815	0.9857	Std. Dev. =	1.751
	3	72.572	0.9853	Cov =	0.0237
				Ave R^2=	0.988
95%	1	73.847	0.993	Ave. =	74.833
	2	76.988	0.9878	Std. Dev. =	1.868
	3	73.665	0.9873	Cov =	0.0250
				Ave R^2=	0.989
90%	1	74.499	0.9937	Ave. =	74.794
	2	77.935	0.989	Std. Dev. =	3.004
	3	71.949	0.9953	Cov =	0.0402
				Ave R^2=	0.993
85%	1	75.152	0.9942	Ave. =	75.524
	2	78.84	0.9899	Std. Dev. =	3.147
	3	72.58	0.9961	Cov =	0.0417
				Ave R^2=	0.993
80%	1	75.761	0.9945	Ave. =	76.272
	2	79.863	0.9905	Std. Dev. =	3.364
	3	73.193	0.9968	Cov =	0.0441
				Ave R^2=	0.994

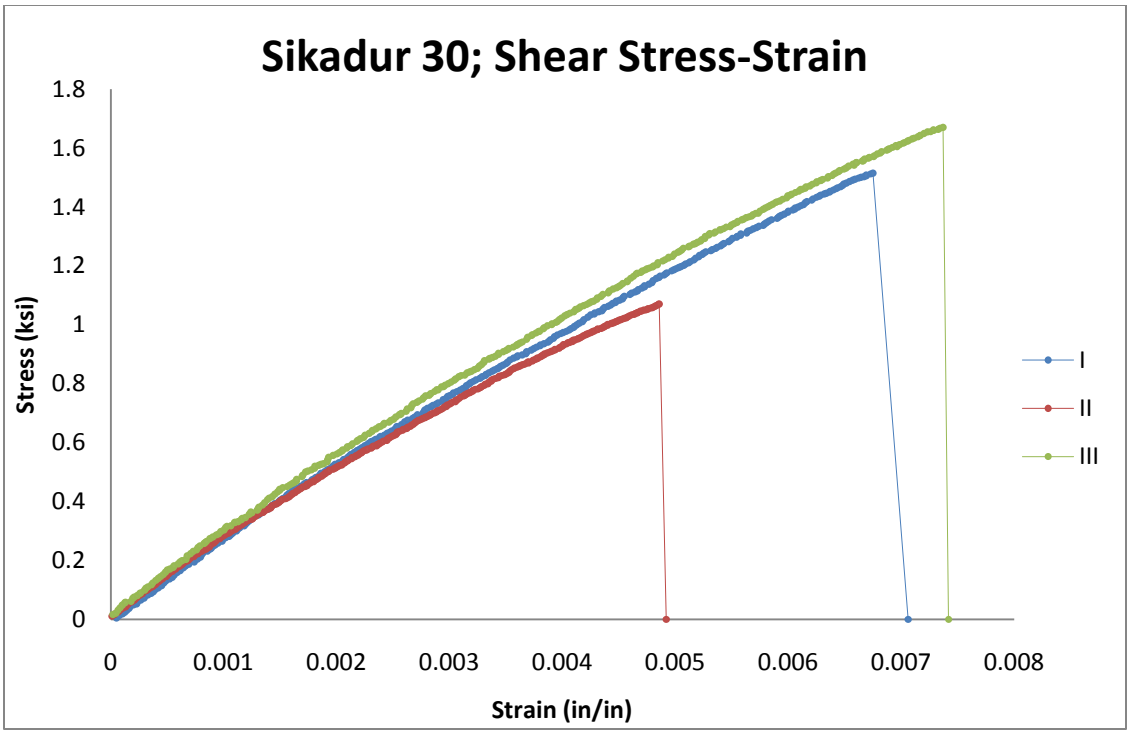

Figure B19. Sikadur 30 shear stress-strain results

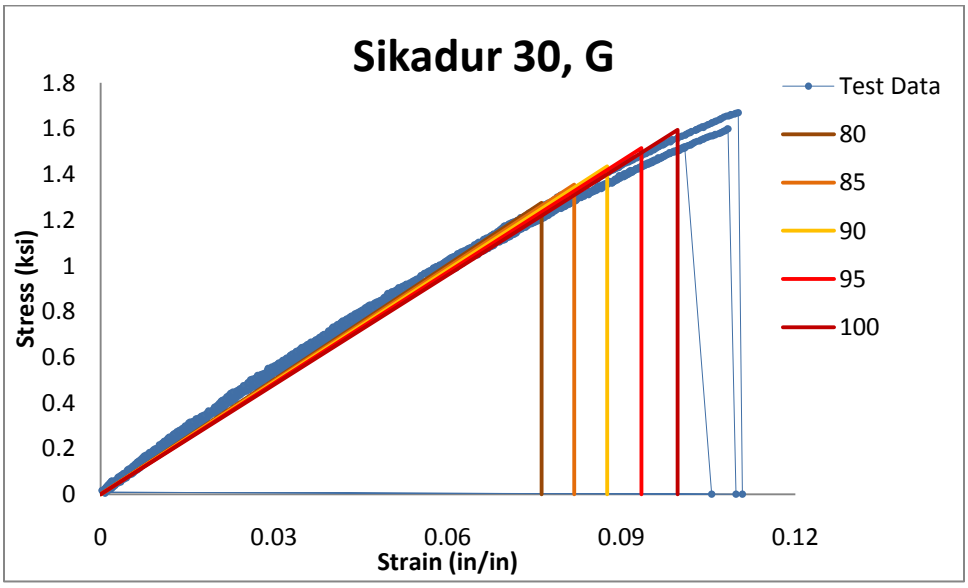

Figure B20. Shear modullus trend lines for Sikadur 30

Table B8. Sikadur 30 shear results from Method A

Method A		
	E	R^2
100%	16.002	0.987
95%	16.221	0.9885
90%	16.401	0.9894
85%	16.575	0.99
80%	16.735	0.9904

Table B9. Sikadur 30 shear results from Method B

Method B					
	Specimen	E	R^2		
100%	1	15.86	0.9923	Ave =	15.988
	2	15.808	0.9862	Std. Dev. =	0.269
	3	16.297	0.9859	Cov =	0.0168
				Ave R^2=	0.988
95%	1	16.029	0.9933	Ave =	16.204
	2	16.047	0.9882	Std. Dev. =	0.288
	3	16.536	0.9877	Cov =	0.0178
				Ave R^2=	0.990
90%	1	16.183	0.994	Ave =	16.388
	2	16.24	0.9893	Std. Dev. =	0.308
	3	16.742	0.9888	Cov =	0.0188
				Ave R^2=	0.991
85%	1	16.305	0.9944	Ave =	16.555
	2	16.424	0.9901	Std. Dev. =	0.335
	3	16.935	0.9896	Cov =	0.0202
				Ave R^2=	0.991
80%	1	16.435	0.9947	Ave =	16.731
	2	16.621	0.9907	Std. Dev. =	0.364
	3	17.138	0.9905	Cov =	0.0218
				Ave R^2=	0.992

Table B10. Sikadur 30 shear capacity

Shear capacity Percentage	τ (ksi)
100	1.418
95	1.348
90	1.277
85	1.206
80	1.135

LTC 4300

Figure B21 shows a specimen of LTC 4300 in the testing apparatus before being loaded. Figures B22 and B23 show specimens after failure. The specimens progressively failed, some remaining intact while not carrying additional load. Again, the cause of failure is the adhesive, as no fibers splintered, yielded, or ruptured. Specimens I and III did not totally separate.

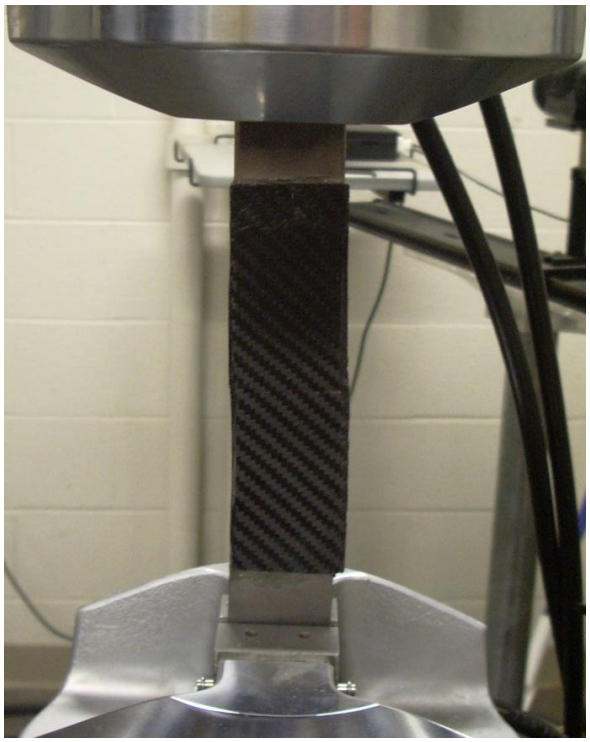

Figure B21. LTC 4300 shear specimen before loading

Figure B22. LTC 4300 shear specimens after failure, side a

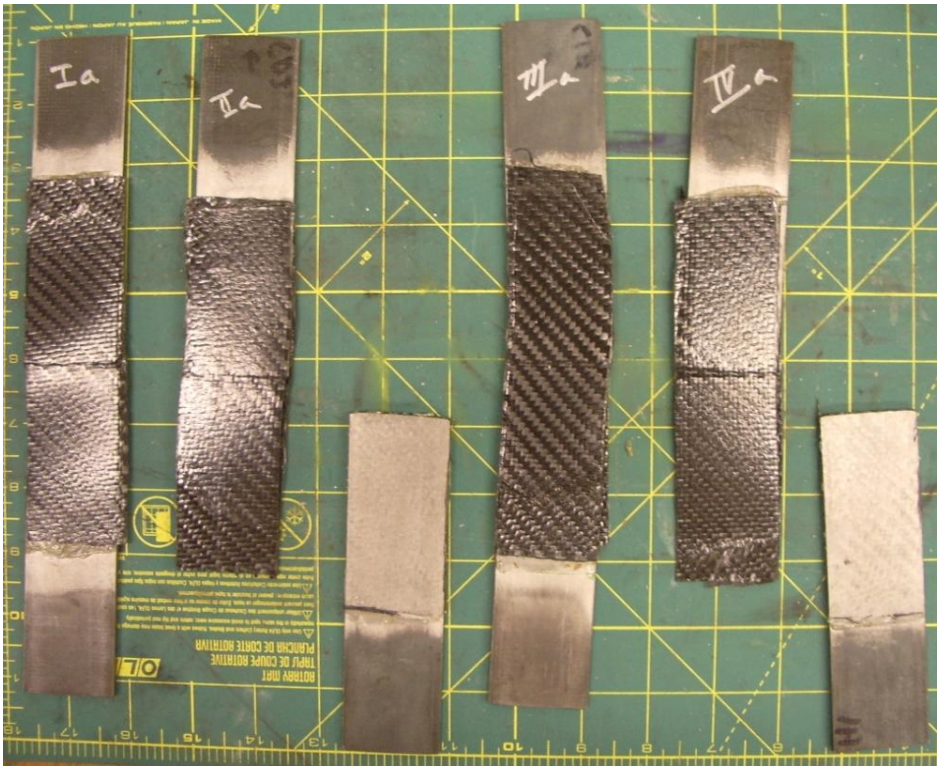

Figure B23. LTC 4300 shear specimen after failure, side b

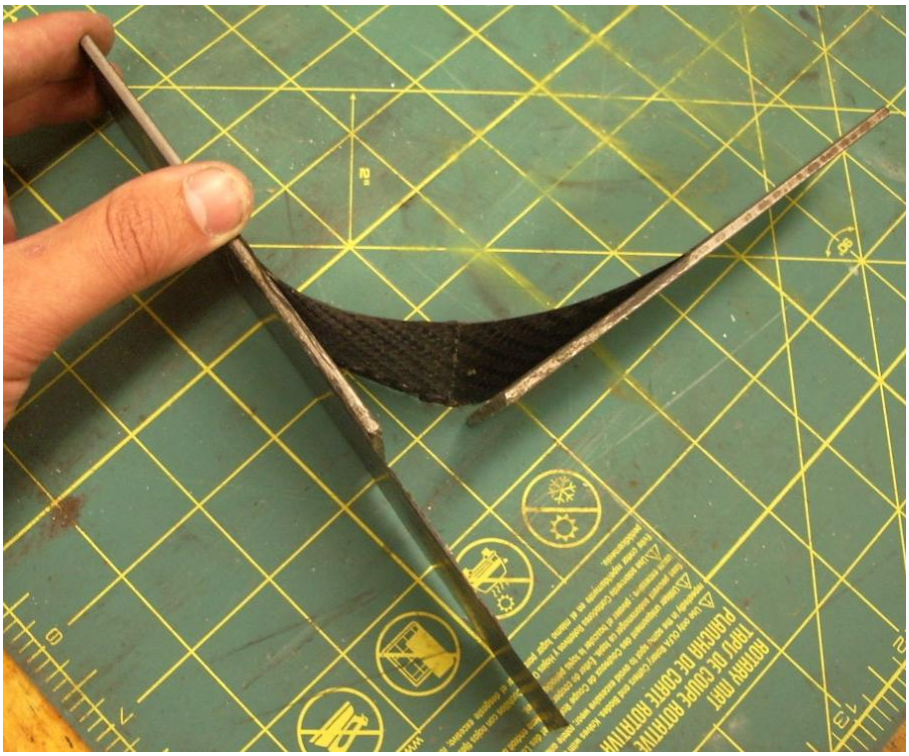

Figure B24. Close up view of specimen I

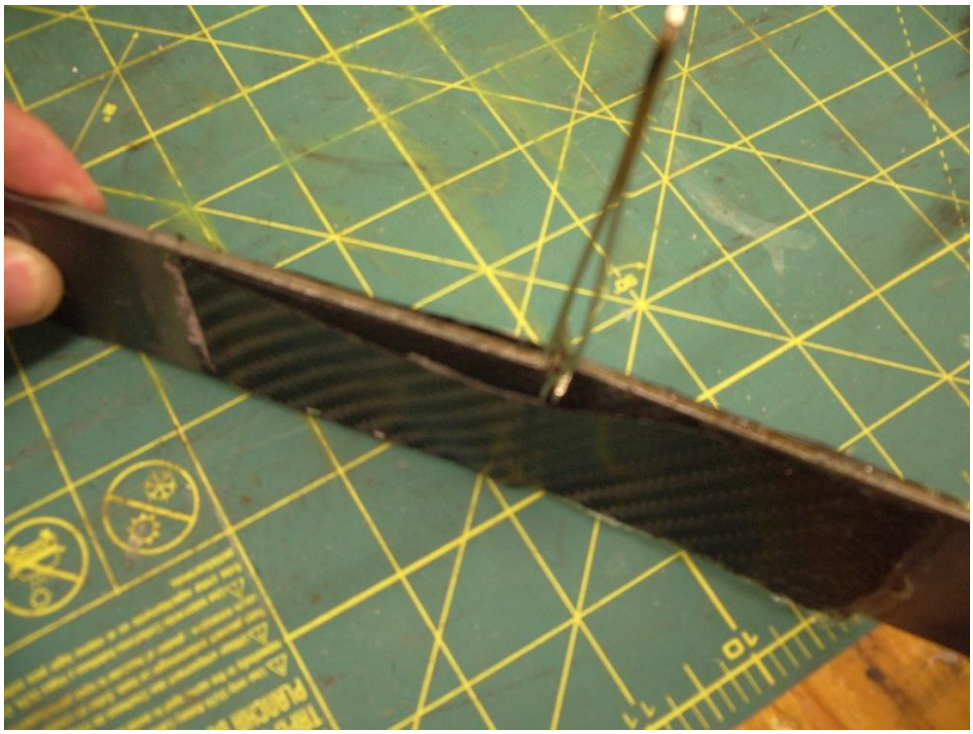

Figure B25. Close up view of specimen III

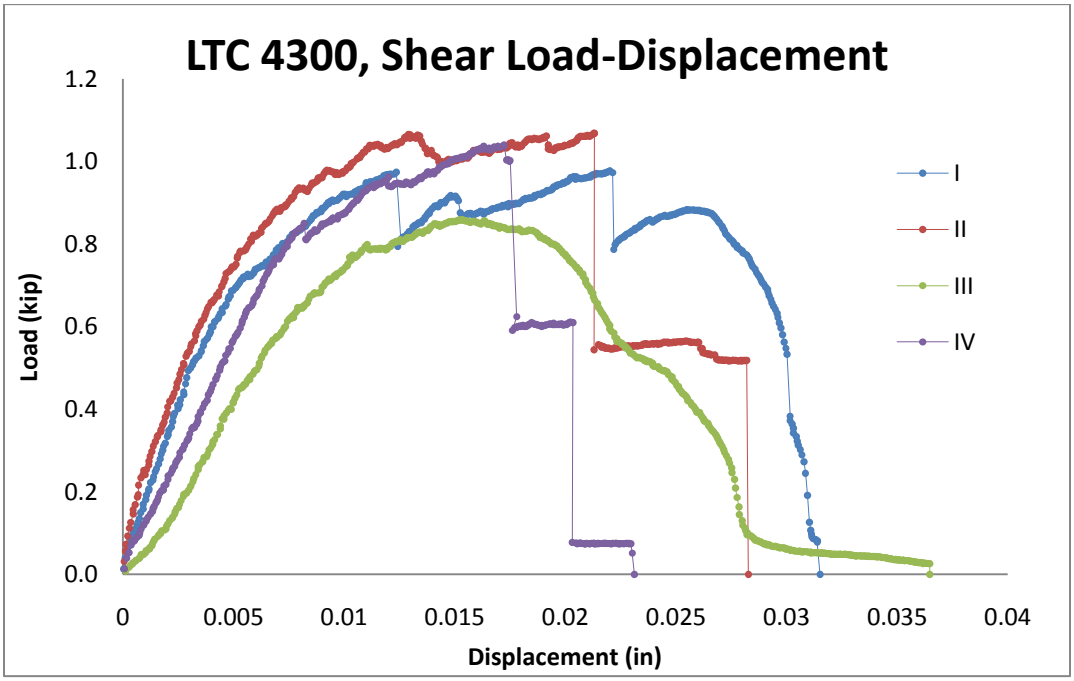

Figure B26. LTC 4300 shear load-displacement results

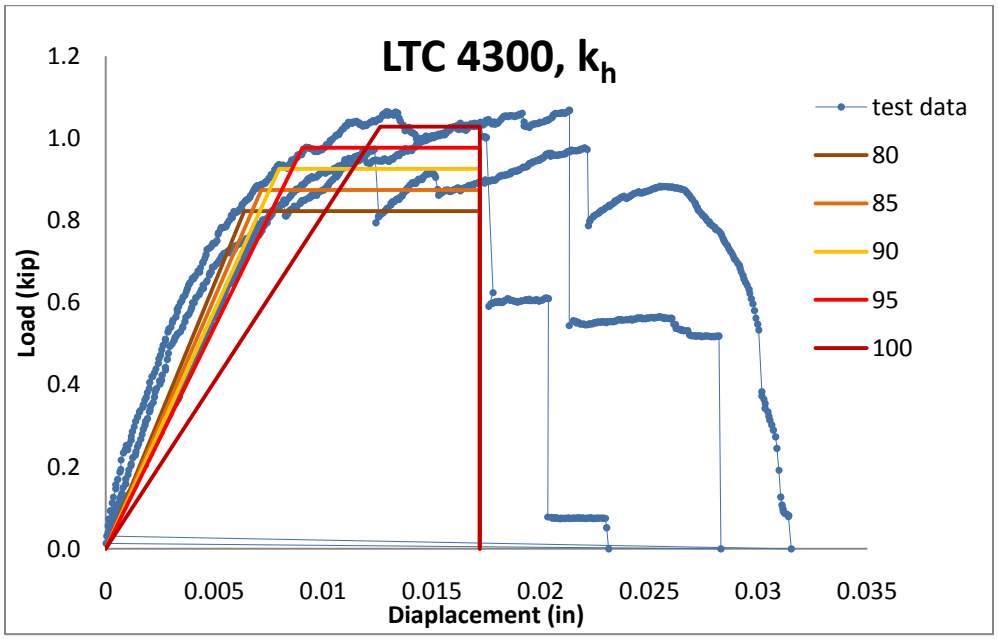

Figure B27. Trendlines of LTC 4300 shear spring constant

Table B11. LTC 4300 shear spring constant results from Method A

Method A		
	k	R^2
100%	5.1702	0.5876
95%	5.7499	0.6734
90%	6.5568	0.7868
85%	6.8424	0.7968
80%	7.3204	0.8335

Table B12. LTC 4300 shear spring constant results from Method B

Method B					
	Specimen	k	R^2		
100%	1	4.5252	0.7616	Ave. =	5.035
	2	6.0531	0.5646	Std. Dev. =	0.882
	3 (exclude)	3.9639	0.9217	Cov =	0.1752
	4	4.5252	0.7616	Ave R^2=	0.696
95%	1	5.0163	0.8434	Ave. =	5.657
	2	6.9394	0.6928	Std. Dev. =	1.110
	3 (exclude)	4.2932	0.9647	Cov =	0.1963
	4	5.0163	0.8434	Ave R^2=	0.793
90%	1	5.743	0.9391	Ave. =	6.426
	2	7.7922	0.7879	Std. Dev. =	1.183
	3 (exclude)	4.5744	0.9877	Cov =	0.1841
	4	5.743	0.9391	Ave R^2=	0.889
85%	1	5.9591	0.9573	Ave. =	6.797
	2	8.4723	0.8363	Std. Dev. =	1.451
	3 (exclude)	4.6454	0.9892	Cov =	0.2135
	4	5.9591	0.9573	Ave R^2=	0.917
80%	1	6.3478	0.9888	Ave. =	7.248
	2	9.0533	0.8659	Std. Dev. =	1.564
	3 (exclude)	4.695	0.9892	Cov =	0.2158
	4	6.3418	0.9888	Ave R^2=	0.948

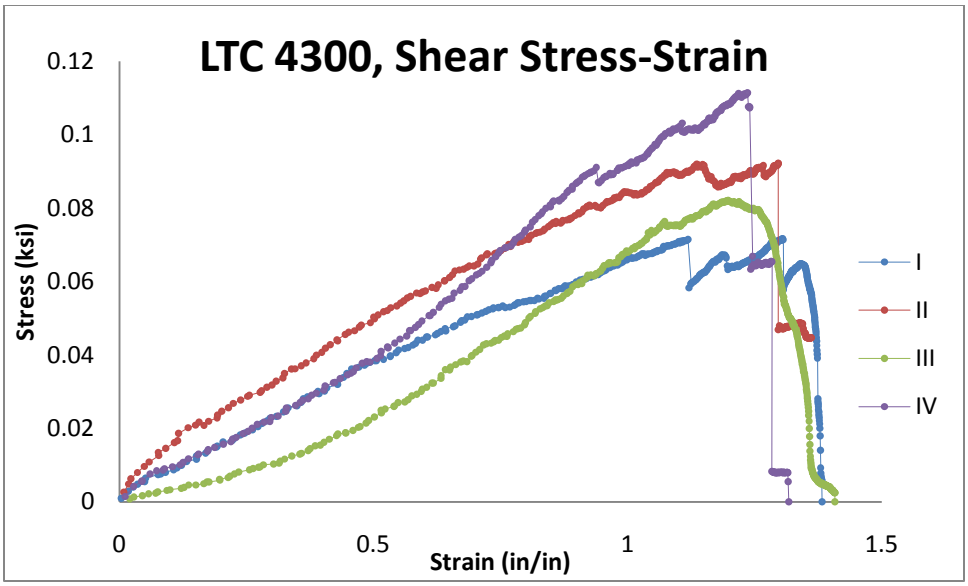

Figure B28. LTC 4300 shear stress-strain results

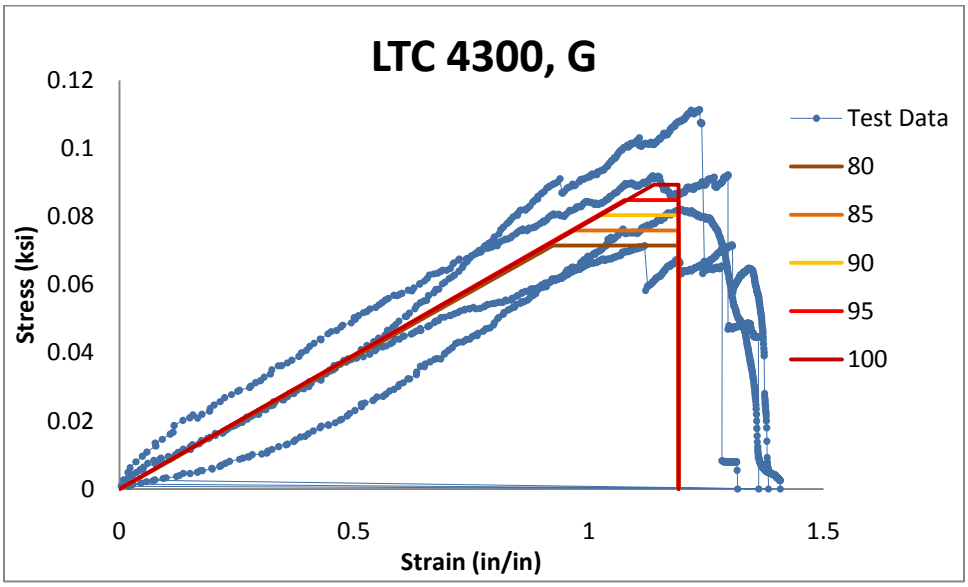

Figure B29. Trendlines for LTC 4300 shear modulus

Table B13. LTC 4300 shear modulus results from Method A

Method A		
	G	R^2
100%	0.0785	0.8666
95%	0.0789	0.8656
90%	0.0786	0.8526
85%	0.0784	0.8439
80%	0.0774	0.8271

Table B14. LTC 4300 shear modulus results from Method B

Method B					
	Specimen	G	R^2		
100%	1	0.067	0.981	Ave. =	0.077
	2	0.0856	0.9571	Std. Dev. =	0.013
	3	0.0661	0.9584	Cov =	0.1639
	4	0.0908	0.9913	Ave R^2=	0.972
95%	1	0.0682	0.9822	Ave. =	0.078
	2	0.088	0.96	Std. Dev. =	0.013
	3	0.065	0.9504	Cov =	0.1706
	4	0.0909	0.9893	Ave R^2=	0.970
90%	1	0.0694	0.9822	Ave. =	0.079
	2	0.0907	0.9655	Std. Dev. =	0.015
	3	0.0629	0.9417	Cov =	0.1851
	4	0.0911	0.9856	Ave R^2=	0.969
85%	1	0.0704	0.9857	Ave. =	0.079
	2	0.0929	0.9668	Std. Dev. =	0.015
	3	0.0617	0.9345	Cov =	0.1945
	4	0.0909	0.9835	Ave R^2=	0.968
80%	1	0.0716	0.9866	Ave. =	0.079
	2	0.0949	0.967	Std. Dev. =	0.016
	3	0.0604	0.937	Cov =	0.2041
	4	0.0906	0.9784	Ave R^2=	0.967

Table B15. Shear capacity of LTC 4300

Shear capacity Percentage	τ (ksi)
100	0.0785
95	0.085
90	0.080
85	0.076
80	0.071

Tensile Testing

Sikadur 330

The tensile properties of the Sikadur 330 are given in a similar order to the shear properties. Figure B30 shows a Sikadur 330/Sikawrap tensile specimen in the loading device of the universal testing machine, followed by the specimens after failure.

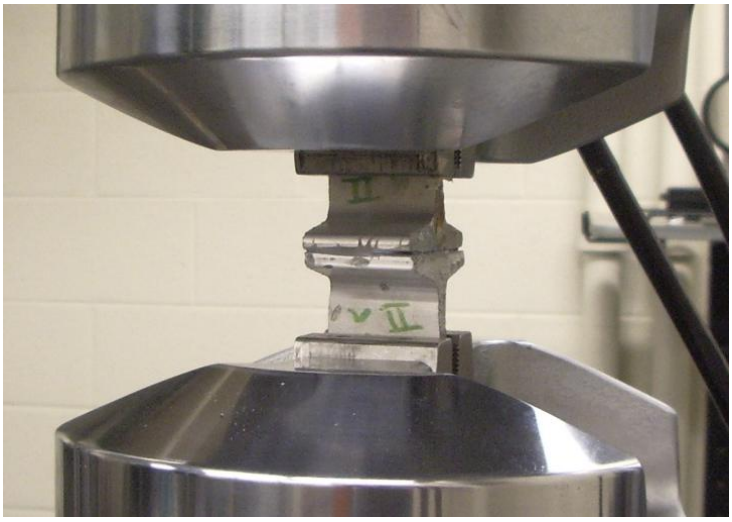

Figure B30. Sikadur 330 tensile specimen before loading

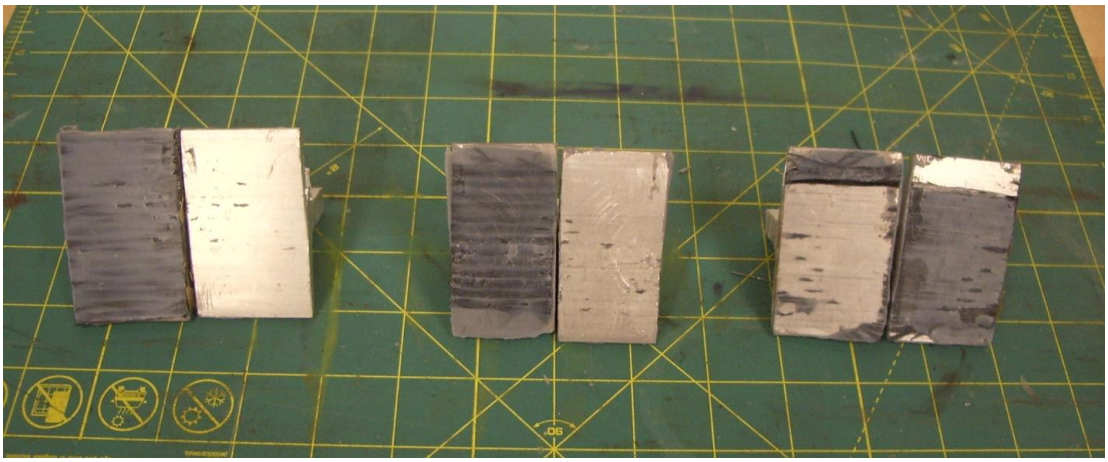

Figure B31. Surfaces of Sikadur 330 tensile specimens after failure

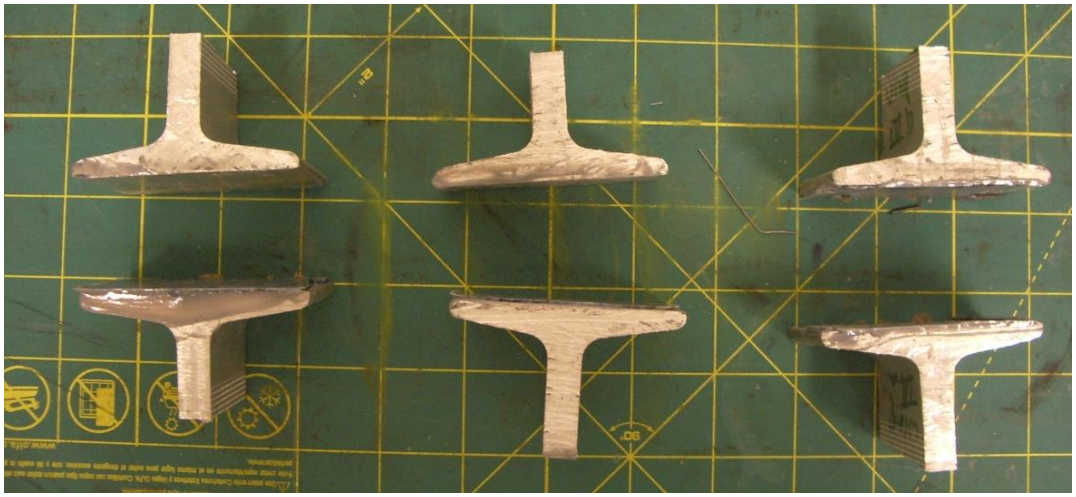

Figure B32. Side profile of Sikadur 330 tensile specimens after failure

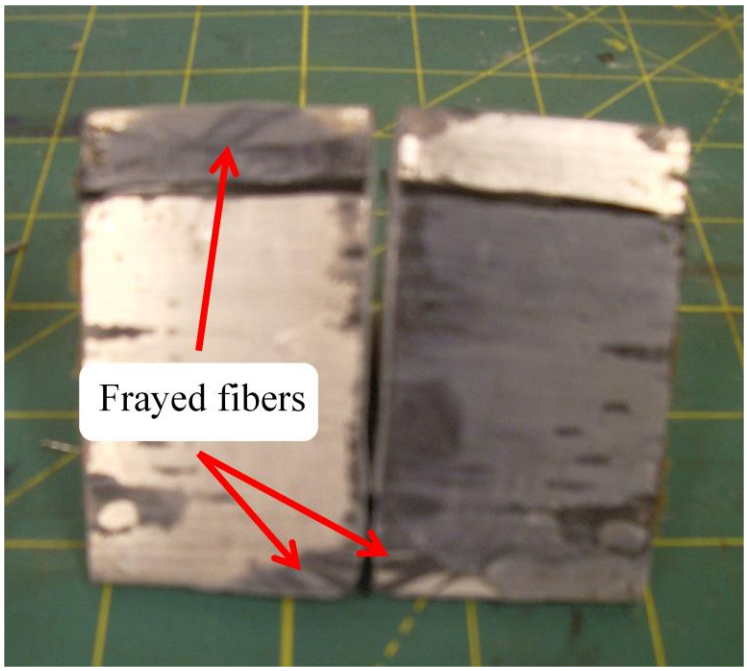

Figure B33. Close up of frayed fibers of Sikadur 330 specimen II

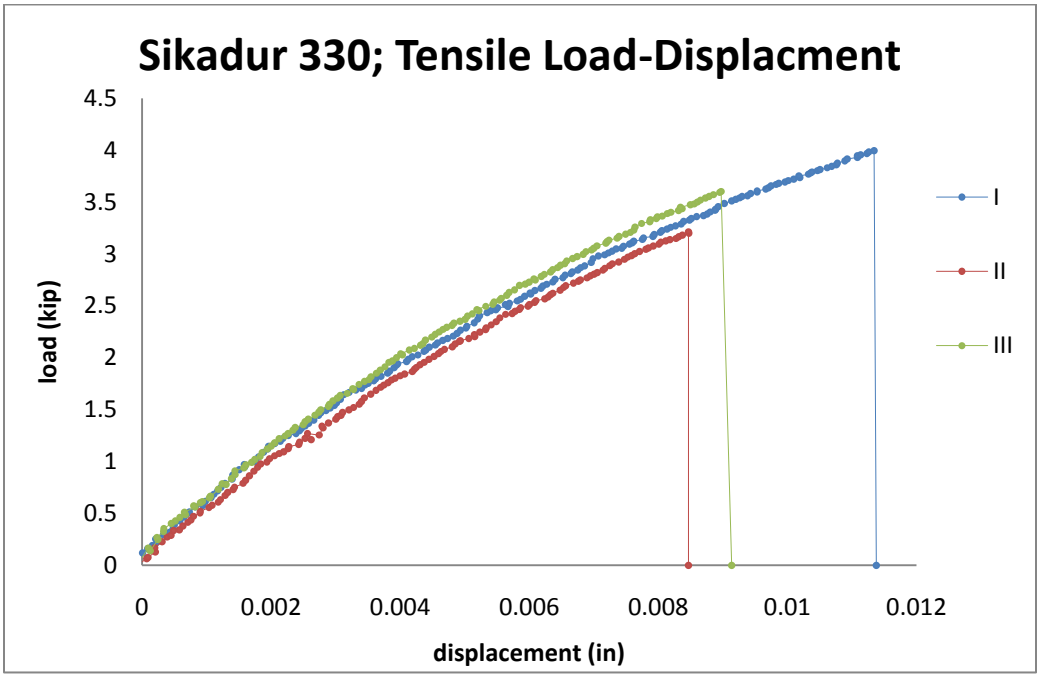

Figure B34. Sikadur 330 tensile load-displacement results

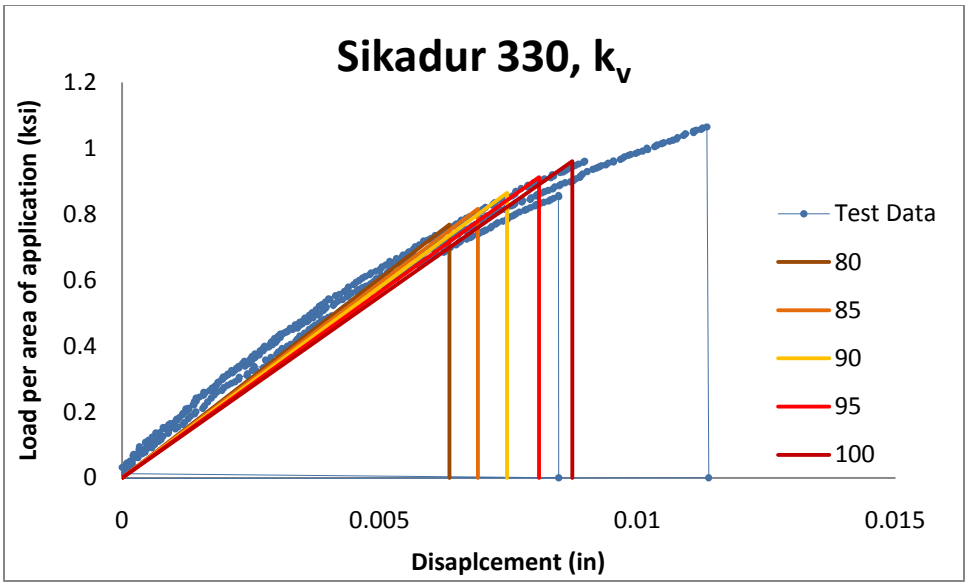

Figure B35. Trendlines for Sikadur 330 tensile spring constant

Table B16. Method A analysis of tensile spring constant for Sikadur 330

Method A	k	R^2
100%	55.035	0.9434
95%	56.46	0.9491
90%	57.97	0.9543
85%	59.175	0.9574
80%	60.53	0.9609

Table B17. Method B analysis of tensile spring constant for Sikadur 330

Method B	Specimen	k	R^2		
100%	1	52.915	0.9379	Ave. =	55.750
	2	55.125	0.9738	Std. Dev. =	3.194
	3	59.21	0.9577	Cov =	0.0573
				Ave R^2=	0.956
95%	1	54.42	0.9422	Ave. =	57.133
	2	56.34	0.9774	Std. Dev. =	3.185
	3	60.64	0.9618	Cov =	0.0557
				Ave R^2=	0.960
90%	1	56.125	0.9499	Ave. =	58.433
	2	57.215	0.9792	Std. Dev. =	3.102
	3	61.96	0.9643	Cov =	0.0531
				Ave R^2=	0.964
85%	1	57.445	0.9532	Ave. =	59.658
	2	58.29	0.9817	Std. Dev. =	3.130
	3	63.24	0.9666	Cov =	0.0525
				Ave R^2=	0.967
80%	1	59.045	0.9577	Ave. =	60.913
	2	59.135	0.9833	Std. Dev. =	3.158
	3	64.56	0.9679	Cov =	0.0519
				Ave R^2=	0.970

Like all the shear specimens, the weakest component of the composite system is the adhesive. Clean separation proves that conclusion. Specimen II shows some type of failure within the fibers. Close inspection showed that several of the fibers frayed at either end of the patch, suggesting poor patch application. Figure B36 shows the location of these frayed fibers. Application error is the most likely cause of the fraying, and is a sign of an inferior application of the carbon fibers. This specimen shows that great care

must be taken applying FRP patches in order to prevent premature fiber failure. Unlike its shear counterpart tests, the Sikadur 330 tensile tests demonstrated an abrupt failure mode.

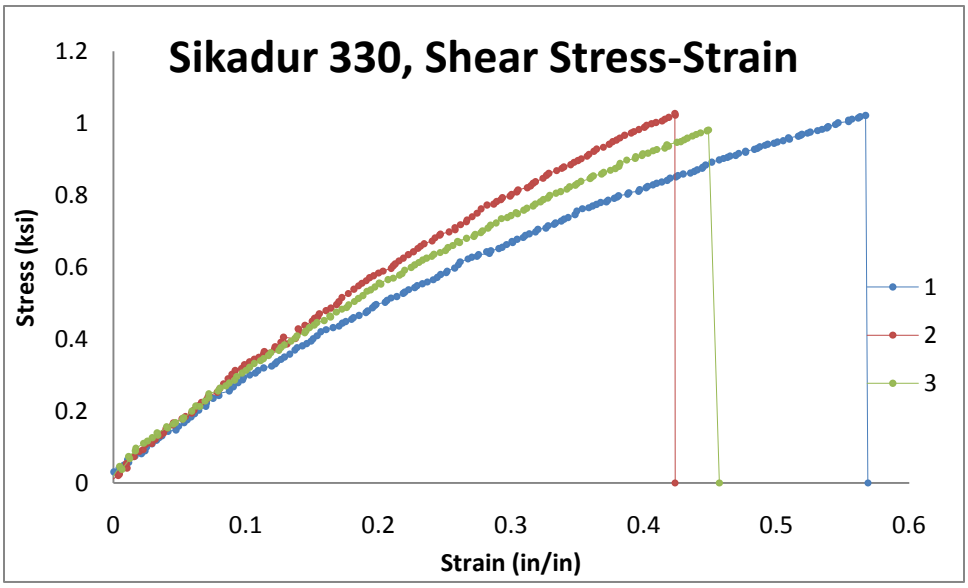

Figure B36. Sikadur 330 tensile stress-strain results

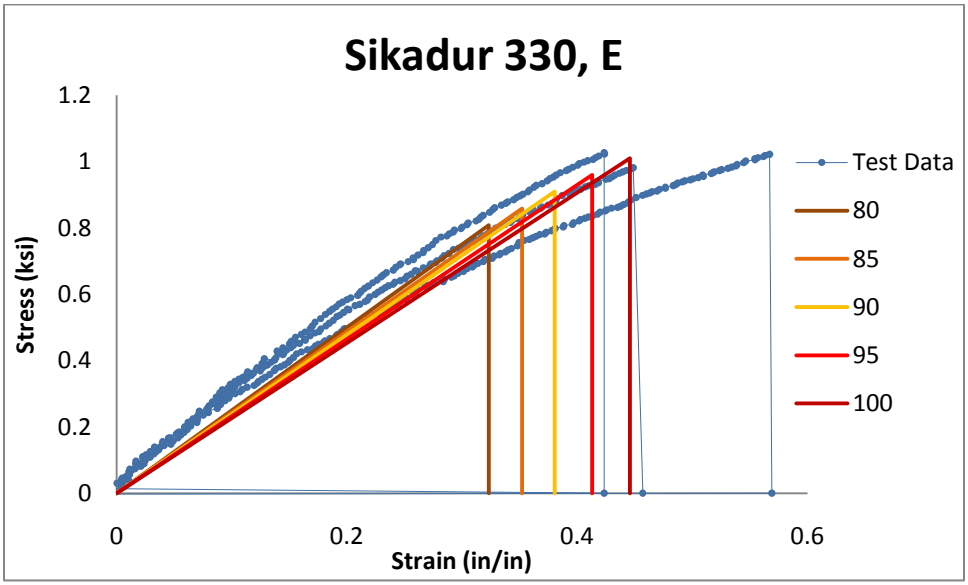

Figure B37. Trend lines for tenisle modulus for Sikadur 330

Table B18. Sikadur 330 tensile results from Method A

Method A		
	E	R^2
100%	0.7694	0.9658
95%	0.7895	0.97
90%	0.806	0.9731
85%	0.8234	0.9759
80%	0.843	0.9782

Table B19. Sikadur 330 tensile results from Method B

Method B					
	Specimen	E	R^2		
100%	1	0.8853	0.9787	Ave. =	0.821
	2	0.7572	0.9563	Std. Dev. =	0.064
	3	0.8214	0.9927	Cov =	0.0780
				Ave R^2=	0.976
95%	1	0.9	0.9811	Ave. =	0.836
	2	0.7779	0.9618	Std. Dev. =	0.061
	3	0.829	0.9936	Cov =	0.0734
				Ave R^2=	0.979
90%	1	0.9149	0.9829	Ave. =	0.849
	2	0.795	0.9656	Std. Dev. =	0.061
	3	0.8367	0.9944	Cov =	0.0717
				Ave R^2=	0.981
85%	1	0.9269	0.9839	Ave. =	0.861
	2	0.813	0.9692	Std. Dev. =	0.059
	3	0.8443	0.995	Cov =	0.0683
				Ave R^2=	0.983
80%	1	0.9397	0.9852	Ave. =	0.875
	2	0.8333	0.9721	Std. Dev. =	0.057
	3	0.8511	0.9951	Cov =	0.0652
				Ave R^2=	0.984

Table B20. Sikadur 330 tensile stress capacity

Tensile Capacity Percentage	σ(ksi)
100%	1.01007
95%	0.95957
90%	0.90906
85%	0.85856
80%	0.80806

Sikadur 30

Figure B38 shows a Sikadur 30/Carbodur tensile specimen in the loading device. Load displacement results are displayed in Figure B41. Figures of the failed specimens follow.

Figure B38. Sikadur 30 tensile specimen before loading

Figure B39. Surface of Sikadur 30 tensile specimens after failure

Figure B40. Profile of Sikadur 30 tensile specimens after failure

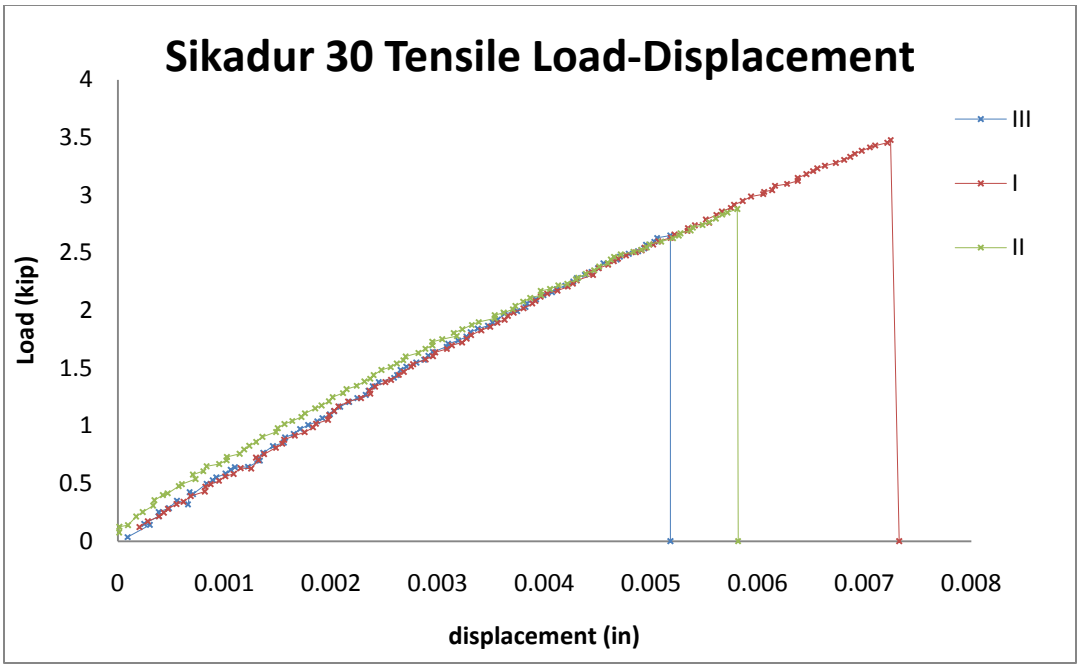

Figure B41. Sikadur 30 tensile load-displacement results

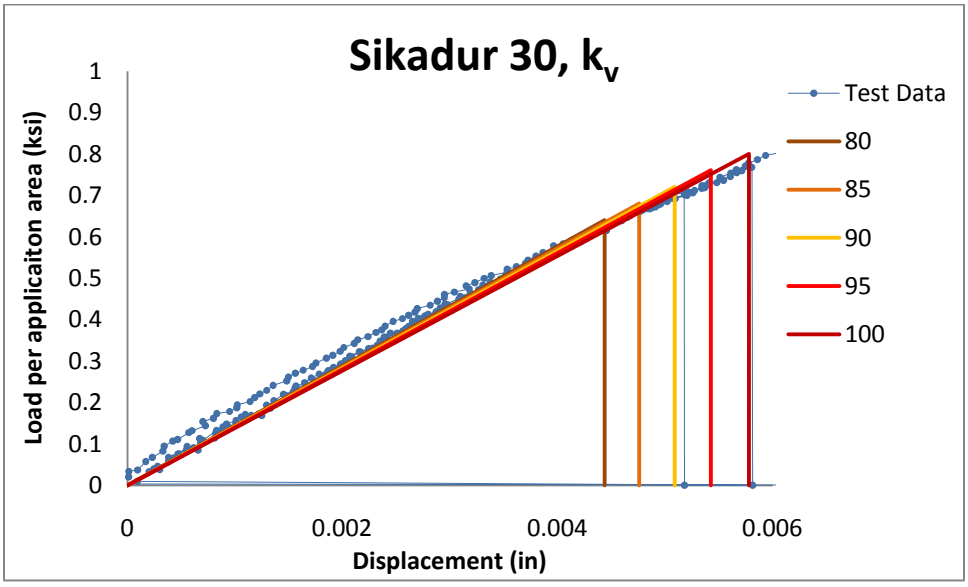

Figure B42. Trend lines for Sikadur 30 tensile spring constant

Table B21. Method A analysis of tensile spring constant for Sikadur 30

Method A		
	k	R^2
100%	63.295	0.9848
95%	70.135	0.9855
90%	70.81	0.9857
85%	71.535	0.9856
80%	72.18	0.9849

Table B22. Method B analysis of tensile spring constant for Sikadur 30

Method B					
	Specimen	k	R^2		
100%	1	67.585	0.9923	Ave. =	71.693
	2	71.26	0.9724	Std. Dev. =	4.341
	3	76.235	0.996	Cov =	0.0606
				Ave R^2=	0.987
95%	1	68.41	0.9934	Ave. =	70.873
	2	72.36	0.972	Std. Dev. =	2.148
	3	71.85	0.9968	Cov =	0.0303
				Ave R^2=	0.987
90%	1	68.59	0.9945	Ave. =	71.480
	2	73.63	0.9743	Std. Dev. =	2.600
	3	72.22	0.997	Cov =	0.0364
				Ave R^2=	0.989
85%	1	69.545	0.9954	Ave. =	72.795
	2	74.756	0.9739	Std. Dev. =	2.835
	3	74.085	0.9972	Cov =	0.0389
				Ave R^2=	0.989
80%	1	70.06	0.9959	Ave. =	72.997
	2	75.84	0.9734	Std. Dev. =	2.891
	3	73.09	0.9975	Cov =	0.0396
				Ave R^2=	0.989

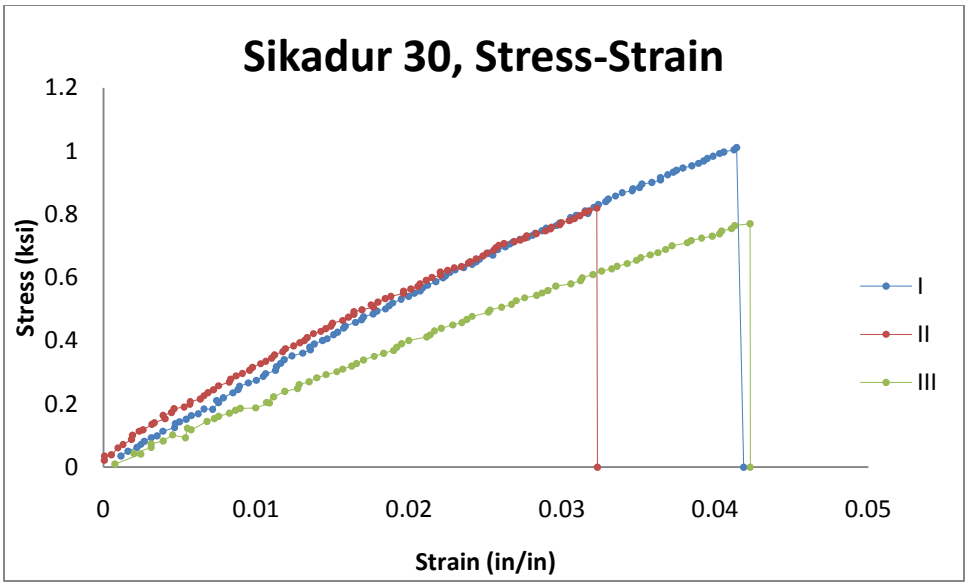

Figure B43. Sikadur 30 tensile stress-strain results

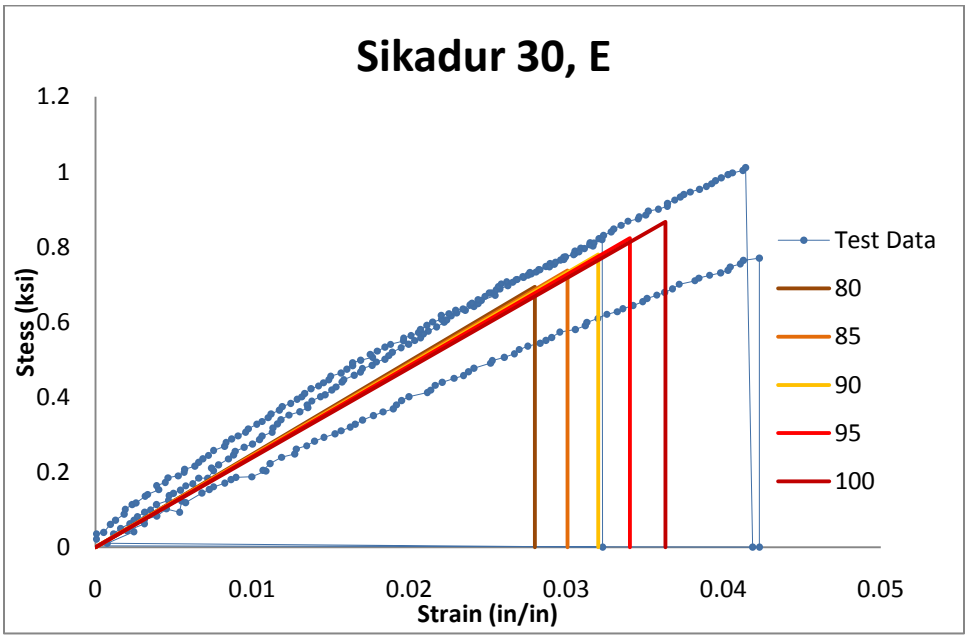

Figure B44. Trend lines for Sikadur 30 tensile modulus

Table B23. Results from Method A application to Sikadur 30 tensile data

Method A		
	E	R^2
100%	23.886	0.8949
95%	24.201	0.8944
90%	24.378	0.891
85%	24.524	0.8852
80%	24.798	0.8848

Table B24. Results from Method B application to Sikadur 30 tensile data

Method B					
	Specimen	E	R^2		
100%	1	25.786	0.9923	Ave. =	24.058
	2	27.369	0.9724	Std. Dev. =	4.435
	3	19.02	0.996	Cov =	0.1843
				Ave R^2=	0.987
95%	1	26.082	0.9938	Ave. =	24.354
	2	27.789	0.973	Std. Dev. =	4.553
	3	19.19	0.9968	Cov =	0.1869
				Ave R^2=	0.988
90%	1	26.288	0.9945	Ave. =	24.615
	2	28.27	9743	Std. Dev. =	4.719
	3	19.288	0.997	Cov =	0.1917
				Ave R^2=	3248.331
85%	1	26.535	0.9954	Ave. =	24.878
	2	28.712	0.9739	Std. Dev. =	4.879
	3	19.386	0.9972	Cov =	0.1961
				Ave R^2=	0.989
80%	1	26.731	0.9959	Ave. =	25.127
	2	29.128	0.9734	Std. Dev. =	5.000
	3	19.521	0.9975	Cov =	0.1990
				Ave R^2=	0.989

Table B25. Sikadur 30 tensile stress capacity

Tensile Capacity Percentage	σ(ksi)
100%	0.86702
95%	0.82366
90%	0.78031
85%	0.73696
80%	0.69361

LTC 4300

Figure B45, illustrates a LTC tensile specimen in the universal testing machine before applying load. Figures B46 and B47 show the specimens after failure.

Figure B45. LTC 4300 adhesive tensile specimen before loading

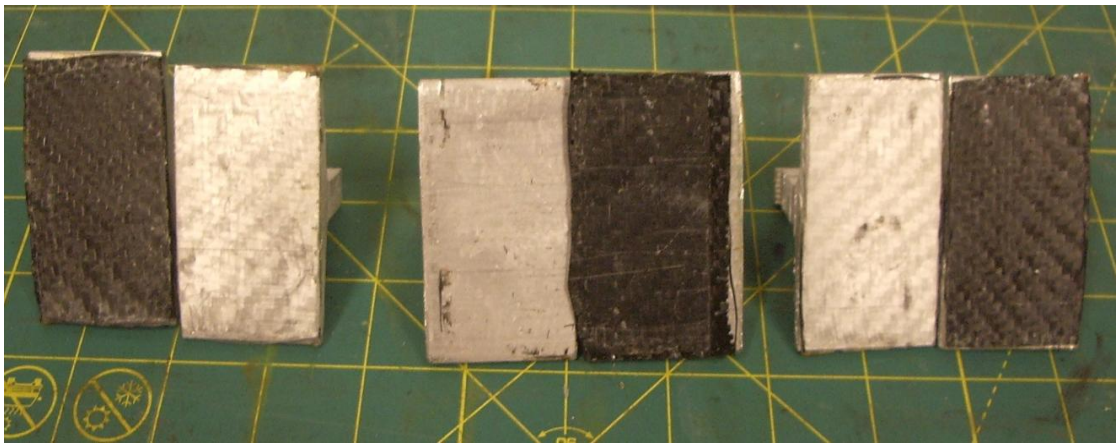

Figure B46. Surface of LTC 4300 tensile specimens after failure

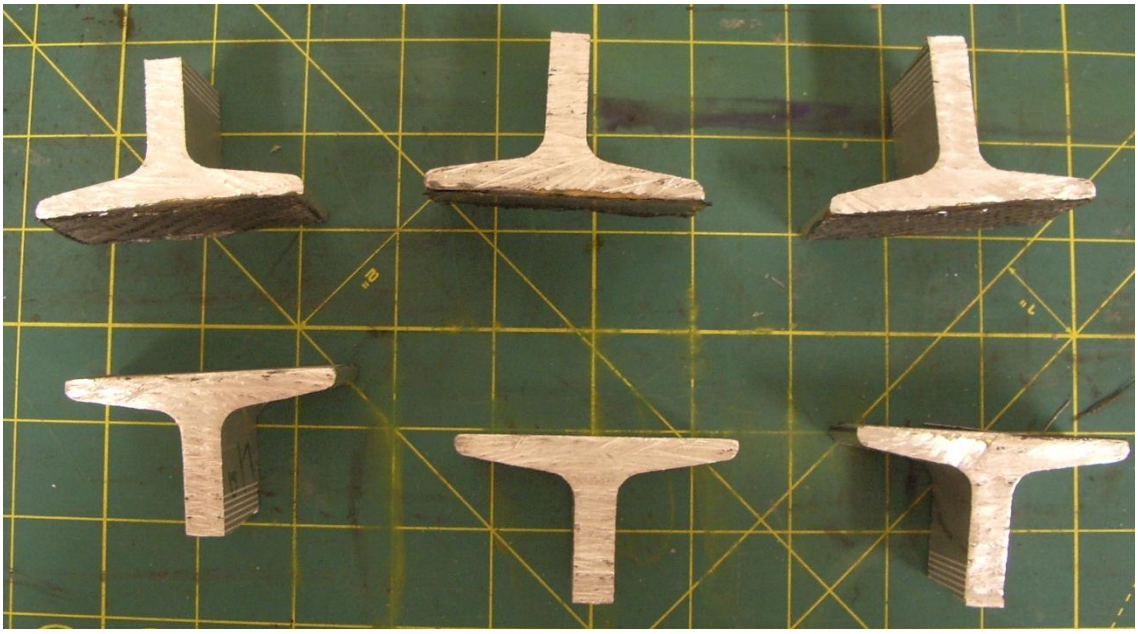

Figure B47. Profile of LTC 4300 tensile specimens after failure

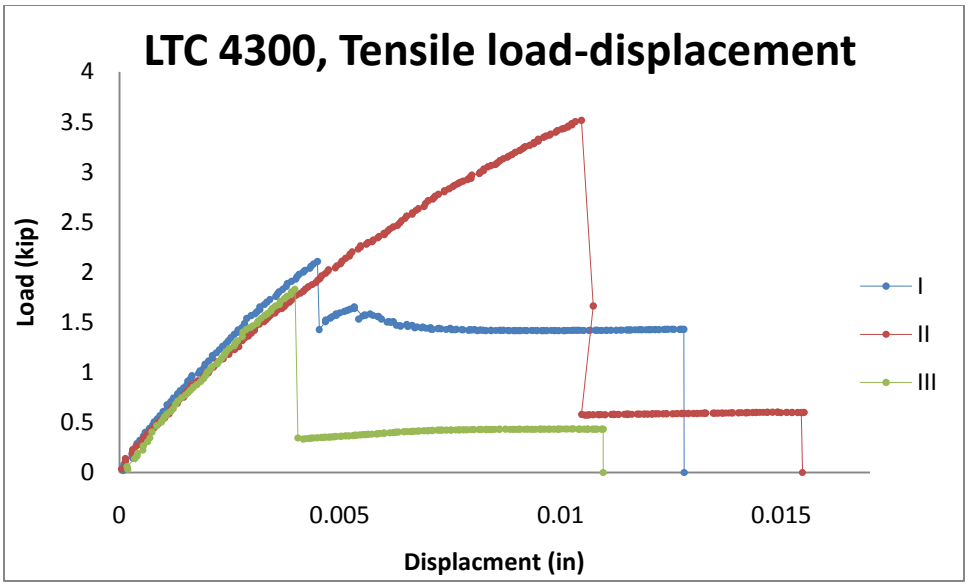

Figure B48. LTC 4300 tensile load-displacement results

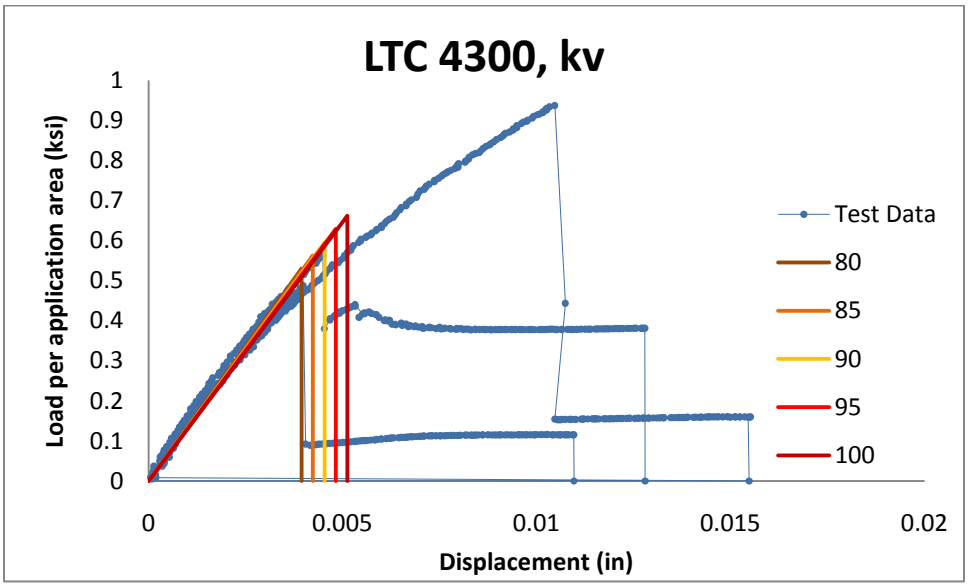

Figure B49. Trend lines for LTC 4300 tensile spring constant

Table B26. LTC 4300 tensile spring constant results from Method A

Method A		
	k	R^2
100%	64.67	0.9762
95%	65.235	0.9754
90%	65.765	0.9744
85%	66.525	0.9748
80%	67.19	0.9748

Table B27. LTC 4300 tensile spring constant results from Method B

Method B					
	Specimen	k	R^2		
100%	1	67.675	0.9787	Ave. =	64.082
	2	61.79	0.9815	Std. Dev. =	3.151
	3	62.78	0.9944	Cov =	0.0492
				Ave R^2=	0.985
95%	1	68.795	0.9814	Ave. =	66.023
	2	125.54/2	0.9822	Std. Dev. =	3.921
	3	63.25	0.9917	Cov =	0.0594
				Ave R^2=	0.985
90%	1	69.94	0.9829	Ave. =	65.758
	2	63.63	0.9833	Std. Dev. =	3.622
	3	63.705	0.9948	Cov =	0.0551
				Ave R^2=	0.987
85%	1	70.86	0.9839	Ave. =	66.485
	2	64.475	0.9838	Std. Dev. =	3.793
	3	64.12	0.9946	Cov =	0.0571
				Ave R^2=	0.987
80%	1	71.67	0.9852	Ave. =	67.112
	2	65.29	0.9873	Std. Dev. =	3.974
	3	64.375	0.994	Cov =	0.0592
				Ave R^2=	0.989

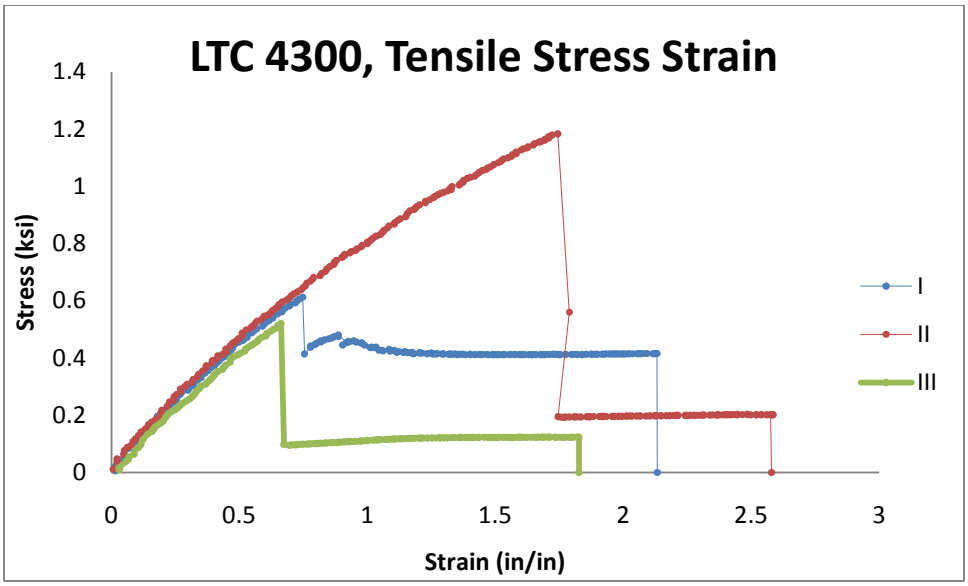

Figure B50. LTC 4300 tensile stress-strain results

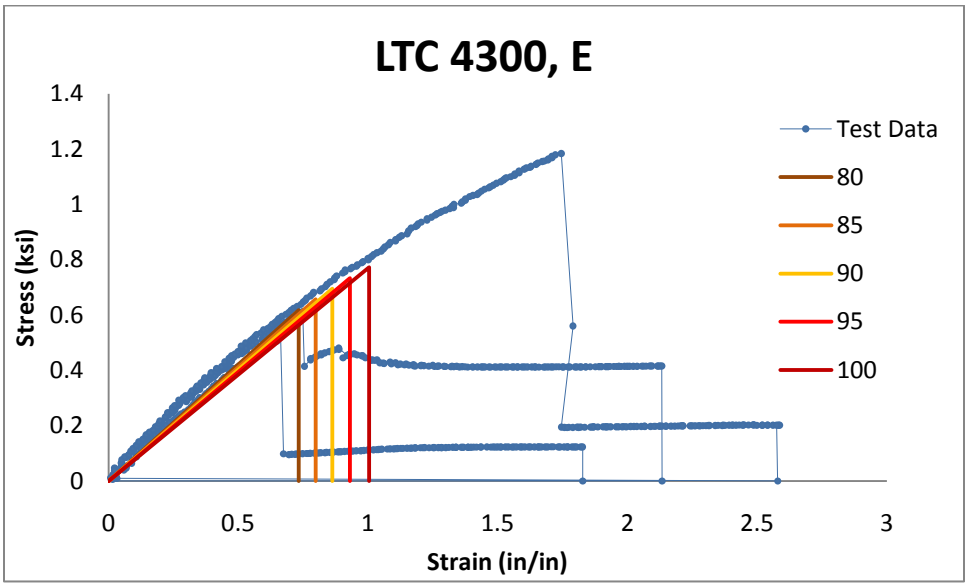

Figure B51. Trend lines for tensile modulus of LTC 4300

Table B28. LTC 4300 tensile modulus results from Method A

Method A		
	E	R^2
100%	0.7694	0.9658
95%	0.7895	0.97
90%	0.806	0.9731
85%	0.8234	0.9759
80%	0.843	0.9782

Table B29. LTC 4300 tensile modulus results from Method B

Method B					
	Specimen	E	R^2		
100%	1	0.8853	0.9787	Ave. =	0.821
	2	0.7572	0.9563	Std. Dev. =	0.064
	3	0.8214	0.9927	Cov =	0.0780
				Ave R^2=	0.976
95%	1	0.9	0.9811	Ave. =	0.836
	2	0.7779	0.9618	Std. Dev. =	0.061
	3	0.829	0.9936	Cov =	0.0734
				Ave R^2=	0.979
90%	1	0.9149	0.9829	Ave. =	0.849
	2	0.795	0.9656	Std. Dev. =	0.061
	3	0.8367	0.9944	Cov =	0.0717
				Ave R^2=	0.981
85%	1	0.9269	0.9839	Ave. =	0.861
	2	0.813	0.9692	Std. Dev. =	0.059
	3	0.8443	0.995	Cov =	0.0683
				Ave R^2=	0.983
80%	1	0.9397	0.9852	Ave. =	0.875
	2	0.8333	0.9721	Std. Dev. =	0.057
	3	0.8511	0.9951	Cov =	0.0652
				Ave R^2=	0.984

Table B30. LTC 4300 tensile stress capacity

Tensile Capacity Percentage	σ(ksi)
100%	1.0037
95%	0.9293
90%	0.8624
85%	0.7972
80%	0.7329

Conclusion of Adhesive Mechanical Properties

Given the above analysis, the magnitude of each parameter was chosen. Ignoring progressive failures and assuming the adhesive behaves in a linear brittle manner is a conservative. Utilizing first failures, even when small, as the failure of the adhesive adds conservatism also to results obtained from methods A and B. Given these considerations, each parameters value was chosen as the magnitude corresponding to 90 percent as described above. This ten percent reduction in capacity and stiffness will yield additional conservatism to the mechanical model. When exploring new frontiers, it is wise to err on the side of conservatism. Table B14 provides all the values used in this research.

In addition to the statistical parameters above, residual analysis of the data was performed. The purpose of residual analysis is to provide a clear image of how well the line trend line fits the data. An excellent trend line not only has an R^2 near 1, but also has a well defined scatter of error. Residual analysis examines the distribution of error between the true data value and the value predicted by the line of best fit. This error should appear as a scatter plot with values near zero along the length of the independent

variable. Figure B52 shows the results of residual analysis performed on an adhesive tensile test of Sikadur 30. This figure is typical of all the specimen groups.

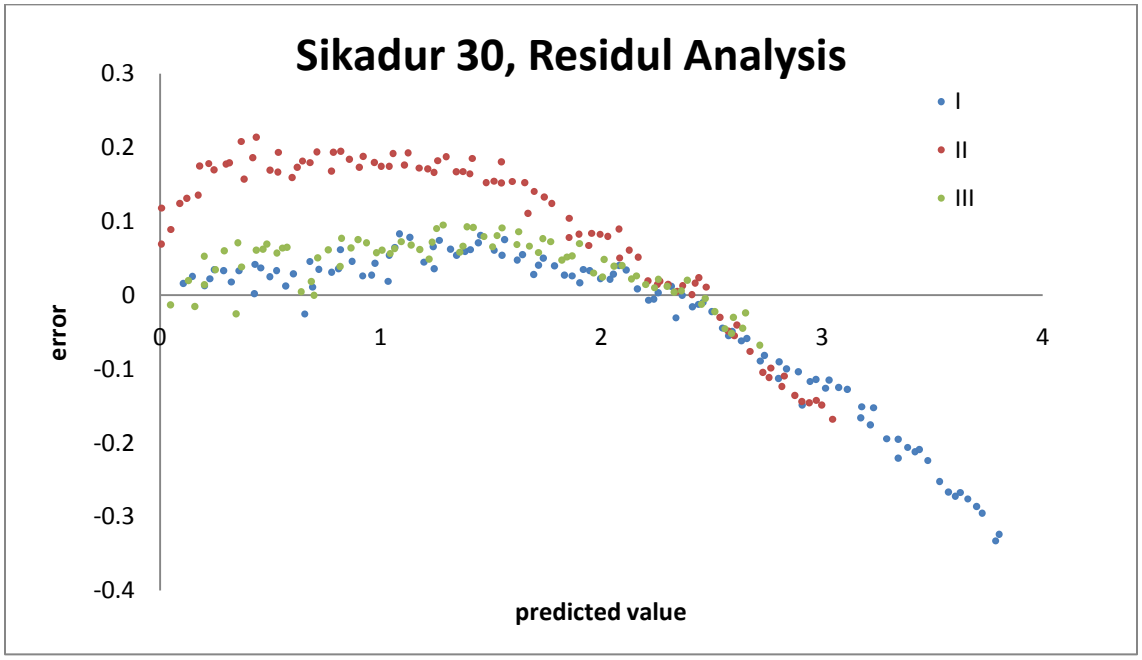

Figure B52. Typical residual analysis for adhesive testing

It is obvious that the points of the graph are not evenly distributed. Instead, a clear pattern emerges. This pattern indicates that a linear trend line is not the optimal choice for modeling the data. Further investigation found that a second degree polynomial modeled the data more closely. However, for the purposes of this research, the linear assumption provides suitable results. Moreover, linear-brittle and linearly elastic-perfectly-plastic assumptions are utilized in modern design practice.

APPENDIX C

CRACK PROPIGATION OF CONCRETE BEAMS

Phase II Testing

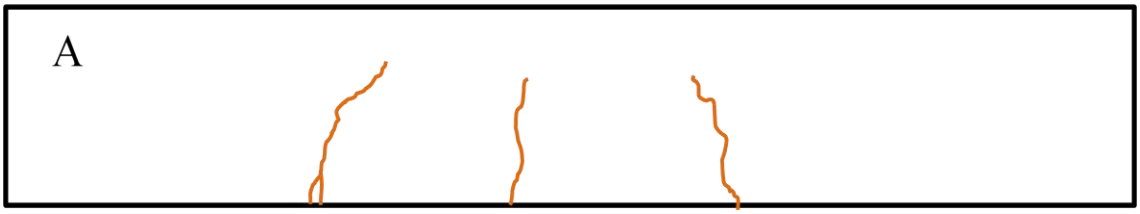

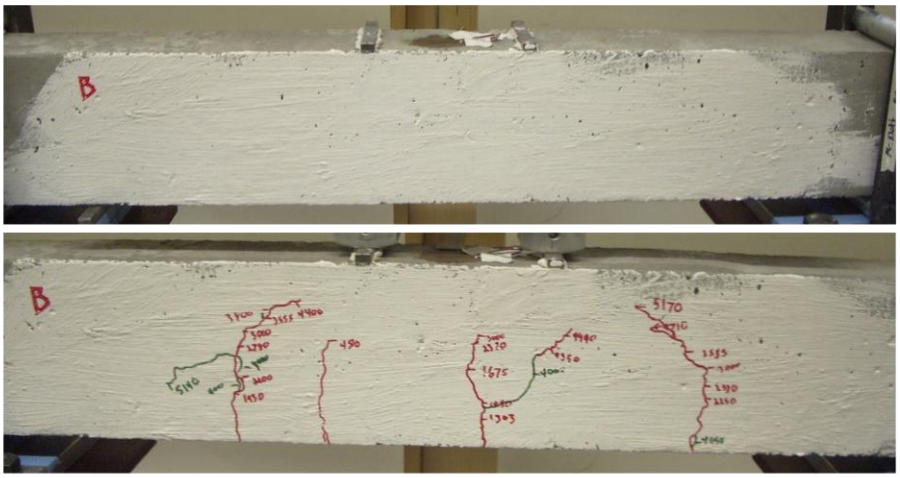

B

C

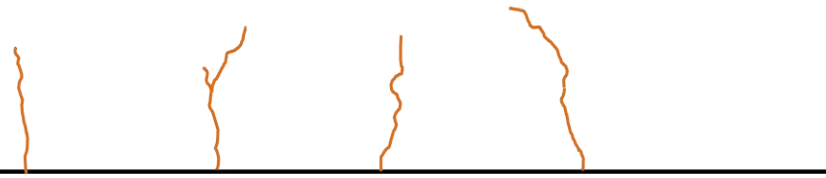

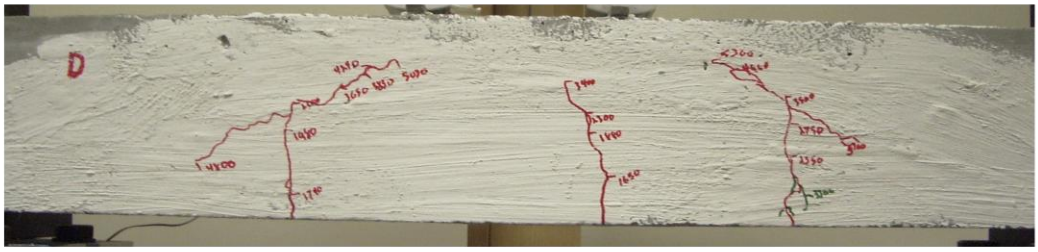

D

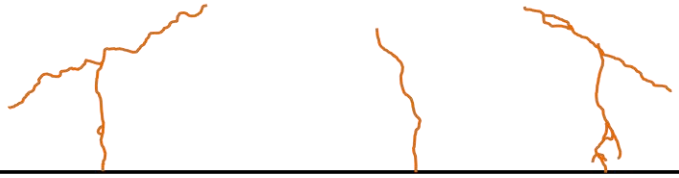

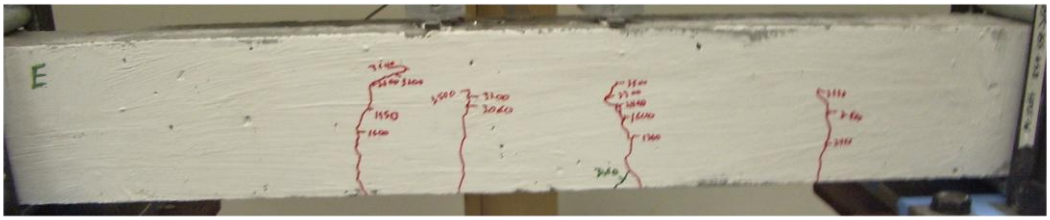

E

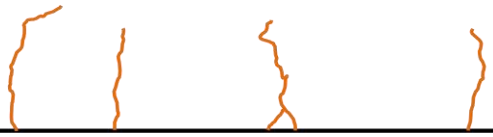

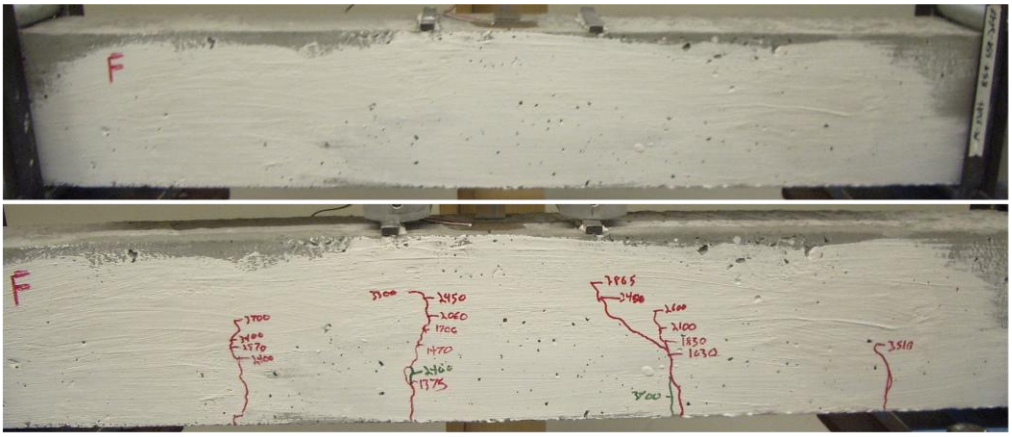
F
F

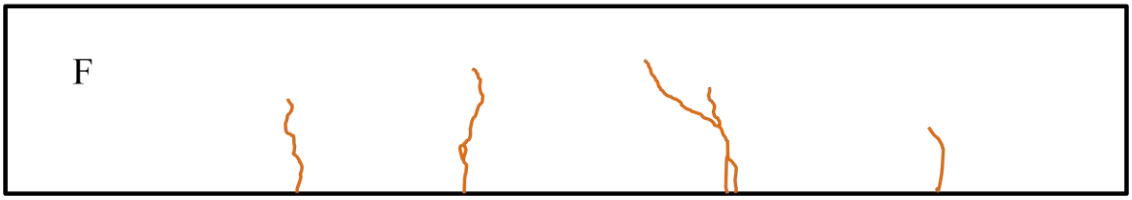
F


G
G


G

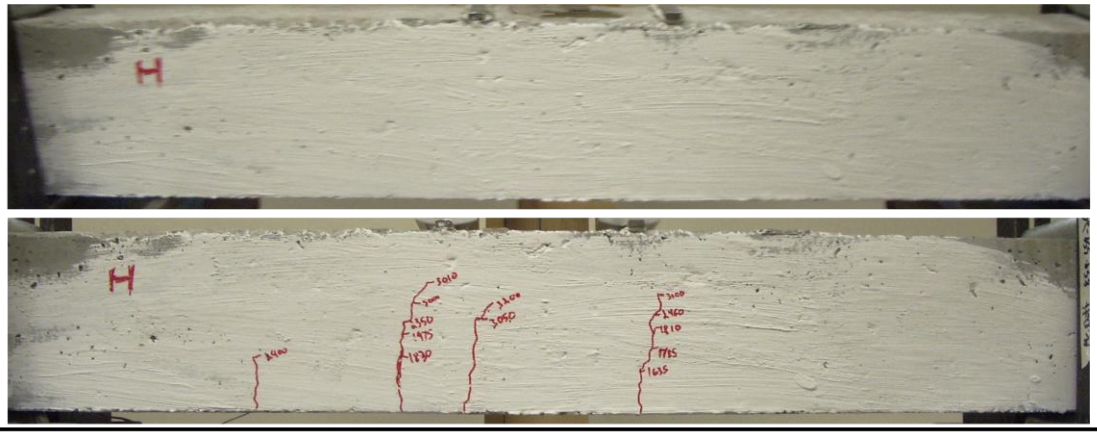
H
H


H

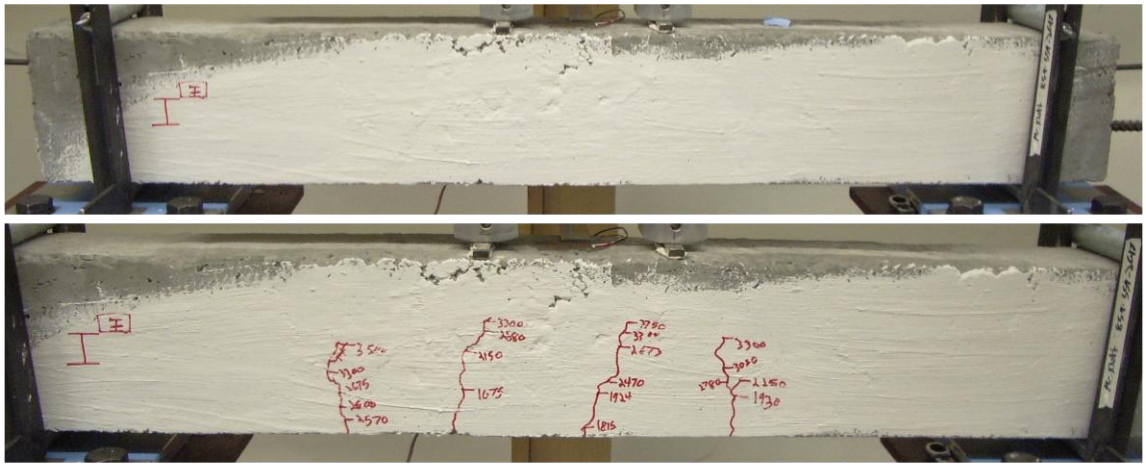

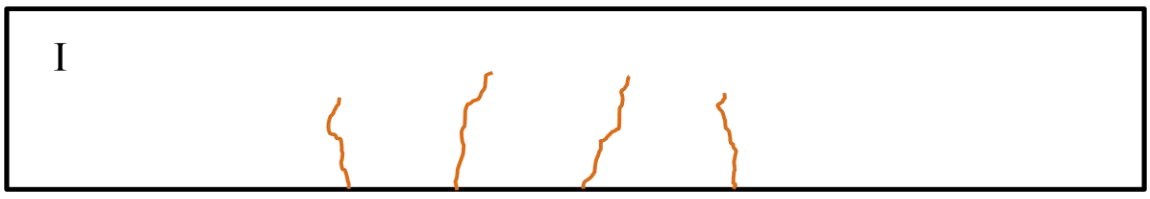
I

1


3


4

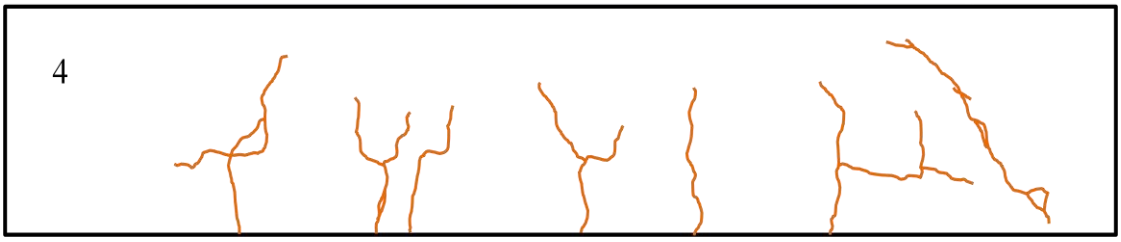
4


5

5

5

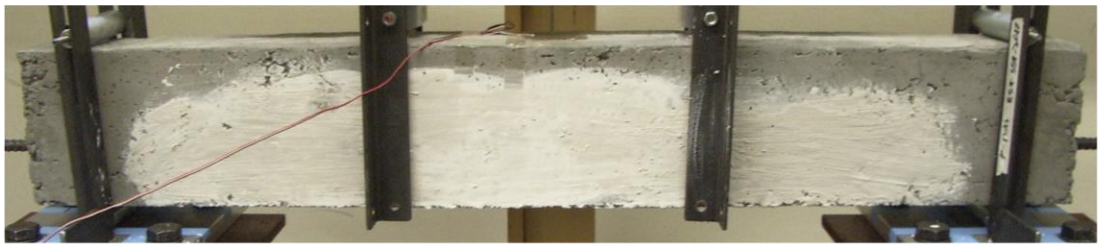

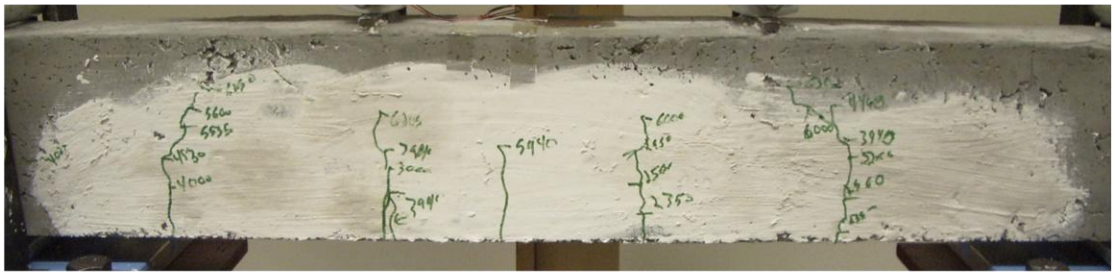

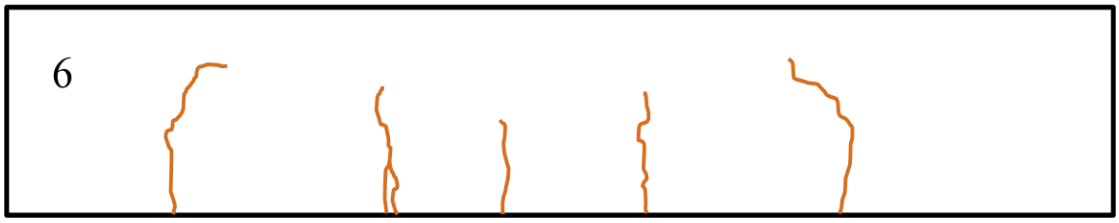
6

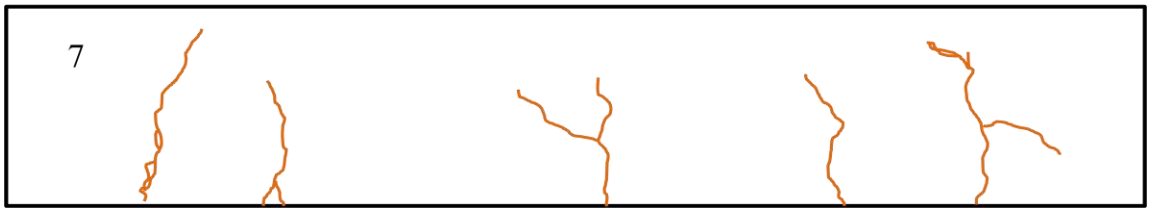
7

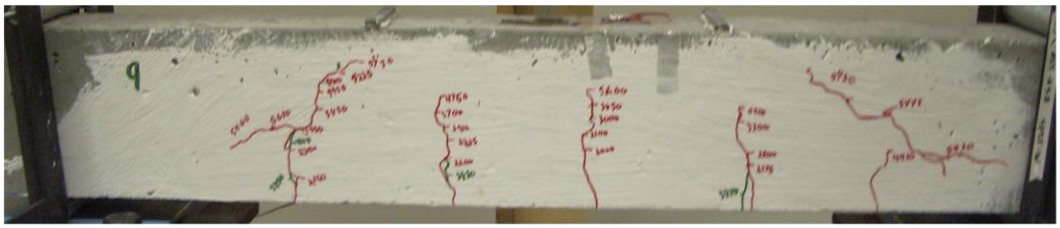

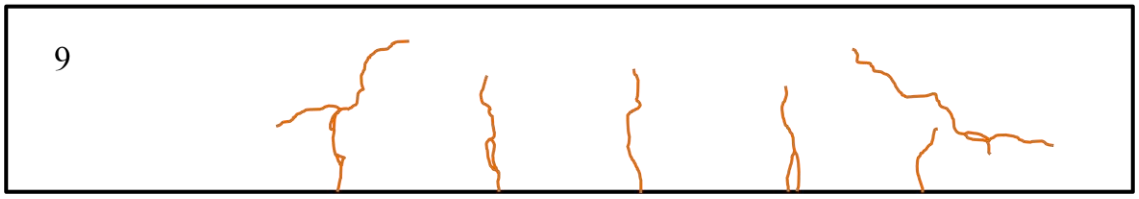
9

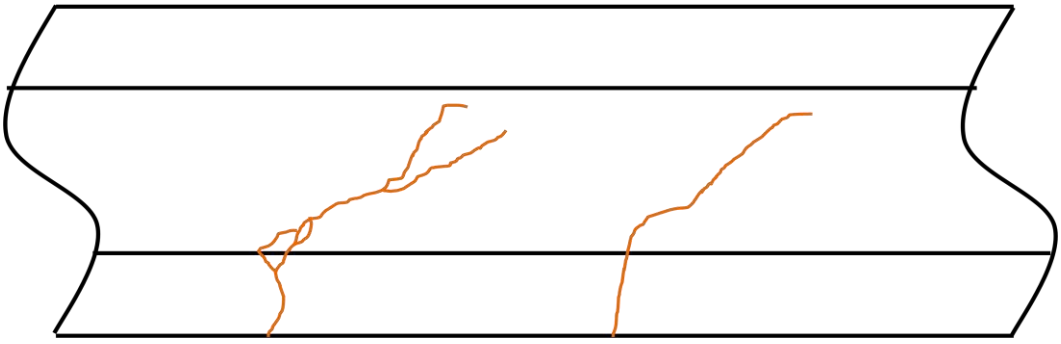

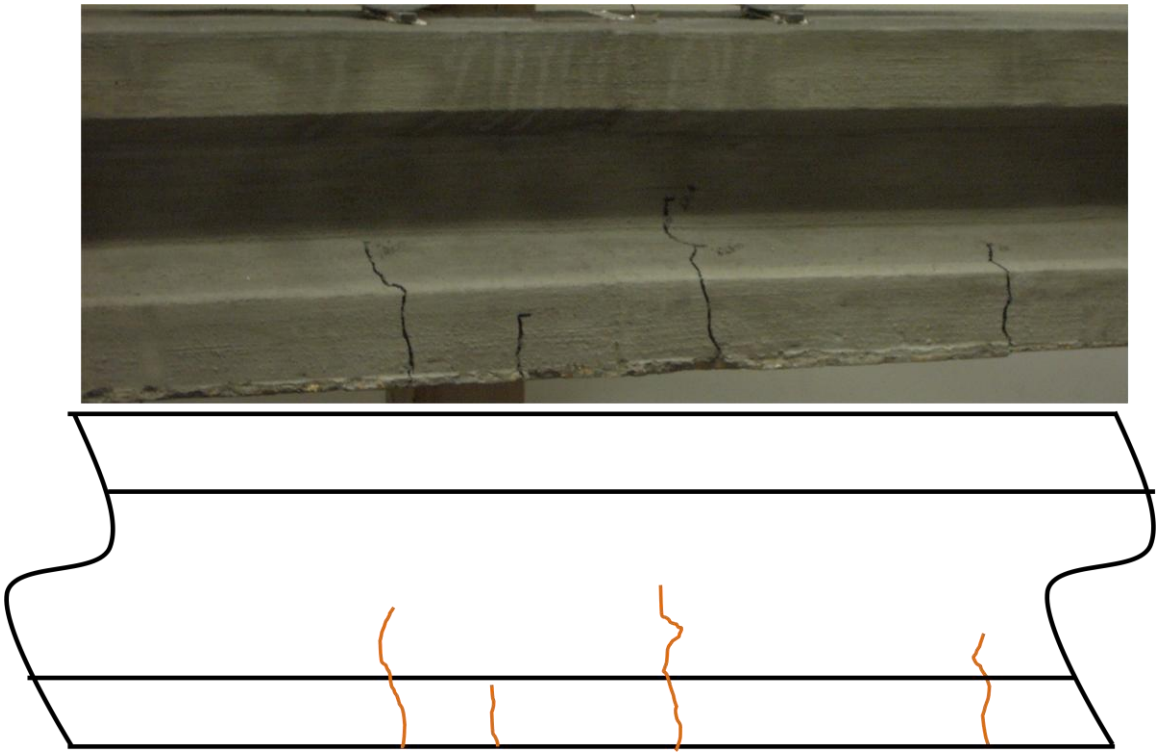

Crack Growth of Phase II Testing

The following figures demonstrate the crack growth of the reinforced concrete specimens. The orange lined cracks were produced from the initial loading performed in phase I of the experimental process. The cracks lined in red are the cracks produced by the second and final loading of the specimens.

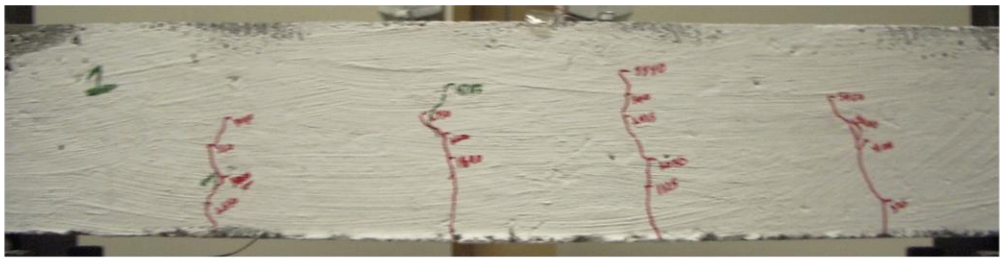

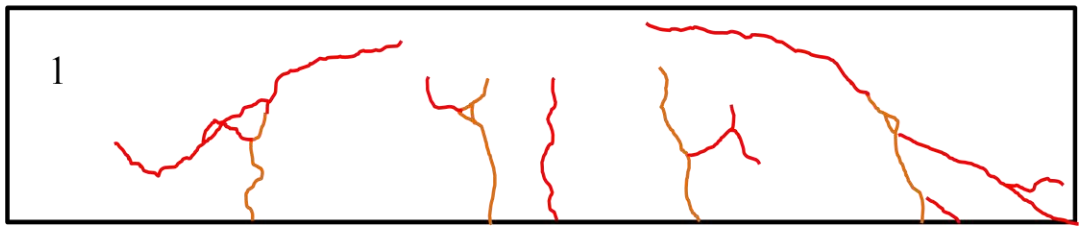
1

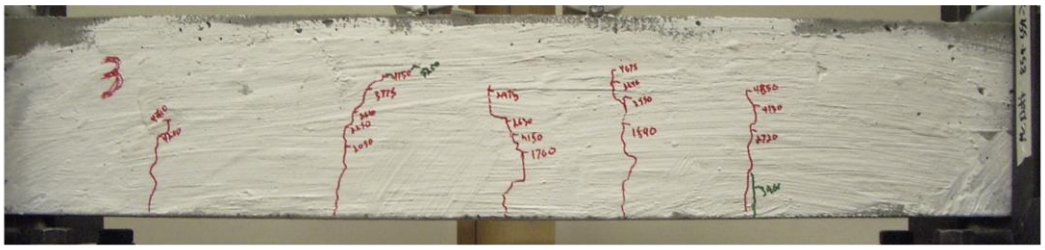


3


A

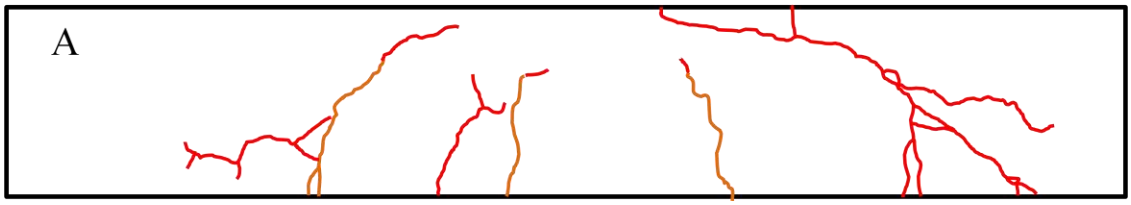
A


B


B


B


C

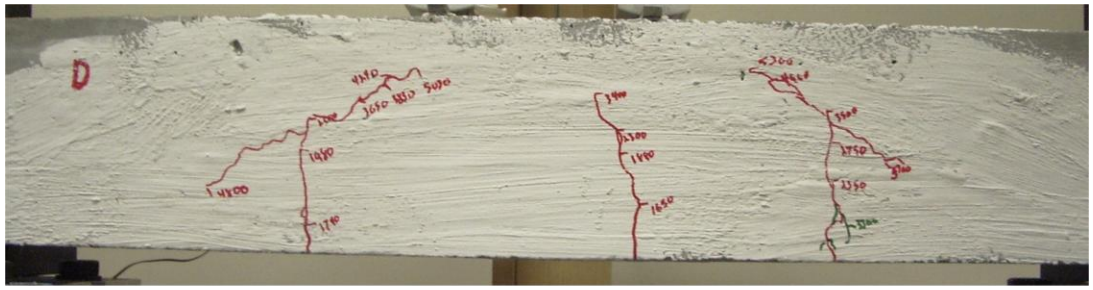
D

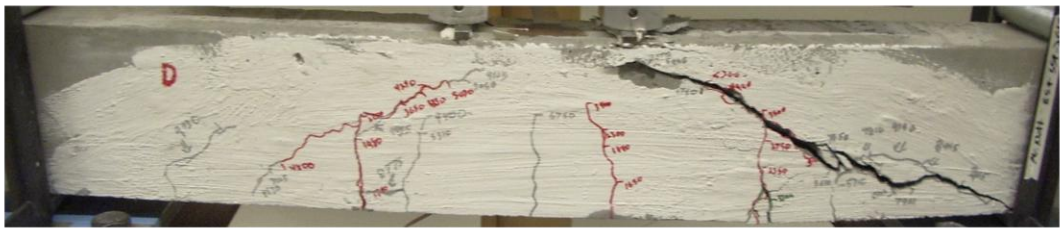
D


D

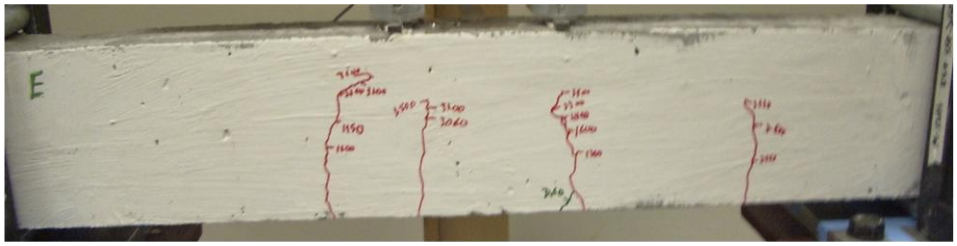
E


E

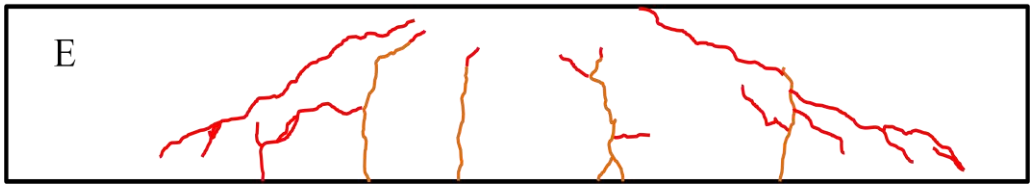
E


F

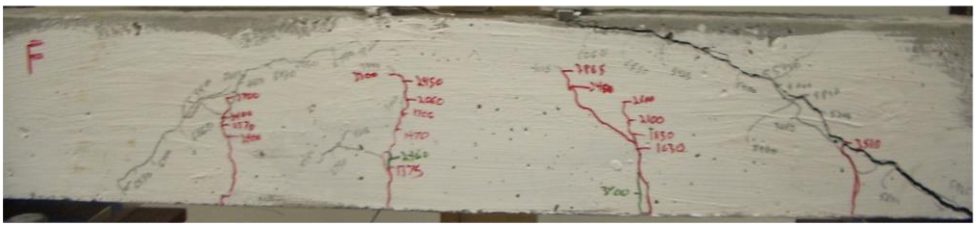
F


F

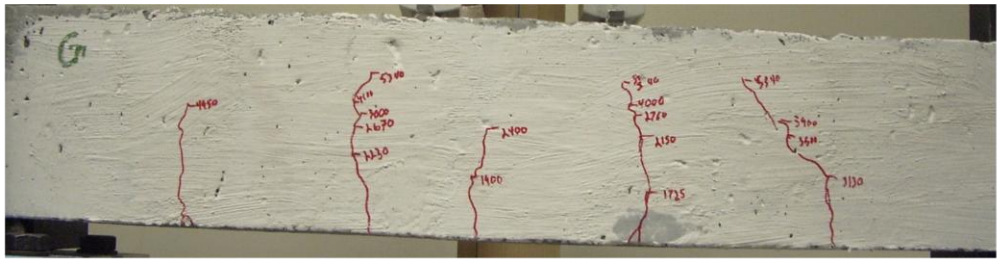

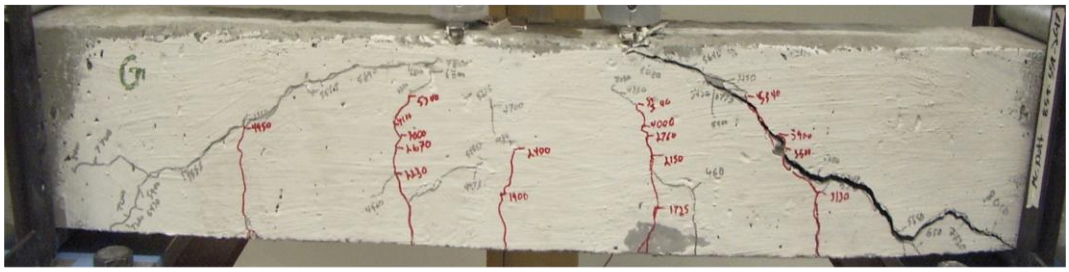


G

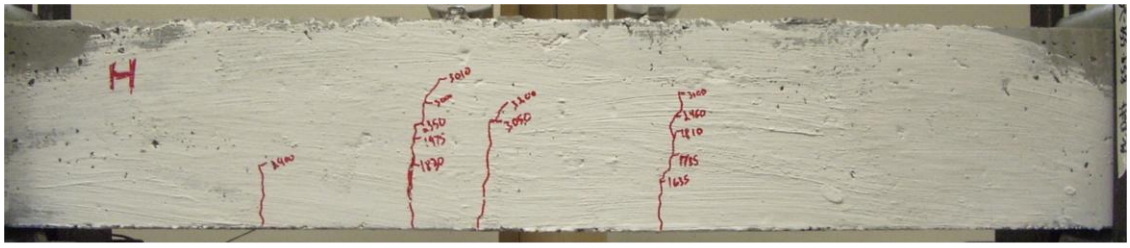

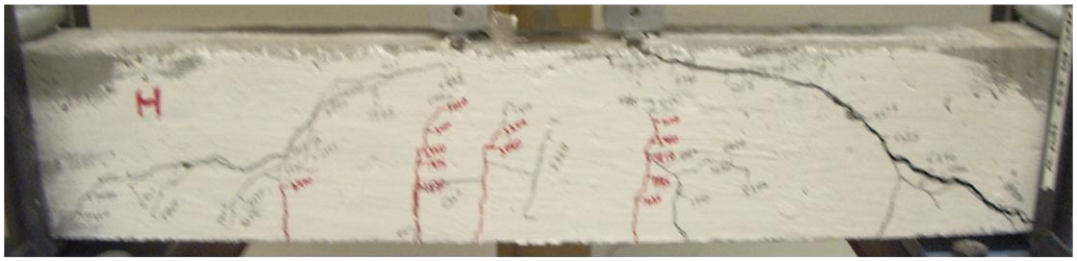


H

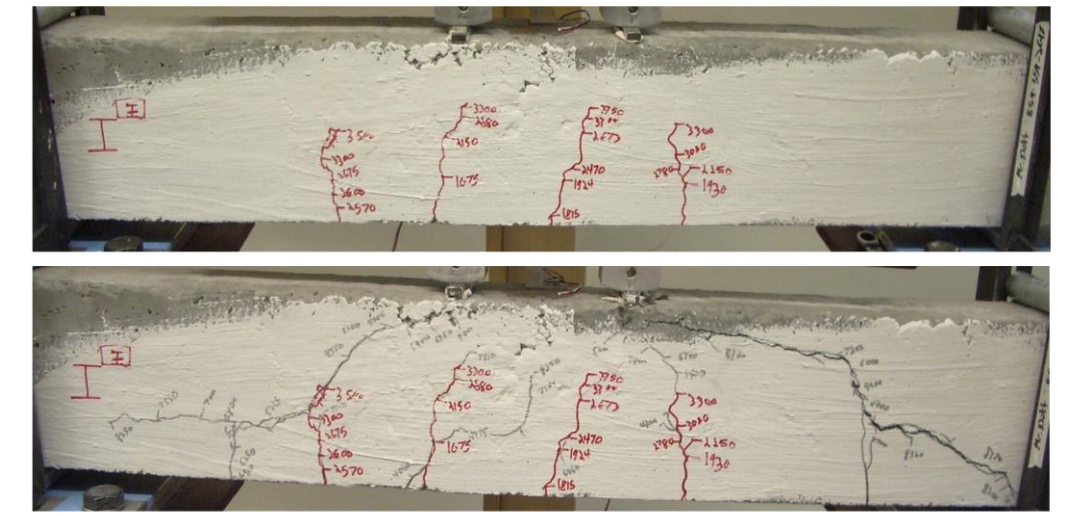

I